Characterisation of the physical environment of embryos throughout *in vitro* culture

A thesis presented in partial fulfilment of the requirements for the degree of

Doctor of Philosophy

at Massey University, Palmerston North

New Zealand

by

Sophia Elizabeth Blomfield

2011

Abstract

Characterisation of the physical environment embryos are exposed to throughout *in vitro* culture for treatments involving *in vitro* fertilisation (IVF) has been limited due to measurement difficulties (since the position of an embryo is the point of interest) and the lack of a theoretical framework. Temperature, oxygen concentrations and pH are all important factors in an oocyte's and an embryo's environment which, if away from desired levels, may impact on embryo viability. The development of mathematical models provides a structured approach which helps to overcome measurement difficulties.

The IVF process was broken down into 70 discrete back-to-back steps, from oocyte aspiration to embryo transfer, which could be modelled. Models of heat transfer were developed for a Petri dish, 4-well dish, Pasteur pipette (un-pulled and pulled), plastic pipette tip (two sizes), denuding pipette and transfer catheter. Models of oxygen and carbon dioxide mass transfer were developed for the Petri dish, in which oocytes and embryos spend the majority of their time in culture. The models were solved by the finite element method in the software package COMSOL Multiphysics 3.3a used in conjunction with MATLAB R2006a. Models were then validated against experimental data.

There is considerable variation in the embryology culture process, with respect to the number and timing of steps, both between and within laboratories. Of all the factors in an embryo's environment embryology practice has the greatest impact on temperature. Embryos are cultured in dishes in incubators which maintain the required gaseous and thermal environment. While paraffin oil, which overlays culture media in

a dish, successfully buffers embryos from great changes in oxygen and pH when dishes are removed from an incubator, maintenance of embryo temperature is dependent on numerous factors including the setting of the surface temperature of microscope stages, whether the lid is on or off the dish, the embryo position across the floor of the dish, the dish's foot height, the time out of incubator and the depth of liquid in the dish. For a period of 5 minutes out of an incubator in a standard Petri dish set up, the pH an embryo is exposed to will not likely rise from pH 7.33, as in an incubator, to above pH 7.38. However, the temperature an embryo is exposed to may change by ± < 0.5 °C or may change by ± 1 to 3 °C, depending on embryology practice. Importantly, an increase of 1 °C in embryo temperature may adversely affect embryo viability while a decrease of 1 °C will likely have little impact.

Transfer of an embryo in a pipette is the step identified which subjects embryos to the greatest rate and magnitude of temperature change. While temperature in a dish may change by 1 to 3 °C during 5 minutes out of an incubator, the temperatures within a pulled glass Pasteur pipette can fall by > 10 °C in 10 seconds. Use of plastic pipette tips instead of glass pipettes is beneficial for maintaining embryo temperature as the temperature will fall by approximately 3 °C in 10 seconds, 7 °C less than in the glass pipette under the same conditions. This work identified many simple practical steps, such as the use of plastic pipette tips instead of glass, which minimise temperature changes embryos are exposed to throughout the culture process.

Applying the Model of mass transfer of O_2 in a Petri dish disproved the belief that equilibration of gas in the dish occurs significantly faster without a lid. The model of O_2 transport in a Petri dish demonstrated that it takes ≈1 hour to reach 67 % and ≈4

hours to reach 95 % full equilibration of oxygen between atmospheric and 5 vol % O_2 at 37 □C. Modelling mass transport of CO_2 provided a means to predict pH changes within a media drop in a Petri dish. In equilibration from atmospheric to 6 vol % CO_2, the pH reached within 0.1 unit of the final value in ≈1.5 hours. An important finding of this work was that sufficient equilibration of gas may be achieved in ≈2 hours and therefore the pre-equilibration time for dishes (currently overnight) may be shortened, reducing the degradation of amino acids, which occurs at 37 °C, to ammonium (embryo toxic).

There is considerable variation in embryology practice. This work successfully utilised engineering knowledge and mathematical modelling to describe the physical environment of temperature, oxygen and pH that oocytes and embryos may be exposed to throughout an open embryo culture system, used by the majority of IVF clinics worldwide. The findings here provide a basis for establishing best practice. Further work is needed to quantify the effects on the embryo of fluctuation in the embryo's environment but this work demonstrates that mathematical modelling of the embryo's environment in IVF is a viable tool for improving laboratory practice.

Acknowledgements

Heartfelt thanks to all my supervisors, Gabe Redding, John Peek, John Bronlund, and John Gawith, for all your academic assistance, support, and encouragement and for some hilarious conference calls. To John Bronlund thank you for all your ideas and invaluable academic input. To John Peek I am so grateful for all your time and advice; I particularly appreciate all your help with the writing process - Victorian subheadings were a breakthrough. To Gabe thank you so much for your sometimes day to day advice and support, despite being in a different city, which enabled me to keep momentum.

I would like to thank everyone at Fertility Associates for their support and encouragement during this project and for making me feel a part of the team. There are too many of you to thank individually. Special thanks to all the laboratory staff, especially Pauline Bigelow, for all your help and for putting up with me. To Bert Stewart many thanks for your day to day help, encouragement and sense of humour.

Thank you to everyone at Massey, Palmerston North, who has helped me with experimental work – finding, fixing and building equipment.

To all my friends many thanks for your encouragement, understanding and distraction – for forcing me to leave it behind at times. Finally a huge thanks to my family, completing this thesis would not have been possible without your love, support, and understanding.

Table of Contents

List of Figures

List of Tables

Nomenclature

α_d	Angle of flaring of the dish walls	°
A	Area	m^2
A_s	Surface area	m^2
β	Thermal expansion coefficient	$°C^{-1}$
Bi	Biot number	-
c	Heat capacity	$J.kg^{-1}K^{-1}$
C	Concentration	$mol.m^{-3}$
C_{O_2}	Concentration of O_2	$mol.m^{-3}$
D	Diffusion coefficient	m^2s^{-1}
ε	Emissivity	-
g	Acceleration due to gravity	$m.s^{-2}$
h	Convective heat transfer coefficient	$W.\ m^{-2}K^{-1}$
H_d	Height of media drop	m
h_{fg}	Latent heat of water	$J.kg^{-1}$
H_{lw}	Height of Petri dish lid wall	m
H_o	Depth of oil	m
H_w	Height of Petri dish wall	m
K	Equilibrium constant	-
k_p	Mass transfer coefficient for a partial pressure driving force	$s.m^{-1}$
M_r	Molar mass	$kg.mol^{-1}$
n	Number	-
P	Partial Pressure	mmHg
P_{v_1}	Partial pressure of water at a surface	mmHg

P_{v_2}	Partial pressure of water above a surface	mmHg
P_{O_2}	Partial pressure of O_2	mmHg
P_{CO_2}	Partial pressure of CO_2	mmHg
P_{aO_2}	Atmospheric O_2 partial pressure	mmHg
P_{iO_2}	Initial partial pressure of O_2	mmHg
P_{eO_2}	Experimentally recorded partial pressure of O_2	mmHg
P_{aCO_2}	Atmospheric CO_2 partial pressure	mmHg
P_{iCO_2}	Initial partial pressure of CO_2	mmHg
pK_a	-log(K)	-
q	Heat flux	$W.m^{-2}$
r	Radial distance	m
R	Thermal resistance	$m^2.K.W^{-1}$
r_a	Radius of air gap beneath Petri dish	m
Ra	Rayleigh number	-
r_d	Radius of media drop	m
Re	Reynolds number	-
R_g	Gas constant	$J.mol^{-1}K^{-1}$
r_i	Internal radius of Petri dish	m
r_l	Radius of Petri dish lid	m
r_o	Radius of the dish at H_o	m
R_x	Cross sectional area/wetted perimeter	m
S	Solubility	$mol.m^{-3}mmHg$
t	Time	s
T	Temperature in Kelvin	K

T_a	Ambient air temperature in Kelvin	K
T_s	Surface temperature in Kelvin	K
U	Apparent heat transfer coefficient	W. $m^{-2}K^{-1}$
v	Velocity	$m.s^{-1}$
V_d	Volume of media drop	m^3
V_{oil}	Volume of paraffin oil	m^3
x	Thickness	m
x_a	Width of the Petri dish foot	m
x_b	Thickness of the Petri dish floor + air gap	m
x_f	Thickness of Petri dish floor	m
x_l	Thickness of the Petri dish lid	m
x_{la}	Thickness of the air gap between the Petri dish and its lid	m
x_{lw}	Thickness of the Petri dish lid wall	m
x_w	Thickness of the Petri dish wall	m
y	Vertical distance	m
θ	Temperature in degrees Celsius	°C
θ_a	Ambient air temperature in degrees Celsius	°C
θ_b	Temperature of base boundary	°C
θ_e	Experimentally recorded temperature	°C
θ_i	Initial temperature	°C
θ_s	Surface temperature in degrees Celsius	°C
λ_{eff}	Effective thermal conductivity	$W.m^{-1}K^{-1}$
ρ	Density	$kg.m^{-3}$
λ	Thermal conductivity	$W.m^{-1}K^{-1}$

μ	Viscosity (kinematic)	m^2s^{-1}
α	Thermal diffusivity	m^2s^{-1}
σ	Stefan-Boltzmann constant	$W.m^{-2}K^{-4}$
Ω	Denotes the subdomain	-

Subscripts

a	Air
g	Glass
m	Media
o	Paraffin oil
p	Polystyrene
pp	Polypropylene

1 Introduction

The use of *in vitro* fertilisation (IVF) is a central part of the growing industry which surrounds assisted reproductive technology (ART). ART is used in the treatment of infertility (the inability to have children when desired). A difficulty to conceive may stem from a range of factors, both known and unknown, affecting one or both partners. At present 1–3% of children born in developed countries are conceived via assisted reproduction treatments (Basatemur *et al*., 2010).

As the *in vitro* culture of human embryos has developed over the last 30 years, the primary focus of research has been the development of culture media specific to human gametes and embryos. Vajta *et al*. (2010) cited seven review articles (published between 1990 and 2008) which detail various components of culture media. While these advances have significantly improved clinical pregnancy rates, very few studies have looked at an embryo's physical environment and how it is affected by steps in the culture process.

Embryo culture aims to keep an embryo's physical environment constant by culturing in incubators at core body temperature (~37□C), 6% carbon dioxide (to maintain the pH of the bicarbonate buffered culture media) and at low oxygen concentration (to mimic the fallopian tubes and uterus). There is debate around the appropriate value for these set points (e.g. Leese *et al*. (2008) query the use of core body temperature). The degree to which changes in the physical environment impact on an embryo has not been described since culture away from the desired set points is not carried out as part of standard IVF. However, it is acknowledged that the variable nature of the

laboratory environment is a source of negative stressors and that accumulation of these may negatively impact embryo development (Thompson *et al*., 2007).

Due to the difficulty of measuring temperature, pH and oxygen concentration *in situ* during embryo incubation and handling, very few studies have looked at the potential changes an embryo experiences in its physical environment *in vitro*. In addition, scientists working in ART seldom have a background in the physical sciences, so what has been done is empirical and is discussed without reference to a theoretical framework of heat or mass transfer. The application of engineering and mathematical modelling alongside measurement will enable description of the physical environments an embryo may be exposed to throughout the culture process. Modelling has recently been applied to some specific aspects in reproduction and ART to investigate physical processes which would otherwise not be described (Redding *et al*., 2007; Redding *et al*., 2008; Stokes *et al*., 2008).

This project aims to describe and quantify changes to an embryo's environment during *in vitro* culture and handling in terms of heat and mass transfer. This involves the application of engineering principles and the development of mathematical models to describe the culture system. Mathematical models are the mathematical, and appropriately simplified, representation of a real life situation and therefore temperatures or concentrations may be investigated at any point within a system (particularly at the position of an embryo).

The use of mathematical models will enable testing of assumptions about a situation and therefore facilitate understanding of the heat and mass transfer processes

involved. Modelling also allows investigation of many situations in the culture system from an embryo's point of view. This allows identification of points in the culture process, at which embryos are exposed to fluctuating conditions.

An understanding of the working environment in the laboratory, the embryo culture process, the physical processes (heat and mass transfer), and the impact of these physical processes on the immediate environment of an embryo provides a basis for identifying potential problems within the embryo culture process. It is hoped that simple solutions can be found to improve laboratory practice, reduce stress on the embryos and thus improve the likelihood with which they will develop into viable pregnancies.

2 Literature Review

The project is directed at understanding and defining the physical environment an embryo experiences *in vitro* and identifying means to optimise this environment. The literature review therefore covers the development and physiology of an oocyte and an embryo from ovulation to implantation in the uterus, and the interaction of the oocyte or the embryo with its environment. This will allow identification of environmental factors which are important to normal embryo development.

2.1 Infertility and in vitro fertilisation (IVF)

Fertility is defined as the capacity to produce offspring. Clinical infertility is commonly defined as the inability to have children within one year of trying and affects approximately 15% of couples at some point throughout their reproductive lifetime (Tavares *et al*., 2009). A difficulty to conceive may stem from a range of factors which may be known or unknown and may affect one or both partners. Only rarely is one partner completely sterile and unable to produce viable gametes (Brinsden, 1999; Pepperell *et al*., 1987).

The development of fertilisation *in vitro* began as a research tool to study mammalian fertilisation and embryo development. Its applications now include conservation of endangered species, selective breeding for improvements to livestock quality and the treatment of human infertility (Bavister, 2002).

Successful IVF was facilitated by major breakthroughs including determining the level of maturity required for a mammalian oocyte to be fertilised and accurately

determining the factors which signal the occurrence of fertilisation (Bavister, 2002). This groundwork paved the way for the birth of Louise Brown in 1978, the first human birth as a result of IVF. IVF quickly became a common practice for the treatment of infertility; pregnancies in Australia and New Zealand grew from 2 in 1979 to ~2000 in 1989 and to ~5000 in 1999 (Campagne, 2006).

The ability to successfully grow human embryos outside the body has led to other developments. Most notable are intra-cytoplasmic sperm injection, a highly effective technique which overcomes most cases of male factor infertility, and pre-implantation genetic diagnosis (PGD); a technique by which genetic screening may be carried out on one or two cells removed from the early *in vitro* embryo. Analysis allows detection of undesirable genes, such as those responsible for cystic fibrosis. As the analysed embryos are still growing in culture, choices can be made as to which embryos are replaced into the uterus, usually those with potential for a higher quality of life. These advances in technology have extended treatment of infertility to a wider range of causes.

IVF is increasingly accepted as a treatment for infertility in the western world. Its uptake has been accelerated because people in Western society frequently delay starting a family until later in life, when a woman's fertility is naturally declining. At present 1–3% of children born in developed countries are conceived via assisted reproduction treatments (Basatemur *et al*., 2010).

2.2 Mammalian oocyte (egg) and embryo development

This section sets out to overview the process of oocyte (egg) maturation, fertilisation, and the subsequent pre-implantation embryo development in a normal human pregnancy, and focuses on the processes and systems which have an impact on this developmental process. Though the focus is on the human oocyte and embryo, pertinent information gathered from experiments involving mammalian models is included.

2.2.1 Oogenesis

Oogenesis is the process of oocyte maturation in the ovary. The development of both oocytes and sperm is coordinated by the central nervous system (CNS). The most important mediator of reproduction by the CNS is gonadotrophin hormone releasing hormone (GnRH) which is released by the hypothalamus (at the base of the brain) and induces the secretion of luteinising hormone (LH) and follicle stimulating hormone (FSH). The regulation of these two hormones and their ratios to each other is highly complex and involves both negative and positive feedback control (Elder & Dale, 2000). The lettering within this section refers to Figure 2.1; which shows the stages of follicular development.

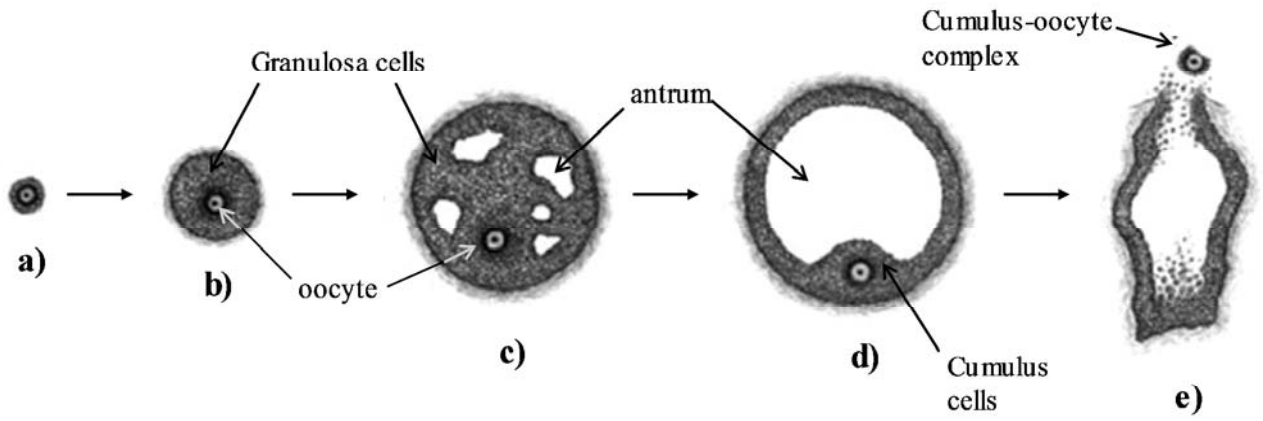

Figure 2.1: Follicular Development in the Ovary. (a) Primordial follicle (containing a primary oocyte), (b) Primary Follicle, (c) Secondary follicle, (d) Mature (Graafian) follicle, (e) Ovulation. Adapted from Soucasaux (1993).

All the oogonia (the precursors to oocytes) available for a woman's reproductive life have entered their first meiotic division to become primary oocytes by the fetal age of five months **(a)**. Primordial follicles are formed (diameter ~50 µm) during the first meiotic prophase before the oocytes arrest in diplotene (a subdivision of the prophase I), in which they may remain viable for up to 50 years (Fauser *et al*, 1999). Primordial follicles consist of an oocyte surrounded by a single layer of granulosa cells.

Recruitment (activation) of some of these primordial follicles begins at puberty. Once selected, primordial follicles grow over a period of 6-7 months, **(b)** to **(d)**, into mature Graafian follicles (diameter ~17-20 mm). Throughout this period of growth the surrounding granulosa cells divide mitotically, the zona pellucida (a glycoprotein coat/shell) is synthesized by the oocyte and intercellular communication systems are formed between the oocyte and the closest layer of granulosa cells which begin to pass developmental information. Most pre-antral follicles **(b)** undergo atresia (cell death) but a small minority develop into antral follicles **(c)** with the formation of a fluid filled cavity (antrum). The cumulus cells are the mass of granulosa cells closely

associated with the oocyte from the antral follicle stage onward. Mature antral follicles are known as Graafian follicles **(d)** and grow in response to the release of follicle stimulating hormone (FSH) (Elder & Dale, 2000).

Once a Graafian follicle is fully mature, a surge in the levels of LH in the blood triggers large scale synthesis of hyaluronic acid by cumulus cells. The bridges between cumulus cells and between cumulus and granulosa cells disappear resulting in the formation of the cumulus-oocyte complex (COC), an oocyte surrounded by loosely bound cumulus cells. The LH surge also causes resumption of nuclear development, and structural changes to the follicle allowing it to rupture (Elder & Dale, 2000). The oocyte is released at ovulation **(e)**, when the follicle ruptures due to the breakdown of the basement membrane. The COC is captured by the oviduct where fertilization may occur *in vivo*. Ovulation occurs within 36-42 hours of the onset of the LH surge (Elder & Dale, 2000).

The meiotic spindle is a crucial structure within the oocyte. It is responsible for the movement (accurate alignment and segregation) of chromosomes during meiosis (Wang & Sun, 2006; Rama Raju, 2007). It is a temporary and dynamic structure composed of cytoskeletal microtubules. These consist of heterodimeric units of α and β tubulin. There are two types of microtubules; those which run from pole to pole between the chromosomes and those attached to the kinetocores of the chromosomes. (Rama Raju *et al*., 2007; Kilani *et al*., 2006). The correct structure of the meiotic spindle is important in order to achieve proper segregation of chromosomes upon cell division. In addition, the location of the meiotic spindle establishes the first cleavage plane and will impact on the quality of the pre-implantation embryo (Wang & Sun,

2006). The morphology and kinetics of the meiotic spindle can be influenced by several factors, particularly temperature (discussed further in Section 2.6.2.2), and *in vitro* manipulations of the oocyte.

2.2.2 Embryo development

The following section describes the fertilisation and subsequent development of the early embryo. It is these stages which take place outside the body in treatments which involve *in vitro* culture (such as IVF). Figure 2.2 is referred to in this section and displays photographs of embryos at progressive stages of development.

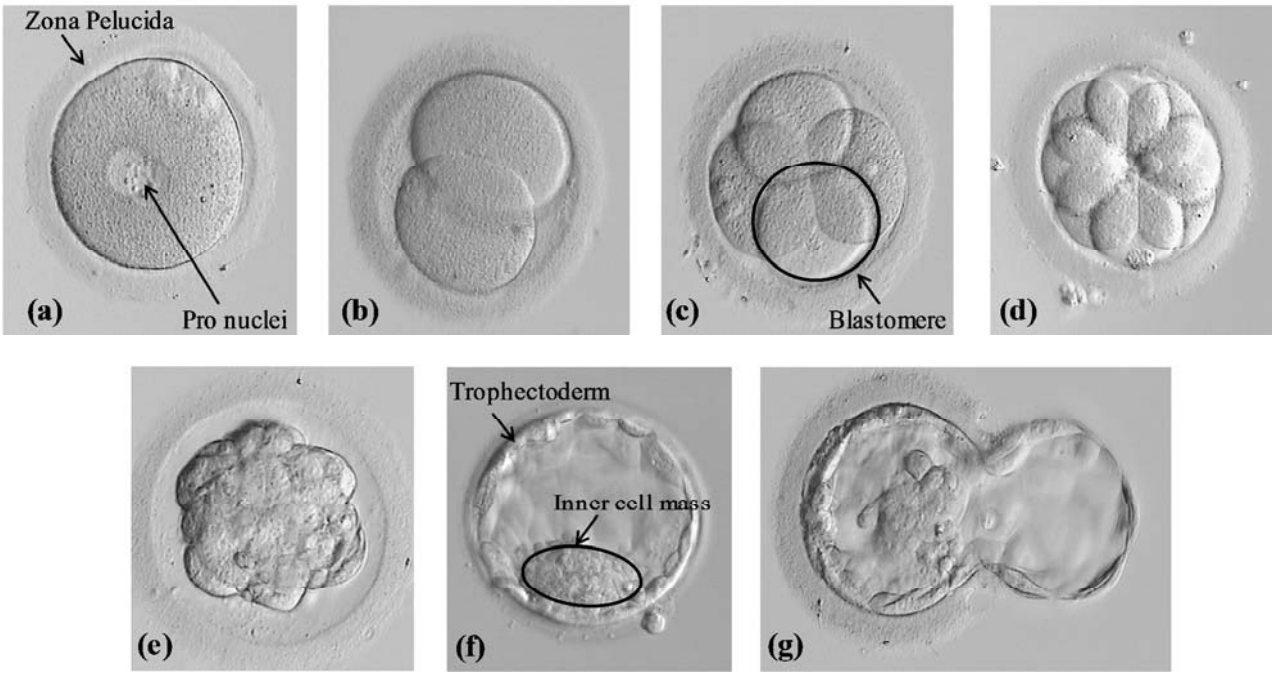

Figure 2.2: Embryo development:(a) normally fertilized oocyte. (b) 2-cell cleavage embryo. (c) 4-cell cleavage embryo. (d) 8-cell cleavage embryo. (e) morula. (f) blastocyst. (g) hatching blastocyst.

2.2.2.1 Fertilisation

The cumulus cells limit the number of spermatozoa (sperm) that are able to reach the oocyte surface. Those that reach the surface need to bind with and then penetrate the

zona pellucida. Binding is dependent on specific molecular interactions between the sperm and the zona associated with the acrosome reaction, in which the release of enzymes from the sperm's acrosome breaks down the vitelline coat and allows entry of single sperm (Elder & Dale, 2000).

The first morphological indication of oocyte activation (sperm entry) is the exocytosis of corticle granules, small spherical membrane-bound organelles containing enzymes and mucopolysaccharides, eliciting the zona reaction. The zona reaction changes the characteristics of the zona to block polyspermy (the entry of multiple spermatozoa) (Elder & Dale, 2000).

Figure 2.2 **(a)** shows a normally fertilized oocyte. Visible, as two circular bodies in the centre, are the pro-nuclei, each containing the chromosomal contribution from the parents.

2.2.2.2 Cleavage

Figures 2.2 **(b)**, **(c)**, and **(d)**, respectively show the progression of the embryo through the 2-cell, 4-cell and 8-cell stages of cleavage. During this period of growth, the mammalian embryo is transported down the oviduct towards the uterus (Elder & Dale, 2000). The zygote cleaves by mitosis into blastomeres (as circled in Figure 2.2 **(b)**). New blastomeres are approximately half the size of the parent cell.

Mitochondria, the cellular organelles responsible for energy production, do not replicate in the early cleavage stage so their number per cell halves with each cell division provided they are uniformly segregated. Uniform segregation of

mitochondria, thus metabolic equivalence among blastomeres, is considered important to embryo development (Van Blerkom, 2004). Early cleavage is a period with intense cell division but with no increase in embryo volume (Booth *et al*., 2005). During this period any protein synthesis is dependent on the remaining maternal mRNA and synthesis declines, likely due to degradation of these mRNA templates (Booth *et al*., 2005). There is a low level of energy production, predominantly by mitochondrial respiration (Thompson *et al*, 1996; Johnson *et al*., 2003).

Activation of the embryo's own genome occurs at approximately the 8-cell stage (Baumann *et al*., 2007; Braude *et al*., 1988). This is accompanied by an increase in protein synthesis and energy production (Booth *et al*., 2005).

2.2.2.3 Morula

At about the stage of the third cleavage (in the human, onset occurs on day 3 around the 6-10 cell stage) the embryo undergoes the process of compaction to form the morula. The blastomeres flatten against each other and begin to form intracellular junctions becoming tightly associated and communicating. Figure 2.2 **(e)** shows a compacted morula; the individual cells (approximately 16 – 32 cells) are no longer discernable. At about the morula stage, energy production significantly increases to support the increase in protein synthesis (Houghton *et al*., 1996).

2.2.2.4 Blastulation (cavitation)

At the 32-cell stage a further morphological change occurs with the formation of the blastocele (a fluid filled cavity) giving rise to a blastocyst. Figure 2.2 **(f)** shows the

blastocyst which is made up of the trophectoderm (flattened cells on the embryo surface), which develops into the placenta, and the inner cell mass (ICM), which develops into the foetus. (Elder & Dale, 2000)

Blastocele formation is essential for both further development and differentiation of the ICM. The blastocele contains a specific fluid medium, the composition of which is controlled by the continuous border of trophectoderm cells. This may contain proteins which influence cell proliferation and differentiation (Elder & Dale, 2000).

2.2.2.5 Blastocyst hatching

The embryo must hatch from the zona – shown in Figure 2.2 **(g)** in order to establish physical contact between the trophectoderm and the endometrium (the lining of the uterus) which is necessary for implantation. The mechanism for hatching is poorly understood but appears to involve both mechanical and chemical factors (Sathananthan *et al*., 2003).

2.3 Culture media

Research into improving embryo culture has predominantly focused on culture media composition which has led to significant increases in embryo implantation rates. Vajta *et al*., (2010) cited seven review articles (published between 1990 and 2008) which detail components of culture media.

Nearly all IVF laboratories now purchase commercially produced proprietary media. Components of culture media which interact with the physical environment in a

laboratory will be discussed when appropriate (e.g. amino acid breakdown and bicarbonate buffering).

In the IVF industry the culture medium is referred to in the plural as "culture media" and drops of culture medium in a culture dish are referred to as "media drops". This convention will be followed throughout this thesis.

2.4 The embryo culture process

The embryo culture process is run by embryologists (specialist laboratory scientists). Oocytes and embryos are held *in vitro* in media drops in dishes (such as Petri dishes). They are transferred between dishes at a number of stages of the process using pipettes.

In open embryo culture, embryo handling (moving embryos between dishes) takes place outside of the incubator environment. The open embryo culture process is similar across different fertility clinics (local and international). The ambient temperatures of open systems depend on climate, clinic size (laboratory temperature control is expensive for small clinics) and local regulations. For example embryo handling throughout Europe must be carried out inside laminar flow hoods to comply with cell culture regulations. Laminar flow hoods blow filtered, room temperature air at a rate of ~0.5 $m.s^{-1}$ over the bench top which limits contamination from the air within the laboratory (from embryologists for example).

In closed culture systems, embryo handling, for all or part of the process, takes place inside a box with a controlled environment (temperature, humidity and gas

composition). These are increasingly used in IVF. The main disadvantage of these, especially for smaller fertility clinics, is the expense. Characterising and identifying limits to the control of an open culture system will enable comparison of a best practise open system with a closed system. Potentially weak points identified in the open system will be points where it would be most useful to consider the use of a closed system. The use of closed culture systems has a higher level of complexity which impact the ease of embryology practices. The closed system causes difficulties in the transfer of sterile equipment and media into it. Electrical equipment such as microscopes generate heat, complicating control of the environment within the system. There are very few totally closed embryo culture systems primarily due to these problems and the large costs involved.

2.4.1 Evolution of the embryo culture process

Improvement of embryology practices is difficult to implement. Some of the reasons for this are outlined by Vajta *et al*. (2010) below:

> "To avoid fiascos, in practice most laboratories simply use their earliest albeit modestly successful routines, painstakingly introducing any innovative procedures which require many years, sometimes a decade or even more to develop. Controversially, even the few new procedures that gain worldwide acceptance are typically implemented and applied without scientifically sound evidence. Consensus among scientists is often lacking. Even the most widely accepted parameter, the application of the core temperature, has been questioned recently and for good reasons. Due to these hurdles and other, not purely scientific factors, mammalian embryology may still be regarded as a

handicapped branch of science especially when compared with other fields, e.g. information technology, nanotechnology and molecular biology."

Due to the delicate nature of human embryo culture for IVF, in both a literal and an emotional sense, IVF scientists and clinicians are reluctant to make any changes in case it is the wrong change. A beneficial technology may be avoided for years simply due to superstition or to a coincidental mishap occurring when it was first introduced. Part of the reason for this mindset is the difficulty in measuring the culture conditions due to the small working volumes (µl to ml). Characterising the physical environment that an embryo experiences will be important to understanding how a process change might impact embryo development.

2.5 Embryo plasticity

The early mammalian embryo has an evident tolerance to some level of variation in its physical environment (as proven by successful *in vitro* culture and subsequent pregnancy). The extent of an individual embryo's plasticity will vary depending on its transcriptome, proteome, and metabolome (the complement of its key macromolecules). An embryo's transcription and protein synthesis will likely deviate further from the norm the further culture conditions are from the ideal *in vivo* environment (Thompson *et al* 2007).

This deviation in transcription and protein synthesis has the potential to impact on subsequent embryo viability and foetal development (Thompson *et al*, 2007). Of particularly sensitivity is the activation of the embryo's own genome as transcription activity is switched over from the maternal transcripts. Genomic activation involves

dramatic reprogramming of the pattern of gene expression. Though initial activation of the embryonic genome may take place earlier (especially since detection is dependent on method sensitivity), significant transcription has not been observed until the 8-cell stage (Braude *et al*., 1988). It has been suggested that stressors in the *in vitro* environment may lead to degradation of the maternal transcript and early dependence of the embryo on its own genome, perhaps triggering developmental arrest and/or apoptosis (Baumann *et al*., 2007).

The increase in synthetic activity and energy consumption observed in *in vitro* cultured embryos has led to the 'quiet' embryo hypothesis (Leese, 2002), where 'quiet' pertains to a lower range of metabolite consumption and turnover rate indicating reduced consumption of energy. Supporting this hypothesis is the evidence that embryos which show successful development to blastocyst have amino acid turnover profiles (used for protein synthesis) and pyruvate consumption profiles distributed within the lower range, compared with those which fail to develop (Baumann *et al*., 2007). The idea is that these quiet embryos are directing their energy towards providing the essential building blocks for development, while less viable embryos have directed metabolic pathways to make up for any beneficial endogenous traits they lack, or in response to negative influences of their environment.

Vajta *et al*., (2010) reviewed observations in the literature which do not support the quiet embryo hypothesis. The opposing line of thought is that an embryo's response to imposed sub-lethal stress may provide resistance to future stress. Expression of proteins, such as the heat shock proteins (expressed upon cellular exposure to environmental stressors such as high temperatures), does not necessarily represent reduced cellular viability, but may demonstrate cell functionality (Rief *et al*., 2002).

To accurately assess any such hypotheses it is crucial to be able to define the embryo's environment. Only then will it be possible to reliably relate differences between embryos with respect to their physical environment.

2.6 Temperature

Temperature is an important environmental factor to both oocytes and embryos. Cooling reduces metabolic rates and depolymerises macromolecules, while heating directs energy into a metabolic survival response, such as the production of heat shock proteins, and denatures proteins and degrades other macromolecules. This section will discuss information available in current literature on the *in vivo* thermal environment, the impact of temperature changes on both oocytes and embryos and temperature control in laboratories. Gaps in this knowledge will be identified.

2.6.1 *in vivo* environment

The *in vivo* environment is accepted as having the target conditions which *in vitro* culture should strive to replicate. Examination of the thermal environment *in vivo* is important in order to gain insight into the typical temperatures an oocyte or an embryo would experience. This is an area of limited research due to the technological limitations to measuring temperature *in vivo* in the female reproductive tract during ovulation and early embryo development (Sutton *et al.*, 2003). Since the beginning of IVF practice it has been assumed that an embryo's temperature should be held constant at the core body temperature of 37°C. Increasingly this 'ideal' of 37°C is questioned and there have been calls for more in-depth study into the actual

temperatures and temperature gradients an oocyte or embryo is exposed to in the reproductive tract (Leese *et al*., 2008; Vajta *et al*., 2010).

A women's core body temperature is not stable. It oscillates over a 0.8-1 °C range between the maximum at day and the minimum at night. The mean value of this daily oscillation varies throughout the menstrual cycle (Cagnacci *et al*., 1997). A decrease in the mean body temperature occurs approximately 24-48 hours before ovulation and is associated with the preovulatory estrogen rise (Coyne *et al*., 2000). Thermosensing has shown that pre-ovulatory follicles of several mammalian species are cooler than the adjoining ovarian stroma; 1.4 ± 0.2 °C cooler in murine, ≥ 1 °C cooler in ovine and approximately 1.5 °C cooler in bovine. It has been suggested that human pre-ovulatory follicles may be up to 2.3 °C cooler than the neighbouring stroma (Hunter *et al*., 2006). Leese *et al*., (2008) conservatively estimates a human oocyte's temperature post ovulation to be 35.5 °C, 1.5 °C cooler than core body temperature.

Whatever the ideal environment for human embryos, at present, the degree of uncertainty around the *in vivo* thermal environment has meant *in vitro* culture systems have focused on maintaining a constant temperature of 37 °C.

2.6.2 *in vitro* environment

The temperature of oocytes and embryos during *in vitro* culture is dependent on the equipment used for temperature maintenance (incubators and heated stages for open culture and the incubation chambers for closed culture), the setting of this equipment to the appropriate temperature, and the use of the equipment and timing of the culture process. Throughout this process there are circumstances where oocytes and embryos

may be heated or cooled. The potential impact that these possible changes have on oocytes and embryos are discussed below.

2.6.2.1 Impact of high temperatures on embryos

How detrimental the effect of heat stress is on development is dependent on its magnitude, duration and the stage of oocyte or embryo development at which it occurs. Barati *et al*. (2008) exposed porcine oocytes to an elevated temperature of 41 °C (porcine body temperature is ≈38.5 °C) for 0, 0.5, 1 or 1.5 hours. The longer the exposure the greater the detrimental impact on the oocytes was, as characterised by an oocyte's ability to undergo the second meiosis, become fertilised and the extent of DNA fragmentation. Sugiyama *et al*. (2003) demonstrated that the impact on bovine embryos on exposure to elevated temperatures depended on the development stage of the embryos. Exposure to 41 °C had a greater impact on the continuing development of embryos exposed on day 1 or 2 (cleavage stage) than those exposed on day 4 (morula/early blastocyst). Similarly it has been shown that exposure of murine blastocysts to 43 °C was required to promote the same expression of a heat shock protein as exposure at the 8-cell stage to 40 °C (Edwards *et al*., 1995). The longer the exposure, the higher the temperature and the earlier the embryo's developmental stage, the greater is the detriment to the embryo.

Heat shock proteins are proteins whose expression increases upon cellular exposure to environmental stressors (such as high temperatures and oxidative stress) as part of a protective mechanism defending the cell against environmental stress (Christians *et al*., 2003; Neuer *et al*., 2000; Lazzari *et al*., 2002). Their expression is triggered by the presence of denatured proteins (Edwards *et al*., 1995) and their function includes

stabilizing denatured proteins which prevents aggregation and enables repair or degradation (Lazzari *et al*., 2002). As expected, due to the increased environmental stressors *in vitro,* higher levels of heat shock proteins are expressed in *in vitro* cultured embryos than in those *in vivo* (Christians *et al*., 2003). Applying the quiet embryo hypothesis (as discussed in Section 2.5; Leese, 2002) to this situation; expression of such proteins for defensive purposes may be detrimental long term for embryo development as energy is directed away from essential development.

Exposing bovine embryos to 41 °C (2 °C above the core body temperature of 39 °C) significantly increased embryo mortality (Sugiyama *et al*., 2003). Since an increase of 2 °C increases embryo mortality, then a lesser increase (perhaps only 0.5 °C above core body temperature) may also impact embryo development, especially if multiple exposures take place. This leaves little leeway in *in vitro* culture for deviations in temperature above the set point.

2.6.2.2 Impact of low temperatures on embryos

Boone & Shapiro (1990) stated that "Early embryos are often adversely affected by elevated temperatures, but seldom harmed by temperatures that are slightly below this optimal maintenance level". However, throughout open embryo culture there is far more opportunity for temperature drop than for overheating as embryos are removed from incubators for observation and manipulation.

A fall in temperature can have a negative impact on an oocyte's meiotic spindle (description Section 2.2.1.) which is required for successful fertilisation. Exposure to low temperatures results in depolarisation of the meiotic spindle. Prolonged exposure

to lower temperatures increases the likelihood of errors occurring in the process of re-association (Rama Raju *et al*., 2007). Abnormalities in the Meiosis II meiotic spindle can be expected to lead to abnormal segregation of chromosomes after fertilisation resulting in aneuploid embryos (Kilani *et al*., 2006).

A number of studies have demonstrated reduced fertilisation rates due to temperature-induced spindle damage of both bovine (Azambuja *et al*., 1998; Pollard *et al*., 1996) and human oocytes (Almeida & Bolton, 1995). Visualization (using a polarised light microscope) of intact meiotic spindles in oocytes prior to fertilization has been identified as an indicator for successful fertilization and superior subsequent development (Wang *et al*., 2001(b); Keefe *et al*., 2003; Petersen *et al*., 2009). Lane *et al*. (2008) compared the development and gene expression levels of murine embryo collected using either heated stages (calibrated to maintain the temperature close to 37 °C) or no heated stage. While development to the blastocyst stage did not differ between the two groups, the level of gene expression was significantly greater for the cold embryos. The authors suggest that the levels of gene expression may indicate the functioning of embryos and that a change in temperature triggered a change in functioning away from 'normal'. The quiet embryo hypothesis (as discussed in Section 2.5; Leese, 2002) would suggest that this increased gene expression triggered by temperature change may be detrimental as the embryo's energy is directed towards 'damage control' instead of necessary development.

Almeida & Bolton (1995) exposed human oocytes in culture to room temperature (23 °C) for 2, 10 or 30 minutes after which their temperatures had fallen to 32 °C, 27 °C and 25 °C respectively. Significant spindle disruption was apparent in all cases. Only

damage to spindles of oocytes exposed for just two minutes was reversed when returned to 37 °C.

2.6.3 Temperature maintenance in the IVF Laboratory

There has been very limited research into the deviations in temperature from the set point that oocytes or embryos experience throughout the IVF process. It was noted in Fleming & Cooke (2009) that the number of peer-reviewed journal articles dealing with this topic could be counted on one hand. Difficulties involved with looking at the thermal environment of a culture system include measurement issues (limits in available technology and its invasive nature) and that the majority of IVF scientists lack background understanding into physical processes like heat transfer. The former makes results unreliable. For example, Barrett *et al*. (2001) suggested that in their study the thermistor probe in the dish was itself cooling the oil. Two examples of the latter were evident in Fleming & Cooke (2009). They were,

1. When discussing the use of a thermocouple to measure temperatures in a dish it was stated that "… enough wire must be coiled up inside the media to enable an accurate and reproducible temperature reading." The temperature read by a thermocouple is dependent on the temperature at the junction. In addition, coiling wire into the media will change the overall thermal properties of the region and thus the temperature being measured.
2. "Dogma suggests that larger volumes of culture media will not retain temperature and that droplets under large volumes of oil will retain temperatures more efficiently than culture media alone; presumably because oil being a dense fluid may be able to be a type of 'heat sink' compared to

culture media alone. This appears not to be the case." Oil floats on top of the water because it has a lower density.

Several studies have looked at variations in the culture process and their impact on embryo development and/or the pregnancy rate.

- Lee *et al*., (2008) and Smuts *et al*., (2008) compared incubator types.
- Higdon *et al*., (2008) compared different shelves in an incubator and determined that embryos positioned on the middle shelf for the duration of culture had a significantly greater chance of achieving a pregnancy.
- Zhang *et al*., (2010) investigated whether a reduction in the time spent out of the incubator for observation could enhance blastocyst formation rate. They found this to be true; the proportion of good blastocysts per patient were significantly lower for embryos assessed every day on days 1-6 than for embryos only assessed on days 1, 3, 5 and 6.
- Cetin *et al*., (2010) looked at impact of embryo transfer duration (measured as the length of time the embryo spent in the catheter) on clinical pregnancy rates. The clinical pregnancy rate was shown to be lower in transfers lasting longer than 1 minute when compared those taking less than 44s.
- Frydman *et al*., (2004) changed the workings of the whole IVF clinic by interspacing 6 weeks of normal work with 2 week breaks to look at quality control. Laboratory practice was scrutinized and, amongst other factors, monitoring of temperature and CO_2 was put in place and an awareness of the impact of opening an incubator door was raised. Pregnancy rates improved significantly in both IVF and intra cytoplasmic sperm injection (ICSI).

Any improvements in these studies may be attributed to a combination of factors including improved control of gas concentrations (O_2 and CO_2 (pH)) and/or of temperature.

Other studies have carried out measurements over time looking at different factors which impact on the temperatures in the dish as it is moved from an incubator onto a surface in the laboratory (Cooke *et al*., 2002; Lane *et al*. 2008). Cooke *et al*., (2002) presented data for heat loss from a dish when changing the type of heated stage, the liquid volumes within the dish and whether the lid was on or off the dish. Lane *et al*., (2008) suggested that culture dishes with flat bottoms should be used, where possible, over those without as the latter are not in contact with the heating surface thus facilitating heat loss.

The greatest temperature loss an oocyte is exposed to is as it is collected from the follicle by vacuum aspiration. Kalan *et al*., (2008) demonstrated that follicular fluid can cool up to 6.6 °C. They also showed that use of a closed, environmentally controlled chamber for handling the oocytes after aspiration failed to eliminate temperature loss though the reason is evident once the mechanism for heat loss is understood. Redding *et al*. (2006), who showed a drop in temperature of 7.7±1.3°C upon aspiration, pointed to evaporation from the collection tube as the source of the heat loss. The low pressure in the tube, required to suck the fluid, and high surface area of the drops of follicular fluid as they enter the tube promotes evaporation and thus significant heat loss (due to water's high latent heat of evaporation). This is an unfortunate start for oocytes as they enter the culture process, as exposure to such low

temperatures will disrupt an oocyte's meiotic spindle and test its ability to re-assemble (Section 2.6.2.2)

Another point in the embryo culture process at which oocytes may be cooled is during intracytoplasmic sperm injection (ICSI) when oocytes may be out of the incubator for up to 20 minutes. Wang *et al*., (2001b) demonstrated that rigorous control of temperature during ICSI procedures significantly enhanced clinical pregnancy rates by comparing the use of three heating systems; one produced a significantly higher clinical pregnancy rate than the other two. The difficulty with such a study is that the temperature of an oocyte in any one system depends on how the system was set up and calibrated. It was stated that the measured temperatures in one of the heating systems were 4 °C below the setting temperature. In practise if this was the case the temperature could be set higher.

As discussed in Sections (2.6.1) the temperature(s) at which oocytes and embryos should be kept through their different stages is open to debate. Higdon *et al*. (2008) compared the clinical pregnancy rates between two incubators (which they had showed to fluctuate by ± 0.2 °C) and attributed the difference to temperature. The incubator providing a significantly higher clinical pregnancy rate had a temperature below 37 °C approximately 50% of the time as opposed to the other incubator which has a temperature below 37 °C only 20% of the time. If indeed this difference is due to such a small change in temperature it indicates how significantly this may impact embryo viability. As with any such study the accuracy of temperature measurements may be questioned; this makes transfer of such information between laboratories

difficult. As a result of this study Higdon *et al*. (2008) changed to setting their incubators to 36.7 °C while other clinics aim for a mean of 37 °C (Wang *et al*., 2001).

Though these studies are all, in one way or another, looking at the impact of temperature control throughout the embryo culture process very few look at the processes in the thermal environment and identify factors which may impact on these or look at new ways of carrying out procedures to better utilise available equipment for thermal control.

2.6.4 Other temperature considerations

Exposing culture media to higher temperatures for longer periods may cause degradation of components of the culture media, for example of amino acids. The presence of amino acids in culture media is likely to improve *in vitro* embryo development by acting as metabolic substrates, as anabolic precursors for protein synthesis, as osmolytes, as chelators of heavy metal ions, as a buffer for pH and as regulators of metabolic function (Edwards *et al*., 1998). Amino acid requirements and their effects on embryonic development vary with species and culture conditions (Lee & Fukui, 1996).

Though amino acid addition to culture media is important for embryo development, ammonium ions (NH_4^+), a by-product of amino acid degradation, are toxic to embryos and detrimental to their survival. Exposure of embryos to ammonium can depress oxidative phosphorylation, decrease blastocyst cell number and adversely affect embryo development (Thompson *et al*, 2007).

Ammonium is broken down by embryo metabolism and also spontaneously. Lane and Gardner (1994), who first supplemented culture medium with amino acids, demonstrated that in a dose dependent fashion, ammonium reduces embryo implantation rates, retards fetal development and induces embryonic exencephaly. Bavister & Poole (2005) cultured hamster embryos in dishes either pre-equilibrated overnight for gas and temperature (at 37.5 °C) or pre-equilibrated for gas overnight at 4 °C and then equilibrated to 37 °C for two hours prior to use. They demonstrated that hamster embryo development was significantly reduced to the blastocyst stage in the dishes previously held at 37 °C overnight and suggested that this was due to the greater degradation of components in the culture media at the higher temperature.

2.7 Oxygen

The oxygen content in the environment is an important factor for oocytes and embryos. Oxygen is vital for embryos aerobic metabolism. Conversely reactive oxygen species (ROS) are formed during the intermediate steps of oxygen reduction for aerobic metabolism, among other metabolic pathways, and enzymatic production is enhanced in higher oxygen conditions (Guérin *et al*., 2001). The main ROS produced by embryos are the super oxide anion radical ($O_2^{-}\cdot$), hydrogen peroxide (H_2O_2) and the hydroxyl radical ($OH\cdot$). Higher levels of ROS lead to embryo damage through alteration of cellular macromolecules including lipids, proteins and nucleic acids (Guérin *et al*., 2001). This section will discuss information available in current literature on the *in vivo* oxygen environments and the impact of different oxygen environments on oocytes and embryos.

2.7.1 *in vivo* environment

As for temperature it is important to examine the oxygen environment an oocyte or embryo would experience *in vivo*.

It is convention in this field to define the oxygen concentration in volume percent (vol %). This means that the oxygen concentration in the solution is in equilibrium with a gas of this concentration. Typically the concentration of gases dissolved in liquid is linear (follows Henry's law) up to a point, but may reach a saturation concentration when equilibrated with gases at very high concentrations (e.g. Langmuir behaviour). At atmospheric pressure water follows Henry's law up to an oxygen concentration in gas of 100 vol. %. This convention is useful as a common unit value can be used to describe any fluid (e.g. blood, plasma, culture media) even though they have different Henry's law coefficients.

In a review covering measurement of *in vivo* oxygen content in the oviduct and uterus of mammalian species the range was presented as approximately 1 to 9 vol % (Burton *et al*., 2002); far below atmospheric oxygen concentration (~21 vol %). Oxygen concentration in the uterus has been shown to be lower than in the oviduct (rabbit, hamster and rhesus monkey). For example the oxygen concentrations in the rhesus monkey's oviduct and uterus have been measured at 8% and 2% respectively (Bavister, 2004, in summary of earlier work). In addition, oxygen levels in the uterus are dependent on the stage of the cycle and decreased oxygen in the uterus is particularly evident at the time of implantation (Harvey *et al.*, 2007).

Jana *et al.* (2010) established an upper limit of ROS in follicular fluid beyond which viable embryo formation would not be expected. For women undergoing IVF who had ROS levels below this upper limit they observed better fertilisation rates, better embryo quality and lower levels of DNA fragmentation.

2.7.2 *in vitro* environment

Multiple studies have reported the benefits of culturing human oocytes and embryos at 5 vol % oxygen instead of at atmospheric oxygen (Ciray *et al*., 2009; Jelinkova *et al*., 2004; Kim *et al*., 2005; Kovačič *et al*., 2008; Meintjes *et al*., 2000). Significant benefits included improved embryo quality, increased numbers of embryos reaching the blastocyst stage, reduced DNA fragmentation and improved pregnancy rates. For example, Kovačič *et al*., (2008) demonstrated that successful embryo development to the blastocyst stage on day 5 of culture was approximately two times more likely when culturing in 5% oxygen than in atmospheric oxygen. Similar results and benefits have been shown for porcine, bovine and rabbit embryos (Karja *et al*., 2004; Kitagawaa *et al*., 2004; Lindenau & Fischer, 1994; Takahashi *et al*., 1999).

5 vol % oxygen is a convenient value within the range of those values which have been measured *in vivo*. Whether it is ideal or not is unknown and investigation has been minimal especially with respect to the human embryo. No significant difference was seen between rabbit embryos cultured in 1% or 5% oxygen, although both showed significantly better development than in 20% oxygen (Lindenau & Fischer, 1994). Yuan *et al*., (2003), in comparing growth of bovine embryos in 2% vs. 5% oxygen, observed that the hatched blastocysts cultured in the 2% oxygen environment showed a significantly lower cell count and a slightly higher tendency for apoptotic

cells. They suggested this was a sign of oxygen deficiency. Thompson (2000) showed that the replication of the *in vivo* oxygen gradient (the decrease in concentration from the oviduct to the uterus) is beneficial to bovine embryo development as blastocyst rate and quality were enhanced when O_2 levels were decreased from 7 to 2%.

Though many studies have reported the benefits of culture in a low oxygen environment the change to 5% O_2 may only have a modest impact on the embryos potential to develop into a successful pregnancy. Several studies have shown minimal benefit of culture in a low oxygen environment. Kovačič *et al*., (2008) compared the growth of human embryos in 5% vs. 20% oxygen. They found that the ratio of successful embryo development to the optimal blastocyst stage on day 5 was approximately 2:1 (5:20%) for IVF and ICSI. This shows an improvement at the blastocyst stage when culturing in low oxygen but this study did not include the pregnancy rates. In a prospective randomized study of 712 embryo transfers Bahçeci *et al*., (2005) found no difference in the pregnancy rates after ICSI between patients whose embryo were cultured at 5% O_2 and those whose embryos were cultured at 20% O_2.

Culture in low oxygen concentrations may improve embryo quality and developmental potential through several mechanisms; by reducing ROS and therefore the extent of macromolecule damage (Karja *et al*., 2004; Kitagawaa *et al*., 2004; Takahashi *et al*., 1999) and by reducing unnecessary gene expression which occurs as a response to oxidative stress (Favetta *et al*., 2007; Correa *et al*., 2007). Applying the quiet embryo hypothesis (as discussed in Section 2.5; Leese, 2002) to this situation, the increased gene expression triggered by oxidative stress may be detrimental to the

embryo as the embryo's energy is directed towards 'damage control' and not reserved for necessary development.

2.8 pH

pH is an important environmental factor for oocytes and embryos. The pH must remain stable as intracellular processes are highly sensitive to pH variation. This section will discuss information available in current literature on the *in vivo* environment with respect to pH and the impact of pH changes on oocytes or embryos. Gaps in this knowledge will be identified.

2.8.1 *in vivo* environment

Throughout the period of pre-implantation development, the oocyte and subsequently the embryo, appear to exist in three distinctly diverse pH environments. The pH of human follicular fluid is reported to be 7.2-7.3, the pH of the oviductal fluid more alkaline (7.6-7.9), and the pH of the uterus is thought to be more acidic again than that of the oviduct (Dale *et al*., 1998).

2.8.2 The internal pH of oocytes and embryos

Intracellular pH regulation in the mammalian oocyte is of vital importance as major intracellular processes are highly sensitive to pH variation. Throughout early development of the human embryo there is no long term change in the internal pH (pH_i); it is stable at pH 7.4±0.1 (Dale *et al*., 1998). As a result of sensitivity, pH control is highly conserved between species so conclusions drawn from studies of

other mammalian species are likely to be applicable to humans. pH sensitivity throughout the pre-implantation period is also partly due to the pH dependence of sperm binding.

Cellular pH is regulated through ion exchangers on the plasma membrane. The Na^+, HCO_3^-/Cl^- and Na^+/H^+ exchangers increase pH_i and the HCO_3^-/Cl^- exchanger lowers pH_i. The mouse embryo has been shown to regulate pH_i increases via a HCO_3^-/Cl^- exchanger (Dale *et al*., 1998) and it is suggested that the human oocyte applies this same mechanism (Dale *et al*., 1998). Furthermore, it seems that the level of activation of this ion exchanger may vary with different oocytes. Activity is perhaps altered by alterations in the ionic balance, or by metabolic integrity of the oocytes (in the case of exchanger regulation by a secondary messenger system) (Dale *et al*., 1998).

Human oocytes and early pre-implantation embryos are unable to recover from acidosis, however, the plasma membrane is highly permeable to H^+ ions at this stage and therefore any pH_i drop due to metabolism may be counteracted by H^+ redistribution. This is possible as the extracellular pH is slightly more alkaline that the pH_i allowing a driving force for H^+ diffusion (Dale *et al*., 1998). The reliance on diffusion of H^+ as the regulatory mechanism for pH control is not sufficient as the presence of weak acids (such as the metabolic product lactate) has been shown to lower the pH_i and perturb the physiology of the early embryo (Edwards *et al*., 1998). Amino acids exist as zwitterions (molecules which contain both acidic and basic groups) at physiological pH. They therefore may act as buffers and their presence in culture media has been shown to counteract the negative effect of lactate (acidosis) on the cleavage embryo by buffering pH_i against acidosis (Edwards *et al*., 1998).

During passage from the oviduct to the uterus (between the morula and blastocyst stages) the embryo develops mechanisms for regulation of acidosis, presumably through expression of pumps on the plasma membrane. This prepares the human blastocyst for a more acidic environment within the uterus (Dale *et al*., 1998). Regulation of pH_i in an acidic environment has been demonstrated by the compacted mouse morula (Edwards *et al*., 1998).

2.8.3 in vitro pH

Embryos are cultured in bicarbonate buffered media. Changes in pH caused by movement to and from the incubator environment (6 vol % CO_2) for embryo manipulation have not been reported in the literature due to measurement difficulties (Fleming & Cooke, 2009).

2.9 Engineering in assisted reproductive technology (ART)

Mathematical modelling so far has had limited use in the field of assisted reproductive technology (ART). It has helped gain an understanding into processes which are otherwise difficult, or not possible, to measure. Mathematical modelling has been used to look at the supply of nutrients (including oxygen and glucose) to an oocyte through different stages of oogenesis (Section 2.2.1) *in vivo*. For example:

- Redding *et al*. (2007, 2008) used mathematical modelling to investigate oxygen concentrations in the developing ovarian follicle.
- Stokes *et al*. (2008) applied mathematical modelling to investigate the glucose concentration through a cumulus-oocyte complex (COC) to investigate glucose supply to the oocyte.

The application of mathematical modelling to the embryo culture process is potentially highly beneficial. It provides a possible means to overcome measurement difficulties, to enable characterisation of the physical environment around an embryo throughout the embryo culture process. It provides a tool to predict how a change to the process impacts on an embryo's environment. This in turn may ease process change and development and enable optimisation.

2.10 Summary

As opposed to the targeted static nature of a Petri dish, the *in vivo* environment is dynamic, with controlled transport of the embryo down the oviduct to the uterus and continual provision of required metabolites and other environmental factors. The *in vivo* environment provides the best basis for ideal culture conditions, however, due to measurement difficulties the exact nature of the *in vivo* environment is unknown.

In vitro studies have identified environmental factors which are important to the successful development of embryos. These include energy substrates (simple sugars and amino acids), oxygen tension, temperature and pH.

A gap in the literature exists in terms of the quantification and understanding of the changing physical environment (temperature, O_2 and pH) an embryo experiences throughout *in vitro* culture, predominantly due to measurement difficulties. While it is accepted that changes in these parameters are important, it is not possible from the literature to prescribe tolerances of how much or for how long these factors can be varied. Generally accepted limits to these physical environments, which embryology laboratories strive to remain within, will be defined in Process Characterisation

(Section 3.6). Mathematical modelling of changes in these variables based on underlying heat and mass transfer principles may provide useful information for future improvement of the IVF process.

3 IVF Process Characterisation Overview

To decide how to utilise engineering tools, such as mathematical modelling, to increase knowledge of the embryo culture process it is first necessary to define the embryo culture process. The culture process was characterised with a focus on steps and conditions which may impact the temperatures or the culture media composition (O_2 and CO_2, thus pH) to which embryos are exposed to.

3.1 Methodology

Fertility Associates New Zealand uses open embryo culture in their three laboratories, where embryo handling takes place outside of the incubator environment. Their process was used as the model process for this research. The process used at Fertility Associates New Zealand is in line with guidelines laid out by the European Society of Human Reproduction and Embryology (ESHRE) (Magli *et al*., 2008) and those laid out by the Practice Committee of the American Society for Reproductive Medicine (ARSM) and the Practice Committee of the Society for Assisted Reproductive Technology (2008).

Process characterisation took approximately two months of observation in Fertility Associates Auckland's embryo laboratory. The goals were to define the steps in the process, to gain an understanding of the extent and sources of process variability and to gain an understanding of the way in which the process had evolved. Information was collected through observation of day to day activity in the laboratory. Twelve full or part time embryologists in the laboratory were shadowed and interviewed. Video was taken of procedures to help identify steps which occur in quick succession.

3.2 The Embryo Culture Process

The primary purpose of the embryo culture process is to 'grow up' embryos to be transferred into the patient and give rise to a pregnancy. It is rarely now that more than one embryo is transferred as this increases the probability of having a multiple pregnancy which increases the risks associated with a pregnancy. Therefore, an important part of this process involves the selection of the most viable embryo for transfer through the use of checks to visually assess their development.

Figure 3.1 displays a block diagram of the major stages in the embryo culture process. Tasks in the process can be divided into three categories. These are essential tasks (egg collection and insemination for example), tasks which ensure best development of the embryos (such as incubation or changing the media type sequentially to support different stages of development) or tasks which involve scoring the embryos (by comparing their morphological characteristics with the 'ideal' expected for each stage of development) to provide a means to select the best embryo for transfer (these stages are referred to as 'checks'). Each stage of the process will be described in detail in this section.

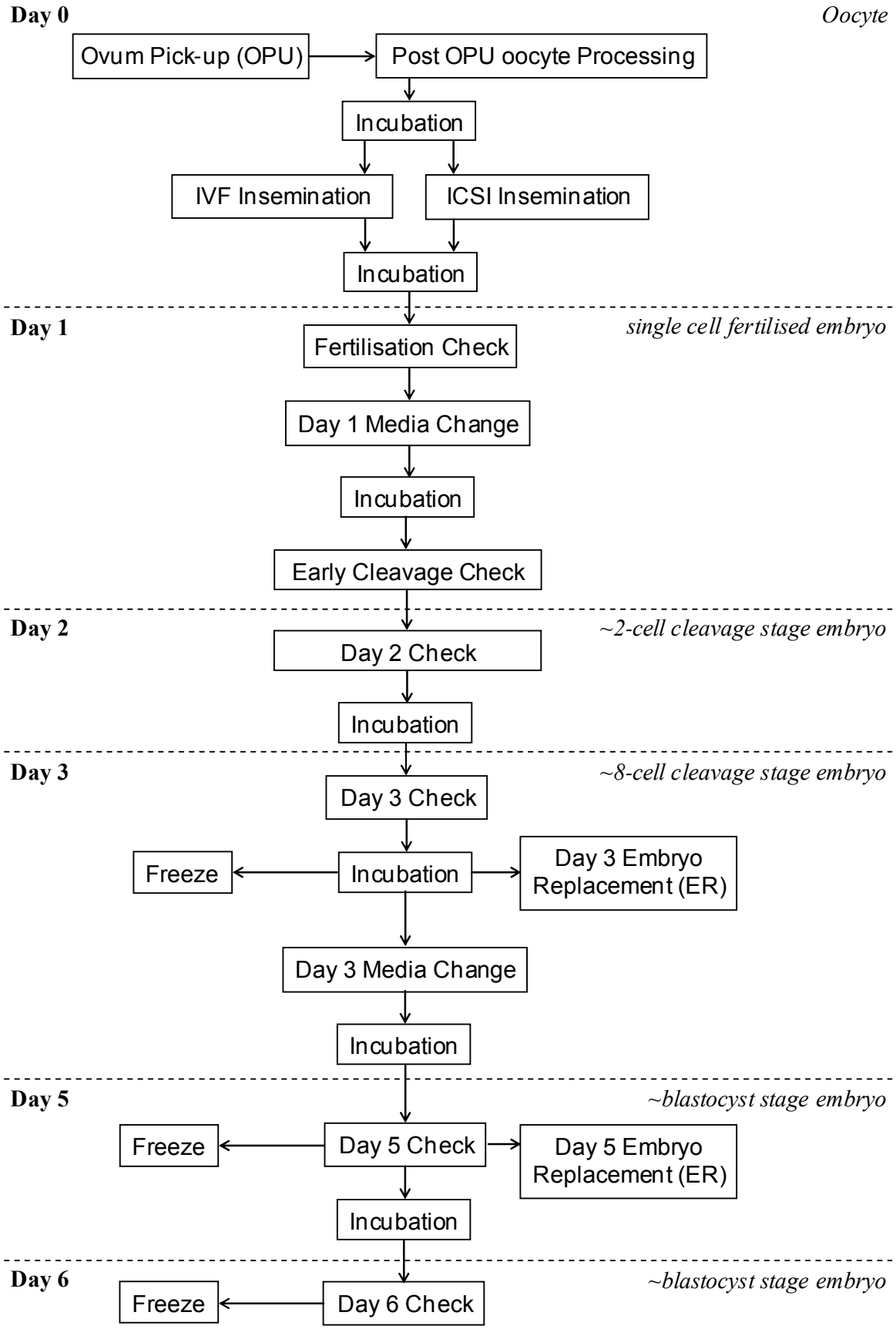

Figure 3.1: Stages of the embryo culture process

3.2.1 Ovum pick up (OPU) (hour 0)

The ovum pick-up (OPU, or egg collection) is the step in which the oocyte is removed from the woman's ovary and enters the process of *in vitro* culture. The following numbering refers to Figure 3.2 below. At the start of the procedure the oocyte is in the ovary surrounded by a large fluid filled antrum which is situated in its Graafian follicle. Homeostasis maintains the physical environment including regulation of temperature and oxygen tension. A needle, guided by ultrasound visualisation, is used to pierce the vaginal wall and enter the follicle. The follicular fluid and cumulus-oocyte complex are aspirated (**1**) (by means of a vacuum) through the needle, through the tubing and into ~2 ml of warmed medium in a test tube held in a heated block (**2**). Usually multiple follicles are aspirated in succession so multiple oocytes may be aspirated into each test tube. The follicle and tubing may be flushed with warm (37 °C) culture medium to help ensure the oocyte(s) is removed. When a suitable volume of fluid fills the test-tube, it is disconnected from the vacuum tubing and transferred to another hot block next to the embryologist (**3**).

Redding *et al*. (2006) identified evaporation as the cause of massive heat losses at egg collection. Under vacuum the follicular fluid, containing the oocyte(s), falls in drops into the test tube from the tubing. The low pressure and the large surface area to volume ratio of the drop promote significant evaporation which cools the follicular fluid, initially at 37 °C in the body, to less than 33 °C. The pre-warmed test tube and culture medium minimises exposure of any aspirated oocytes to low temperatures as the drops will rapidly heat up again when they reach the fluid in the bottom of the tube.

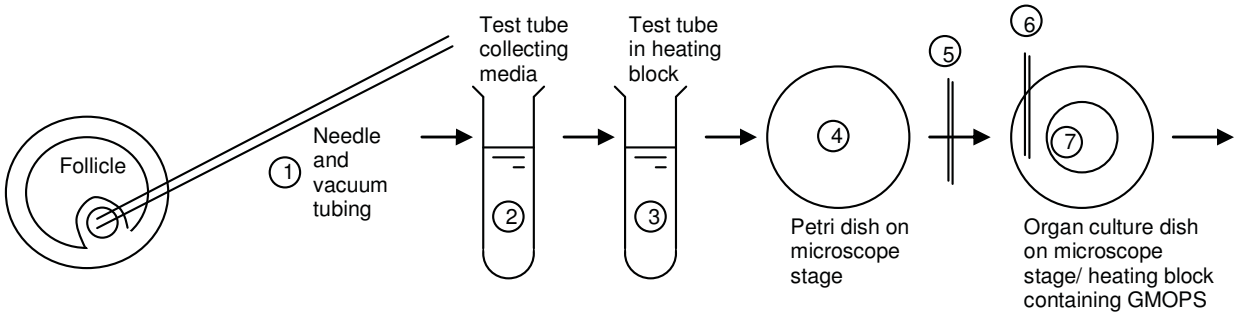

Figure 3.2: The steps involved in ovum pick-up (OPU).

The embryologist removes the test-tube and transfers the contents into one, or several, small Petri-dishes on a microscope stage (**4**). Throughout the culture process all microscope stages are heated in order to maintain the temperature of oocytes and embryos close to 37°C. Under the microscope, the dish is searched for oocytes which are collected into a pipette and transferred to the moat of an organ culture dish (**5**) containing a self-buffered culture medium. All dishes contain G-MOPS^{TM} (The G5 Series, Vitrolife Sweden AB, Kungsbacka, Sweden), a 3-(N-morpholino)propanesulfonic acid (MOPS) buffered culture medium, and have been pre-equilibrated to 37 °C in an incubator prior to use. In order to remove blood, follicular fluid and excess cumulus cells, the oocyte is washed (**6**) and then transferred into the central well (**7**). Washing the oocyte involves lifting up and expelling the oocyte, or embryo in later steps, from the pipette several times (which may vary approximately between 2 and 20 times due to process variation, discussed in Section 3.4). A lid is placed onto the dish which is then transferred onto a coin (aluminium disc) on a heating block. This single dish is used to collect all oocytes collected during the OPU. Therefore, for every oocyte found subsequently, the dish will be returned to the microscope stage, its lid removed, then replaced and the dish returned to the heating block.

There is potential for changes in temperatures and gas concentrations. Temperatures will likely change when;

- the test tube contents are transferred into a dish
- an oocyte is lifted into a pipette, since the thermal mass of the small pipette system is low and therefore rapid heat loss may be expected
- a dish is moved through the cooler laboratory air
- a dish is placed onto an aluminium coin as this will replace the air gap beneath the dish with metal enabling faster heat transfer to the dish

While the MOPS buffered medium has been pre-equilibrated in 5 vol % oxygen this is not maintained out of the incubator and therefore some change in oxygen concentrations in the droplet is expected

3.2.2 Oocyte Processing Post OPU

The following numbering refers to Figure 3.3. The dish carrying the oocytes is transferred back to the microscope stage and the lid is removed. The oocytes are transferred by pipette into the central well of an organ culture dish (**1**) also containing the self-buffered medium. The oocytes are washed in a pipette (as described above in Section 3.2.1) (**2**) before transfer to the centre of another organ culture dish, this one containing G-IVF (G-IVF, The G5 Series, Vitrolife Sweden AB, Kungsbacka, Sweden), the fertilisation medium (**3**). This is the first dish containing a bicarbonate buffered medium. At equilibrium, the pH of such media is dependent on the surrounding concentration of CO_2 so dishes are pre-equilibrated in an incubator with 6 vol % CO_2.

Throughout the culture process culture media is covered with a layer of paraffin oil (OVOIL, Vitrolife Sweden AB, Kungsbacka, Sweden) as this prevents loss of water

through evaporation thus preventing concentrating the culture media) and is thought to slow the loss of CO_2 from the media to the air. Despite the presence of paraffin oil, some change in pH due to loss of CO_2 is likely.

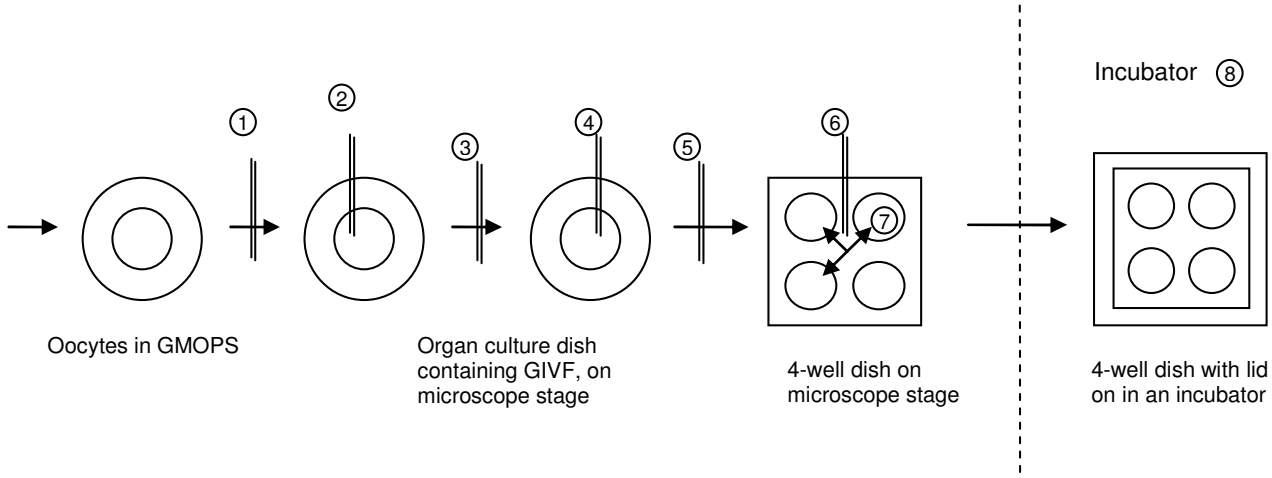

Figure 3.3: The steps involved in post ovum pick-up (OPU) processing.

The oocytes are washed in a pipette (**4**) before transfer to the centre of a 4-well dish (**5**) where another wash takes place (**6**). Each oocyte is then placed into one of the four wells (**7**). Each well contains 0.5 ml of G-IVF culture medium overlaid with 0.3 ml of Paraffin oil. A lid is placed on the 4-well dish which is transferred into the incubator (**8**). Changes in temperature are expected with transfer of the dish through the air and lifting the embryos in a pipette. Changes in O_2 and CO_2 are likely while the dish is in the atmospheric environment.

3.2.3 Insemination (IVF) (hour 4-6)

The following procedure is used if the oocyte is to be inseminated by conventional IVF. This usually takes place if sperm is available in sufficient numbers and quality. The 4-well dish containing the oocyte(s) is removed from the incubator and placed onto a microscope stage, the lid is removed and a preparation of sperm, pre-equilibrated to 37 °C, is pipetted into each oocyte-containing well. The preparation of

sperm is approximately 5-10 µl which is a 100th to a 50th of the volume of medium in each well (0.5 ml) and therefore if it cools during transfer in a pipette it will be unlikely to impact on the temperatures or gaseous concentrations within the dish. The lid is then replaced and the dish is returned to the incubator; the oocytes and sperm cultured together.

3.2.4 Insemination (ICSI) (hour 4-6)

Intracytoplasmic sperm injection (ICSI) is a procedure involving the injection of a single sperm directly into the oocyte. It is frequently used as an alternative to standard IVF in the treatment of male infertility when sperm numbers and/or quality are poor. The following numbering refers to Figure 3.4.

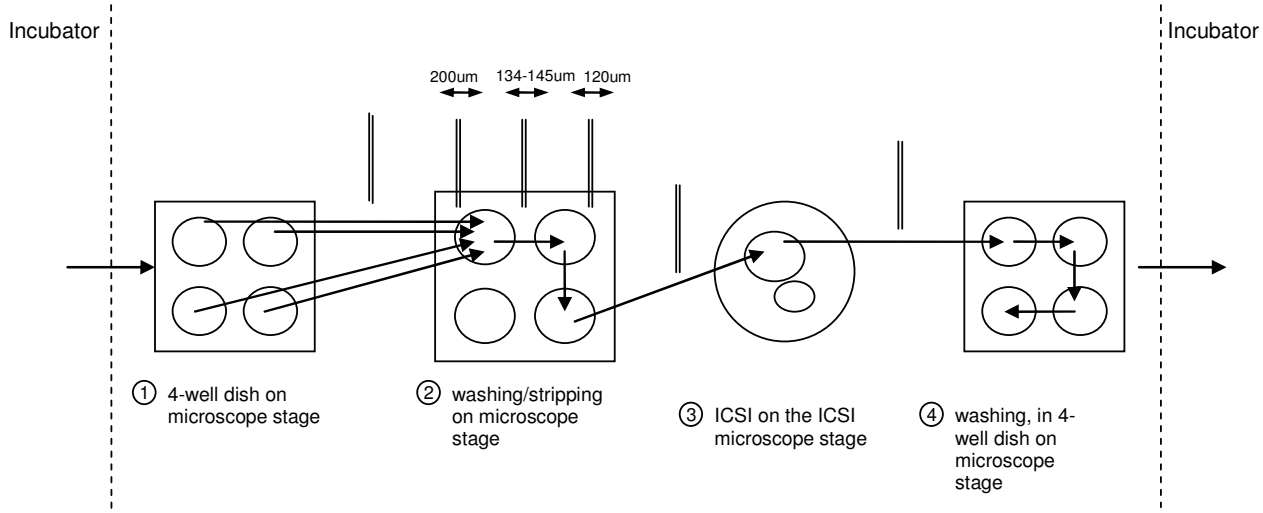

Figure 3.4: The steps involved in insemination by intracytoplasmic sperm injection (ICSI).

The first step required for ICSI is the removal of the cumulus cells from around the oocyte. This is known as denuding or stripping. Denuding provides the injection needle direct access to the oocyte and prevents cellular material from these cells entering the oocyte with injection of the sperm. The 4-well dish containing the

oocyte(s) is removed from the incubator and placed onto a microscope stage (**1**). The oocytes are transferred into well 1 of another 4-well dish. They are washed in wells 1, 2 and 3 of this dish and the internal diameter of the pipette used is decreased for each wash (**2**). Well 1 in the stripping process contains hyaluronidase, an enzyme which breaks down the hyaluronan molecules forming part of the matrix connecting the cumulus cells, to aid denuding. The final pipette has an internal diameter approximately the same as that of the oocyte (~120μm) and thus removes all cumulus cells which may remain attached.

If more than 5 or 6 oocytes are suitable for ICSI, the denuding step (described above) would be carried out before preparation of the ICSI microscope, and the 4-well dish is returned to the incubator for this time. ICSI would then be carried out with batches of oocytes to limit the time an oocyte spends out of the incubator.

For fewer than 5 or 6 oocytes, immediately after stripping, the lid is returned to the 4-well dish and a separate dish for ICSI is prepared on the microscope stage. The stripped oocytes are transferred to their droplet in the ICSI dish, the lid placed onto this dish, and the dish lifted across the lab and placed onto the ICSI microscope stage.

ICSI (**3**) is then carried out. For every oocyte a single sperm has its tail broken, using micromanipulation techniques on the ICSI microscope, to induce reactions which would normally occur with sperm penetration of the oocyte. The sperm is then injected into an oocyte. Though 20 minutes may be suggested as a maximum for a five or six oocyte ICSI, the total time this process takes is highly variable (5 minutes to several hours), and depends on the embryologist, the quality of sperm and oocytes,

and very much upon the oocyte number. Upon completion the lid is returned to the dish which is moved back across the lab to the microscope stage.

All ICSI fertilised oocytes are transferred by pipette into well 1 of a new 4-well dish (**4**). They are then washed around wells 1-3 and placed in well 4 for continued culture. With more oocytes only wells 1 and 2 are used for washing, the oocytes are kept in groups in wells 3 and 4. The lid is placed onto this 4-well dish and the dish is transferred to the incubator.

3.2.5 Fertilisation Check (~ hour 18)

The following discussion refers to numbering in Figure 3.5 below. The dish containing the embryos to be checked is removed from the incubator and placed on a microscope stage. Embryos fertilised by ICSI are transferred straight from well 4 (or from wells 3 and 4) of the 4-well dish into well 1 of another 4-well dish (**2**). Embryos fertilised by IVF are firstly washed in well 4 of the 4-well dish (**1**) in which they were fertilised, in order to remove any cumulus cells or sperm still attached, and then transferred into well 1 of another 4-well dish.

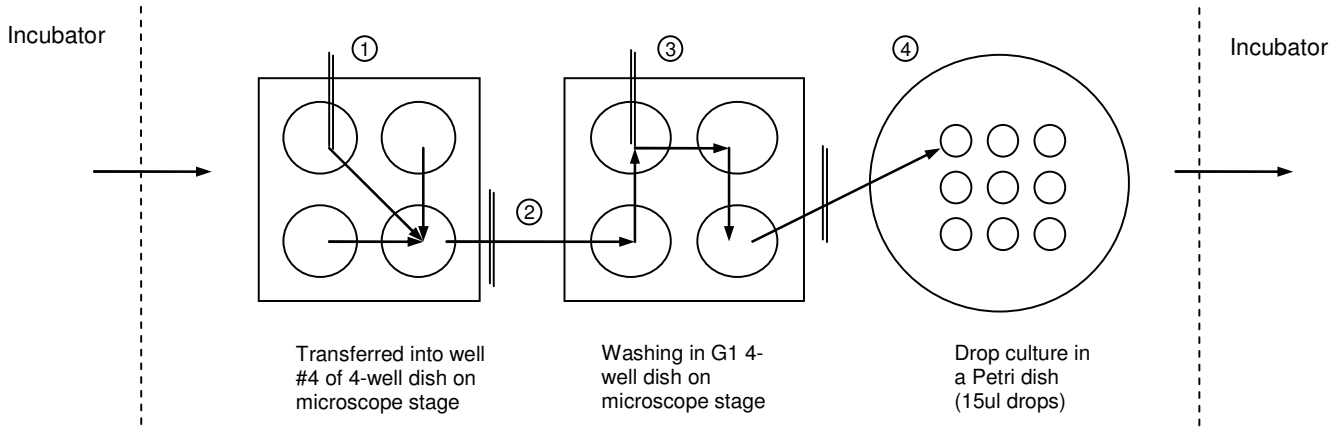

Figure 3.5: The steps involved in a fertilisation check.

The embryos are washed through each well of this 4-well dish (**3**) which contains the G-1 culture medium used for day 1-3 culture (G-1^{TM}, The G5 Series, Vitrolife

Sweden AB, Kungsbacka, Sweden), a bicarbonate buffered medium. They are transferred by pipette (**4**) from well 4 of the 4-well dish into individual 15 µl droplets (of G-1) under oil. There is a maximum of 10 droplets per dish. The dish is then transferred into an incubator. It is important to keep embryos separate so that individuals are identifiable for scoring; therefore only 4 embryos may be in the wash dish at one time (one in each well).

3.2.6 Early Cleavage Check (~hour 25)

The dish containing the embryos is removed from the incubator and placed on a heated microscope stage. The embryos are checked and scored based on their morphology. Ideally at the early cleavage check the embryo has divided into two cells. In addition to cell number, the presence or absence of features including uniform cell size and cellular fragmentation are taken into account with the scoring. The lid remains on the dish throughout the check. On occasion the lid may be removed, for example to discard a 3PN embryo (embryos in which 3 pro-nuclei are visible indicating an incorrect chromosome complement). After the check the dish is the returned to the incubator.

The time required for a check is dependent on the number of embryos, the number of embryos to be discarded and the presence of any abnormal features. It would not often exceed five minutes.

3.2.7 Day 2 Check (hour 43 is desirable – usually 42-45)

The embryos are checked and scored based on their morphology. Ideally an embryo is at the 4 cell stage on day two. The dish containing the embryos is removed from the

incubator and placed on a heated microscope stage. The lid remains on the dish throughout the check. After the check the dish is then returned to the incubator. The expected time frame is similar to that for the early cleavage check (Section 3.2.6).

3.2.8 Day 3 Check (hour 65-70)

The embryos are checked and scored based on their morphology. Ideally an embryo is at the 8 cell stage on day 3. The decision to replace an embryo on day 3, to continue culture until day 5 and/or to freeze embryos is made at this check and, if there is to be a day 3 replacement, an embryo (or two) is chosen. The dish containing the embryos is removed from the incubator and placed on a microscope stage. The lid remains on the dish throughout the check unless embryos are discarded. After the check the dish is returned to the incubator. The expected time frame is similar to that for the early cleavage check (Section 3.2.6) and the day 2 check (Section 3.2.7).

3.2.9 Day 3 Embryo Replacement (ER) (hours 65-70) and Media Change

The embryo replacement (ER) is the transfer of an embryo back into the mother's uterus. The ER may take place on day 3 or day 5 depending on many factors which include the number of embryos in culture and the ease of best embryo selection at this time. The following discussion refers to numbering shown in Figure 3.6.

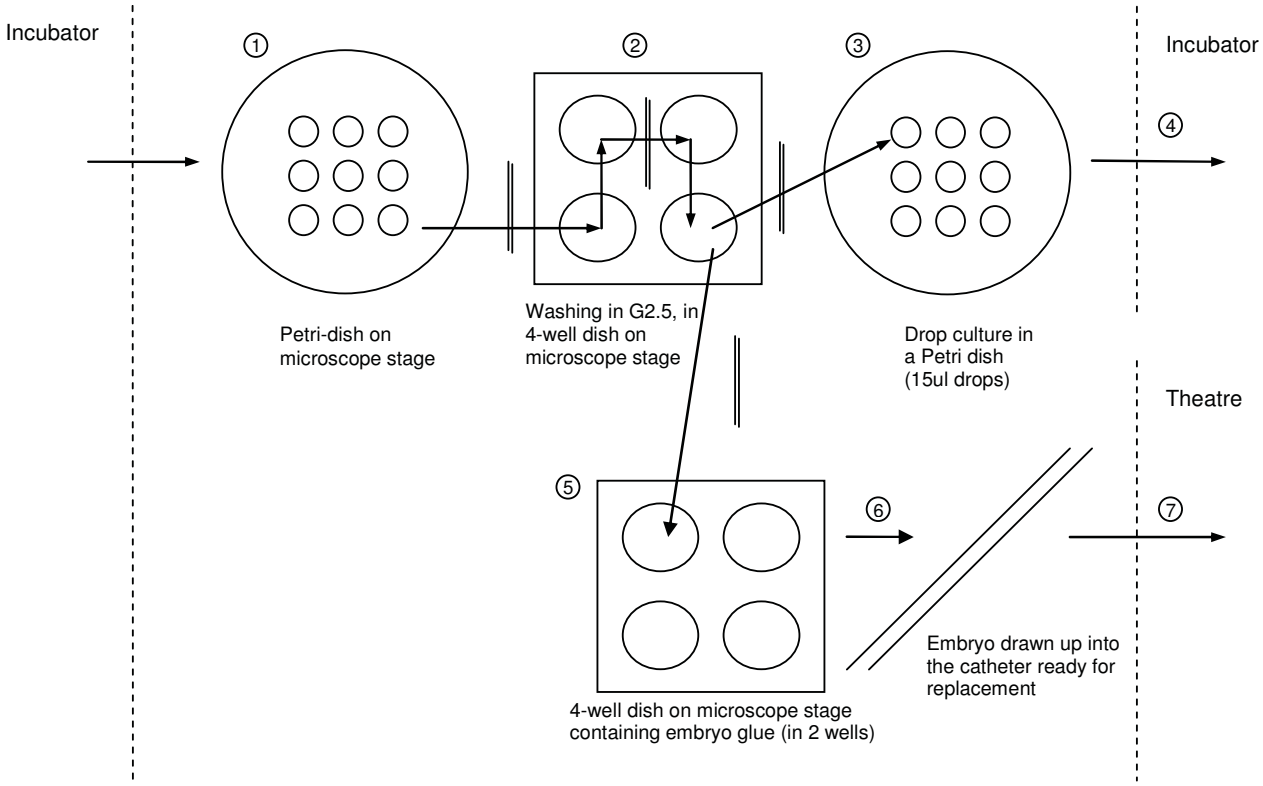

Figure 3.6: The steps involved in an embryo replacement.

The dish containing the embryos is removed from the incubator and placed on a heated microscope stage (**1**). The lid is removed from the dish and the embryo of choice is washed through each well of a 4-well dish (**2**) and subsequently transferred into a well of a 4-well dish containing embryo glue (a culture media designed for embryo transfer) (**5**).

The 4-well dish containing the chosen embryo (**5**) also contains embryo glue in a separate well and G-1 medium in the central moat for flushing the catheter. Depending on timing, the 4-well culture dish may be transferred to the incubator, to be removed just prior to replacement. At the time of replacement, the embryo is loaded into a catheter (**6**). The catheter is transferred through to the doctor in theatre (**7**).

The day 3 media change for embryos remaining in culture may be carried out at the same time as the preparation for the embryo replacement or later in the day. For

embryos that are not replaced on day 3, embryo culture continues. The dish containing the embryos is removed from the incubator and placed on a microscope stage. The lid is removed from the dish and the embryo(s) are individually washed through each well of a 4-well dish (**2**) which contains G-2 culture medium used for day 3-5 culture (G-2^{TM}, The G5 Series, Vitrolife Sweden AB, Kungsbacka, Sweden), a bicarbonate buffered medium. They are then transferred by pipette (**3**) from well 4 of the 4-well dish into individual 15 µl droplets (of G-2 medium) under oil. This dish is then transferred into an incubator (**4**).

3.2.10 Day 5 Check

The embryos are checked and scored based on their morphology. Ideally embryos are at the early blastocyst stage on day 5. The decision to transfer an embryo on day 5 or to continue culture through until day 6 is made at this check. If there is to be a day 5 replacement an embryo is chosen. The dish containing the embryos is removed from the incubator and placed on a microscope stage. The lid remains on the dish throughout the check unless embryos are discarded. The dish is returned to the incubator. The expected time frame is similar to that for the early cleavage check (Section 3.2.6), the day 2 check (Section 3.2.7) and the day 3 check (Section 3.2.8).

3.2.11 Day 5 ER and Day 5 Media change

The day 5 media change and ER procedure is identical to the process for day 3 (Section 3.2.9), all that differs is that the embryos are at a different stage of development. They should be blastocysts by day 5.

3.2.12 Day 6 Check

Any embryos not replaced or ready to freeze on day 5 are left in the incubator overnight and a decision is made whether to discard or freeze them on day 6. The dish containing the embryos is removed from the incubator and placed on a microscope stage. The lid remains on the dish throughout the check unless embryos are discarded. After the check the dish is returned to the incubator.

3.3 Process Simplification

Characterisation of the embryo culture process in addition to the review of the current literature highlighted three factors in an embryo's environment which are a) important to embryo development and b) affected by steps in the culture process. These factors are temperature, CO_2 concentration (pH), and O_2 concentration.

The purpose of this section is to define the steps in the process which may be modelled. This will identify the number of models required to represent the system. To aid transformation of the process into a series of models, the geometries (the form of embryo containment) and the various boundary conditions (the processes/conditions at the boundary of the model(s)) are described in more detail.

3.3.1 Geometries

Defining the structure within which oocytes and embryos are contained is vital for understanding the environment to which they are exposed. These structures are limited to pipettes, dishes, test tubes and catheters. Figure 3.7 displays the major geometries in which embryos are contained throughout the culture process.

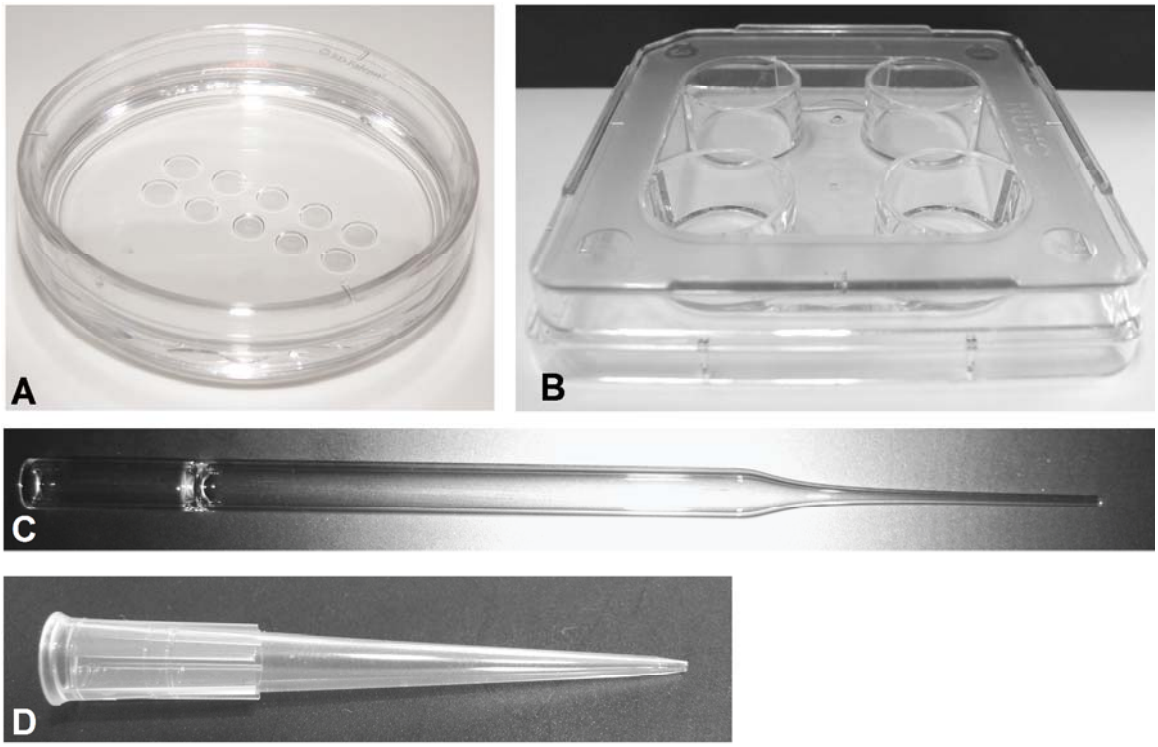

Figure 3.7: Structures which hold embryos throughout the embryo culture process. A) A Petri dish (BD Falcon, BD Biosciences, NJ USA) containing 10 media drops overlaid by paraffin oil. B) A 4-well dish (NUNC brand, Thermo Fisher Scientific Inc., MA USA) C) A glass pipette (VOLAC® Disposable Pasteur Pipettes, Poulten & Graf Ltd, Barking, England). D) A plastic pipette tip (Axygen Inc, CA USA).

Embryos spend the majority of their time throughout the culture process in drop culture within a Petri dish (**A**). Oocytes briefly pass through organ culture dishes at OPU. For initial culture (including insemination) oocytes and embryos are situated in a well of a 4-well dish (**B**) and 4-well dishes are utilised for tasks including media changes and preparation for embryo replacements.

Oocytes are aspirated into test tubes at OPU. A pipette is used any time oocytes or embryos are transferred between dishes and for numerous washing stages carried out during the process. The choice of pipette type is dependent on the task and on personal preference of the embryologist. Glass pipettes (Figure 3.7**C**) may be used as they are, or they may, be pulled. A pulled (fine drawn) glass pipette is a standard

('unpulled') glass Pasteur pipette which has been softened in a hot flame and pulled quickly to thin the barrel. The diameter of a pulled pipette will vary but, for example, the total diameter may decrease from ~0.9 mm to ~0.2 mm when a pipette is pulled. Plastic pipettes are also used (Figure 3.7**D**). A catheter carries the embryo(s) for replacement.

Seven different model geometries are required to represent the entire process. These are the Petri dish, organ culture dish, 4-well dish, test tube, glass pipette, plastic pipette and catheter.

3.3.2 Boundary conditions

The seven geometries described above are exposed to the environment(s) within the laboratory. Figure 3.8 displays some of the equipment which provides the various environments surrounding the embryos.

3.3.2.1 Incubators

For the majority of the culture process, dishes are kept in an incubator. The majority of incubators conform to two types, each of which may utilise different ways of controlling temperature and gas composition.

(i) Open volume incubators (Figure 3.8B), which typically range from 50-250 litres, maintain a large cavity at the required temperature, humidity and gas concentrations. Culture vessels, such as Petri dishes, sit on perforated metal trays within the incubation chamber. Normally larger volume incubators will have several trays stacked vertically to maximise utilisable space. Temperature within the chamber is

maintained by convection from heating elements within the chamber floor, walls and door. Many contain fans, not to provide air flow within the chamber, but to thoroughly mix gases within the vicinity of gas sampling ports.

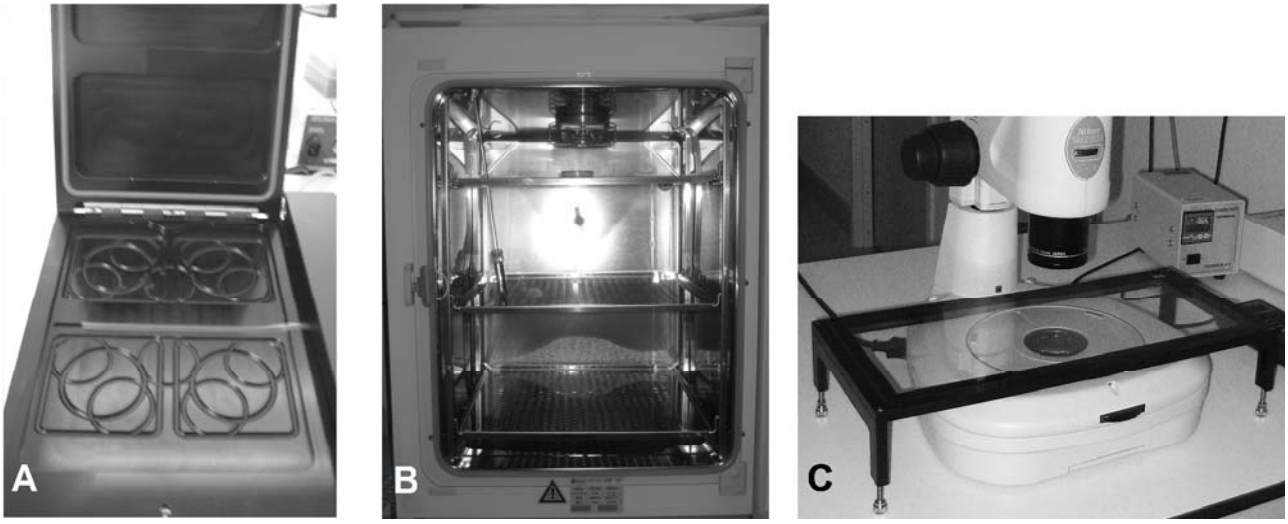

Figure 3.8: Boundary Conditions for dish systems in an embryo laboratory. A) One of the two chambers of the MINC Benchtop Incubator (Cook Medical, Cook Group Inc., IN USA) incubator which may hold four dishes. B) An open volume SANYO incubator (SANYO Biomedical, IL USA). C) A glass heated microscope stage (Thermoplate, Tokai Hit, Japan).

Open volume incubators control gas composition by injecting pure gas directly into the chamber. The gas is mixed with the existing incubator atmosphere and samples of the gas pass over feedback sensors. Injection of the pure gas will continue until the required concentration has been achieved. The minimum requirement of any incubator is to maintain a concentration of CO_2 higher than atmospheric levels by injecting pure $CO_{2.}$ A concentration of 5-6% is required in the chamber to maintain the correct pH within a bicarbonate buffered culture medium. Other incubators are also capable of maintaining a chamber with a low oxygen atmosphere. In such incubators, the O_2 level is lowered by displacing atmospheric air within the chamber with pure $N_{2.}$ Absolute levels will vary between laboratories.

(ii) The second type of incubator, the MINC (Figure 3.8A), has very low internal volume. The culture vessels sit directly on a heated plate, and are covered by a heated lid. A pre-mix of humidified gas (at appropriate CO_2 and O_2 concentrations) is either perfused through the chamber, or may purge and soak the chamber.

3.3.2.2 Laboratory temperature

The ambient laboratory air surrounds all geometry systems at some stage throughout the process and is invariably cooler (typically 23-27 °C) than the generally targeted embryo temperature of 37 °C. Optimally, laboratories would be maintained at a constant temperature allowing accurate calibration of equipment while trying to maintain a balance between minimising temperature fluctuations (for embryos while they are out of the incubator) and maintaining a comfortable working environment. Culture critical gasses such as CO_2 and O_2 are sub-optimal at atmospheric concentrations. Air flow is likely to be minimal in a lab environment but it is worth noting the position of equipment – such as a heated stage – with respect to any air conditioning unit as increased air flow will affect both heat and gaseous mass transfer.

3.3.2.3 Heated surfaces

Dishes are removed from the incubator for embryo manipulation and observation under the microscope. Heated stages provide the base boundary of dishes outside an incubator. There are many types of heated microscope stages available (different materials and makes). Two main types of heated stage are used at Fertility Associates Auckland and they provide significantly different boundaries. With the first, a metal heating plate provides a heated surface. The advantage of metal is that the rate of heat transfer within the metal itself is high and so the temperature throughout the body of

the stage will remain fairly uniform. The disadvantage is that metals are opaque and as embryo observations require transmitted light, a transparent aperture must be provided. The aperture may be a physical space or be filled with a transparent material such as plastic or glass. The rate of heat transfer within either material is significantly reduced in comparison to the surrounding metal which increases the difficulty of maintaining a uniform temperature across the entire working area. In contrast, glass heated stages (Figure 3.8**C**) are transparent so the entire surface is homogenous. However, the properties of glass do not facilitate heat transfer as fast as in metal, so a localized heat loss / gain will not be as quickly dispersed across the stage, slowing any response by the temperature controller.

Heating blocks are used to hold test tubes and for temporary placement of dishes. These are deep metal blocks held within a heated channel and provide a uniformly heated surface. Test tubes sit within cylindrical cut outs of the heating block; these holders are dry so air gaps exist between the test tube and the wall. Depending on the make of heating block and the volume of test tube, a proportion of the test tube will stand proud of the top surface of the block. Thermocoins (aluminium disks) sit under dishes on the heating block replacing the air gap beneath the dish and therefore provide direct contact between the heated surface and the dish floor.

The way in which the temperatures of heated microscope stages or heated blocks are set is laboratory dependent. Several methods used are listed here:

- setting the temperature of the control system for the heated microscope stage to read 37 °C

- by placing a thermistor (or other temperature measuring device) onto the surface of a stage, and adjusting the set point of the control system to read either 37 °C or another value which has proved, by trial and error to give better pregnancy rates
- by placing a thermistor (or other temperature measuring device) into a dish (with its lid on and with or without liquid in it) on the surface of a stage, and adjusting the set point of the control system to read either 37 °C (or another value which has proved, by trial and error, to give better pregnancy rates) at steady state.

3.4 Process variation

The evolution of the embryo culture process was discussed in Section 2.4.1. Due to the delicate nature of the human embryo, assisted reproduction is a very conservative field and changes are difficult to implement. Changes may be implemented without scientifically sound evidence (Vajta *et al*., 2010), likely due to the inability to use human embryos for research, and beneficial technology may be avoided for years simply due to superstition or coincidental mishap occurring when it was first introduced.

The culture process described in this Chapter is an example of the process an embryo may go through in the laboratory at Fertility Associates Auckland. The process varies between laboratories due to multiple factors including differing views of those running laboratories, differing size and layout of laboratories and differing equipment choices and settings used within the laboratories. This is the environment within which embryologists work. Embryology is a specialised branch of laboratory science

which, for the most part is learnt on the job though within the last 10 years masters courses have become available at several universities worldwide.

The process within a single laboratory will also vary. The main source of this variability is the embryologist. Individual embryologists have their own way of performing different procedures which have evolved during their careers. They will have been influenced by the views and practises of the clinics they have worked in, the embryologists they have been taught by, or worked with, and will have further been shaped by experiences they have had or observed, both successes and failures. They therefore all have their own ideas as to what is important to the embryos and what is not. These influences affect the exact procedures they use, the care with which they perform a task and the time they take to complete a task. External factors such as how busy the laboratory is and interruptions to an embryologist's work by other staff members also have an impact. The environmental changes experienced by two individual embryos going through the same laboratory will therefore differ and it is likely that neither will experience the best the process has to offer. Embryologists have the ability to optimise the environment an embryo is exposed to throughout the culture process if changes to the process for optimisation are well defined and will more likely carry out changes if the reasoning for them is well explained and understood.

3.5 Approach to the modelling

A goal throughout an open embryo culture process is to minimise changes to the embryos environment (temperature, oxygen and pH) during the short periods embryos

are removed from the incubators for observation and manipulation. Therefore modelling will be applied to identifying factors which may minimise these changes.

Section 3.4 showed there was a high degree of variation within the embryo culture process. It would be interesting to define the temperature-time profile of specific embryos as they go through the culture process. A full characterisation of this variation would be useful and would be a useful exercise for individual clinics to carry out. In order to gain information which may be transferrable within and between laboratories, modelling will be used to identify the factors that impact on changes in the embryo environment for each step of the process. With this knowledge clinics could identify strategies to reduce variation and develop better protocols.

3.6 Commonly accepted limits to an embryo's physical environment

It is not possible from the literature to prescribe tolerances of how much or for how long an embryo's temperature, oxygen and pH can be varied. Generally accepted limits to these physical environments, which embryology laboratories strive to remain within, will be defined here to provide a basis upon which to evaluate the outcomes of the modelling work.

In laboratories it is considered, by embryologists, to be desirable to keep embryos close to 37 °C and within a range of 36 - 37.1 °C. As it is known that embryo temperature is not maintained within this range during observation and manipulation, the outer limits acceptable for brief exposure are arbitrarily defined to be 33-37.5 °C, although 34 °C is sometimes interchanged with 33 °C as the desired lower limit.

Since embryo's can survive in an atmospheric oxygen environment, limits to the oxygen environment embryos are exposed to during manipulation are not considered by embryologists beyond ensuring the incubator environment is at 5%. Conversely the pH is an important environmental factor to an embryo. The G5 series Vitrolife culture media specifies that the pH of the culture media under a 6% CO_2 atmosphere is 7.27±0.07. The pH of the media will increase, become more alkaline, with removal into the ambient laboratory environment for embryo observation and manipulation as CO_2 diffuses out of the dish contents. The CO_2 environment will not, unless accidentally, be increased above 6%. Therefore only an upper level of pH is defined. Though rarely measured in a laboratory, a pH of 7.4 is commonly considered by embryologists to be the desired upper limit of pH.

3.7 Process Flow Diagram

The process flow diagram shown in Figure 3.10 displays an example of the embryo culture process as a sequence of steps. The legend for this flow diagram is displayed in Figure 3.9. Each step may be represented by a single model simulation. Consecutive steps differ in geometry and/or boundary conditions, with initial conditions being carried over from the final state of the previous step. To break up the process the steps are grouped into stages. Each stage of the process is a major task such as the ovarian pick-up, the early cleavage check, or a media change. Table 3.1 defines the environments (which are the boundary conditions to the model geometries) and assigns a code to each. Table 3.2 defines the geometry and identifies the environment surrounding the geometry for every step in the process as numbered in the process flow diagram (Figure 3.10).

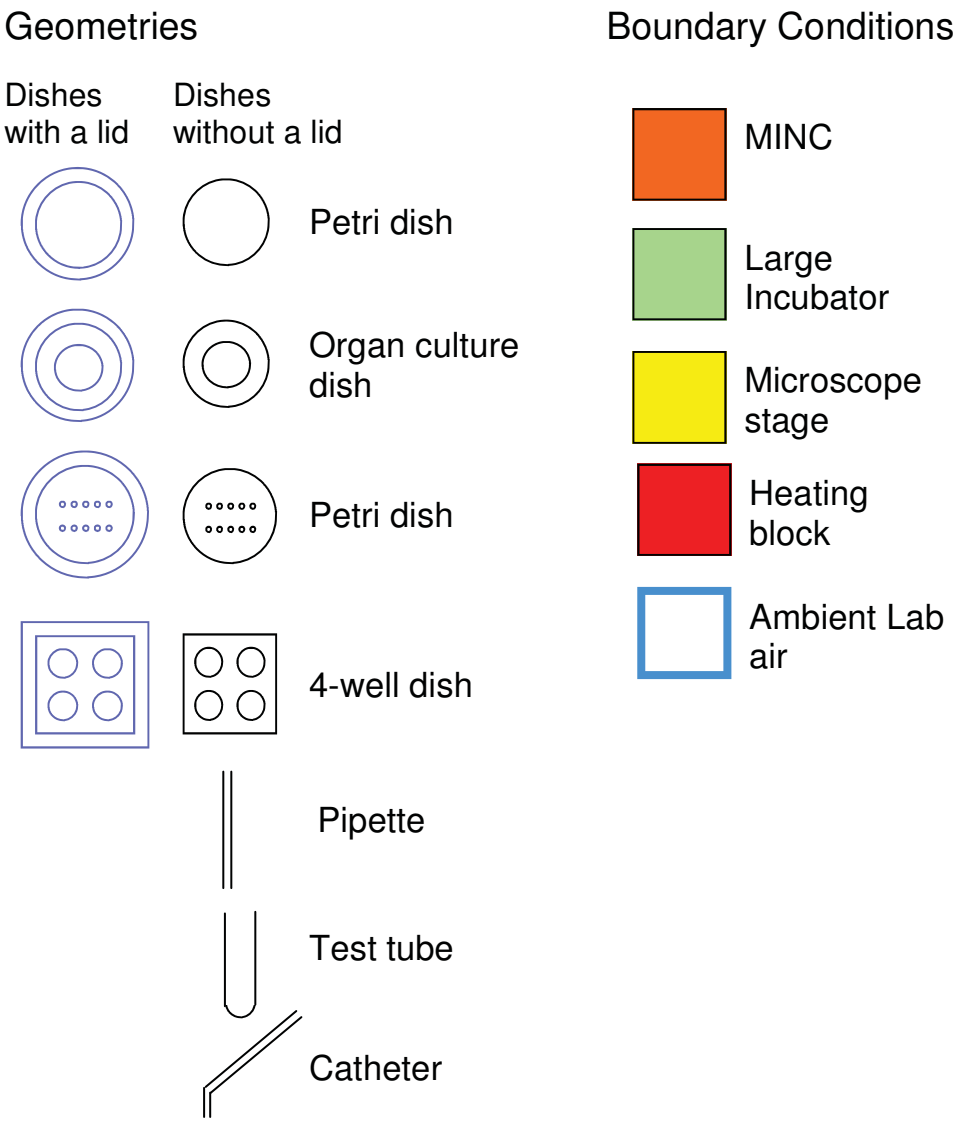

Figure 3.9: Summary of the symbols and colours used in the process flow diagram to represent process geometries and boundary conditions.

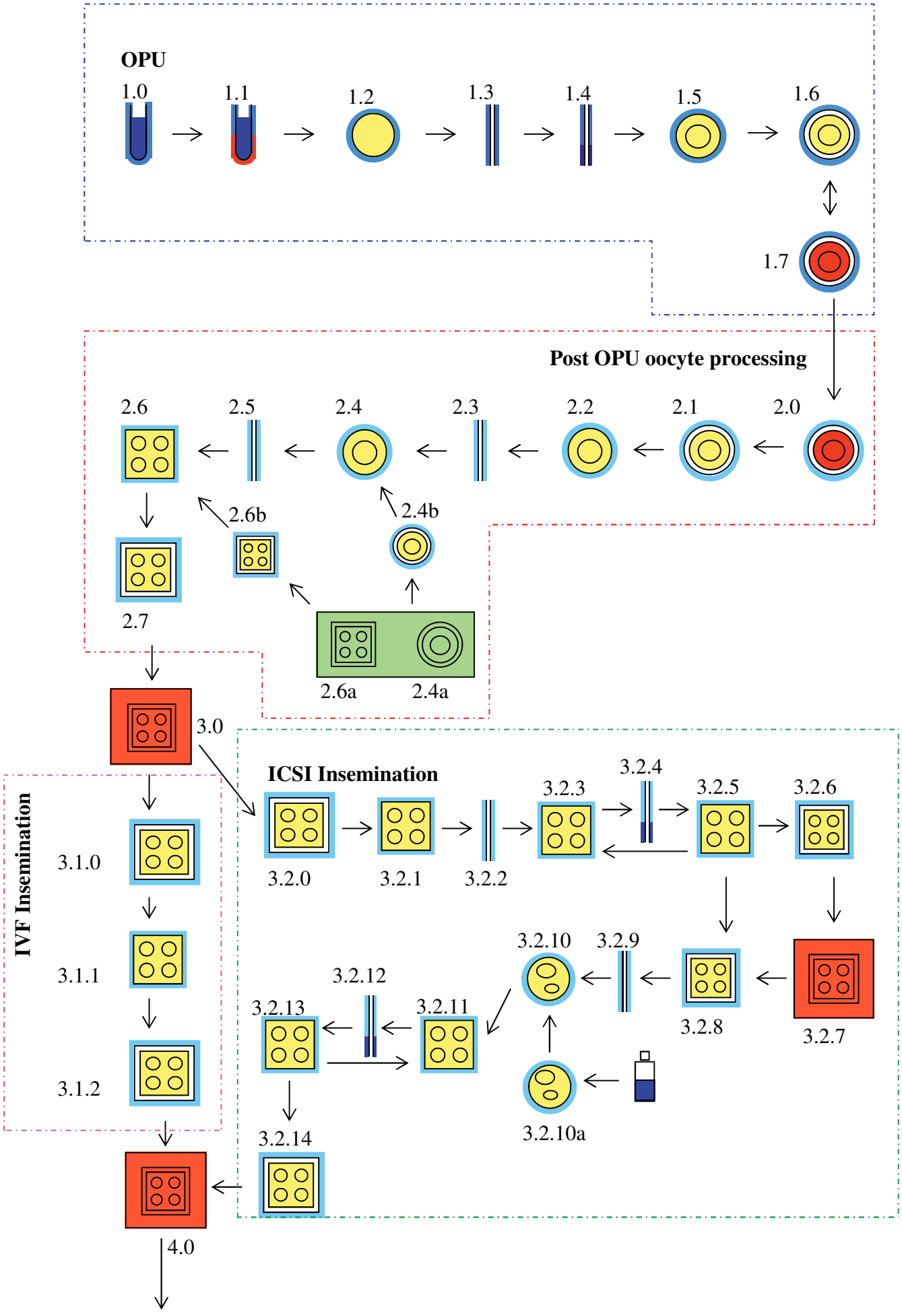
OPU
1.0
1.1
1.2
1.3
1.4
1.5
1.6
1.7
Post OPU oocyte processing
2.6
2.5
2.4
2.3
2.2
2.1
2.0
2.6b
2.4b
2.7
2.6a
2.4a
3.0
IVF Insemination
3.1.0
3.1.1
3.1.2
ICSI Insemination
3.2.0
3.2.1
3.2.2
3.2.3
3.2.4
3.2.5
3.2.6
3.2.7
3.2.8
3.2.9
3.2.10
3.2.10a
3.2.11
3.2.12
3.2.13
3.2.14
4.0

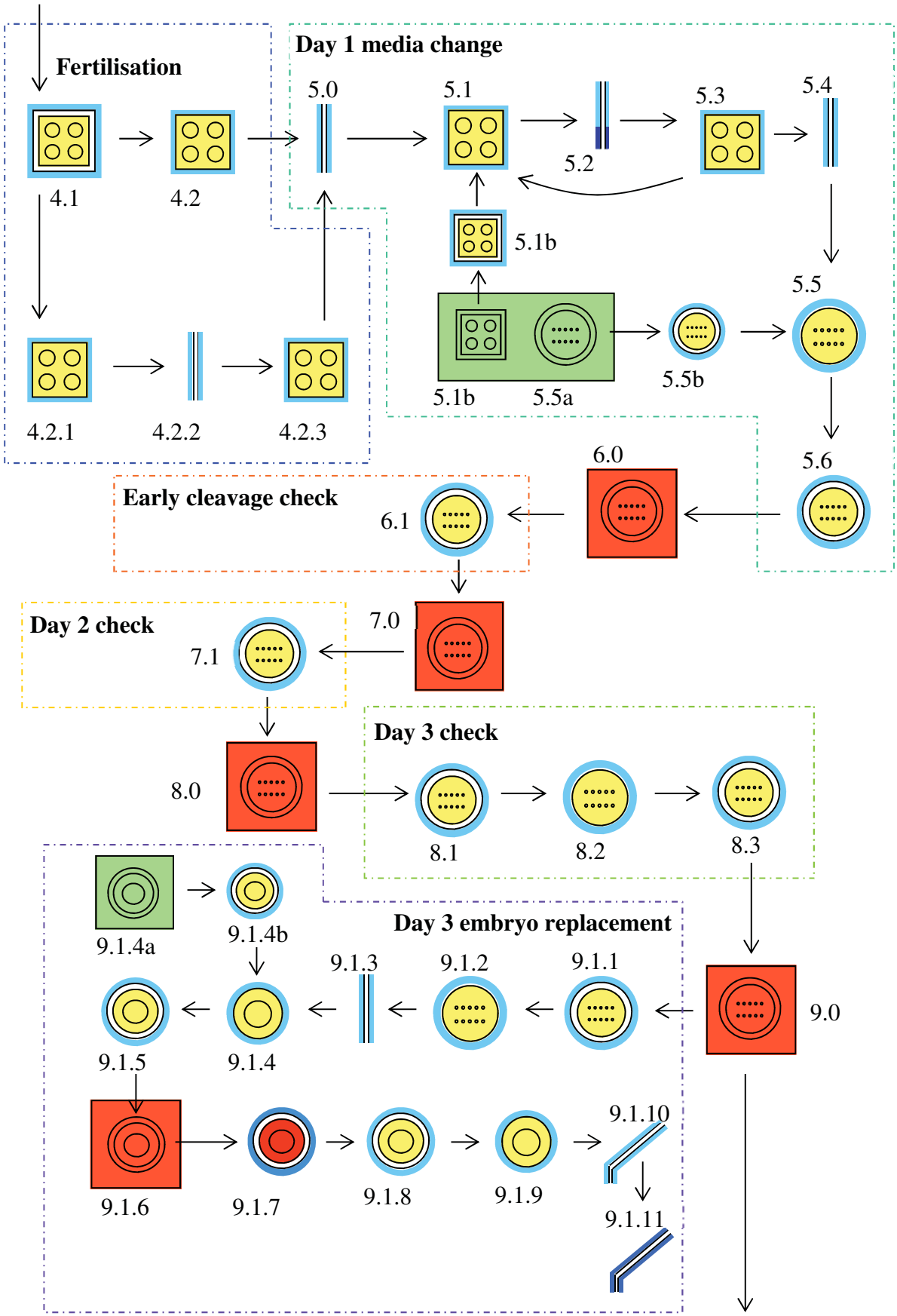
Fertilisation
Day 1 media change
5.0
5.1
5.2
5.3
5.4
4.1
4.2
5.1b
5.5
4.2.1
4.2.2
4.2.3
5.1b
5.5a
5.5b
6.0
5.6
Early cleavage check
6.1
7.0
Day 2 check
7.1
Day 3 check
8.0
8.1
8.2
8.3
Day 3 embryo replacement
9.1.4a
9.1.4b
9.1.3
9.1.2
9.1.1
9.0
9.1.5
9.1.4
9.1.10
9.1.6
9.1.7
9.1.8
9.1.9
9.1.11

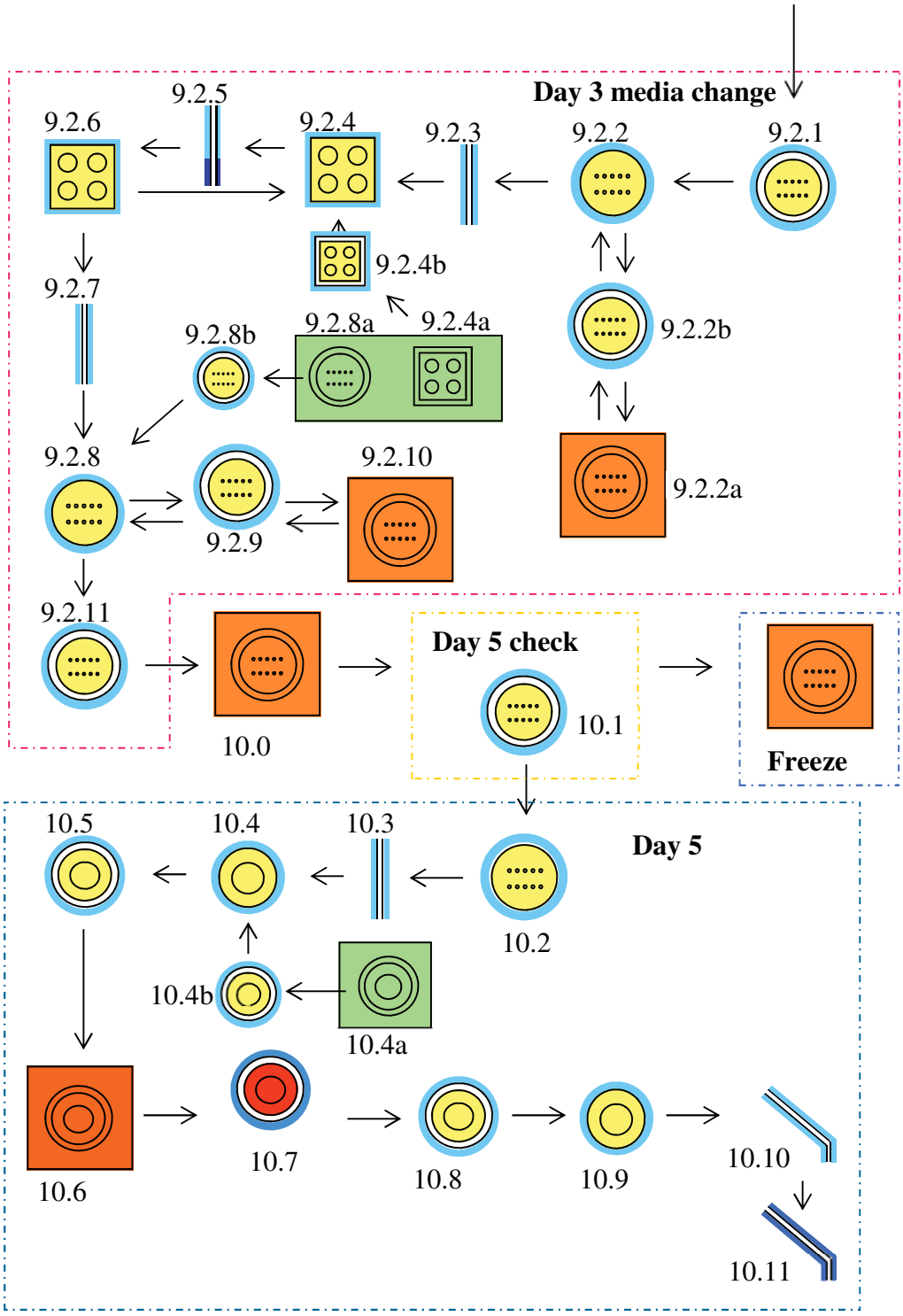

Figure 3.10: Process flow diagram of embryo culture. The movement of an embryo from one step to the next is indicated by arrows. Steps are grouped into the stages of the culture process as indicated by surrounding dotted lines. Refer to Figure 3.9 for a description of the meanings of colours and symbols.

Code	Description	Temperature	Gaseous
Incubation:			
MINC	MINC	~37 ^{o}C	5% O_2, 6% CO_2
I	Large incubator	~37 ^{o}C	5% O_2, 6% CO_2
Surroundings:			
A	Ambient lab air	~23-27 ^{o}C	Atmospheric
Base of dish:			
S	On heated microscope stage	~37 ^{o}C	Atmospheric
HB	On heating block	~37 ^{o}C	Atmospheric

Table 3.1: Description of the environments which provide the boundary conditions for modelling. A code is defined for each environment and these are attached to the steps in the culture process in Table 3.2

Step	Geometry	Surrounding environments
1.0	test-tube	A
1.1	test-tube	A, HB
1.2	small petri dish – no lid	A, S
1.3	pipette	A
1.4	pipette	A
1.5	organ culture dish – no lid	A, S
1.6	organ culture dish – with lid	A, HB
1.7	organ culture dish – with lid	A, HB
2.0	organ culture dish – with lid	A, HB
2.1	organ culture dish – with lid	A, S
2.2	organ culture dish – no lid	A, S
2.3	pipette	A
2.4a	organ culture dish – with lid	I
2.4b	organ culture dish – with lid	A, S
2.4	organ culture dish – no lid	A, S
2.5	pipette	A
2.6a	4-well dish – with lid	I
2.6b	4-well dish – with lid	A, S
2.6	4-well dish – no lid	A, S
2.7	4-well dish – with lid	A, S
3.0	4-well dish – with lid	MINC
3.1.0	4-well dish – with lid	A, S
3.1.1	4-well dish – no lid	A, S
3.1.2	4-well dish – with lid	A, S
3.2.0	4-well dish – with lid	A, S
3.2.1	4-well dish – no lid	A, S
3.2.2	pipette	A
3.2.3	4-well dish – no lid	A, S
3.2.4	pipette	A
3.2.5	4-well dish – no lid	A, S
3.2.6	4-well dish – with lid	A, S
3.2.7	4-well dish – with lid	MINC
3.2.8	4-well dish – with lid	A, S
3.2.9	pipette	A
3.2.10a	petri dish	A, S

3.2.10	petri dish	A, S
3.2.11	4-well dish – no lid	A, S
3.2.12	pipette	A
3.2.13	4-well dish – no lid	A, S
3.2.14	4-well dish – with lid	A, S
4.0	4-well dish – with lid	MINC
4.1	4-well dish – with lid	A, S
4.2	4-well dish – no lid	A, S
4.2.1	4-well dish – no lid	A, S
4.2.2	pipette	A
4.2.3	4-well dish – no lid	A, S
5.0	pipette	A
5.1	4-well dish – no lid	I
5.1a	4-well dish – with lid	A, S
5.1b	4-well dish – with lid	A, S
5.2	pipette	A
5.3	4-well dish – no lid	A, S
5.4	pipette	A
5.5a	Drop culture – with lid	I
5.5b	Drop culture – with lid	A, S
5.5	Drop culture	A, S
5.6	Drop culture – with lid	A, S
6.0	Drop culture – with lid	MINC
6.1	Drop culture – with lid	A, S
7.0	Drop culture – with lid	MINC
7.1	Drop culture – with lid	A, S
8.0	Drop culture – with lid	MINC
8.1	Drop culture – with lid	A, S
8.2	Drop culture – no lid	A, S
8.3	Drop culture – with lid	A, S
9.0	Drop culture – with lid	MINC
9.1.1	Drop culture – with lid	A, S
9.1.2	Drop culture – no lid	A, S
9.1.3	Pipette	A
9.1.4a	Drop culture – with lid	I
9.1.4b	Drop culture – with lid	A, S
9.1.4	Drop culture – no lid	A, S
9.1.5	Drop culture – with lid	A, S
9.1.6	Drop culture – with lid	MINC
9.1.7	Drop culture – with lid	A, HB
9.1.8	Drop culture – with lid	A, S
9.1.9	Drop culture – no lid	A, S
9.1.10	Catheter	A
9.1.11	Catheter	A
9.2.1	Drop culture – with lid	A, S
9.2.2a	Drop culture – with lid	MINC
9.2.2b	Drop culture – with lid	A, S
9.2.2	Drop culture – no lid	A, S
9.2.3	pipette	A
9.2.4a	4-well dish – with lid	MINC
9.2.4b	4-well dish – with lid	A, S
9.2.4	4-well dish – no lid	A, S

9.2.5	pipette	A
9.2.6	4-well dish – no lid	A, S
9.2.7	pipette	A
9.2.8a	4-well dish – with lid	MINC
9.2.8b	4-well dish – with lid	A, S
9.2.8	4-well dish – no lid	A, S
9.2.9	4-well dish – with lid	A, S
9.2.10	4-well dish – with lid	MINC
9.2.11	4-well dish – with lid	A, S
10.0	4-well dish – with lid	MINC
10.1	4-well dish – with lid	A, S
10.2	4-well dish – no lid	A, S
10.3	pipette	A
10.4a	4-well dish – with lid	I
10.4b	4-well dish – with lid	A, S
10.4	4-well dish – no lid	A, S
10.5	4-well dish – with lid	A, S
10.6	4-well dish – with lid	MINC
10.7	4-well dish – with lid	A, HB
10.8	4-well dish – with lid	A, S
10.9	4-well dish – no lid	A, S
10.10	Catheter	A
10.11	Catheter	A

Table 3.2: The geometries and surrounding environments are defined for the steps in the culture process as labelled in Figure 3.10

3.8 Summary

Every step in the process flow diagram (Figure 3.10) may be modelled for heat and mass transfer in order to characterise the thermal, oxygen, carbon dioxide environments immediate to an embryo throughout the culture process. Though the process has many steps it is made up of repeated units. For example:

- Every time a dish is used in the process it is removed from an incubator, its lid is removed, embryo manipulation takes place, the lid is returned to the dish and the dish is returned to the incubator.

- Every time a pipette is used in the process it lifts liquid from a dish and expels the liquid, most often at another location.

Modelling heat and mass transfer in these frequently repeated steps for the major dish and pipette types will provide a description of the physical environment embryos and oocytes may be exposed to throughout the process. Models will provide an investigative tool to identify the factors in the process which have the most impact on the embryos' environment and will thus aid process optimisation.

4 Heat transfer in a Petri dish

Previous chapters have suggested that modelling heat and mass transfer in the steps of the culture process is a means to overcome difficulties in characterising the physical environment around an embryo. Characterisation of the embryos' environment may identify changes to clinical practice which may minimise environmental stress on embryos and potentially improve IVF success rates.

An embryo spends the majority of its time throughout the culture process within a Petri dish. Modelling heat transfer in dishes is a good starting point when investigating the physical environment an embryo is exposed to throughout the culture process due to the intrinsic importance of temperature to the embryo and the universal use of the Petri dish for its culture. Temperature sensors (required for collecting data for model validation) are smaller, cheaper, and more robust than those for O_2, CO_2, or pH. Dishes are the largest systems in the culture process. Consequently, experimental set up for model validation at a specific point in a dish system is easier and likely to be less invasive than in the smaller systems (e.g. pipettes and catheters). The thermophysical properties of many of the materials in a Petri dish system are well characterised, providing a wide range of resources for parameter estimation. The aim of this chapter is to develop and validate appropriate models of heat transfer in the Petri dish which may be used to simulate conditions in every day clinical practice.

The model will be validated against experimental set-ups similar to steps in the culture process (as identified in Chapter 3).

4.1 Drop culture in a Petri dish

As demonstrated in Chapter 3, embryos spend the majority of their time *in vitro* in Petri dish drop culture. The purpose of this section is to describe the development of a model for heat transfer in this system.

4.1.1 The system

Drop culture in a Petri dish is the culture of embryos in individual drops of media on the floor of a Petri dish which are overlaid by paraffin oil. Keeping the embryos separate enables identification of individual embryos throughout the process for the scoring of their morphological parameters.

The following procedure is used at Fertility Associates New Zealand for Petri dish set-up but this is representative of standard industry practice. Ten 7.5 µl drops of media are pipetted onto the floor of a Petri dish (IVF Dish, BD Falcon, BD Biosciences, NJ, USA) in two rows of five and overlaid with 7 ml of paraffin oil (Figure 4.1). These drops are removed leaving thin layers of liquid on the dish floor (footprints). 15 µl of culture media is pipetted into each footprint forming the drops for embryo culture. This procedure produces drops of media which retain the footprints of the smaller liquid drops and stand up above the dish floor.

Figure 4.1: Photograph of drop culture in a Petri dish a) Side view showing 10 media drops standing up above the dish floor. b) From above displaying the drop layout.

Throughout the culture process the Petri dish system is only removed from the stable environment of the incubators (37 °C) for embryo observation and manipulation. The Petri dish is subsequently placed on heated microscope stages or heated blocks which

are set to maintain appropriate temperatures at the dish floor while the remainder of the dish boundary is exposed to laboratory air (typically 24-27 °C).

The centre floor of the media drops is always the temperature of interest as an embryo is always found in the centre of a media drop (an observation made by embryologists). This is likely due to surface tension forces.

4.1.2 Model requirements

A model of heat transfer within a Petri dish is required to simulate the heat transfer processes which occur within and at the boundaries of the Petri dish system. Comparison of the model with experimental data (Model validation, Section 4.5) provides an opportunity to validate the assumptions made with respect to the modes of heat transfer considered.

If the basis of the model is appropriate, the accuracy of input parameters to the model (such as heat transfer coefficients and thermophysical properties) will determine how closely the model can predict the real life situation. A good model is a model which predicts the actual temperatures (judged by comparison with experimental data) to an acceptable accuracy, bearing in mind that experimental measurement has its own level of uncertainty.

A Petri dish, due to its relatively large thermal mass, will not change temperatures rapidly compared to a small system e.g. a thin glass pipette. Therefore high prediction accuracy may be expected. Predicting heat transfer in a Petri dish to an accuracy of ± 0.3 °C would be sufficient for the model to be used for predictive purposes and to

compare different procedures. With such a degree of accuracy, if the model was used to simulate a situation and the temperature was predicted to be 37.1 °C then the maximum value may be assumed at 37.4 °C – still within the 33-37.5 °C range (the outer acceptable limits as defined in Section 3.6).

4.1.3 Conceptual model development

The aim of this section is to develop a conceptual model to describe the heat transfer processes which take place within and at the boundaries of the defined Petri dish model geometry. To do this, assumptions are made based on a theoretical understanding of heat transfer.

4.1.3.1 Model geometry

The model geometry is a geometric representation of the system including appropriate simplifications. The ideal geometry will be the simplest geometry which enables an adequate description of heat transfer within the system. Such a geometry will ease solution of the model by reducing the required number of mesh elements in the model while not significantly reducing the accuracy of the predictions (see Section 4.2.2.2). Figure 4.2 displays the model geometry for which dimensions, as labelled, are defined in Table 4.1.

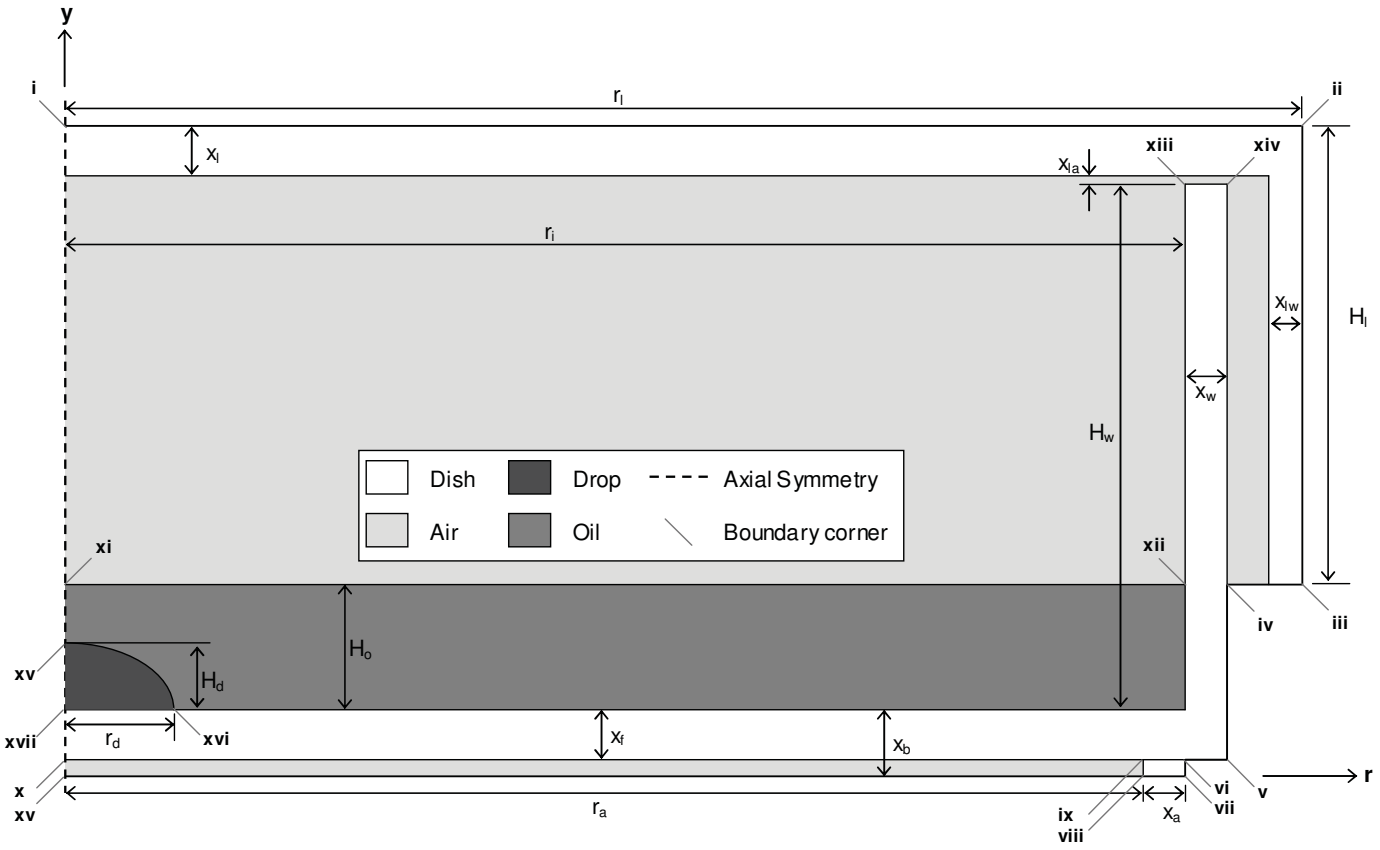

Figure 4.2: Displays the two-dimensional model geometry of drop culture in a Petri dish. Roman numerals (i-xv) label corners of the dish system boundaries. Dimensions are defined in Table 4.1.

Dimension	Length (mm)	Dimension	Length (mm)
r_i	25.9	x_l	1.03
r_a	24.85	x_{la}	0.17
r_l	28.62	x_{lw}	0.89
r_d	2.45	H_d	1.43
x_f*	1.09	H_w	12.71
x_b*	1.51	H_{lw}	9.65
x_a	0.93	H_o*	3.09
x_w	0.94		

Table 4.1: Defines the dimensions for the two-dimensional model geometry of drop culture in a Petri dish (Figure 4.2). Values marked (*) are dimensions which were measured for each individual dish during model validation.

The dimensions (Table 4.1) were taken from measurement of a single Petri dish. Initially, when these dimensions were first taken, there seemed to be negligible variation (≈ 0.02 mm) between the dimensions of different dishes. However during model validation variation was identified in dimensions which have a significant impact on heat transfer to and from the floor of the dish. For model validation these dimensions, the thickness of the dish floor and the thickness of the air gap beneath the dish (as labelled by '*' in Table 4.1, along with oil depth (H_o)), were measured for every dish used in experimental work.

Little variation is apparent between dishes in a batch and between batches at any one time however there is significant variation between batches over time, perhaps due to changes in manufacture. For example Table 4.2 displays the thickness of the dish floor and the thickness of the air gap beneath the dish for two dishes, A and B, which were from two separate batches (used by Fertility Associates during intervals approximately two years apart). The distance between the floor of the dish and the surface beneath the dish is 1.51 mm and 1.97 mm for Dish A and Dish B respectively, an increase of ≈30%, which increases the resistance to heat transfer between a heated surface and the dish floor. The purpose of this thesis was not to describe the variation in dish dimensions, which is manufacturer dependent. Rather this work considers identification of dimensions which affect heat transfer to and from the position of an embryo as these are important for controlling the temperatures embryos are exposed to.

	Thickness of the dish floor (x_f) (mm)	Thickness of the air gap beneath the dish (x_b-x_f) (mm)
Dish A	1.09	0.42
Dish B	1.36	0.61

Table 4.2: Dimension of two Petri dishes, from batches used at fertility associates approximately two years apart as an example of the variation which can occur between batches.

Modelling a single drop at the centre of a Petri dish enables axial symmetry to be applied, simplifying the geometry to two dimensions. In practice embryos may be placed in drops anywhere across the floor of the dish. The 2D geometry cannot be used to model drops placed anywhere other than centrally. As paraffin oil and aqueous culture media have similar thermophysical properties and media droplets have a very small volume relative to the rest of the system, we may assume that heat transfer at a given point on the floor of the dish is not significantly altered by the presence/absence of a media drop. However any effect caused by the presence of a drop on the dish floor may be investigated by altering thermophysical properties of the centralised drop in the 2D model.

Several other simplifications were made to the system; these are shown in Figure 4.2. The lid is raised above the dish by small lid lugs to form an air gap between the lid and the base of the dish. This air gap is potentially important to heat transfer as the properties of air differ significantly to those of polystyrene (the Petri dish material). The lugs themselves take up less than 2% of this space, so they are ignored while the air gap is included in the geometry.

The walls of the dish and its lid are slightly flared, with the internal radius of the dish increasing by 0.63 mm (±0.03 mm, n=10) over its 15 mm depth. This flaring was considered insignificant and the radius was taken to be that at the floor of the dish. This only decreases the surface area of the dish wall to 98.77% of its magnitude when flaring is incorporated.

Fertility Associates protocol states that 7 ml of paraffin oil overlays the drops in the Petri dish in order to prevent evaporation. The exact depth of oil is not considered important in the embryology lab and therefore a range of depths may exist depending on how accurately the volume is assessed, and on the embryologist's technique and preference. As a result variation in oil volume was investigated. Dishes were pre-weighed and three embryologists each dispensed oil into three dishes which were then reweighed. The volume of oil dispensed into each dish was calculated using the oil density at 25 °C (843.97 $kg.m^{-3}$; Table 4.6, Equation 4). The mean volume dispensed was 6.56 ml with a standard deviation of 0.30 ml (n=9, limited due to the expense of oil).

The depth of the paraffin oil and the variation in this value can be calculated from the dimensions of the dish and the measured oil volume. The flaring of the dish wall is taken into account to maximise accuracy. The depth was calculated from the equation for the volume of a cone segment (Equation 4.1) derived below. The dimensions used in the calculations are labelled in Figure 4.3.

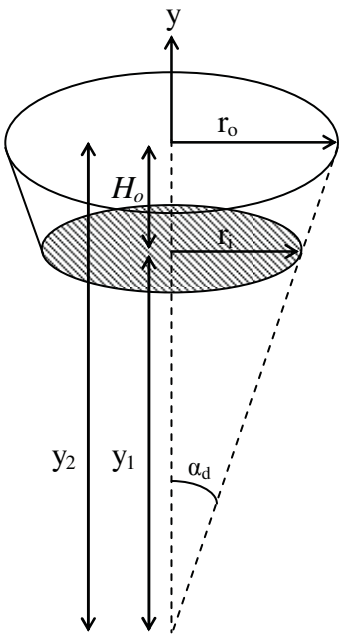

Figure 4.3: A segment of a cone

$$V = Ay \ \therefore \ V = \int \pi r^2 dy$$

Since $r_x = h_x \tan\alpha$ and $V = \int \pi (y \tan^2 \alpha) dy$:

$$V_{oil} = \pi \tan^2 \alpha_d \int_{y_1}^{y_2} y^2 dy = \left[\frac{\pi \tan \alpha_d y^3}{3} \right]_{y_1}^{y_2}$$

$$V_{oil} = \frac{\pi}{3}\left(r_o \times y_2 - r_i \times y_1\right)$$

Since $r_o = r_i + H_o \tan\alpha_d$, $y_1 = \dfrac{r_i}{\tan\alpha_d}$ and $y_2 = \dfrac{r_o}{\tan\alpha_d}$;

$$V_{oil} = \frac{\pi}{3}\left[(r_i + H_o \times \tan\alpha_d)^2 + \frac{r_i + H_o \times \tan\alpha_d}{\tan\alpha_d} + r_i^2 \left(\frac{r_i}{\tan\alpha_d} \right) \right] \qquad \text{Equation 4.1}$$

For model validation, the mass of oil used in each experiment was determined from this relationship to enable the model to represent the system as accurately as possible. A single 15 µl drop at the centre of the dish was used in model validation

experiments. As this is such a small volume, approximately 0.2% of the 7 ml of paraffin oil, it was not taken into account when determining the depth of oil. For applications of the model an oil depth of 3.09 ± 0.29 mm (± twice the standard deviation) was used. This corresponds to the mean and standard deviation in the volume of dispensed oil described above.

The 15 µl media drops are formed with the footprint of a 5 µl drop. The footprint diameters of ten 15 µl drops were measured with a micrometer defining a mean of 4.9 mm and the variability was conservatively taken to be ±0.16 mm (twice the standard deviation of 0.08 mm).

The 15 µl drops stand up above the dish floor and bulge slightly making their exact geometry hard to define. To enable prediction of drop height, their shape was defined as a segment of a sphere with a volume of exactly 15 µl.

Equation 4.2 (derived below) was solved for a given drop volume (V_d) and footprint radius (r_d). The dimensions used in the calculations are labelled in Figure 4.4.

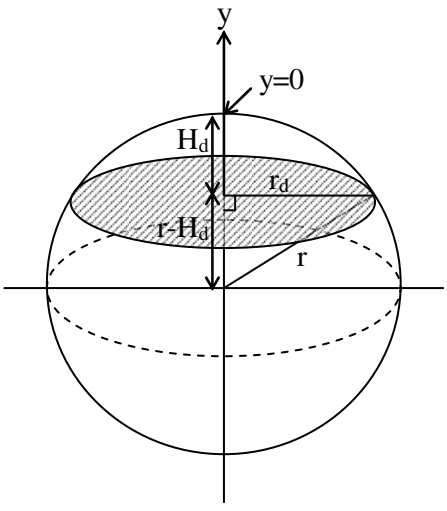

Figure 4.4: The segment of a sphere

$$V = Ay = \int \pi r^2 dy$$

Since $r_d{}^2 = r^2 - (r - H_d)^2 = 2rH_d - H_d{}^2$

$$V_d = \int_0^{H_d} 2\pi y r dy - \int_0^{H_d} \pi y^2 dy$$

$$V_d = \pi r H_d{}^2 - \frac{\pi H_d{}^3}{3}$$

Since $r = \frac{r_d{}^2 + H_d{}^2}{2H_d}$

$$V_d = \frac{\pi H_d}{6}\left(3r_d{}^2 - H_d{}^2\right) \qquad \text{Equation 4.2}$$

A 15 µl sphere-segment (drop) with a footprint diameter of 4.9 mm will have a drop height of 1.43 mm. A footprint diameter of 4.9 ± 0.16 mm, as defined above, equates to a drop height of 1.43 ± 0.07 mm.

The geometric parameters defined in this section are summarised in Table 4.3.

Dimension	Best Estimate	Range
Oil depth (H_o)	3.09 mm	±0.29
Drop diameter (r_d)	4.9 mm	±0.16
Drop depth (H_d)	1.43 mm	±0.07

Table 4.3: Summary of the variable geometric model parameters. These values are used during application of the Petri dish model.

4.1.3.2 Heat transfer model assumptions

Several assumptions must be made when defining the means by which heat is transferred both within the system and to and from the boundaries of the system.

Forced convection within the paraffin oil and media drops

Though perhaps present in the process at times, forced convection both within the oil layer and drops was assumed to be negligible. Transfer of embryos to and from the incubators is done with care. Any mixing is purposely avoided to prevent drops moving and running together. At all other times, dishes are placed on flat surfaces. Pulled glass pipettes, used for embryo manipulation, have a small diameter (200 μm) and lift embryos in a minimal volume causing little movement in the bulk liquid.

Natural convection

To investigate the significance of internal convection the dimensionless Rayleigh number (*Ra*) was calculated (Equation 4.3) for the liquid layers in the system. The dimensionless Rayleigh number is the ratio of inertia forces to viscous forces. In the fluid, above a critical value, the inertial forces (buoyancy due to density differences and the result of a temperature gradient) outweigh the viscous force of the fluid and convection takes place.

$$Ra = \frac{g\beta(\theta_s - \theta_\infty)L^3 c\rho}{\mu\lambda} \qquad \text{Equation 4.3}$$

where g is acceleration due to gravity (9.81 $m.s^{-2}$), β is the thermal expansion coefficient ($°C^{-1}$), θ_s is the temperature of the surface (°C), θ_∞ is the temperature at the oil surface (°C), L is the thickness of the oil layer (m), c is the heat capacity of the oil ($J.kg^{-1}K^{-1}$), μ is the oil's kinematic viscosity ($m^2.s^{-1}$) and λ is the oil's thermal conductivity ($W.m^{-1}K^{-1}$), ρ is the density ($kg.m^{-3}$).

Mikheyev (1968) showed how the contribution of natural convection changes as a function of the Rayleigh number using a convective coefficient (λ_{eff}/λ). The convective coefficient is the effective rate of heat transfer relative to when there is no convection (so conduction only). This showed that natural convection is only significant at $Ra>10^3$.

The Rayleigh number was calculated both for the oil layer and for the air layer trapped by the lid of the dish. The values for the density, heat capacity and thermal conductivity of paraffin oil and air were determined from Table 4.6 Equations 4-6 (oil) and Table 4.6 Equations 10-12 (air) assuming a temperature of 30 °C, approximately midway between the incubator and laboratory air temperature. The thickness was taken, from Figure 4.2, to be 0.0098 m and 0.00309 m for air and oil respectively. The thermal expansion coefficients used were 0.0033 for air (assuming air is an ideal gas and thus β=1/T) and 0.878×10^{-3} for paraffin oil (Koster, 1997) and the kinematic viscosities used were 1.67×10^{-5} m^2s^{-1} for air (Geankoplis, 2003) and 7.6×10^{-5} m^2s^{-1} (Koster, 1997).

For a Petri dish system within the culture process the greatest temperature gradients will occur across the dish when the dish is on a heated microscope stage (~37 °C) and exposed to the ambient laboratory air. Since this temperature gradient will be spread across multiple layers (the air gap beneath the dish, the dish floor, the paraffin oil and the air trapped by the lid of the dish), a temperature difference of 10 °C was assumed across the two layers to give an estimate of the Rayleigh number.

The calculated Rayleigh numbers were 809 and 443 for the air and the paraffin oil layers respectively. These Rayleigh numbers are less than 10^3 and therefore the convective coefficient is 1 and no significant natural convection will occur within the layer. Therefore heat transfer induced density differences will not drive bulk mass transfer within the system.

Convective heat transfer between the dish and its surroundings

At the boundaries, where the dish or pipette is exposed to the air, heat is transferred by convection. The varying resistance to heat transfer between bulk air and a surface in convective heat transfer is theoretically represented by conduction of heat though a layer of still air adjacent to the surface (the boundary layer). The greater the rate of airflow adjacent to the surface, the thinner is the boundary layer. In addition, the thickness of the boundary layer is dependent on the material, finish and orientation of the surface. The effect of boundary layer thickness on heat transfer is accounted for by a convective heat transfer coefficient (h), the thinner the boundary layer the higher the convective heat transfer coefficient for any given surface.

At the boundary of the model geometry, it is possible to assume that the convective heat transfer coefficient is infinitely high and therefore that the surface temperature is equal to the surrounding temperature, as long as the resistance to heat transfer from the external environment to the boundary of interest (external resistance) is significantly less than the resistance within the object (internal resistance). The dimensionless Biot number (Bi) gives a ratio between the two resistances to heat transfer and may be used to indicate whether the assumption that the external

resistance is negligible is reasonable. If the Biot number is >20 negligible external resistance may be assumed (McCabe et al., 2005).

For a Petri dish without a lid containing a depth of 3.09 mm of oil (see Figure 4.2), assuming convective heat transfer coefficients of 15 $W.m^{-2}K^{-1}$ and 5 $W.m^{-2}K^{-1}$ (a broad range for still air) the Biot numbers are 0.188 and 0.0627 respectively. For a Petri dish with a lid and therefore 9.2 mm of trapped air (see Figure 4.2) assuming convective heat transfer coefficients of 15 $W.m^{-2}K^{-1}$ and 5 $W.m^{-2}K^{-1}$ the Biot numbers are 2.56 and 0.85 respectively. For the dish, both with and without a lid, the Biot numbers are <20 so the external resistance to heat transfer cannot be negated. Therefore a convective boundary condition at the external boundaries was applied to the model in all situations.

Radiation

Heat may be lost from the dish to the surrounding air via a number of modes of heat transfer. Here, heat loss due to natural convection from the lid of the dish (in still air at 25 °C) immediately after removal from an incubator (37 °C) is compared to heat loss due to radiation. This is the situation with the greatest temperature difference and therefore greatest rate of heat transfer from the lid of the dish to its surroundings. For convective heat transfer the heat flux from the surface is given by;

$$q = h\Delta\theta \qquad \text{Equation 4.4}$$

$$= 10 \times (37 - 25)$$

$$= 120 \ W.m^{-2}$$

and for radiative heat transfer;

$$q = \varepsilon\sigma(T_s^4 - T_a^4) \qquad \text{Equation 4.5}$$

$$= 0.9 \times 5.676 \times 10^{-8} \times (310.15^4 - 298.15^4)$$

$$= 69 \ W.m^{-2}$$

Where q is the heat flux (W.m^{-2}); ε is the emissivity of the dish surface (~0.9 for plastics, Gaudina *et al*., 2011); σ is the Stefan-Boltzmann constant (5.676×10^{-8} W.m^{-2}K^{-4}); T_s is the dish surface temperature (310.15 K); T_a is the ambient room temperature (298.15 K). All thermophysical properties were taken at 30°C.

Heat flux from the surface of the dish lid due to radiation is approximately half of that due to convection. Therefore radiation is significant. However, since determination of the convective heat transfer coefficient is subject to significant uncertainty in its determination, this radiation may be included as convection.

Evaporation and condensation

Air within an incubator is kept humid. The degree of humidity is not closely controlled; water is held in a tray on the floor of open volume incubators and the air is bubbled through water before entering the MINC bench top incubators. Therefore the possible effects of evaporation and condensation must be considered. The air trapped by the lid of an equilibrated dish will have a relative humidity equal to that in the incubator. Upon removal of this dish into the cooler ambient air some of this moisture will condense. It is necessary to determine whether the amount of energy released when this process takes place will impact significantly on the temperatures within the dish.

Approximately 3.4×10^{-5} m^3 (an overestimate, assuming a cylinder of radius 30 mm and height of 12 mm) of air is trapped by the lid of a dish. Assuming the air is saturated, the humidity ratio in the incubator at 37 °C is 41.45 g of water per kg dry air, therefore the air trapped by the lid of the dish may contain a maximum of $1.6\times10^{-3}\,g$ of water (air density calculated at 37 °C from Equation 10, Table 4.6). When the dish is removed from the incubator, assuming a laboratory temperature of 25 °C, the humidity ratio falls to 23 g water per kg dry air and the air trapped by the lid of the dish may contain a maximum of $9\times10^{-4}\,g$ of water (air density calculated at 25 °C from Equation 10, Table 4.6). This means that the difference between the water contents at 37 °C and at 25 °C of $7\times10^{-4}\,g$ must condense.

Condensation of $7\times10^{-4}\,g$ of water releases only 1.58 J of energy. Approximately 4.18 J is required to heat 1 g (approximately 1 ml) of water by 1 °C hence the impact of 1.58 J on 7 ml of liquid is negligible. Therefore the impact of the humid environment may be ignored throughout model development.

4.1.4 Model formulation

Given the above assumptions the sole mode of heat transfer within the geometry is conduction (thermal diffusion). Thermal diffusion within the dish is described by Equation 4.6.

$$\rho c\frac{\partial\theta}{\partial t}=\lambda\nabla^2\theta \qquad \text{Equation 4.6}$$

The boundary conditions which apply to the model are defined below. The boundaries to which these conditions apply vary depending on the process step being simulated. For a given condition the steps are specified along with the boundary (described by the Roman numerals in reference to Figure 4.2).

1. The line of axial symmetry down the centre of the dish, about which the 2D model rotates.

$$\lambda \frac{\partial \theta}{\partial r} = 0 \qquad \text{Equation 4.7}$$

for i-x, $t \geq 0$ *when all of the dish is exposed to the surrounding air as occurs while the dish is moved across a laboratory or if the dish is sat on a mesh tray in an incubator*

for i-xv, $t \geq 0$ *when the dish is sat on a surface*

2. The exposed external boundaries of the model geometry, in which convection from the surface is equal to the conductive flux normal to the boundary.

$$\lambda \nabla \theta = h(\theta_A - \theta_S) \qquad \text{Equation 4.8}$$

for i-ii-iii-iv-v-vi-vii-viii-ix-x, $t \geq 0$ *when all of the dish are exposed to the surrounding air as occurs while the dish is moved across a laboratory or if the dish is sat on a mesh tray in an incubator*

for i-ii-iii-iv-v-vi-vii, $t \geq 0$ *when the dish is sat on a surface*

for xi-xii-xiii-xiv-iv-v-vi-vii, $t \geq 0$ *when the dish is sat on a surface and the lid is off the dish*

3. The boundary at which the model's subdomains meet the surface upon which the dish is sat. The nature of this boundary condition depends on the surface upon which the dish is sat.

$$\theta = \theta_b$$ Equation 4.9

for vii-viii-vv, $t \geq 0$*, where* θ_b *is the constant and uniform surface temperature*

$$\theta = \theta_b(t)$$ Equation 4.10

for vii-viii-vv, $t \geq 0$*, where* θ_b *is the surface temperature as a function of time.*

$$\theta = \theta_b(t, r)$$ Equation 4.11

for vii-viii-vv, $t \geq 0$*, where* θ_b *is the surface temperature as a function of time and position*

Initial Conditions

If it is assumed that the initial temperature gradient through the dish is negligible, the initial conditions are:

$\theta_i(\Omega_a, \Omega_p, \Omega_m, \Omega_o) = \theta_e$ at t=0

'Ω' denotes the subdomain (with the subscripts: *a*=air, *p*=polystyrene, *m*=media, *o*=Paraffin oil), θ_i = the initial temperature and θ_e = experimentally recorded temperature (for example this may be 37°C if the dish is initially in the incubator or at the ambient air temperature if the dish is initially on a bench).

If it cannot be assumed that the temperature gradient through the dish is negligible then the initial temperature values are defined as the output values from the model of the preceding situation.

$\theta_{i(x)}(y,r) = \theta_{f(x-1)}(y,r)$ at t=0

$\theta_{i(x)}$ = Initial temperature #*(x)*, $\theta_{f(x-1)}$ = Final temperature #*(x-1)*

4.2 The model solution

This section overviews the tools applied to solve this model and the checks which demonstrate that the solution was reliable.

4.2.1 The simulation

The model was solved by the finite element method in the software package COMSOL Multiphysics 3.3a (COMSOL, Stockholm, Sweden). The default linear system solver, the direct UMFPACK solver, was used.

The geometry was defined by equations in MATLAB (MATLAB R2006a, The MathsWorks, Inc.) and subsequently imported into COMSOL (COMSOL Multiphysics 3.3a). Defining the model geometry in MATLAB provides flexibility and eases the ability to test the sensitivity of the model prediction to changes in geometric dimensions. Additional parameters are entered into COMSOL as either constants or functions and assigned to the relevant subdomains and/or model boundaries. The mesh, which defines the size and position of model elements (triangles), is generated automatically in COMSOL; the mesh density may be refined in manually selected areas. The simulation time is specified. Figure 4.5 displays examples of the model geometry (A), the meshed model geometry (B), and the temperature profile through the geometry at the end of a simulation (C) with the temperature profile over time at the centre floor of the dish. The temperature profile over time may be obtained for any position within the model geometry. COMSOL and MATLAB files used are provided in Appendix A.

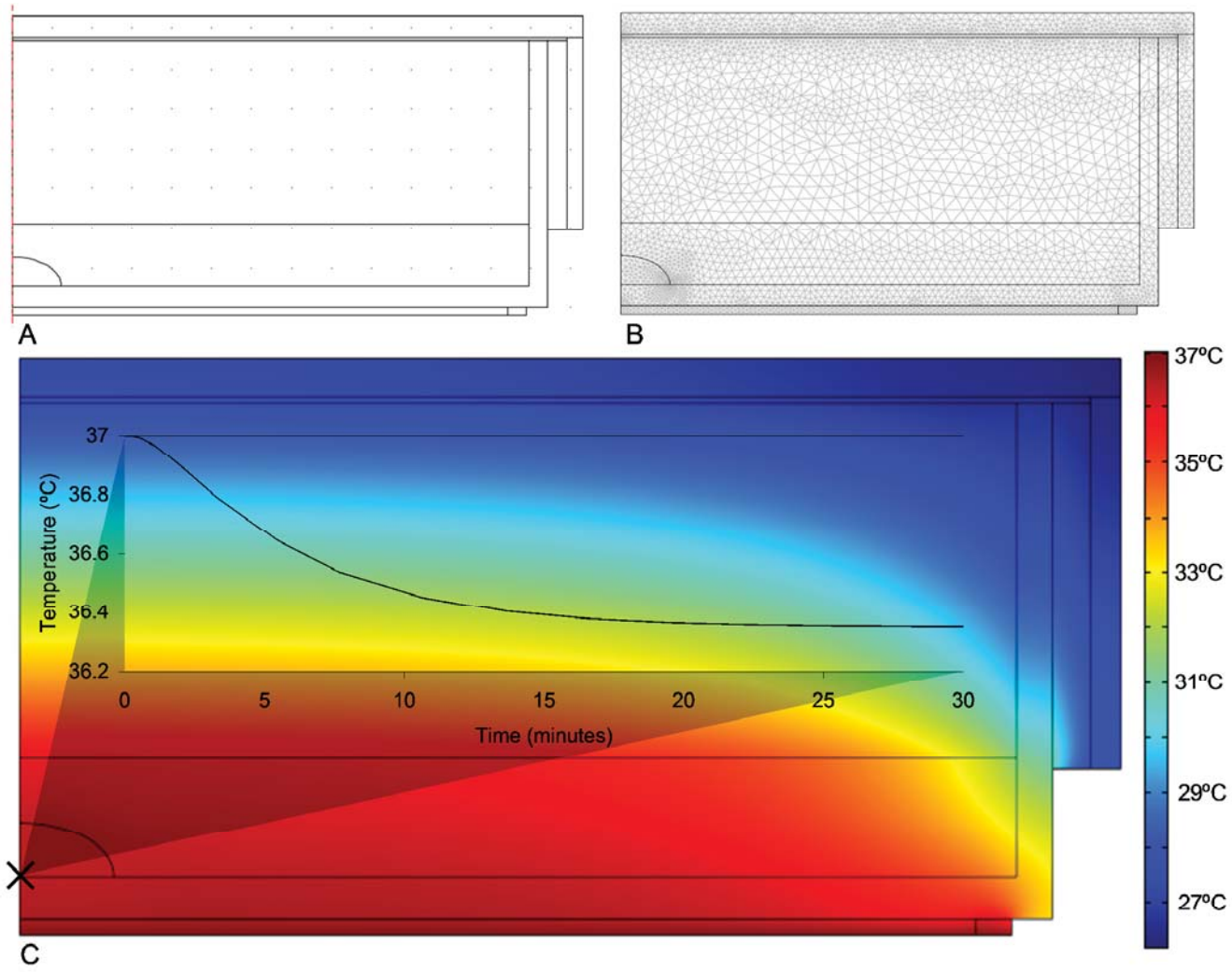

Figure 4.5: Example of the COMSOL Multiphysics 3.3a for modelling. A) The model geometry. B) The meshed model geometry. C) The temperature profile across the Petri dish geometry after 30 minutes with the base boundary set at 37 °C and the exposed external boundaries to 27 °C). C(insert): The temperature profile over time at the centre floor of the dish (×) ; this information may be obtained at any position within the model geometry.

4.2.2 Error checks

It is important to discern whether the model solver has been implemented correctly and that numerical errors are controlled before testing the model against experimental data. Simple tests are used to check the mathematics and the accuracy of the solver.

4.2.2.1 Mathematical error checks

These simply check that the correct mathematics underlie the model. The simplest mathematical checks are to run simulations where the solution, from an alternative source, is known. For example the model was set up to predict the temperature on the dish floor over 10 minutes when the system's uniform initial temperature and the temperature at each boundary was 25 °C. The output was a uniform and consistent 25 °C as expected.

To check that thermal diffusion was accurately predicted by the model, the model output at steady state was compared with a one dimensional analytical solution. The horizontal surface of the dish lid was set to 20 °C and the base set to 40°C. Thermal insulation was applied to the remainder of the exposed boundaries. This enabled the model to be approximated as an infinite slab. The diagram in Figure 4.6 displays the situation used in comparing the COMSOL model with an analytical solution. The model was solved in COMSOL and the temperatures at steady state were taken at the four points where the subdomains interface along the line of symmetry. The temperature at each of these four points was also determined using an analytical solution as described below.

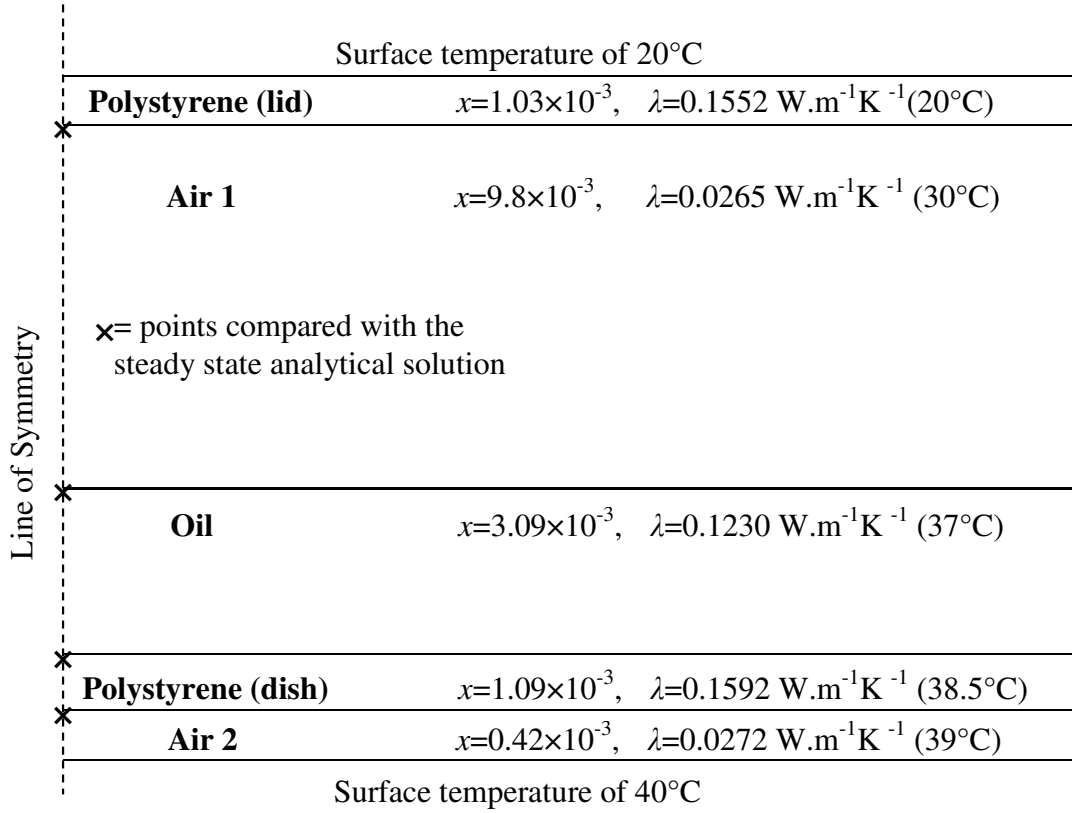

Figure 4.6: A schematic of the comparison between the COMSOL model output with an analytical solution. The boundary condition along the top surface of the lid was set to 20 °C, the base boundary condition was set to 40 °C, and the boundary conditions along the line of symmetry and the dish walls were set to thermal insulation. The thickness (x) and thermal conductivity (λ) of each subdomain are presented. The temperatures at which individual thermal conductivities were calculated are displayed in brackets.

The thermal resistance across each subdomain was calculated and from these the total heat flux across the dish was calculated;

$$R_{polystyrene(lid)} = \frac{x}{\lambda} = 0.006636 \text{ m}^2\text{K.W}^{-1}$$

$$R_{air1} = \frac{x}{\lambda} = 0.3457 \text{ m}^2\text{K.W}^{-1}$$

$$R_{oil} = \frac{x}{\lambda} = 0.02512 \text{ m}^2\text{K.W}^{-1}$$

$$R_{polystyrene(dish)} = \frac{x}{\lambda} = 0.006847 \text{ m}^2\text{K.W}^{-1}$$

$$R_{air2} = \frac{x}{\lambda} = 0.01544 \text{ m}^2\text{K.W}^{-1}$$

$$q = \frac{\Delta\theta}{\Sigma R} = \frac{40 - 20}{0.0066366 + 0.34566 + 0.025122 + 0.0068467 + 0.015441} = 50.029 \text{ W.m}^{-2}$$

As the same flux will occur through each layer, the temperature of each interface point could be calculated. These are compared to the steady state temperatures from the COMSOL solution in Table 4.4. The greatest percentage difference between the two solution types at an interface is a negligible 0.05% (a difference of 0.02 °C) which suggests that the model has been implemented correctly.

Interface	COMSOL Model Steady State Temperature	Analytical Steady State Temperature	% Difference
Polystyrene (lid) – Air1	20.33 °C	20.33 °C	0.00%
Air1 – Oil	37.61 °C	37.63 °C	0.05%
Oil – Polystyrene (dish)	38.87 °C	38.88 °C	0.025%
Polystyrene (dish) – Air2	39.22 °C	39.23 °C	0.025%

Table 4.4: A comparison of the COMSOL solution with the Analytical solution at steady state

4.2.2.2 Solver accuracy checks

Solver parameters including mesh density and the relative tolerance (controls the error in the integration steps) may affect the accuracy of the prediction. The finer the mesh (the more elements) and the lower the relative tolerance, the more accurate the prediction will be. This means there are more calculations for the computer to process and it will take longer and may not run to completion (memory dependent). In

addition, too small time steps can result in rounding errors. Therefore accuracy must be balanced with suitable simulation settings to ensure that the model solution runs and is stable.

A typical situation was simulated multiple times. The mesh density and relative tolerance were varied whilst holding the other constant. The initial temperature of the system was set to 25 °C, the base boundary to 37 °C and the exposed boundaries to 25 °C with a convective heat transfer coefficient of 12 $W.m^{-2}K^{-1}$. The estimated temperatures at the centre floor of the dish at t=5 minute and t=2 hours are displayed in Table 4.5.

The estimated temperatures at t=5 minutes across all variations of mesh density and relative tolerance ranged between 36.6136 °C and 36.6150 °C; a range of only 0.0026 °C. Any difference in temperature of this magnitude is insignificant to the requirements of this model. In addition after 2 hours all simulations had stabilised at 36.2465 °C demonstrating that the model is stable; there was no error accumulation in this time frame.

Thus all subsequent simulations were run with a relative tolerance of 0.01. A minimum standard for the mesh density of ~7000 elements was used for this work which allowed the simulation to run efficiently and without memory issues compared to higher mesh densities.

Solution Parameters	Range	Solutions at the 5 minutes
Mesh Density (reltol of 0.01)	**High value:** 12,200 elements	36.6150 °C
	Low value: 3,600 elements	36.6143 °C
Relative Tolerance (reltol) (mesh density of ~7000 elements)	**High value:** 0.01	36.6144 °C
	Low value: 0.005	36.6136 °C

Table 4.5: Comparing the model output (Temperature (°C) at t=5 min and t=2 min) for defined high and low values of the mesh de

4.3 The Monte Carlo simulation

A purpose of developing this model is to predict the range of temperatures embryos are exposed to in a step in the culture process. A Monte Carlo simulation can be used which runs the model using values of all the input parameters selected randomly from their distribution. In this work it was assumed that each variable had a normal distribution. Running multiple simulations in this way produces a distribution of temperatures at any point in time. This methodology identifies a possible range of temperature predictions within which one would expect the 'mean' of the real experimental data to fall given the variability of the model input parameters (Cronin & Gleeson, 2006).

Monte Carlo analysis was used to characterise the impact of the uncertainty present in the estimates of thermophysical properties. Human controlled factors (such as oil height and droplet volume) were not included because they could be controlled within tight bounds (the effect of variations in these during clinical practice was explored in latter sections).

In order to implement a Monte Carlo simulation a value for the standard deviation of every thermophysical property was required. Where possible the standard deviation was determined from experimental data or, if it was explicitly stated, taken from the literature. Where this was not possible, the reported range or estimated error was used to estimate the standard deviation. The estimate of the standard deviation was calculated by assuming that the standard deviation is equal to a quarter of this range or half the error value. Assuming a normal distribution, 95% of all values are expected to lie within two standard deviations of the mean. Therefore estimating the standard

deviation as a quarter of the range will be most accurate when the specified dataset had extreme values which fell close to these limits. This will likely be true for typical datasets which contain sufficient samples to reflect the majority of the population, but few enough samples to make the presence of extreme outliers unlikely. This assumption will be inaccurate when the sample size was very small however it represents the best compromise likely to cover the greatest number of datasets.

4.4 Parameter estimation

The final model must be able to produce reliable predictions upon which decisions about future work may be based. For this to be possible the values of the model's subdomain parameters, the thermophysical properties of each subdomain (media, paraffin oil, polystyrene, and air), are required.

Every parameter was defined as an equation representing its temperature dependency. An estimate of the standard deviation of the data was defined for use in the Monte Carlo simulations. The equations defining each of the thermophysical properties and their errors are presented in Table 4.6 and discussed below.

Media (water)

Culture media (G5 Series, Vitrolife, Kungsbacka, Sweden) is a dilute aqueous solution (all 280±5 $mOsm.kg^{-1}$) and was therefore assumed to have the same thermophysical properties as water. Values of thermal conductivity, heat capacity, and density are available in a large number of engineering textbooks (examples include Perry et al., 1997; Dincer, 2003; and Tennent, 2001) to a high degree of accuracy over a wide range of temperatures. Equations 1, 2, and 3 (2^{nd} order polynomials) in Table

4.6 define the parameters of water with respect to their temperature dependency. The percentage error margin of "within 3.9%" was generalised, encompassing other parameter equations for more complex food substances published together in Choi & Okos (1986), and therefore, given the defined nature of water, is likely an overestimate of actual error. This is suitable as any overestimate of error will most likely compensate for slight differences between pure water and embryo culture media. It will be assumed, for Monte Carlo simulations that the standard deviation is 1.95% (half the assumed error).

Paraffin oil

The range of values available in the literature for paraffin oil was limited. As the means to measure the density and heat capacity of the paraffin oil used at Fertility Associates (OVOIL-100, Vitrolife, Kungsbacka, Sweden) was available, they were determined experimentally.

To determine the density a 10 ml density bottle was weighed, filled with the oil at room temperature (22 °C) and reweighed. This was repeated a further four times (n=5). The same set of experiments was carried out at both 30 °C and 37 °C in order to define the parameter's temperature variation. The data with a linear fit is shown in Figure 4.7, and the equation representing this line of best fit is presented in Equation 4 of Table 4.6. The greatest standard deviation at a single temperature (30 °C) was used in Monte Carlo simulations (a value of 0.024 % at 30 °C). The measured density values are within 5.5 % of the value (of 800 kg. m^{-3}) presented in Tennent (2001).

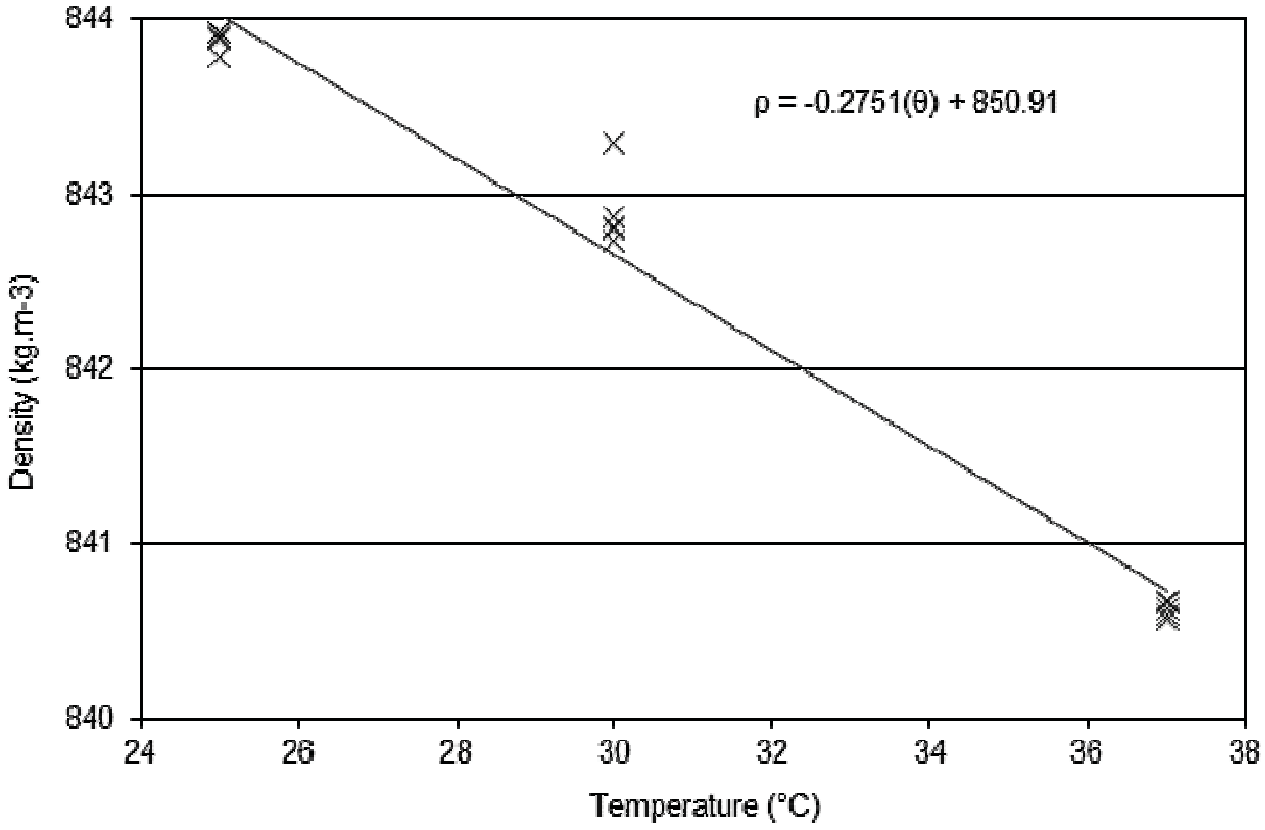

Figure 4.7: The measured densities of paraffin oil are displayed at 25, 30 and 37 °C (×). A linear best fit was applied to the data and is presented in equation form.

The heat capacity of paraffin oil was determined experimentally by differential scanning calorimetry in a DSC Q100 with a DSC refrigerated cooling system (TA instruments, Michigan USA). The method used was described by Yang et al. (1997).

Calibration of the instrument was attained with sapphire and indium standards. Samples were held in hermetic aluminium pans, the chamber purged with dry nitrogen, and a ramp test was run, heating from -20 to 60 °C at a constant rate of 5 $°C.min^{-1}$. A blank curve was obtained with an empty hermetic aluminum pan. The ramp test was carried out on five samples (~20 µl); the mass of each sample was recorded. Each sample was re-weighed after completion of the run to confirm no sample loss.

The blank curve was subtracted from each sample run and the heat capacity calculated over the temperature range at every step in temperature (intervals of approximately 0.02 °C). Figure 4.8 displays the mean heat capacity (n=5) ± 2× the standard deviation over the temperature range 10-40 °C. The greatest standard deviation, for use in Monte Carlo simulations, was 2.3%. A 2nd order polynomial was fitted (displayed in Figure 4.8) to the experimental data to provide an equation (Table 4.6, Equation 6) defining the heat capacity's temperature dependency. The mean value of the heat capacity is within 12% of the single value of 2130 J.kg^{-1}K^{-1} presented in Tennent (2001) at temperatures above 20 °C.

Kaye & Higgins (1928) reported experimental data for the thermal conductivity of liquids including medicinal paraffin (paraffin oil). A linear equation was derived from this data to define the temperature dependency of medicinal paraffin (Table 4.6, Equation 5). A conservative error estimate of ± 5%, and therefore an assumed standard deviation of 2.5% for Monte Carlo simulations, was applied.

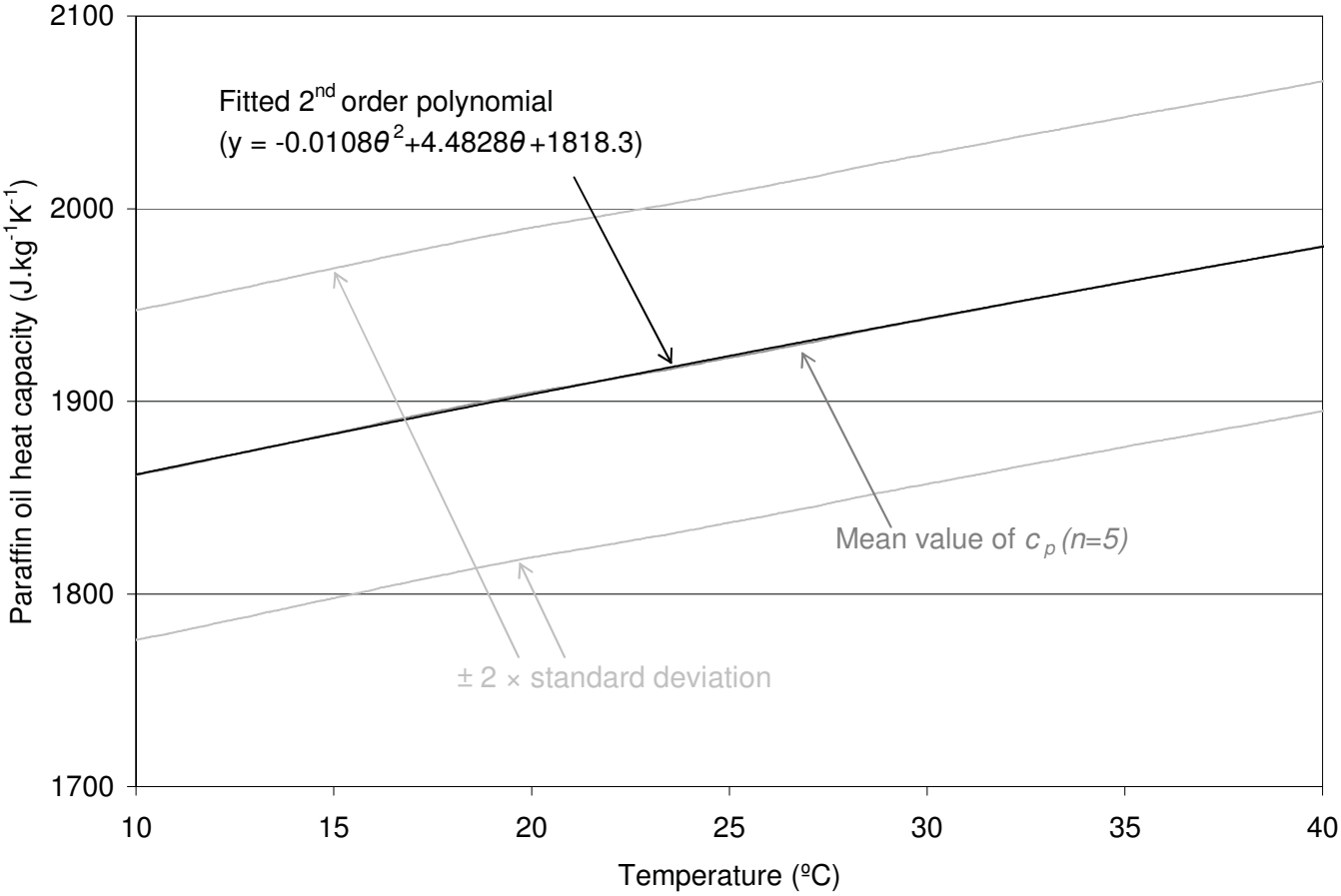

Figure 4.8: The experimentally determined heat capacity of paraffin oil. The mean heat capacity (n=5) ± 2 × standard deviation is displayed. A 2nd order polynomial is fitted to the mean ($c_o = -0.0108\theta^2 + 4.4828\theta + 1818.3$).

Polystyrene

The density of polystyrene was presented by Fox and Flory (1949) as a temperature dependent linear relationship. The authors stated that the reproducibility of the data "was generally within ±0.1%". A linear relationship (Table 4.6, Equation 9) was used to represent the temperature dependency of the heat capacity of polystyrene as presented by Abu-Isa and Doyle (1965) with an experimental uncertainty of ± 0.5% (over the temperature range -50-65 °C). Given the small error margins presented for these two values a conservative error estimate of ± 5%, and therefore an assumed standard deviation of 2.5% for Monte Carlo simulations, was assumed.

Carwile and Hoge (1966) presented a thorough review on published values of the thermal conductivity of polystyrene and selected best values. These values were believed to be correct within ± 6% between room temperature and 120 °C. A 2nd order polynomial (Table 4.6, Equation 8) was fitted to this data to define the temperature dependency. For Monte Carlo simulations it was assumed that the standard deviation is 3% (half the presented error).

Air

The thermophysical properties of air are well characterised and may be found in a range of literature sources. Second order polynomials were fitted to the data presented in Geankoplis (2005) for all three parameters. Given no estimate of variability was presented for the data a conservative error estimate of ± 5%, and therefore a standard deviation of 2.5%, for Monte Carlo simulations was assumed.

Parameter	Units	Equation	Equation #	SD	R
ρ_m	kg.m^{-3}	$\rho_m = 9.9718\times10^{2} + 3.1438\times10^{-3}\theta - 3.7574\times10^{-3}\theta^{2}$	1	1.95%$^{+}$	Cl
λ_m	W.m^{-1}K^{-1}	$\lambda_m = 5.7109\times10^{-1} + 1.7625\times10^{-3}\theta - 6.7036\times10^{-6}\theta^{2}$	2	1.95%$^{+}$	Cl
c_m	J.kg^{-1}K^{-1}	$c_m = 4176.2 + 9.0864\times10^{-2}\theta - 5.4731\times10^{-3}\theta^{2}$	3	1.95%$^{+}$	Cl
ρ_o	kg.m^{-3}	$\rho_o = -0.2751\theta + 850.91$	4	0.026%*	Ex
λ_o	W.m^{-1}K^{-1}	$\lambda_o = -7\times10^{-5}\theta + 0.1257$	5	2.5%	K
c_o	J.kg^{-1}K^{-1}	$c_o = -0.0108\theta^{2} + 4.4828\theta + 1818.3$	6	2.3%*	Ex
ρ_p	kg.m^{-3}	$\rho_p = \frac{1}{0.00025\theta + 0.943}\times1000$	7	2.5%	Fo
λ_p	W.m^{-1}K^{-1}	$\lambda_p = -2\times10^{-6}\theta^{2} + 0.0003\theta + 0.1488$	8	3%$^{+}$	Ca
c_p	J.kg^{-1}K^{-1}	$c_p = 4.2873\theta + 1086.5$	9	2.5%	Al
ρ_a	kg.m^{-3}	$\rho_a = 8.8\times10^{-6}\theta^{2} - 4.34\times10^{-3}\theta + 1.2904$	10	2.5%	Ga
λ_a	W.m^{-1}K^{-1}	$\lambda_a = -9.63\times10^{-9}\theta^{2} + 7.596\times10^{-5}\theta + 0.0242$	11	2.5%	Ga
c_a	J.kg^{-1}K^{-1}	$c_a = 5.12\times10^{-4}\theta^{2} + 8.612\times10^{-3}\theta + 1004.66$	12	2.5%	Ga

Table 4.6: Model Parameter Inputs and Error. Parameters: ρ=density, λ=thermal conductivity, c= heat capacity. Subscripts: m=m

The standard deviations were determined from experimental data (*), derived from variability data presented in the literature ($^{+}$), or

Estimating the convective heat transfer coefficient

The heat transfer coefficient was calculated from experimentally determined values for a dish in both the still laboratory air and a laminar flow hood (air velocity = 0.5 $m.s^{-1}$). This approximates the range of values which are applicable to a Petri dish in the lab setting.

A Petri dish, without its lid, was equilibrated on a hot block in both environments. The steady state temperatures of the air, centre floor of dish and surface of the hot block were recorded and the thermal conductivity of each layer between the air and hot block (oil, polystyrene floor and air) were calculated (from equations presented in Table 4.6) at appropriate temperatures. The heat flux is predominantly vertical and therefore it may be assumed that the dish is an infinite slab and therefore that the calculation is one dimensional. The heat flux from the stage surface to the dish floor can be calculated from the known heat transfer resistances and the measured temperature difference. At steady state this heat flux is equal to that lost by convection, therefore an estimate of the heat transfer coefficient can be made. The calculations for the convective heat transfer coefficient in both situations are displayed in Table 4.7.

The convective heat transfer coefficient at the dish boundary in the relatively still laboratory air was found to be ~13 $W.m^{-2}K^{-1}$. This is less than half the value found in the laminar flow hood (29 $W.m^{-2}K^{-1}$). Therefore in a laboratory environment the convective heat transfer coefficient may feasibly range between 10 $W.m^{-2}K^{-1}$ and 30 $W.m^{-2}K^{-1}$ depending on the air flow conditions. This calculated range is sufficiently wide to have a large impact on model simulations. Therefore, for model validation,

the convective heat transfer coefficient was defined independently for the different geometries modelled in this thesis (Petri dish, 4-well dish, glass Pasteur and plastic pipette tips), as described in Section 4.5.3.

	Laminar flow hood	Still air
θ_{air}	28.57 °C	27.84 °C
$\theta_{\text{dish floor}}$	36.87 °C	38.41 °C
$\theta_{\text{surface hot block}}$	39.98 °C	40.73 °C
$R_{oil} = \frac{x}{\lambda}$	$\frac{3.09e^{-3}}{0.1234} = 0.02504$ m^2.K.W^{-1}	$\frac{3.09e^{-3}}{0.1232} = 0.02508$ m^2.K.W^{-1}
$R_{polystyrene} = \frac{x}{\lambda}$	$\frac{1.09e^{-3}}{0.1589} = 0.006860$ m^2.K.W^{-1}	$\frac{1.09e^{-3}}{0.1591} = 0.006851$ m^2.K.W^{-1}
$R_{air} = \frac{x}{\lambda}$	$\frac{0.42e^{-3}}{0.0272} = 0.01544$ m^2.K.W^{-1}	$\frac{0.42e^{-3}}{0.0272} = 0.01544$ m^2.K.W^{-1}
$q = \frac{\Delta\theta}{\Sigma R}$	$\frac{39.98 - 36.87}{0.01544 + 0.006860} = 139.46$ W.m^{-2}	$\frac{40.73 - 38.41}{0.01544 + 0.006851} = 104.08$ W.m^{-2}
h	$\frac{39.98 - 28.57}{0.01544 + 0.006860 + 0.02504 + \frac{1}{h}} = 139.46$	$\frac{40.73 - 27.84}{0.01544 + 0.006851 + 0.02508 + \frac{1}{h}} = 104.08$
	$h = 29.006$ W.m^{-2}K^{-1}	$h = 13.075$ W.m^{-2}K^{-1}

Table 4.7: Calculations for the convective heat transfer coefficient (h) in still laboratory air and in the laminar flow hood (air flow ≈ 0.5 m.s^{-1}).

4.5 Model validation

The purpose of model validation was to determine whether or not the model is able to accurately predict the temperatures which occur within the dish system in a real life situation in the laboratory. Experimental work was carried out to provide data for two purposes:

1. To provide data set(s) for comparison with the model predictions at the point(s) of interest in the model (i.e. centre floor of the dish).
2. To provide input data for the model's initial conditions and boundary conditions.

In this section the experimental equipment and methodology are described, and the results presented.

Validating the model in a simple, controlled experimental situation has a number of benefits. Experimental data collection is simplified thereby minimising error in the data. The complexity of the initial conditions and boundary conditions are minimised making it easier to attribute discrepancies between the model and the experimental data to parameter(s) within the dish model. Therefore the dish model was validated for pre-equilibration of a Petri dish, initially fully equilibrated on the bench top to the ambient laboratory temperature, to 37 °C° in a dry Sanyo incubator. Pre-equilibration of the Petri dish takes place prior to dish use in the process as in steps 5.5a and 9.2.8a as defined in the process flow diagram (Figure 3.10).

4.5.1 Equipment

4.5.1.1 Temperature measurement

Requirements

The equipment for the validation experiments had to meet the following requirements:

- Temperatures must be measured and logged continuously.

- The temperature probe itself should be minimally invasive (have minimal impact on the measured temperature).
- The temperature probe should have a rapid response time to enable accurate measurement of the dynamics.
- The temperature probe should be easily positioned at the position of an embryo for the duration of the experiment.
- It should be possible to carry out multiple measurements; collecting data for the boundary conditions and point(s) of interest.

Thermocouples

Thermocouples proved to be the most appropriate means of temperature measurement for this application. A thermocouple is simply a closed circuit formed by two unlike conductor wires around which a current flows when a temperature difference exists between two junctions, for measurement and for reference. The voltage which produces the current is dependent on this temperature difference.

To measure at the small point of interest – the position of an embryo – is a challenge. Thermocouples have fewer limitations with respect to their physical size than other forms of contact sensor. K Type thermocouples were chosen with a wire diameter of 150 μm and a solder junction.

Agilent data logger

The Agilent data logger (34970A Data Acquisition Switch Unit, Agilent Technologies, Santa Clara CA) enables simultaneous temperature measurement with multiple thermocouples and continuous data collection in small time steps (1 second

used throughout this work). This measurement hardware was connected via serial port to a computer where the data was collected by the Agilent Benchlink Data Logger Software, enabling monitoring and easy export of data.

4.5.1.2 Incubator

In the Sanyo incubator (MCO-5M: 1.7 cu. ft. CO2 Cell Culture Incubator, SANYO Biomedical, Wood Dale IL) dishes sit on metal trays within a chamber which is controlled to the required temperature by natural convection from heating elements within the chamber floor, walls and door. The incubator was dried by replacing the water tray with a dish of silica gel crystals. This removed any effects the humidity may have on heat transfer properties and the potential for evaporative effects.

A plastic tray with a low plastic to air surface ratio was placed into the incubator in preference to the incubator's own metal tray. This low ratio significantly reduces dish-tray contact and allows air to pass freely beneath the dish. This enables the air gap under the dish to be excluded from the model and the boundary condition to be considered uniform at all outer surfaces of the dish.

4.5.2 Experimental methodology

Prior to an experimental run, a two point calibration of the thermocouple was carried out against a calibrated platinum electrode in an ice-water slurry at 0 °C and a water bath at 37 °C.

The Petri dish was set up on the bench top in the laboratory (ambient air temperature of 25-27 °C). Figure 4.9 displays a photograph of the thermocouple set-up as described below. The thermocouple measuring the centre floor temperature of the dish was positioned across the floor of the dish (perpendicular to the major direction of heat flux), carefully ensuring that the thermocouple's junction was in contact with the dish floor. The thermocouple was held in position by small strips of aluminium tape. Aluminium tape is thin, has a high thermal conductivity and low heat capacity and so has minimal interference with temperature gradients in the dish. Potential for interference was further minimised by avoiding placement of the tape over the thermocouple's junction. 7.5 µl of medium was pipetted onto the junction of the thermocouple at the centre floor of the dish and 7.5 ml of oil overlaid. The 5 µl of medium was then removed and replaced with 15 µl of media to create the drop. Once prepared, the dish was left on the bench adjacent to the incubator to equilibrate to the ambient air temperature.

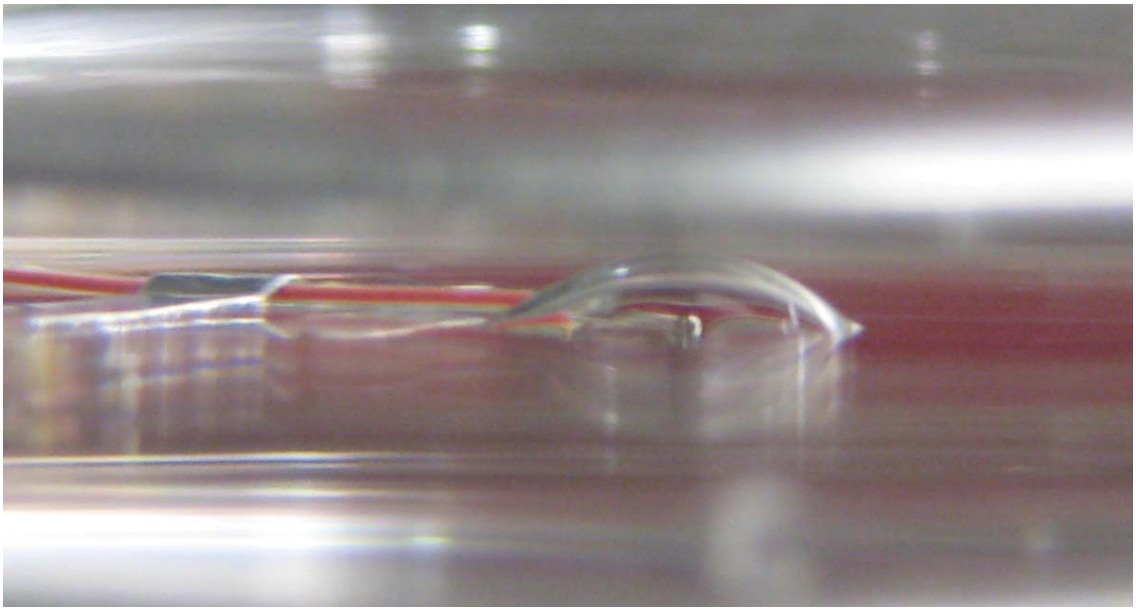

Figure 4.9: Photograph of a thermocouple with the junction positioned at the centre floor of a Petri dish overlaid with a media drop.

Two thermocouples were positioned within the incubator to measure the air at the side (front and back) of the dish position. The small diameter of the thermocouple wire allowed them to pass through the seal around the incubator door with ease, avoiding any mechanical damage.

Data collection commenced once the dish had reached a steady state temperature (the measured temperature on the dish floor had changed by <0.1 °C over a 5 minute period). The temperature was measured for a minimum of two minutes without moving the dish off the bench in order to collect data for the initial temperature of the dish and to demonstrate it was constant. The dish was then carefully transferred onto the tray in the incubator. Disturbance of the oil and the length of time the incubator door was open were minimised. Data collection continued until the measured temperature in the dish had reached steady state. The measured temperatures of each thermocouple were adjusted based on the two point calibration data.

4.5.3 The boundary conditions

Every surface of the dish and therefore external boundary of the model was exposed to the air in the incubator. The condition at this boundary is described by Equation 4.8. Therefore, as discussed in Section 4.4, the convective heat transfer coefficient (h) within the incubator must be defined. To define the heat transfer coefficient (h) the experiment for model validation was carried out five times. Simulation outputs from models using the best estimate of each input parameter but varying h (incrementally by 0.5 $W.m^{-2}K^{-1}$) were compared with each set of experimental data and the best fit was estimated by sight (thus estimating h to the nearest 0.5 $W.m^{-2}K^{-1}$. The outcome was a mean of 12 $W.m^{-2}K^{-1}$ with a standard deviation of 1 $W.m^{-2}K^{-1}$.

4.5.4 Model validation

Figure 4.10 displays the data collected while equilibrating a dish to 37 °C in a dry Sanyo incubator. The measured incubator air temperature provided a temperature data set for the exposed boundary condition of the dish. Due to the air temperature of the incubator recovering to 99.5% of its initial temperature within 30 seconds after the door was opened, a single air temperature value of 36.9 °C (the average steady state incubator air temperature) was applied to the exposed boundary with a convective heat transfer coefficient of 12 $W.m^{-2}K^{-1}$ as defined in the previous section. The initial temperature of the dish model was set to 25.4 °C; the initial steady state temperature of the dish on the bench (where $t<0$).

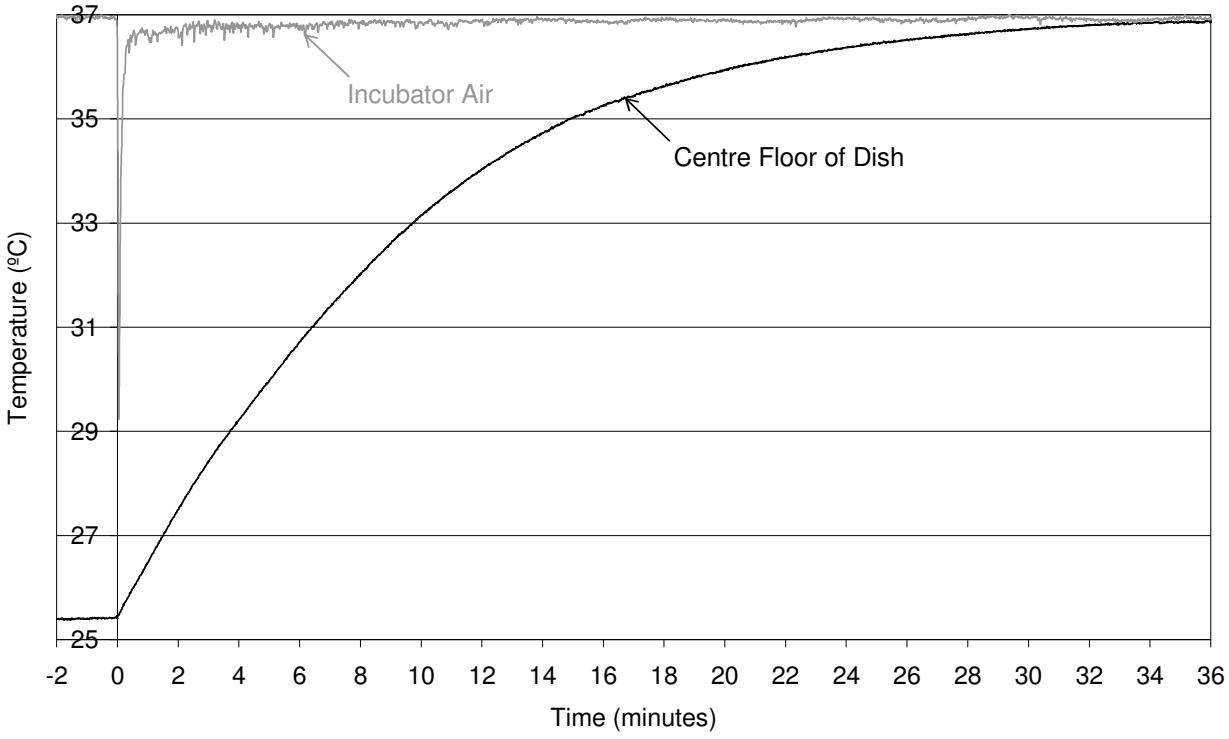

Figure 4.10: Experimentally measured temperatures at the centre floor of a Petri dish and in an incubator as the dish (initially 25.4 °C) was placed into the incubator at t=0 (with opening and closing of the incubator door) and equilibrated to the incubator temperature (36.9 °C). Oil depth (H_o) = 3.06 mm, foot height (*xb-xf*) = 0.40 mm, thickness of dish floor (*xf*) =1.12 mm.

Monte Carlo simulations were run with the initial conditions and boundary conditions described above. The thermophysical properties and their standard deviations were used as defined in Table 4.6. The oil mass (5.48 g) was measured and its depth calculated (3.06 mm) and the thickness of the base of the dish (1.12 mm) and the foot height of the dish (0.40 mm) were measured.

Forty Monte Carlo simulations were run. After every simulation the standard deviation was calculated at every time step for all the existing simulations. The maximum standard deviation across time steps for any given run was determined. Figure 4.11 is a plot of the maximum standard deviation of the first 'n' samples vs. the number of simulations (n). After approximately 30 simulations the standard deviation levels out and stays relatively constant indicating that there is little change in the data spread. This analysis shows that additional Monte Carlo simulations were not required. A similar analysis was carried out in all Monte Carlo simulations for the remainder of this thesis.

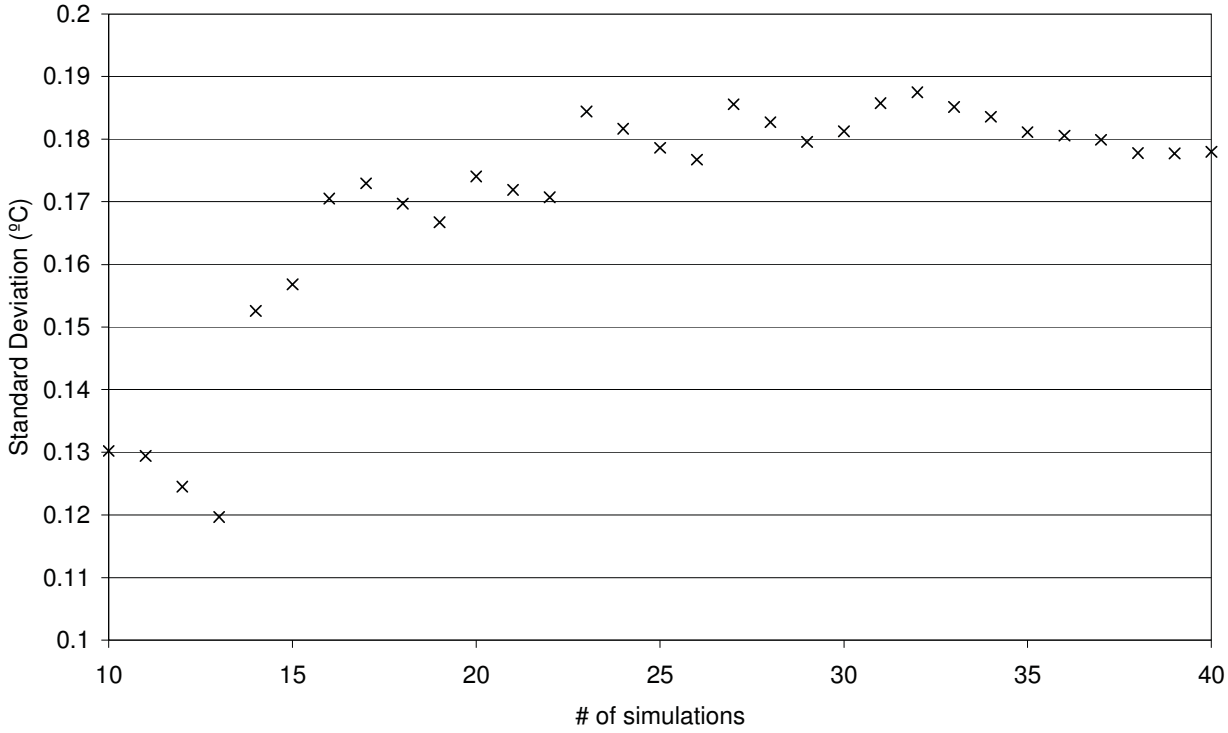

Figure 4.11: The maximum standard deviation for the first 'n' simulations (over the simulation's time steps) vs. the number of simulations run (n) for equilibration of a Petri dish.

The model can only be validated against a single experimental run since input parameters, such as dish dimensions, oil depth and initial conditions, are specific to an individual run. A good model fit was defined when the experimental data fits within the mean ± 2 standard deviations of this simulation since we would expect any random data set, such as an experimental run, to fall between these limits 95% of the time. This definition of model fit is only valid if the distribution of the Monte Carlo simulation output is normal (or at least approximately so). Figure 4.12 demonstrates that the distribution of the Monte Carlo simulations, while skewed slightly toward higher temperatures, is close to normal justifying this approach. It is worth noting that the model output being sufficiently normal is not a given. In general the distribution of the output of a model will be affected by the action of the model itself on the input parameters. Hence, as has been done here, the distribution of the model

output should be checked if conclusions which rely on a certain output distribution are to be drawn.

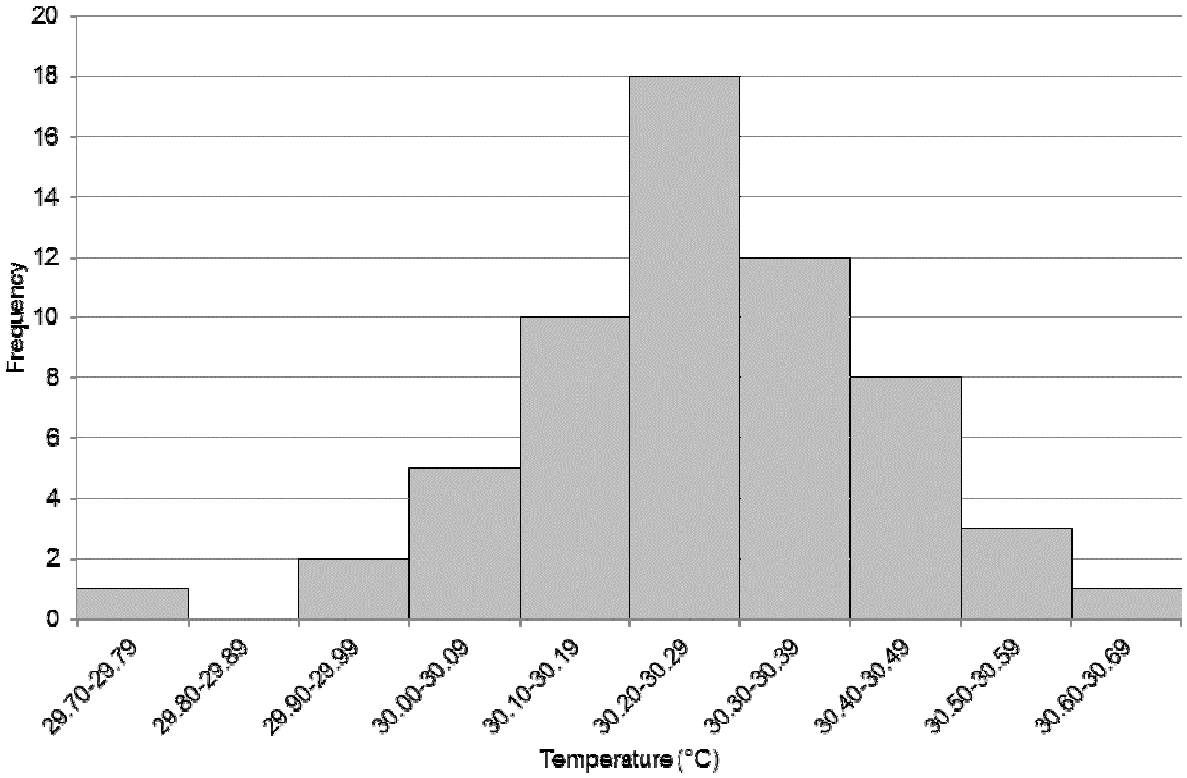

Figure 4.12: A histogram displaying a typical example of the temperature frequency of 60 Monte Carlo Simulations (at t=5 minutes) for equilibration of a Petri dish.

The comparison between the mean simulation (± 2 standard deviations) and the experimental data is displayed in Figure 4.13. The experimental data remained within two standard deviations of the mean simulation output, validating the model. The width of this prediction band does not exceed 0.59 °C.

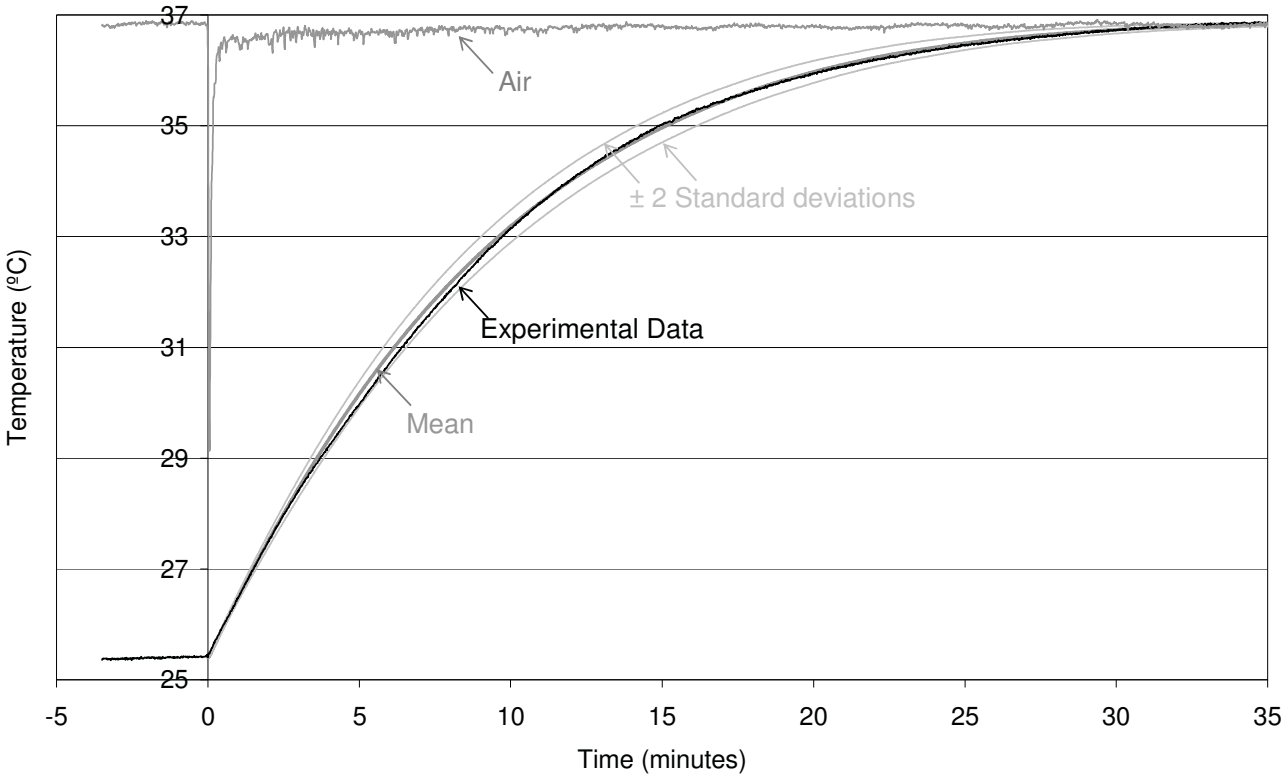

Figure 4.13: Measured temperature rise at the centre floor of a well of a Petri dish compared with the model simulation output (mean ± 2 standard deviation, 30 Monte Carlo simulation outputs) after placement into an incubator at t=0. Oil depth (H_o) = 3.06 mm, foot height (xb-x_f) = 0.40 mm, thickness of dish floor (xf) =1.12 mm.

While only a single validation experiment is presented here four were carried out for a Petri dish equilibrating in a dry incubator. The model displayed a good fit with the experimental data in every case and the difference between the model and the experimental data did not exceed 0.3 °C. The model is further validated in Chapter 5 through comparison with experimental data for a number of other steps in the culture process.

Validating the model against data collected during Petri dish pre-equilibration enabled information to be collected about Petri dish temperature pre-equilibration in the culture process (steps 5.5a and 9.2.8a in the process flow diagram, Figure 3.10). The

temperature at the centre floor of a Petri dish, initially at room temperature, equilibrates to within 0.3 °C of the incubator temperature in 28 minutes. It is standard practice to pre-equilibrate dishes overnight prior to use to ensure the gaseous and thermal environment is optimal for embryos when they are transferred into a dish. However, shortening this equilibration time is potentially beneficial since degradation of amino acids to ammonium increases with temperature (As discussed in section 2.6.4). Limiting the exposure of the culture media to 37 °C will limit ammonium production which is potentially beneficial since ammonium is embryo toxic. Thermal pre-equilibration for <1 hour prior to embryo placement into the dish will enable embryo placement into media at 37 °C media while limiting the exposure of the culture media to 37 °C.

A <1 hour pre-equilibration time, while sufficient for thermal equilibration to 37 °C, may not be an adequate period for equilibration of oxygen and CO_2 (thus pH). Before any practical recommendations with respect to the period of pre-equilibration may be made, the time required for equilibration of oxygen and CO_2 (thus pH) must be addressed.

4.6 Summary

A model of heat transfer within the Petri dish drop culture system was developed and validated within this chapter. This model may be applied for the following purposes:

- To investigate more complex thermal boundary conditions which are present throughout the embryo culture process.
- To identify factors in the environment which have a significant impact on heat transfer to and from the dish floor (an embryo's position).

- To predict changes to an embryo's temperature given changes in boundary condition or dish geometry.

Validation of the model for pre-equilibration of a Petri dish identified that the temperature at the centre floor of a Petri dish (initially at room temperature) equilibrates to within 0.3 °C of the incubator temperature in 28 minutes. This suggests that shortening the current overnight pre-equilibration may be a possibility but no recommendations can be made until pre-equilibration of oxygen and carbon dioxide have been assessed.

For this model the thermophysical properties of air, culture media (water), paraffin oil and the polystyrene dish were defined. These properties may be applied when modelling other systems throughout the culture process such as the 4-well dish, which involves identical materials in a different geometry, and the pipettes, which can contain air, paraffin oil and culture media.

5 Petri dish model application

The purpose of this chapter is to apply the model of heat transfer in a Petri dish, as validated in Chapter 4, to steps in the culture process in order to characterise the temperatures embryos are subjected to, the main factors which influence the thermal environment and the limits (due to setup, time and equipment) to temperature control.

5.1 The Petri dish as part of the culture process

The Petri dish is an integral component in the culture process used widely in IVF laboratories worldwide. Its exact use frequently differs between clinics in terms of the steps in which it is utilised and the protocol for setting up media and oil in the dish (volumes and drop placement). Input parameters to the Petri dish model, validated in Chapter 4, may be altered in order to simulate multiple dish set ups and situations. However, for the purpose of this section, the dish set up and the process steps used at Fertility Associates (as described in Chapter 4 Section 4.1 and Chapter 3 respectively) will be the focus.

5.1.1 Process steps

When a Petri dish is used to hold embryos the following steps are likely to take place:

- Equilibration of a dish in a humidified incubator
- Transfer of a Petri dish (from the incubator onto a heated surface)
- Placement of a dish onto a heated stage for embryo manipulation
- Lid removal for embryo manipulation
- Lid replacement after completion

- Transfer back into the humid incubator
- Re-equilibration in the incubator

5.2 Equilibration of a Petri dish

Pre-equilibration of a Petri dish in an incubator from room temperature to 37 °C was the step in the process for which the model was validated in Chapter 4. Pre-equilibration of a Petri dish is represented by steps 5.5a and 9.2.8a as defined in the process flow diagram (Figure 3.10). The temperature at the centre floor of the dish reached within 0.3 °C of full equilibration (37 °C) in 28 minutes.

In the laboratory the temperature of the dish contents as it is placed into the incubator will vary. All dishes required for the following day are set up together in a laminar flow hood at room temperature. The culture media and paraffin oil are initially at fridge temperature (4 °C) however throughout the process of setting up all the dishes paraffin oil is transferred into dishes which, without their lids on, sit for an extended period while media drops are added. The process of dish set up may take more than an hour but it varies depending on the number of dishes required for the following day and the embryologist completing this task. It is reasonable to assume that the dish contents are close to, if not at, room temperature by the time a dish is transferred into an incubator.

It was assumed (Section 4.1.3.2) that the humidity of the incubator would not significantly impact on the temperatures embryos are exposed to within a Petri dish since calculations showed that condensation of water out of the air within the dish when removed from the incubator would negligibly affect the temperature of the dish

system. Therefore it was not considered in the model. The incubators were dried out to ensure this assumption was valid and to remove any affect the humidity may have on the heat transfer properties. To investigate the general validity of this assumption experimental data for the equilibration of a dish in a humid incubator was collected. This data is compared with the model simulation (mean ± 2 standard deviations of 30 Monte Carlo simulations), which applies the thermophysical properties of dry air, in Figure 5.1.

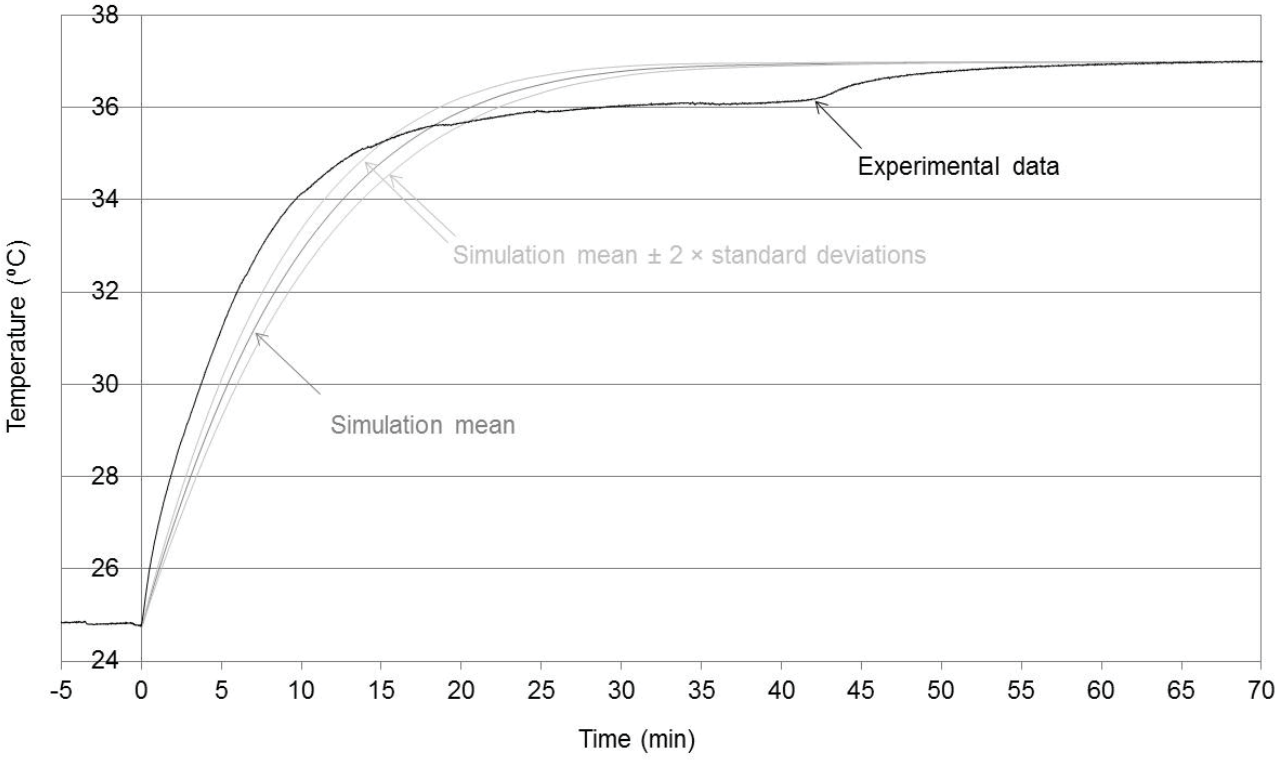

Figure 5.1. Experimentally measured temperature rise at the centre floor of a Petri dish (containing 7 ml of oil) as it is placed into a humid incubator (t=0). This is compared with the modelled temperature rise (mean ± 2 standard deviations of 30 Monte Carlo simulations). Dish system initially at 24.7 °C, incubator air temperature = 37 °C, h = 12 $W.m^{-2}K^{-1}$.

There are clear discrepancies between the experimental data and the simulation output as the experimental data reaches an intermediate steady state at approximately 36.1 °C before it equilibrates to the incubator temperature (37 °C).

At t=0 a cool dish (≈25 °C) is placed into the humid, 37 °C air in the incubator. The air surrounding the dish cools and consequently holds less water. Water condenses onto the surface of the dish and the temperature of the dish system begins to rise quicker than the model predicts. As the dish system heats, the water on the dish surface begins to evaporate. The intermediate steady state at ≈36.1 °C (the temperature reaches within 0.3 °C of this value after ≈23 minutes) is the temperature at which the rate of heat gained from the incubator equals the rate of heat loss due to the latent heat of evaporation. Once all the water has evaporated the dish heats to the incubator temperature, the final steady state. The temperatures reached to within 0.3 °C of the final steady state value after ≈48 minutes

The implications of this phenomenon are likely not to be significant to an embryo. Placing a cool dish into a humid incubator will only occur for pre-equilibration when there are no embryos in the dish. A dish containing an embryo will be maintained close to 37 °C while outside the incubator which will minimise condensation upon return to an incubator.

In a humid incubator the dish equilibrates to within 0.3 °C of the final steady state value in ≈48 minutes. This is longer than the ≈28 minutes in a dry incubator (as determined in section 4.5.4) but still offers the same potential for shortening the thermal equilibration time.

5.3 Transfer of a Petri dish

In the laboratory dishes are transferred between incubators, stages, and heated blocks. They are hand held or are carried on a tray or specialised dish carrier. This is

potentially a vulnerable time for an embryo as heat is lost to the surrounding air or the carrier (tray, hand etc.). Transfer of a Petri dish was not incorporated as an individual step in the process flow diagram (Figure 3.10) but is represented by the transition between two steps. For example in the transition between steps 6.0 and 6.1 (Figure 3.10) a Petri dish with its lid on is transferred from an incubator onto a heated stage.

The degree of air flow around the dish has a significant impact on heat loss. The higher the air flow around the dish, the lower the resistance to heat transfer and the higher the rate of heat transfer between the dish and surrounding air. This resistance to heat transfer is described mathematically by the convective heat transfer coefficient. Multiple factors contribute to air flow around a dish in the laboratory; the position of air conditioning units, doors and hatches, the movement of people about the laboratory and the speed of dish transfer between incubators and stages.

To simplify the investigation, heat loss from the dish was investigated in two parts. Firstly, it was assumed that heat loss to the carrier is negligible so the system could be approximated by assuming that all external boundaries of the dish were exposed to the laboratory air. Then the impact of a carrier on heat loss from the dish was investigated.

Heat transfer in the oil layer is assumed to be by conduction only. Bulk flow of the paraffin oil in the Petri dish during transfer is minimised since the delicate nature of the dish contents lends itself to careful handling. Any movement of liquid within the dish is easily visualised since the media drops can be seen to move relative to their

base with any oil movement. This allows easy identification of good practice and minimisation.

5.3.1 Heat loss to the laboratory air

Heat loss to the air from a Petri dish may be modelled simply. The boundary condition is uniform for all the external boundaries of the dish. The speed of transport is characterised by variations in the convective heat transfer coefficient.

The data displayed in Figure 5.2 was collected at the centre floor of a dish as it was transferred at a careful, steady pace from an incubator onto an adjacent heated stage. The dish was in the air approximately 20 seconds and the laboratory temperature was approximately 27 °C. Overlaying the experimental data in Figure 5.2 is the output from seven model simulations which differ only in the value of the convective heat transfer coefficient (h) at the boundary: a range from 10 – 22 $W.m^{-2}K^{-1}$.

The experimental data lies within the bands formed by these values of h (10 – 22 $W.m^{-2}K^{-1}$). The convective heat transfer coefficient best representing the movement of the dish in this particular situation is between 16 and 20 $W.m^{-2}K^{-1}$. The value of h is dependent on air flow around the dish. This is due to a combination of the air flow in the laboratory and the movement of the dish relative to the air. The faster the dish is moved, the higher the apparent air flow and the greater the value of h. Air flow around a dish will not be uniform or constant during any transfer and so the theoretical value of h will also vary. In any such situation we must therefore consider a range of values of h.

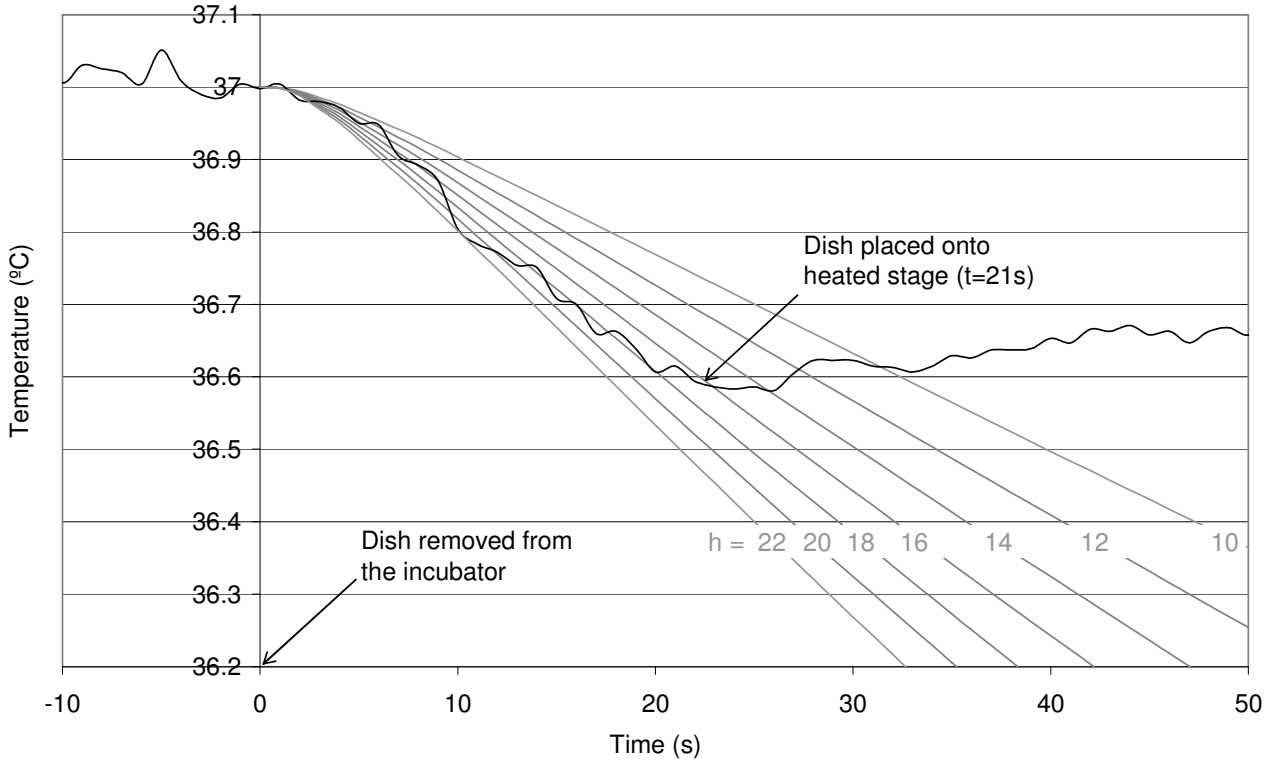

Figure 5.2: Experimentally measured temperature loss from the centre floor of a Petri dish as it was removed from an incubator at t=0 and transferred, at a careful, steady pace, to a heated stage onto which it was placed at t=21 s. Ambient air = 27 °C. Temperature loss from the centre floor of a Petri dish during transfer was modelled in 7 simulations which vary in the value of h (10-22 $W.m^{-2}K^{-1}$).

Figure 5.3 is a graph of more practical use. This looks at three factors which have an impact on heat loss from the Petri dish to the laboratory air during transfer; the convective heat transfer coefficient (h), the laboratory air temperature (θ_a) and the time of transfer. A range of feasible values for both h and θ_a were selected and a model simulation was run with the values of each that resulted firstly in the highest rate (θ_a =18 °C, h=60 $W.m^{-2}K^{-1}$) and secondly in the lowest rate (θ_a=27 °C, h=10 $W.m^{-2}K^{-1}$) of heat transfer between the dish and the surrounding air. Between these two lines lies the range of temperatures the centre floor of the dish may feasibly drop to at every time interval.

In Chapter 4 (Section 4.4) the range of 10 – 30 $W.m^{-2}K^{-1}$ was defined for the convective heat transfer coefficient (h), a range of values which may feasibly exist within a lab for a still dish. When transferring a dish we may consider the convective heat transfer coefficient as dependent on the speed the dish is moved. A worst case scenario value for h of 60 $W.m^{-2}K^{-1}$ was approximated experimentally by briskly walking a dish across the laboratory (at a pace which would be risky if carrying embryos) and fitting the model to the recorded experimental data.

By imposing a lower limit to an embryo's acceptable temperature it is possible to identify time constraints to Petri dish transfer. In Figure 5.3, for example, where the cut-off temperature was set to 36 °C (the lower end of the desired temperature range, Section 3.6), the shaded area represents the times within which a dish may be transferred while its contents remain above 36 °C. This shows that the centre floor of a dish is very unlikely to drop below 36 °C in under 11 seconds, and is very likely to have dropped below 36 °C after 85 seconds. In a small laboratory 11 seconds is a plausible time in which to move a dish from an incubator to a stage.

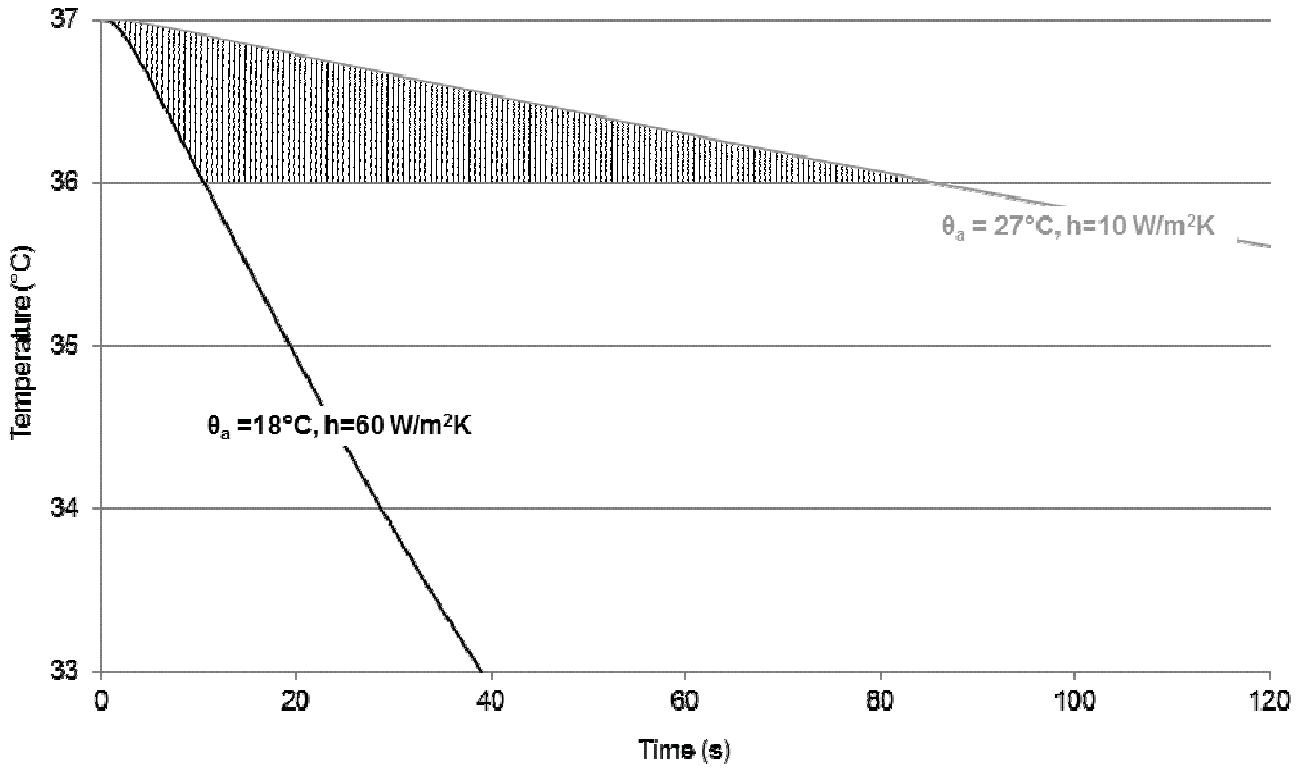

Figure 5.3: The impact of the laboratory environment on heat loss from a Petri dish during dish transfer through air. Values of h and θa were chosen to give a high rate (θa=18 °C, h=60 $W.m^{-2}K^{-1}$) and a low rate (θa=27 °C, h=10 $W.m^{-2}K^{-1}$) of heat transfer between the dish and the surrounding air. The shaded area represents the range of temperatures, above 36 °C, to which the centre floor of the dish may drop at every time interval.

Figure 5.4 takes this approach a step further. Figure 5.4 is a contour plot displaying the time in seconds it takes for the floor of the dish to drop below 34 °C (frequently considered to be the desired lower limit for embryo temperature, Section 3.6) as a function of the convective heat transfer coefficient and the laboratory air temperature. For the purpose of this plot the range of the convective heat transfer coefficient has been narrowed to 30-60 $W.m^{-2}K^{-1}$.

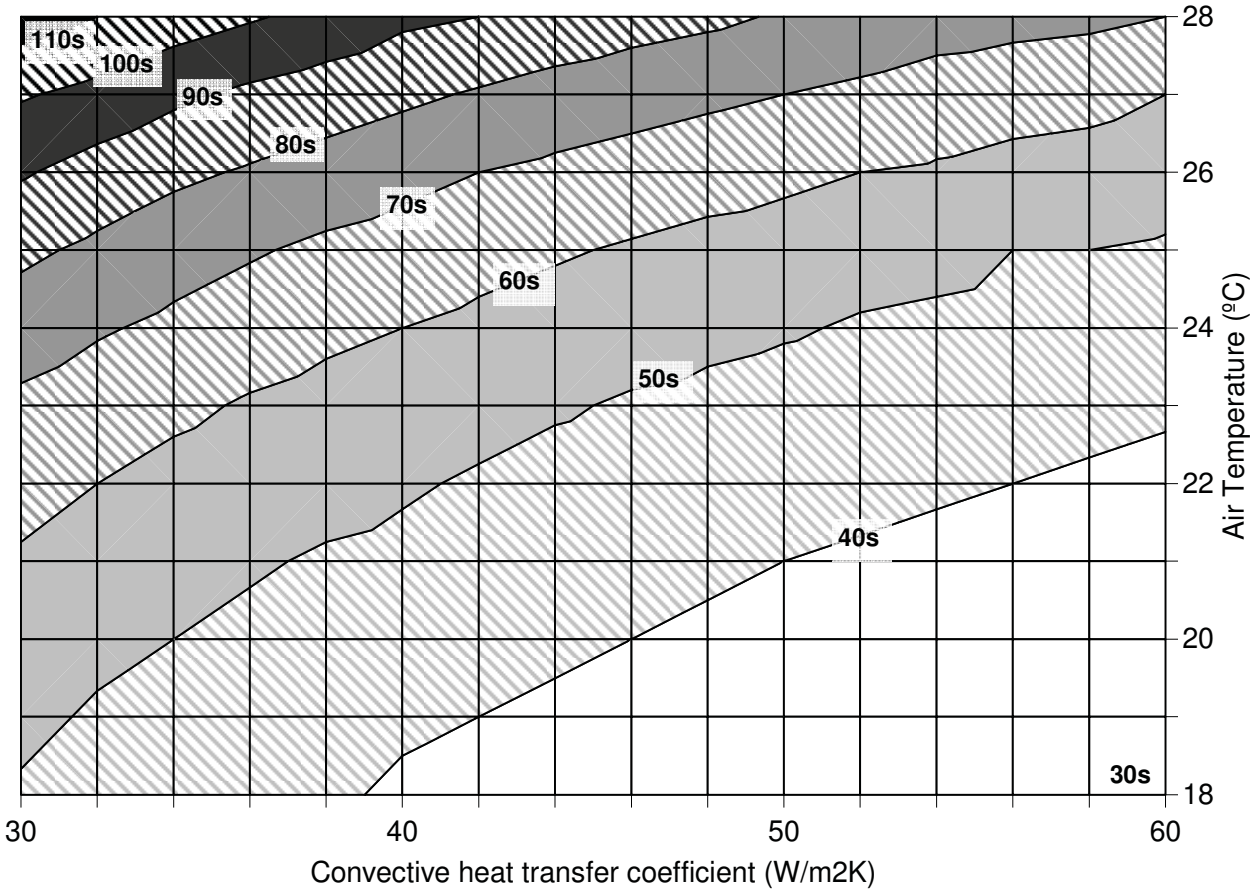

Figure 5.4: Contour plot displaying the time in seconds it takes for the centre floor of a Petri dish, containing a central media drop and 7 ml of paraffin oil, initially equilibrated at 37 °C to drop below 34 °C as a function of h ($W.m^{-2}K^{-1}$) and the laboratory air temperature (°C).

When transferring a dish from an incubator onto a heated stage through 25 °C laboratory air in relatively little air flow (a slow walk with similar air flow to a laminar flow hood (0.5 $m.s^{-1}$), h=30) the temperature drops to 34 °C in 80 s while a faster transfer of a dish (brisk walk and dish movement, h=60) the temperature drops to 34 °C in 50 *s*. In a well set out laboratory, transfer of a dish from the incubator to a nearby stage may only take a few seconds and so the impact on the embryo is likely to be insignificant.

5.3.2 Heat loss to the carrier

In reality, heat loss to the carrier of the dish may not be negligible. Carrying a dish, whether by hand or on a tray, may have a significant impact on heat loss from the dish to the laboratory air. In relatively still air, heat transfer by conduction is faster than that by convection. Heat may be conducted from the dish to its carrier and/or from the carrier to the dish while it is simultaneously lost to the surrounding air by convection.

The use of a tray or an incubator insert to carry a dish may be beneficial as long as the carrier is equilibrated to temperature (37 °C) with the dish. If the carrier is initially cold it will act as a heat sink and cool the dish at a greater rate than the air alone. If the carrier is warm, then the dish-carrier system will have a greater thermal mass than the dish alone and will therefore take a longer time to cool down. The effectiveness of a particular carrier is dependent on its geometry and thermophysical properties.

Figure 5.5 compares (θ_a =18 °C, h=30 $W.m^{-2}K^{-1}$) the model output from four carrier systems under the same conditions. For the carrier models the properties of two different materials (a metal and a ceramic) were applied to two different geometries, a tray with an air gap and a tray fitted to the dish (no air gap), which are depicted in Figure 5.5. The thermophysical properties are displayed in Table 5.1. At t=0 the dish-carrier system, initially at a uniform 37 °C, is removed from the incubator into the air (θ_a =18 °C, h=60 $W.m^{-2}K^{-1}$).

Heating or cooling time of a particular material is dependent on its thermal diffusivity and its thickness (in the direction of heat transfer). It is inversely proportional to the material's thermal diffusivity and proportional to the square of the thickness (Wilson

1959). The thermal diffusivity of the tray materials (defined in Equation 5.1) were calculated from their physical properties and are displayed with them in Table 5.1.

$$\alpha = \frac{\lambda}{\rho c}$$ Equation 5.1

Material	Property (units)	Value	Reference
Porcelain	λ (W.m^{-1}.K^{-1})	1	Laughton & Warne, 2003
	c (J.kg^{-1}.K^{-1})	800	Laughton & Warne, 2003
	ρ (kg. m^{-3})	2400	Laughton & Warne, 2003
	α (m^{2}s^{-1})	5.21×10^{-7}	-
Aluminium	λ (W.m^{-1}.K^{-1})	160	COMSOL material/coefficients library
	c (J.kg^{-1}.K^{-1})	900	COMSOL material/coefficients library
	ρ (kg. m^{-3})	2700	COMSOL material/coefficients library
	α (m^{2}s^{-1})	6.5×10^{-5}	-

Table 5.1: Thermophysical properties (thermal conductivity, heat capacity, density and thermal diffusivity) of aluminium and porcelain.

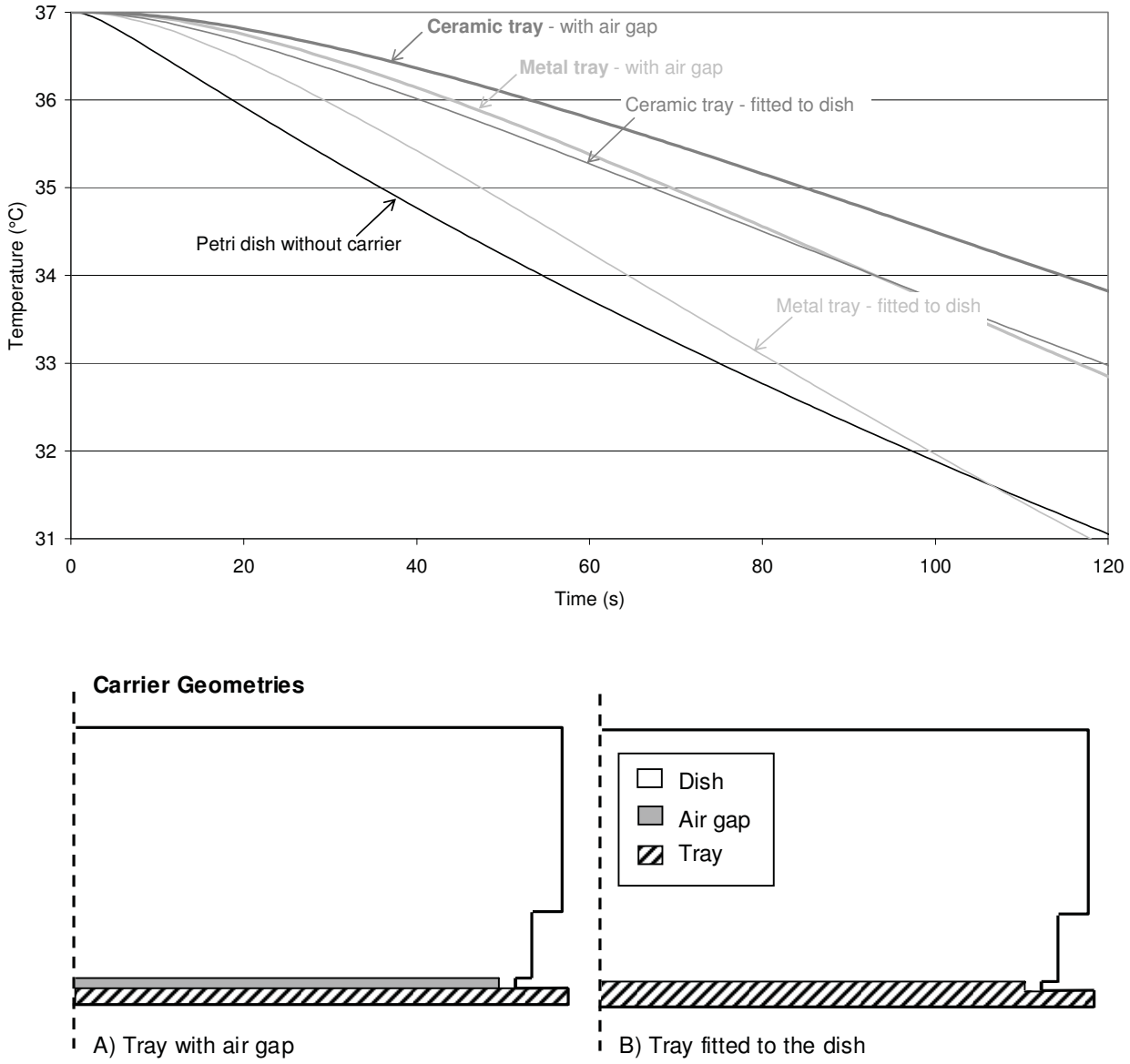

Figure 5.5: Modelled heat loss from a Petri dish without a carrier and Petri dishes with metal and ceramic carriers of both geometries. A) Tray with an air gap (1 mm thick). B) Tray fitted to the dish (1.42 mm thick beneath the dish floor).

Figure 5.5 shows that heat loss is slower from the centre floor of a Petri dish on a ceramic tray than on a metal tray for both tray geometries. The thermal diffusivity of aluminium is 126 times higher than that of porcelain. Therefore, since time for heating or cooling of a material is inversely proportional to its thermal diffusivity, for the same tray dimensions porcelain will take longer to cool than aluminium. This gives the ceramic carrier an apparent advantage, but if the carrier is to be re-heated

with the dish on a stage or in an incubator then metal will perform better as it will more effectively transfer heat to the dish.

The first tray geometry (Figure 5.5A) is simply a flat disk and so an air gap the height of the dish feet is present between the dish and the tray. The second (Figure 5.5B) is moulded to sit flush to the floor of the dish leaving no air gap. For both materials, geometry A maintains the temperature of the dish more effectively than geometry B. This is due to the presence of an insulating air gap in geometry A rather than the increase in the thermal mass of geometry B. While not investigated in Figure 5.5 the thickness of the dish carrier will significantly affect its rate of cooling. As stated above the rate of cooling is proportional to the square of the carrier thickness. The situation with the geometry of the dish carrier is similar to that with the dish material in that the arrangement most appropriate for slowing cooling of the dish system during transfer (the presence of an air gap and increasing the thickness of the tray) will also slow heating of the dish back in the incubator or on a stage.

From Figure 5.5 a ceramic dish with an air gap, geometry A, would be the best option for a carrier as long as it is pre-warmed to 37 °C. It is important to note the implications of the fact that the properties of a dish carrier which most aid temperature maintenance (a low rate of heat transfer away from the dish) are the opposite properties to those desired when heating or re-heating a dish in an incubator (a high rate of heat transfer to the dish). Therefore, the use of incubator inserts as dish carriers, a common accessory for incubators, is not appropriate since opposing thermophysical properties and geometries are optimal for each situation.

The most common dish carriers are hands. Heat loss from the dish is dependent on hand temperature (though this will be <37 °C) and the surface area of contact between the dish and the hands. A mistake frequently made is cradling the dish with both hands as this feels warm. However, this is not keeping the dish contents warm it is heat being transferred away from the dish.

5.4 The Petri dish-heated surface thermal environment

In open culture, maintaining the temperature of an embryo during observation and manipulation is dependent on the use of heated microscope stages and hot blocks. The purpose of this section is to apply the model as a tool to aid understanding of this thermal environment and how to control the temperatures an embryo may experience.

Petri dishes are removed from the incubator fully equilibrated to the incubator temperature and are placed onto heated microscope stages for embryo manipulation and observation many times throughout the embryo culture process. In the process flow diagram (Figure 3.10) 22 steps involve a Petri dish (with or without a lid) on a heated microscope stage (the first of these is step 5.5b).

5.4.1 Heated stage use

Heated microscope stages are used throughout the culture process with the goal to maintain the temperature of embryos when they are removed from the stable incubator systems (37 °C) into the laboratory environment (≈25 °C). Heated blocks are also used for this purpose, to hold a dish of embryos just prior to or after use. It is a common perception by embryologists that all stages are a constant and uniform

temperature. In embryology laboratories the temperature of the surface of microscope stages and heated blocks are set by a number of methods, as described in Section 3.3.2.3. Heated stages may be built into the microscope or may be stand-alone and used with a variety of different microscopes.

Traditionally stages are a heated metal surface with a hole in the centre to enable light to pass through for the microscope. The size of the stage and the hole varies with manufacturer. Some stages have an open hole in the stage, an obvious cool spot, while others have warm air blowing underneath the hole or a plastic or glass insert (which may or may not be heated). There are two makes of metal stage at Fertility Associates Auckland, one has a small, open hole at the centre, and the other has a hole with a plastic insert (not heated).

Glass stages are transparent and therefore do not require a hole. Because of this they are perceived as having a uniform temperature and they are preferred by many clinics for this reason. Fertility Associates Auckland have two types of glass stage (both Tokai Hit), a small stage insert attached to the micromanipulator (used for ICSI) and large stand-alone stages.

Heated blocks are a system for heating aluminium blocks. These blocks provide a surface to place a dish on and to hold test tubes (some blocks are test tube holders). During many procedures, dishes of media drops with or without embryos are placed on such blocks for considerable periods of time.

The use of heated stages does not generally follow a set protocol. Every embryologist has their own way of doing things which has evolved over time. For example some prefer to remove their dishes from the incubator and place them on a heated block before they pull their pipettes, while some prefer to pull their pipettes before finding the embryos.

It is possible to model the heated stage systems and to incorporate the dish model to simulate dish placement on a stage. As there is so much variation, even within a single embryology laboratory, modelling any one of the different stage types would be of limited practical use. The metal stages, except for the hole in the centre of the stage, and the heated blocks may be assumed to be of a constant and uniform temperature. This provides a boundary condition which may be easily applied to the dish model. Modelling a dish system on a stage of constant and uniform temperature enabled investigation of factors within the dish system which impact on an embryo's thermal environment while outside of the incubator. The environment provided by the popular glass microscope stage was investigated through experimental measurement.

5.4.2 Validation of the model on a surface of constant and uniform temperature

A copper heat exchanger purpose made for cooling computer chips (Apogee GT, Swiftech, Long Beach CA, USA) provides a surface just large enough to hold a Petri dish. The properties of this heat exchanger promote the desired constant and uniform surface temperature:

- Copper has a very high thermal conductivity (approximately 1.6 times greater than that of aluminium)

- The inlet and outlet pipes provided the capacity for a large flow rate of water through the block and the inside was a corrugated surface promoting turbulence (increasing the convective heat transfer coefficient between the water and the copper) and providing a large surface area for heat transfer.

Water from a water bath set to 37 °C was pumped through the copper heat exchanger. Heat losses from the pipes were assumed to be constant as changes in the flow rate of water, the laboratory air temperature and air flow were negligible. Measuring surface temperature is difficult. Good contact is required and this is not sufficiently provided by taping down small thermocouples. Rather, the surface temperature of the copper heat exchanger could be calculated from experimental data and the known properties of the dish system since;

- It may be assumed to be a constant value
- Validation of the model in Chapter 4 demonstrated that the heat transfer processes within the dish system are suitably defined
- The ambient temperature may be accurately measured
- A range of convective heat transfer coefficients has been defined for relatively still laboratory air

The stage surface temperature was therefore the only unknown in the system.

For a Petri dish, with its lid on, at steady state equilibrated on the copper heat exchanger the heat flux is predominantly vertical and therefore it may be assumed that the dish is an infinite slab and the calculation of surface temperature may be considered as a one dimensional problem. The surface temperature of the heat

exchanger may be calculated from known values: the ambient air temperature, the steady state temperature at the centre floor of the dish and the resistances to heat transfer of each layer between the laboratory air and the surface of the heat exchanger (polystyrene lid, air trapped by the lid of the dish, oil, media, polystyrene floor of the dish, air trapped beneath the dish). The heat flux lost by convection can be determined and at steady state this is equal to the heat flux from the stage to the surface of the dish floor. The calculations are presented in Table 5.2.

θ_{air}	24 °C
$\theta_{\text{dish floor lid on}}$	34.78 °C
$\frac{1}{h}$	$\frac{1}{12} = 0.083\ m^2.K.W^{-1}$
$R_{polystyrene\ (lid)} = \frac{x}{\lambda}$	$\frac{1.03e^{-3}}{0.1565} = 0.00658\ m^2.K.W^{-1}$
$R_{air\ trapped\ by\ lid} = \frac{x}{\lambda}$	$\frac{9.82e^{-3}}{0.267} = 0.368\ m^2.K.W^{-1}$
$R_{oil} = \frac{x}{\lambda}$	$\frac{1.66e^{-3}}{0.1232} = 0.0135\ m^2.K.W^{-1}$
$R_{media} = \frac{x}{\lambda}$	$\frac{1.43e^{-3}}{0.622} = 0.00230\ m^2.K.W^{-1}$
$R_{polystyrene\ (dish\ floor)} = \frac{x}{\lambda}$	$\frac{1.35e^{-3}}{0.156} = 0.00862\ m^2.K.W^{-1}$
$R_{air\ beneath\ dish} = \frac{x}{\lambda}$	$\frac{0.44e^{-3}}{0.0267} = 0.0168\ m^2.K.W^{-1}$
$q = \frac{\Delta\theta}{\Sigma R}$	$\frac{34.78 - 24}{0.0830 + 0.00658 + 0.368 + 0.0135 + 0.0023} = 22.77\ W.m^{-2}$
	$\frac{\theta - 24}{0.083 + 0.00658 + 0.368 + 0.0135 + 0.0023 + 0.00862 + 0.0168} = 22.77$
	$\theta = 35.36\ °C$

Table 5.2: Calculations to determine the temperature of the surface of the copper heat exchanger.

Figure 5.6 displays the experimental data together with the prediction band (the average ± two standard deviations of 30 Monte Carlo model simulations). The room

temperature was 24 °C and the heat transfer coefficient was estimated to be 12 $W.m^{-2}K^{-1}$ with a standard deviation of 2 $W.m^{-2}K^{-1}$.

At t=0 the dish, at room temperature, was placed on to the copper surface. After steady state was reached the lid was removed from the dish at t=23 min 30 s. Removing the lid removes a layer of insulating air, cooling the dish. The prediction band noticeably broadens at this point as the importance of external resistance to heat transfer (defined numerically by the convective heat transfer coefficient (h)) increases since, with the loss of the air layer trapped by the dish and the polystyrene lid, it becomes a greater proportion of the total resistance to heat transfer.

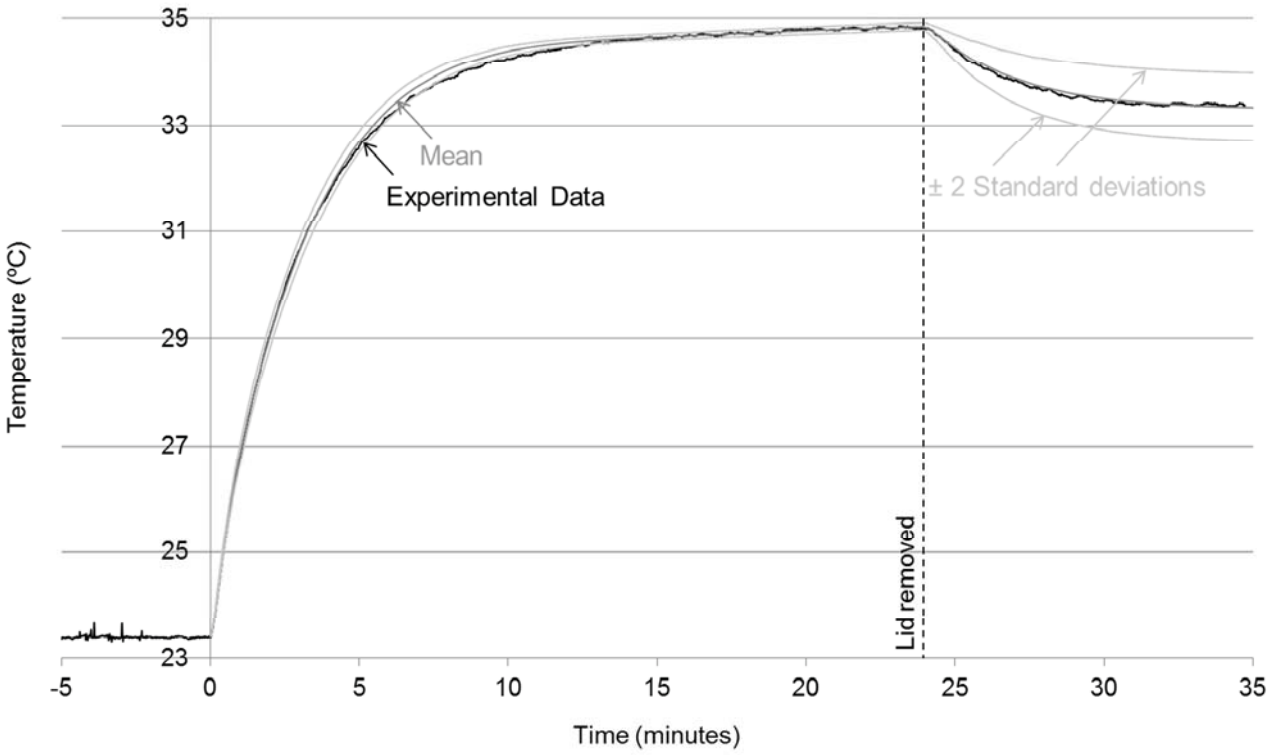

Figure 5.6: Compares experimental data with the modelled temperature rise (mean ± 2 standard deviations) at the centre floor of a Petri dish, initially at 23.4 °C, after placement on a heated stage at t=0 (of assumed constant and uniform temperature of 35.36 °C) and subsequent heat loss after removal of the dish's lid at t=24 min. Ambient air = 24 °C, h=12 $W.m^{-2}K^{-1}$. For the Petri dish system: foot height = 0.45 mm, base thickness = 1.35 mm, oil depth = 3.07 mm.

The three steady state temperatures were well within the prediction band, the model slightly over predicts the rate of heat transfer. This is likely due to thermocouple placement for experimental data collection. Setting up a thermocouple in a drop at the centre of the dish is delicate. Placing the drop so that its centre is over the thermocouple junction is difficult and the thermocouple itself tends to disrupt the drops footprint leading to a slightly wider, shorter droplet. A reduced drop height over the thermocouple or thermocouple placement away from the centre of the drop reduces the proportion of culture media in the liquid depth above the thermocouple. Water has a greater thermal mass ($\rho \times c_p$) than paraffin oil and it therefore requires more energy to heat the same volume. Therefore for a constant depth of oil, the greater the depth of culture medium above the thermocouple the slower the thermocouple will heat up. This is demonstrated in Figure 5.7 which displays the temperature profile of a cross section through the drop (standard dimensions) after the dish has been on the stage for two minutes; the point on the floor of the dish at the drop edge is the warmest. That a temperature difference of 0.5 °C exists within this small drop highlights the sensitivity of measured values to thermocouple placement within the drop.

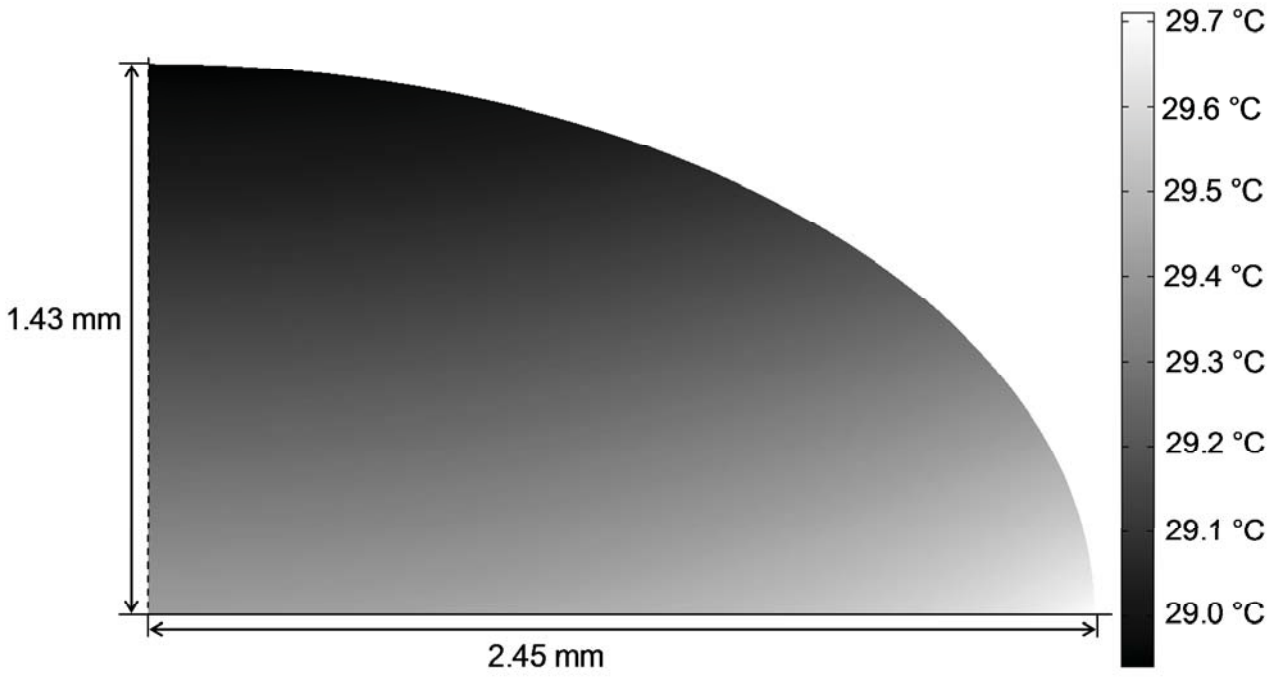

Figure 5.7: Modelled temperature profile through cross section of a media drop at the centre floor of a Petri dish, initially at 23.4 °C, 2 minutes after placement on a heated stage (constant and uniform temperature of 35.36 °C). Ambient air = 24 °C, h=12 $W.m^{-2}K^{-1}$. At *t*=2 minutes from the model simulation displayed in Figure 5.6.

5.4.3 Factors which affect the temperatures on the dish floor

The ease of modelling with a constant and uniform boundary condition provides a simple tool to investigate and identify geometric parameters in the model which have an impact on the temperatures embryos may experience on the dish floor. Three parameters were considered; whether the lid is on or off the dish, the dish's foot height and drop placement within the dish.

In practise the temperatures of heated microscope stages are set by a number of methods as described in Section 3.3.2.3. For the purpose of this modelling work the surface temperature was set so that the temperature at the centre floor of the Petri dish system (with a defined liquid content and with or without a lid as specified) rises as

close to, without exceeding, 37.1 °C. As discussed in Section 3.6, 37.1 °C is the upper limit of the temperature range embryologists consider desirable for embryo culture.

Lid on or off the dish

The resistances to heat transfer of each layer along the central axis of the Petri dish are displayed in Table 5.2. The greatest resistance to heat transfer between the heated surface and the ambient laboratory air is the air trapped by the lid of the dish which is more than double the resistance to heat transfer of any other layer. Therefore the thickness of this air layer is expected to have a significant effect on the steady state temperature of the dish floor. For oocyte collection and embryo manipulation the lids must be removed from the dish, the loss of this insulating layer of air under the lid will lower the steady state temperature at the dish floor.

This is illustrated in Figure 5.6. As the lid is removed from the dish (at t=23 min 30 s) the steady state temperature falls from 34.8 °C to a new steady state of 33.35 °C. As described above, the temperatures within the dish fall since the lid and, more importantly, the air trapped by the lid insulated the dish contents from the surrounding cool air.

Figure 5.8 compares the modelled temperature change at the centre floor of a Petri dish (initially at 37 °C), both with and without a lid, after placement onto a constant and uniform surface. The surface temperature was set to maintain temperatures at the centre floor of a dish with its lid on at 37.4 °C (Figure 5.8A) or off at 38.5 °C (Figure 5.8B).

Figure 5.8A shows that setting the surface temperature (of a stage of constant and uniform temperature) can successfully maintain the temperature at the centre floor of a Petri dish with its lid on between 36.7 and 37.1 °C over a 10 minute period. For a Petri dish without a lid on the same surface, temperatures fall to 34.8 °C after 10 minutes.

Figure 5.8B shows that by setting the surface temperature (of a stage of constant and uniform temperature), the temperature at the centre floor of a Petri dish with no lid can be maintained between 35.7 and 37.1 °C over a 10 minute period. Maintaining temperatures within a dish with its lid off is especially important during longer manipulations such as ICSI.

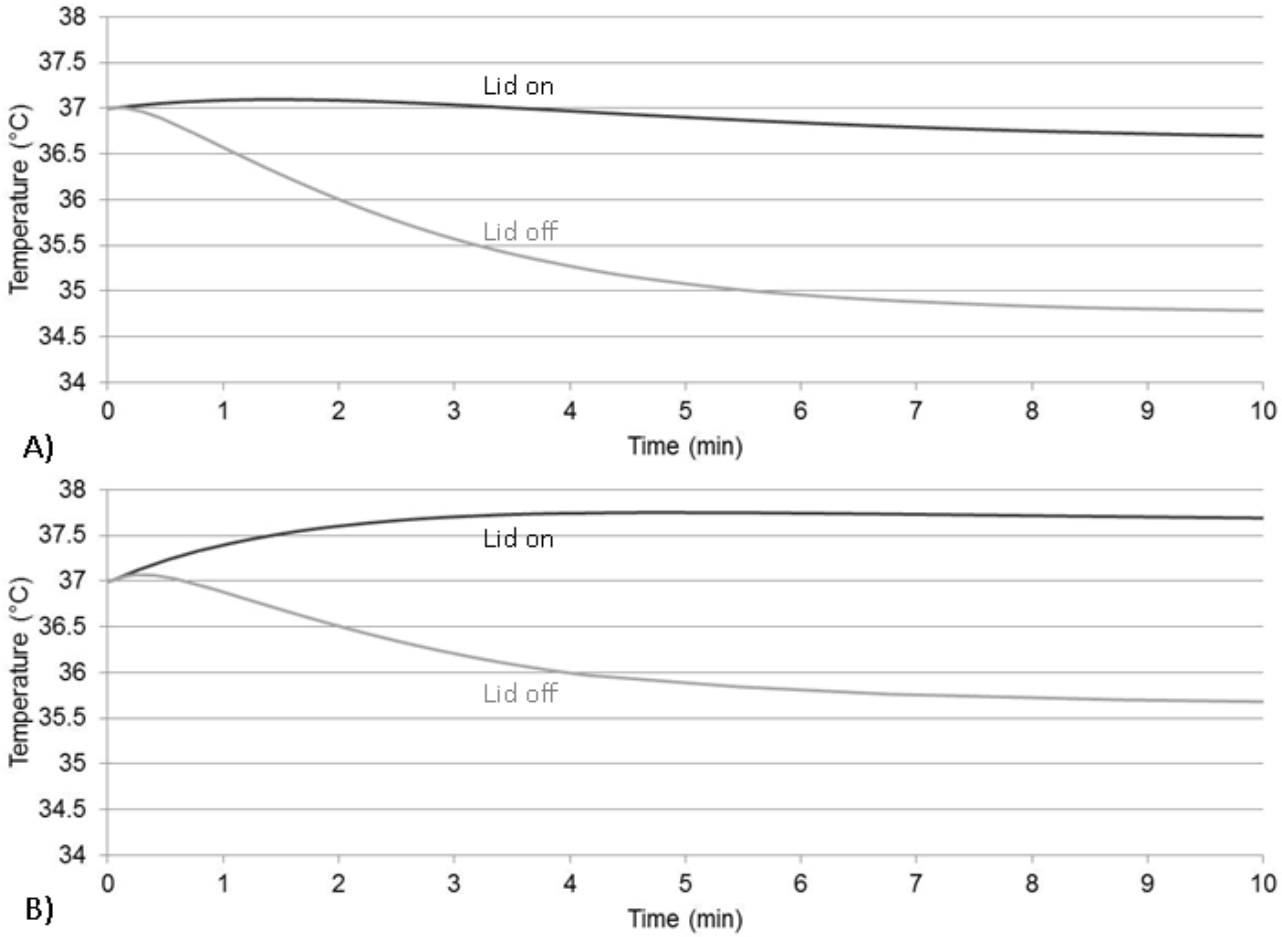

Figure 5.8: A) Displays the modelled temperature profiles at the centre floor of a Petri dish with its lid either on or off when the surface of the stage of constant and uniform temperature was set to 37.4 °C. B) Displays the modelled temperature profiles at the centre floor of a Petri dish with its lid either on or off when the surface of the stage of constant and uniform temperature was set to 38.5 °C. In both cases the air temperature was 25 °C, initial temperature of the dish system was 37 °C and the convective heat transfer coefficient was set to 12 $W.m^{-2}K^{-1}$.

The temperature at the centre floor of a Petri dish without a lid falls to 35.7 °C after 10 minutes on a stage of constant and uniform temperature (38.5 °C). The stage could not be set to a higher temperature as the temperature at the centre floor of the dish would initially rise above 37.1 °C. As described in Section 5.3.2 the rate a particular layer of material takes to heat or cool is inversely proportional to the material's thermal diffusivity and proportional to the square of the thickness. Table 5.3 displays the values of the thermal diffusivity (α), the square of the thickness (x) and the value

of α/x^2 for each layer along the central axis of a Petri dish (assuming an infinite slab). The value of α/x^2 is inversely proportional to the time the material takes to heat or cool. Table 5.3 demonstrates that the layer of paraffin oil heats or cools the slowest and the air gap beneath the dish heats or cools the fastest. Initially when the dish (at a uniform 37 °C) is placed onto the stage (whether the lid is on or off the dish) the layers beneath the dish floor heat quicker from the stage below than the layers above the dish floor (including the oil layer) are cooled by the surrounding laboratory air. This results in the initial rise in temperature at the floor of the dish which is seen at t= 1.5 minutes for a dish with its lid on in Figure 5.8A and at t=20 s for a dish with no lid in Figure 5.8B. It is this initial rise in temperature which limits the maximum set point for the stage surface temperature. This highlights the importance of understanding that heat transfer after placement of a dish onto a heated surface is dynamic and thus setting the surface temperature to fit the steady state temperatures alone may result in unintentional overheating of embryos.

	α ($m^2.s^{-1}$)	x (m)	$\frac{\alpha}{x^2}$ (s^{-1})
polystyrene (lid)	1.21×10^{-7}	0.00103	0.114
air (trapped by lid)	2.07×10^{-5}	0.00982	0.215
oil	7.55×10^{-8}	0.00166	0.0274
media	1.48×10^{-7}	0.00143	0.0724
polystyrene (dish floor)	1.21×10^{-7}	0.00135	0.0664
air (trapped beneath dish)	2.07×10^{-5}	0.00044	106.9

Table 5.3: The thermal diffusivity, the square of the thickness and the value of α/x^2 of the layers along the central axis of the Petri dish system with its lid on. The larger the value of α/x^2, the faster is the rate of heating or cooling.

If a microscope stage setting is intended for a dish with its lid off, then, if a dish is placed onto the stage with its lid still on, the temperatures at the centre floor of that dish would likely rise above 37.5 °C (the outer upper limit as defined in Section 3.6). Figure 5.8 B shows that where the stage is of a constant and uniform temperature the centre floor of the dish rises above 37.5 °C after 1 minute 25 seconds.

The foot height

The foot height, the height of the air gap beneath the dish, has a significant impact on the temperatures on the dish floor. The resistances to heat transfer of each layer through the centre of the dish (displayed in Table 5.2) were calculated for determining the heat exchanger surface temperature. The greatest resistance to heat transfer between the heated surface and the dish floor (displayed in Table 5.2) is the air gap which, despite being less than half the thickness of the dish floor, has double the resistance ($R_{air\ beneath\ dish}$=0.0168 $m^2.K.W^1$, $R_{polystyrene\ (dish\ floor)}$=0.00862 $m^2.K.W^1$). Therefore the thickness of this air layer is expected to have a significant effect on the steady state temperature of the dish floor.

While relatively consistent within a batch (observed to be approximately ± 0.02 mm) the foot height has been found to vary between batches. For example, the foot height was found to differ by 0.19 mm (0.61 mm and 0.42 mm) between two Petri dishes from different batches (Dishes A and B as described in Section 4.1.3.1). Figure 5.9 displays the impact on the steady state temperature at the centre of the dish floor of varying a dish's foot height over a 0.3 mm range (0.35 mm to 0.65 mm). With the lid off the dish the steady state temperature varies by 0.64 °C over this range.

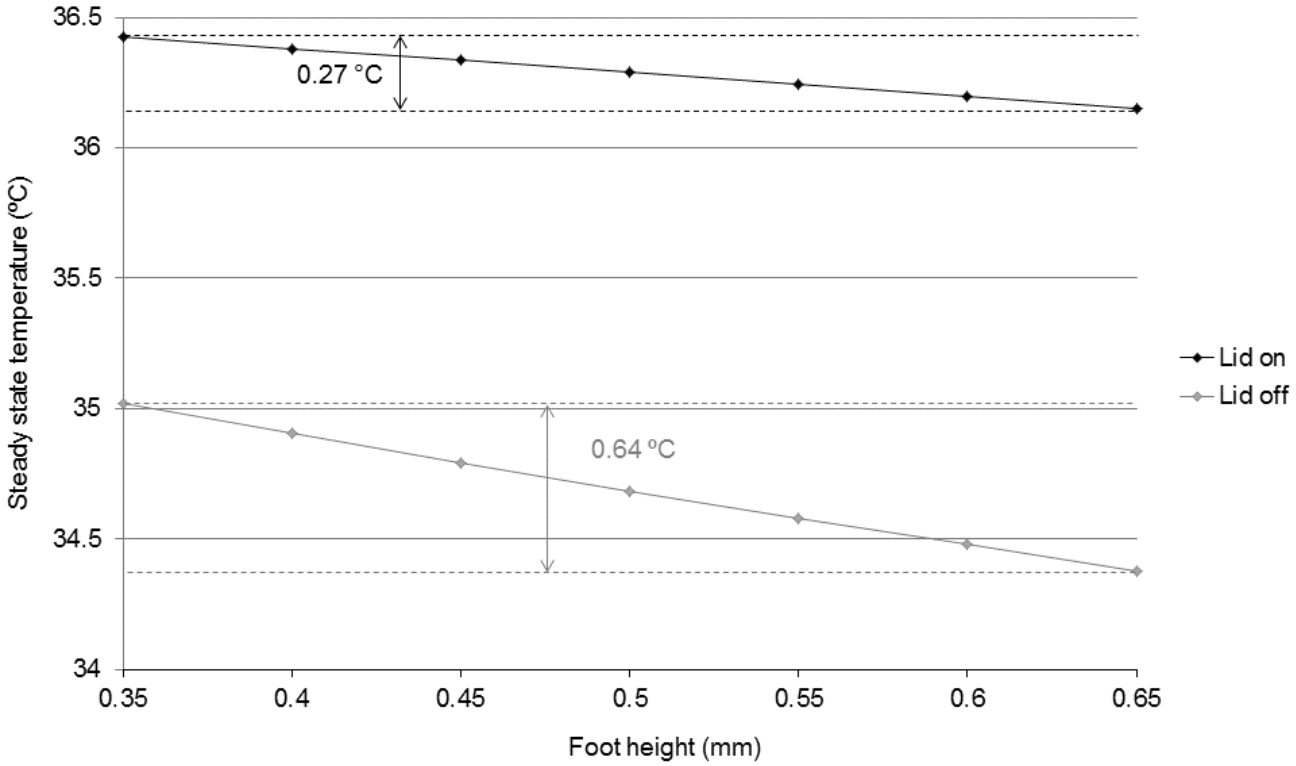

Figure 5.9: Petri dish foot height vs. the modelled steady state temperature at the centre floor of a Petri dish on a surface of constant and uniform temperature (37 °C) for a Petri dish both with and without a lid. Ambient air temperature = 27 °C, h= 12 W.m^{-2}K^{-1}, thickness of dish floor = 1.09 mm.

This variation in equipment is another source of variation in the culture conditions and has the potential to negatively impact embryo culture. This is likely to have more significance where several types of dish are used on one stage as foot heights vary widely with type and make of dish (e.g. Falcon Petri dish ~0.4 mm, 4-well dish ~0.7 mm). This will be further investigated when modelling the 4-well dish (Section 6.4.2).

Drop placement within the dish

Embryo placement, in terms of radial distance from the dish centre, greatly affects temperature during periods outside the incubator. Since heat is lost through the dish wall a radial temperature gradient builds up across the dish floor. The greater the distance from the dish centre, the greater the impact of heat loss through the dish walls and therefore the faster an embryo will cool.

Figures 5.10 and 5.11 display the modelled temperature gradients across the radius of the floor of a Petri dish, respectively with and without a lid, at the following times; 30 s, 60 s, 120 s and 300 s.

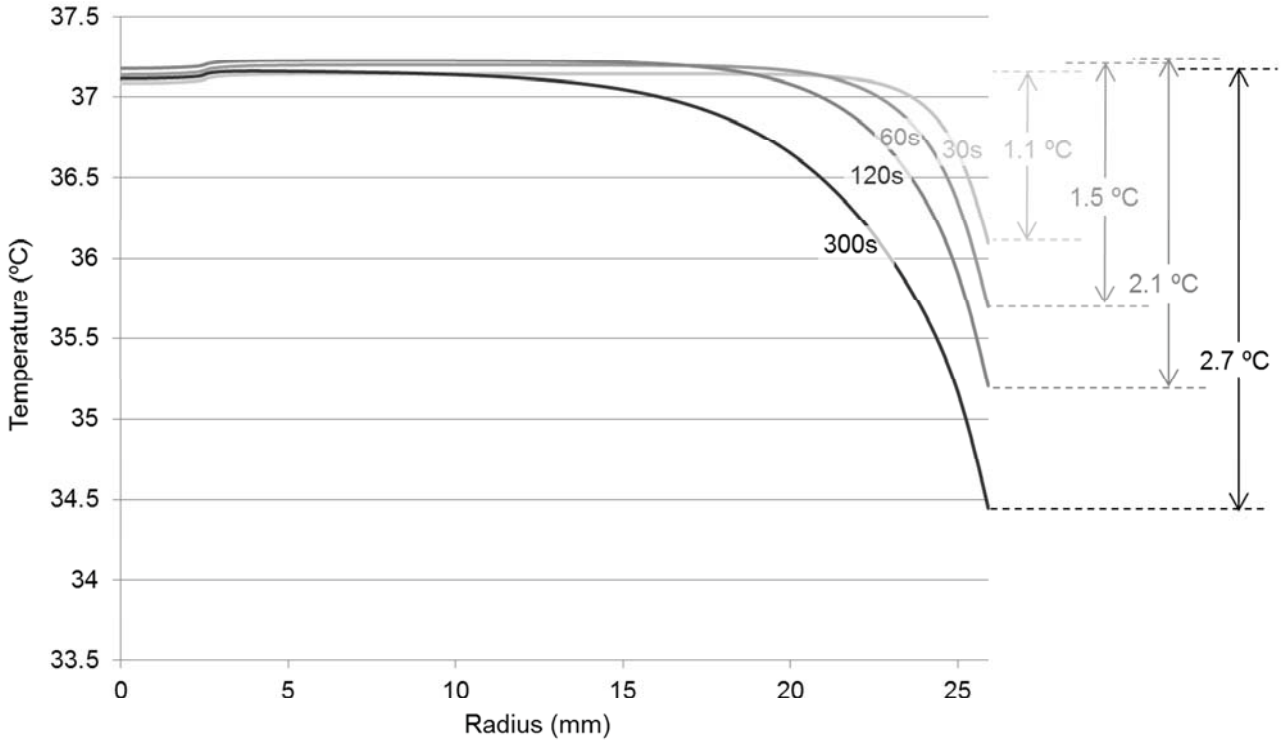

Figure 5.10: Displays the modelled temperature profile across the floor of a Petri dish with its lid on at times 30 s, 60 s, 120 s and 300 s. The Petri dish system was initially at 37 °C. At t=0 it was placed onto a stage of constant and uniform temperature (37.6°C). The maximum temperature difference across the radius of the dish at each of the displayed times is labelled. Ambient air = 27 °C, h= 12 W.m^{-2}K^{-1}, oil depth = 3.09 mm, foot height = 0.42 mm, thickness of dish floor = 1.09 mm.

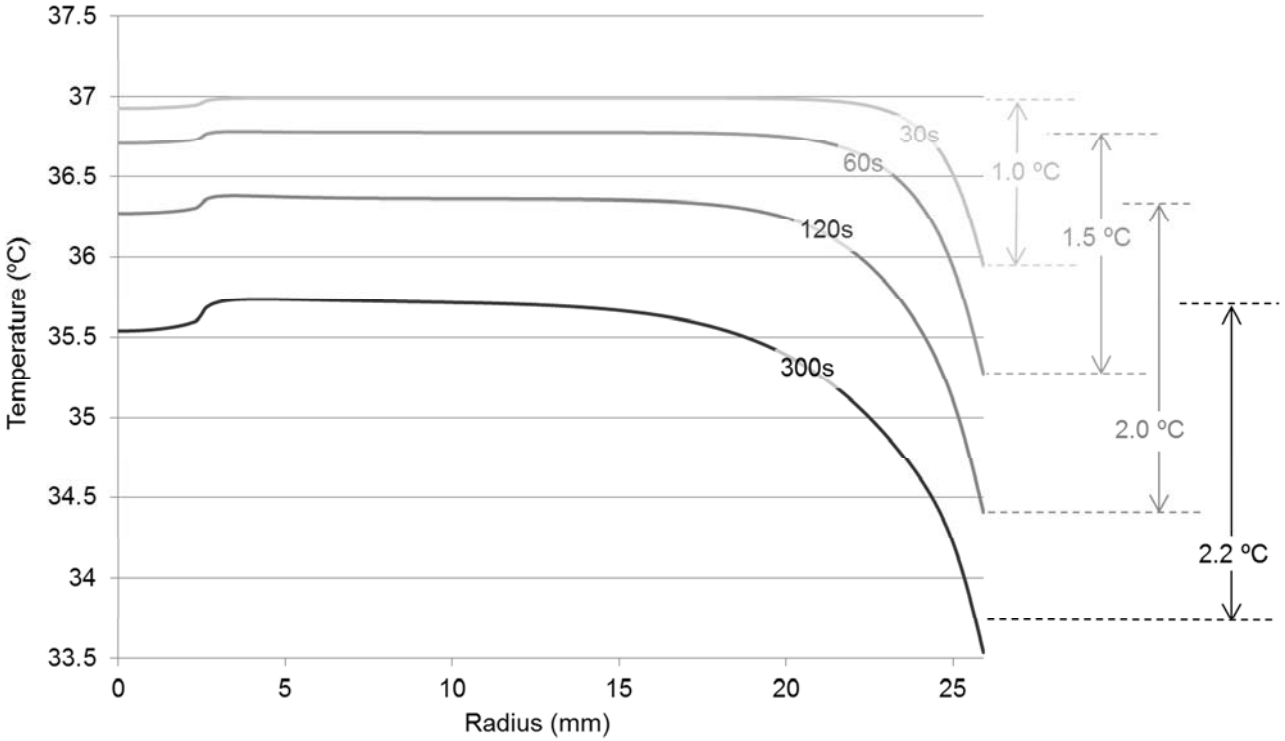

Figure 5.11: Displays the modelled temperature profile across the floor of a Petri dish with its lid off at times 30 s, 60 s, 120 s and 300 s. The Petri dish system was initially at 37 °C. At t=0 it was placed onto a stage of constant and uniform temperature (37.6 °C). The maximum temperature difference across the radius of the dish at each of the displayed times is labelled. Ambient air = 27 °C, h= 12 $W.m^{-2}K^{-1}$, oil depth = 3.09 mm, foot height = 0.42 mm, thickness of dish floor = 1.09 mm.

On a surface of constant and uniform temperature the temperatures of embryos placed across the Petri dish radius differ by up to 2.7 °C, when the lid is on the dish, or 2.2 °C, with the lid off the dish, after 300 s (5 minutes). Different methods may be used to minimise such temperature differences between embryos:

- Restricting the placement of embryos to within 15 mm of the dish centre the maximum temperature difference can be limited to within 1 °C.

- Restricting embryo placement to a ring at a set distance from the dish centre (i.e. 20 mm) and setting the microscope stage temperature to keep this ring

within the desired temperature range would ensure all embryos are maintained at the same temperature. Note that temperatures closer to the dish centre would then be > 37.1 °C.

5.4.4 Investigating the glass heated microscope stage

The stand-alone glass microscope stages (pictured in Figure 3.8C) are one of the main stage types used at Fertility associates. The attraction of the glass stage is that since it is transparent it does not require a hole in it for microscope function (as in a metal stage). The physically uniform stage (300×150×2.1 mm) therefore appears to provide a uniform thermal environment making it an apparently attractive option for maintaining embryo temperature.

Figure 5.12 shows the measured temperature changes at the centre floor of a Petri dish and on the surface of the glass stage immediately below this point as the Petri dish is placed onto the stage at t=0 and the lid is removed from the dish at t=27.4 minutes. The Petri dish was placed onto the centre of the glass microscope stage as it would be in embryology practise.

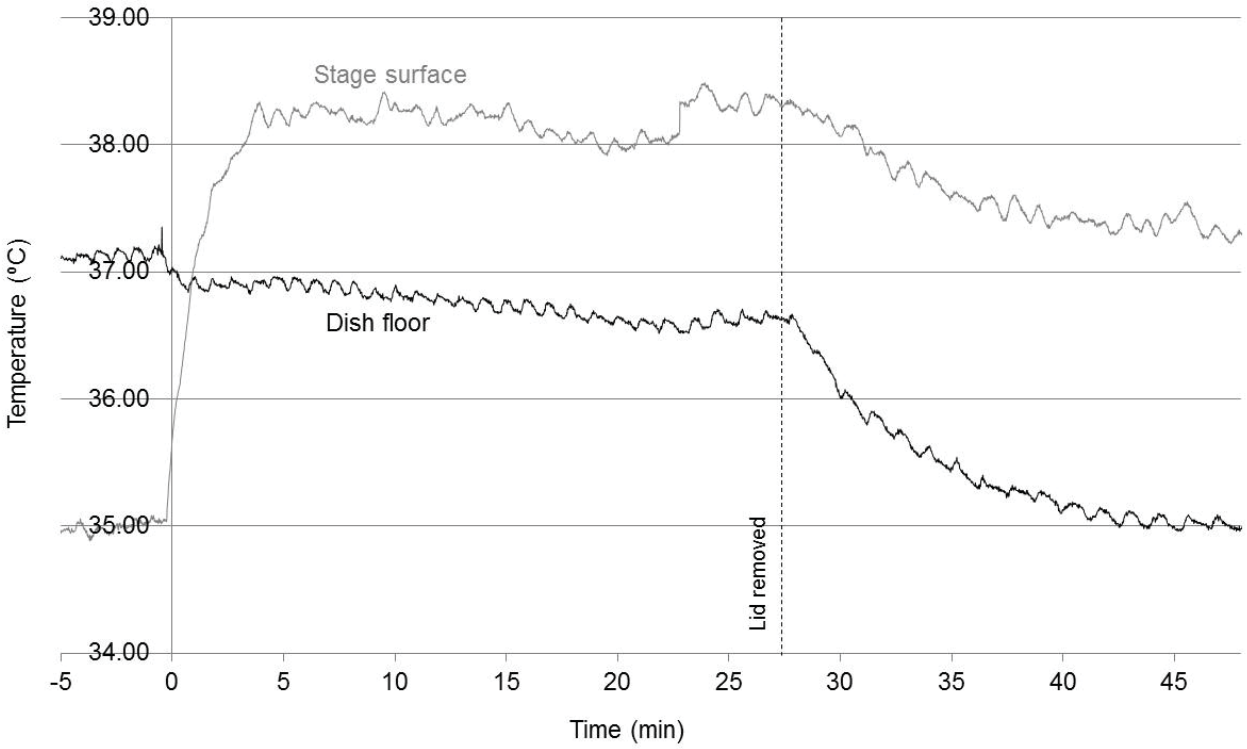

Figure 5.12: Experimentally measured temperatures at the centre floor of a Petri dish and on the surface of a glass heated microscope stage immediately below the centre floor of the dish. At t=0 the Petri dish (initially at ≈37.2 °C) was transferred from an incubator onto the glass heated microscope stage (Surface temperature of 35 °C). At t=27.4 min (dashed line) the lid was removed from the Petri dish on the glass heated microscope stage.

The single feedback sensors (thermistors) for the control system of glass stages are located at the edge of the stage, a minimum of 70 mm from the centre of a dish placed along the centre of the stage. These sensors do not pick up changes in the central stage temperature as, due to the relatively low thermal conductivity of glass when compared with a metal stage, heat transfer through the stage is slow.

Initially, before the dish is placed onto the stage, the stage is controlled at a constant temperature. At this time the heat flux into the stage from the element ($q_{element}$, as defined in Equation 5.2) is equal to the rate of heat loss by convection to the

surrounding air from both the top (q_{top}, as defined in equation 5.3) and the bottom (q_{bottom}) of the glass surface.

$$q_{element} = q_{bottom} + q_{top}$$ Equation 5.2

$$q_{top} = h(\theta_{top} - \theta_a)$$ Equation 5.3

θ_{top} is the temperature of the stage's top surface

If a dish is placed on the surface of the stage, as at t=0 in Figure 5.12, the resistance to heat loss from the top surface increases and at steady state:

$$q_{top} = U(\theta_{top} - \theta_a)$$ Equation 5.1

where $U << h$ (equation 5.3) as the resistance to heat transfer has increased.

If $q_{element}$ remains the same, which is the case if the feedback sensor does not pick up a temperature change, then θ_{top} must increase to compensate. This is evident in Figure 5.12 in the rise in surface temperature of the stage after the dish is placed onto it at t=0 suggesting that the stage's control system is not compensating for this change in stage temperature (there is no change in $q_{element}$). At t=27.4 minutes in Figure 5.12 the lid is removed from the Petri dish, reducing the resistance to heat transfer (and therefore the value of U in the above equation). Again there is no change in $q_{element}$, the temperatures of the centre floor of the Petri dish and of the stage surface beneath it fall at an equal rate.

Figure 5.13 displays the stage surface temperatures measured by five thermocouples spaced 15 mm apart across the surface of the glass stage from the stage centre. A cold (27 °C) Petri dish (containing 7 ml of oil) was placed over the thermocouple at the stage centre at t=0. The stage surface temperature was initially set to 37 °C. The surface of the stage under the Petri dish cooled due to heat transfer to the cold dish. It then heated with the dish to reach temperatures above the set point showing, as in

Figure 5.12, that the stage's control system had not altered $q_{element}$ in order to compensate for the steady state heat transfer being slower than that originally lost by convection directly to the air when no dish was present. The surface temperature of the stage 15 mm away from the Petri dish does not significantly change throughout the 30 minute equilibration of the dish and the stage beneath it. This clearly demonstrates that the stages feedback sensor, a minimum of 70 mm from the centre of the dish (44 mm from the edge of the dish), will not pick up on temperature changes due to dish placement on the stage.

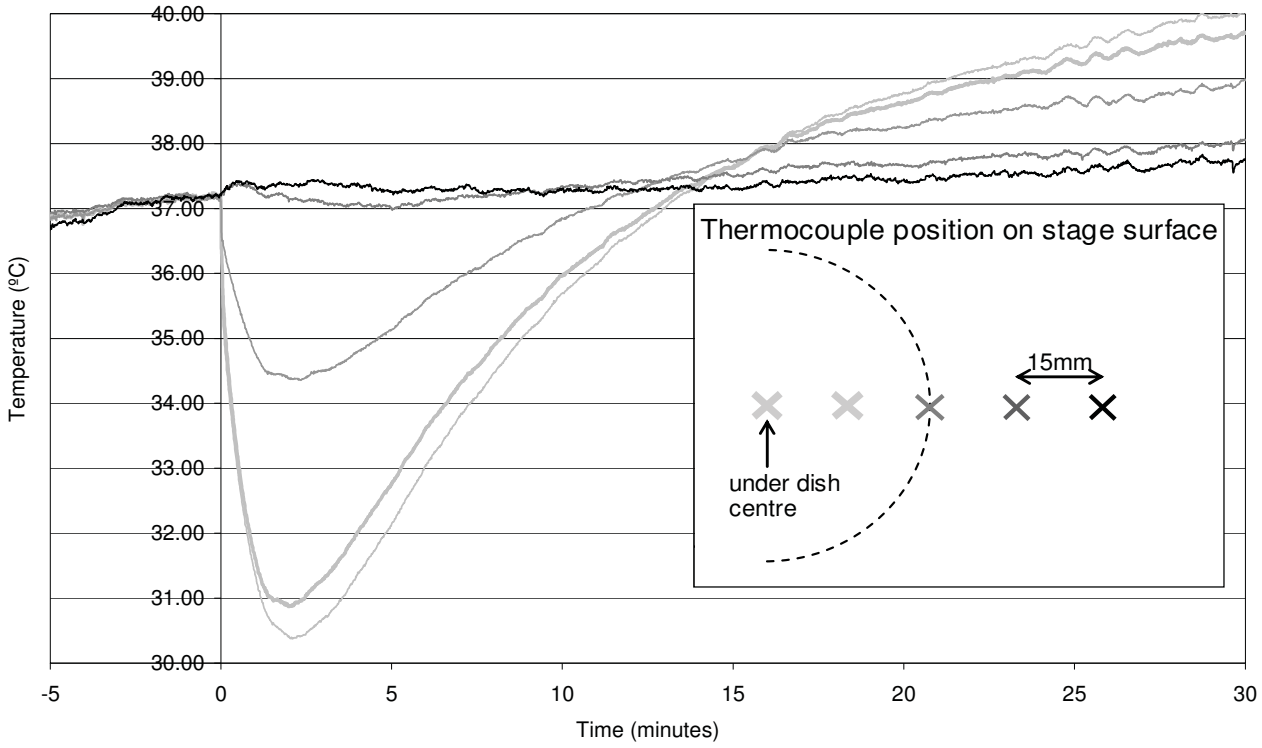

Figure 5.13: The experimentally measured temperatures at points across the surface of a glass microscope stage as a cold Petri dish (27°C) is placed over the centre of the stage at t=0. The thermocouples are placed 15 mm apart. The insert shows placement of the thermocouples.

Figure 5.13 demonstrates that when a Petri dish is placed onto a glass stage a radial temperature gradient will build up within the stage itself. The radial temperature gradients across the floor of the Petri dish when placed onto a stage of constant and

uniform temperature were investigated in Section 5.4.2. With temperature gradients building up across the glass stage beneath the Petri dish, larger temperature differences would be expected to develop across the floor of the Petri dish compared to one on a stage of constant and uniform temperature.

Through experimentation, this work has shown the dynamic nature of the thermal environment when a Petri dish is placed onto a glass heated microscope stage. If the temperature of a glass stage is set appropriately, so than an embryo at the centre floor of a Petri dish does not exceed 37.1 °C, glass stages may be used effectively to maintain the temperature of embryo's within a Petri dish during observation and manipulation. As placement of a Petri dish onto a glass stage sets up significant temperature gradients within the stage, placement of multiple dishes onto a glass stage at any one time should be avoided as this would further complicate the thermal environment making the temperatures embryos are exposed to less predictable.

As long as the complexities of the thermal environment are understood and glass stages are set appropriately, their use is likely beneficial for maintenance of embryo temperature compared to metal stages since metal stages which require a hole in the centre to enable light to pass through for microscopy and therefore are not heated at this point.

5.5 Summary

The model of heat transfer in a Petri dish system, validated in Chapter 4, was further validated in this chapter and was applied to investigate the range of temperatures an

embryo may be exposed to within the Petri dish system and the factors which influence these. The main findings were:

- In a humid incubator the dish equilibrates to within 0.3 °C of the final steady state value in 48 minutes, 20 minutes longer than the 28 minutes to equilibrate in a dry incubator.
- Modelling estimated that after considering the likely variations in air speed and laboratory condition the centre floor of a dish is very unlikely to drop below 36 °C in less than 11 seconds, and is very likely to have dropped below 36 °C after 85 seconds.
- The use of a tray or an incubator insert to transfer a dish may be beneficial if the tray is pre-warmed. Opposing thermophysical properties of the tray or insert material facilitate either maintaining the temperature of the dish floor during transfer or re-warming of the dish upon return to an incubator.
- For a Petri dish on a heated microscope stage the presence of the lid has a significant impact on the temperatures on the dish floor due to the trapping of an insulating layer of air. The steady state temperatures of a Petri dish with a lid, and one without a lid, differ by ≈2 °C on a stage of constant and uniform temperature.
- For a Petri dish with its lid on, appropriately setting the surface temperature (of a stage of constant and uniform temperature) can be done to maintain the temperature at the centre floor of the dish between 36.7 and 37.1 °C over a 10 minute period after removal from an incubator.
- For a Petri dish with its lid off, appropriately setting the surface temperature (of a stage of constant and uniform temperature) can be done to maintain the temperature at the centre floor of the dish between 35.7 and 37.1 °C over a 10

minute period after removal from an incubator. However, if a dish is placed onto this surface with its lid accidentally left on, the temperature at the centre floor of the dish could rise above 37.5 °C in < 2 minutes.

- For a Petri dish with its lid off on a stage of constant and uniform temperature, a change in the foot height from 0.35 mm to 0.65 mm (expected in different batches) changes the steady state temperature at the centre floor of the dish by 0.64 °C. For this reason stage temperature should be reset for each batch.
- For a Petri dish on a stage of constant and uniform temperature, the temperatures of embryos placed across the radius of the Petri dish may differ by up to 2.7 °C with the lid on and 2.2 °C with the lid off after 5 minutes. Temperature differences between embryos can be minimised to < 1 °C by restricting the placement of embryos to within 15 mm of the dish centre, or can be eliminated by restricting embryo placement to a ring at a set distance from the dish centre.

Similar models of other structures within the culture process, such as the 4-well dish, may be developed on this basis in order to further the understanding of the temperatures embryos are exposed to.

6 The 4-well Dish

The purpose of this section is to develop and validate a model for heat transfer in a 4-well dish. Model development has been eased significantly as the system only differs from the Petri dish model (developed and validated in Chapter 4) in its geometry. Therefore, in this chapter the Petri dish model was adapted to suit the 4-well dish system.

The application of the validated Petri dish model in Chapter 5 highlighted the complex nature of the dish-stage thermal environment. An aim of this chapter is to ascertain the differences and similarities in the dish-stage relationship between the Petri and the 4-well dishes as the same heated microscope stages are often used for both.

6.1 Drop culture in a 4-well dish

6.1.1 The System

The 4-well dish is used throughout the embryo culture process at Fertility Associates for a range of tasks. The major benefit of 4-well dishes is the provision of five separate compartments (4-wells and a central moat) as shown in Figure 6.1. At Fertility Associates the standard set up for a single well of a 4-well dish is 0.5 ml of culture media overlaid with 0.3 ml of paraffin oil; not all wells are necessarily filled. In some situations the moat between the wells may contain media for rinsing pipettes or a catheter, but embryos are not placed into the moat and it usually remains empty. For the purposes of this chapter it will be assumed that the moat is empty ('air filled').

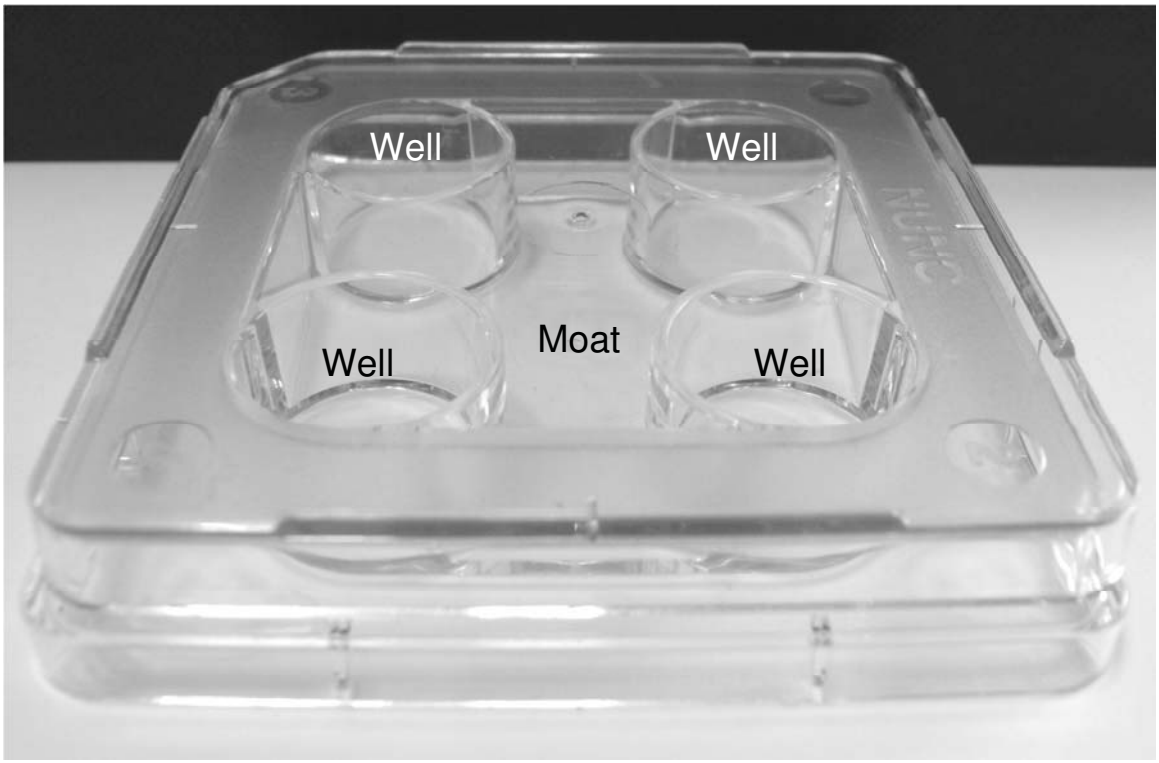

Figure 6.1: Photograph of a 4-well dish without a lid showing moat and wells

6.1.2 Conceptual Model Development

The aim of this section is to develop a conceptual model describing the heat transfer processes which take place within, and at the boundaries of, a defined model geometry. To do this, the geometry of the 4-well dish will be described. In addition, assumptions around the modes of heat transfer made in the development of the Petri dish model will be discussed with respect to the 4-well dish. This will enable a judgment to be made as to whether the model formulation for the Petri dish is applicable to the 4-well dish.

6.1.2.1 Model geometry

Figure 6.2 displays the geometry of a 4-well dish for which the dimensions, as labelled, are defined in Table 6.1. As described in Section 4.1.3.1, fully characterising

the variation in dish dimensions is not a focus of this thesis. Model validation of the Petri dish identified dimensions which have a significant impact on heat transfer to and from the floor of the dish. As for the Petri dish, for model validation these dimensions (as labelled by '*' in Table 6.1), the thickness of the dish floor ('j', Table 6.1) and the thickness of the air gap beneath the dish ('p-r', Table 6.1), were measured for each dish used in experimental work for model validation.

The 4-well dish model may not be simplified into two dimensions in a way that maintains geometries key to the thermal environment. This is because the air spaces, both with the lid on and off, differ around the well. Air insulates and therefore is important to the thermal environment. However, a simplified three dimensional geometry can be formed by taking two vertical lines of symmetry which split the 4-well dish into four individual wells (as shown in Figure 6.2). Therefore a single well will be modelled in three dimensions. This forces the assumption that the contents of each well are identical and does not enable investigation of alternatives through modelling. This is not a great handicap to the model as the impact of one well on another is very likely minimal since the majority of heat flux is vertical. When the lid is off the dish for embryo manipulation (the time during which heat loss from the system is most likely) all that connects the four wells is the thin air gap beneath the dish and the thin polystyrene dish floor which run perpendicular to the main direction of heat flux.

Several other simplifications were made to the system. As with the Petri dish model, the small lugs on the lid which form an air gap between the lid and the base of the dish were ignored while the air gap was included. The slight flaring of the dish walls

(see Figure 6.1) and the curved corners were ignored. There is no flaring of the well walls. Therefore the depth of oil and media may be easily calculated from mass. For model application, an oil depth of 1.5 mm and media depth of 2.6 mm, which respectively correspond to 0.3 ml and 0.5 ml, was used.

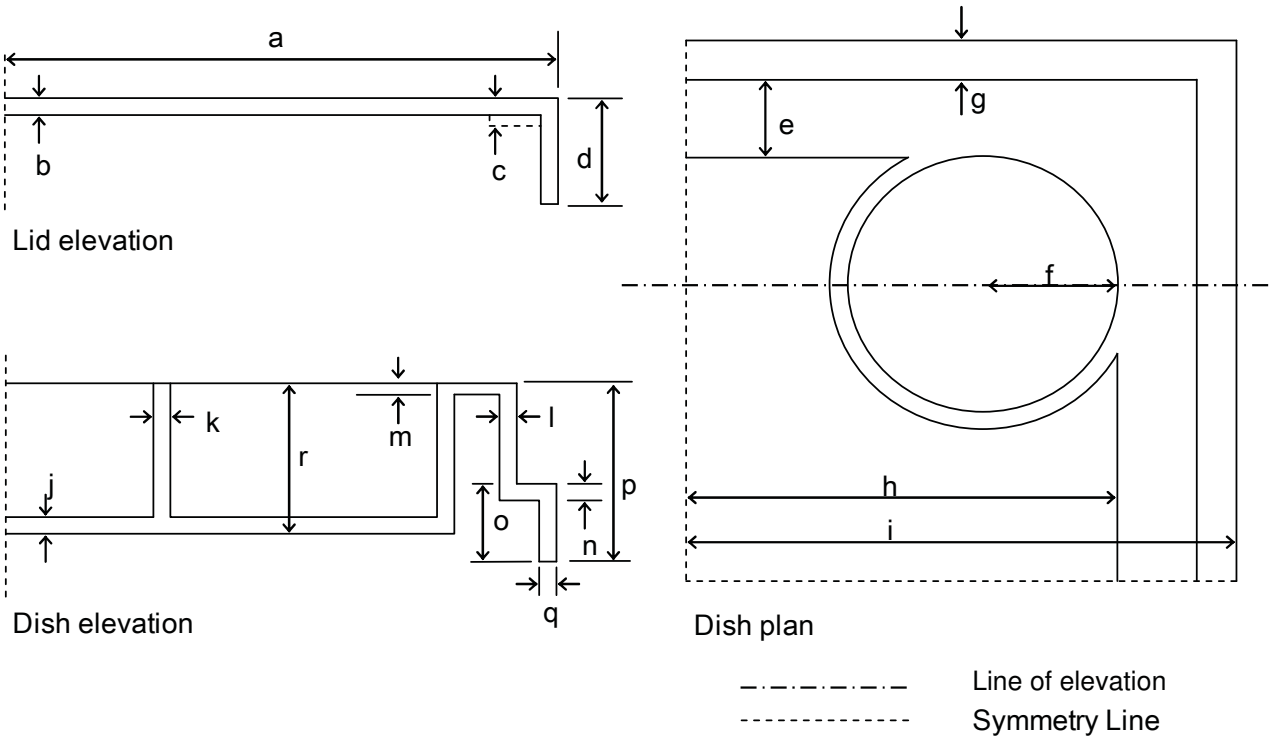

Figure 6.2: A plan and elevation of one quarter of a 4-well dish, and the elevation of its lid. Dimensions are defined in Table 6.1.

Dimension	Length	Dimension	Length	Dimension	Length
a	32.00 mm	g	2.35 mm	m	1.10 mm
b	1.00 mm	h	21.50 mm	n	1.10 mm
c	1.25 mm	i	32.80 mm	o	5.35 mm
d	5.95 mm	j*	1.10 mm	p*	11.30 mm
e	8.90 mm	k	1.40 mm	q	1.15 mm
f	7.80 mm	l	1.15 mm	r*	10.57 mm

Table 6.1: Dimensions of the 4-well dish (Figure 6.2). Measurements were taken from a single dish; each dimension value is the average of three measures from different parts of the dish. Values marked (*) are dimensions which were characterised for each individual dish during model validation.

6.1.2.2 Model Assumptions

The assumptions made in Chapter 4 (Section 4.1.3.2) that enabled the mode of heat transfer in a Petri dish system to be defined as conduction will be re-visited in this section to ensure they are applicable to the 4-well dish system.

Forced and Natural convection

Both forced and natural convection were assumed not to be significant in the Petri dish system (Section 4.1.3.2). There are a number of aspects of the 4-well dish geometry which make convection even less likely to develop than in a Petri dish. The 4-well dish is divided into five separate compartments further preventing bulk liquid movement across the whole dish and the 4-well dish is shallower than a Petri dish.

Convective heat transfer between the dish and its surroundings

The Biot numbers determined for the Petri dish (Section 4.1.3.2) ranged between 0.0627 and 2.56. These are << 20 so the external resistance to heat transfer could not be negated. The 4-well dish model is likely to be even more sensitive to this value as the small wells increase the surface area to volume ratio of the liquid, promoting heat loss to the air.

Radiation

The surface area, material and temperatures generally occurring in the 4-well dish system are similar to those in the Petri dish. Therefore the ratio of heat flux from the surface due to convection to that due to radiation will to be similar, radiation being approximately half that of convection. As with the Petri dish, since determination of the convective heat transfer coefficient is subject to significant uncertainty, the heat

loss by radiation may be included using a slightly elevated convective heat transfer coefficient.

Evaporation and condensation

The impact of the humid environment was ignored in model development for the Petri dish. The condensation of water from the air trapped under the lid upon removal from the incubator, based on the mass of water the air in the Petri dish could hold at 37 °C, was shown to be negligible (Section 4.1.3.2). This will be true for the 4-well dish as it will hold a similar volume of air.

The impact of water condensing onto the walls of a cold Petri dish when it is placed into a humidified incubator for equilibration was demonstrated in Chapter 5 (section 5.2). The only importance to the embryo culture process is that full thermal equilibration takes a little longer but still significantly less time than gas equilibration. A similar delay in thermal equilibration is likely to be seen in the 4-well dish (due to a similar surface area and initial temperature to the Petri dish) and will be discussed when validating the model.

6.1.3 Model Formulation

The assumptions made in defining conduction (thermal diffusion) as the mode of heat transfer in the Petri dish system are all applicable to the 4-well dish. Therefore formulation of the 4-well dish model is identical to that of the Petri dish. Refer to Section 4.1.4.

The 4-well dish system is made up of the same materials as the Petri dish drop culture system: paraffin oil, media, polystyrene and air. Therefore, the thermophysical properties of the subdomains are identical. These are defined in Table 4.6 Chapter 4. The heat transfer coefficient was defined for the 4-well dish in the laboratory environment to be 12 ± 2 $W.m^{-2}.K^{-1}$, using the methodology described for the Petri dish in Section 4.5.3

6.2 The Model Solution

The 4-well dish model was solved via the finite element method in the software package COMSOL Multiphysics 3.3a (COMSOL, Stockholm, Sweden). The factors involved in solving this 3D model using COMSOL Multiphysics are similar to those described in Section 4.2 for the 2D model of a Petri dish. The mesh elements in the 3D model are tetrahedrons. The conjugate gradients with the algebraic multigrid preconditioner is a linear solver that is the default for 3D models. This solver was used as it is more memory efficient than the direct solvers used for 1D and 2D models.

Solver accuracy checks were carried out, as detailed for heat transfer in a Petri dish in Section 4.2.2.2. As a result all subsequent simulations were run with a relative tolerance of 0.01. A mesh density of ≈7100 elements was used.

6.3 Model Validation

The 4-well dish was validated in the same simple, controlled situation as the Petri dish. That was pre-equilibration of the 4-well dish from an ambient laboratory

temperature to ~37 °C in a dry incubator. Pre-equilibration of the 4-well dish takes place prior to dish use in the process as in steps 2.6a, 5.1b and 9.2.4a, defined in the process flow diagram (Figure 3.10). This situation was shown to minimise the complexity of the initial conditions and boundary conditions making it easier to attribute discrepancies between the model and the experimental data to parameter(s) within the dish model.

Validating the 4-well dish after the Petri dish provided a number of opportunities. It reinforces validation of the thermophysical property estimates made when developing the Petri dish model. It also aids trouble shooting, in that any great discrepancy between the experimental data and the simulation output may initially be attributed to a) the experimental methodology or set up, or b) to the model geometry.

6.3.1 Experimental set up

The experimental set up for model validation is similar to that used for the Petri dish (Sections 4.5.1-2). A thermocouple was used to measure the centre floor temperature in one well. The thermocouple was threaded through a hole in the dish wall and the wire bent so that it ran down the wall and then across the well floor to the centre, carefully ensuring that the thermocouple's junction was in contact with the dish floor. The thermocouple was held in place with aluminium tape. 0.5 ml of media was pipetted into each of the four wells and overlaid by 0.3 ml of oil. Though only the centre floor of one well was measured for comparison with the model, in order to maintain system symmetry all wells were filled with the same amount of liquid. The mass of oil and media was weighed as it was added to the well containing the thermocouple so that the depth could be accurately determined for use in the model.

6.3.2 Model Validation

Figure 6.3 displays the data collected while equilibrating a 4-well dish, initially fully equilibrated on the bench top to the ambient laboratory temperature, to 37 °C in a dry Sanyo incubator. The incubator air temperature recovered quickly to a constant 36.8 °C so, as for the Petri dish, this was applied to the exposed boundary of the model with a convective heat transfer coefficient of 12 $W.m^{-2}K^{-1}$. The initial temperature of the dish model was set to 25.4 °C; the initial steady state temperature of the dish on the bench when t<0.

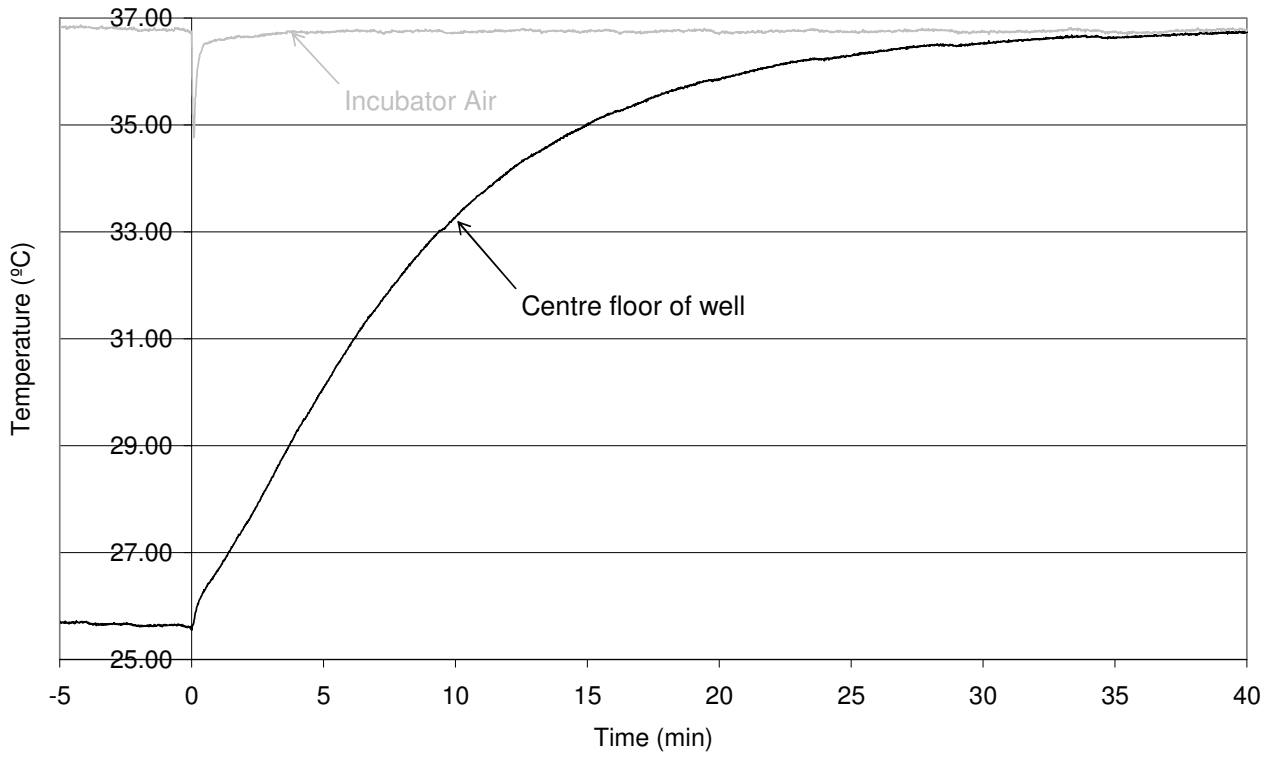

Figure 6.3: Experimentally measured temperatures at the centre floor of a well of a 4-well dish and in an incubator as the 4-well dish (initially 25.6 °C) was placed into the incubator at t=0 (with opening and closing of the incubator door) and equilibrated to the incubator temperature (36.8 °C)

30 Monte Carlo simulations were run. Figure 6.4 is a plot of maximum standard deviation of the first 'n' samples vs. the number of simulations (n). Increasing the number of simulations from 20 to 30 decreases the standard deviation by less than

0.01 °C, a negligible temperature difference, so the number of simulations was limited to 30 for subsequent model validations.

To validate the model, the experimental data set should lie within the mean ± 2 standard deviations of these simulations 95% of the time, assuming the distribution of the Monte Carlo simulations is normal enables this definition of model fit. Figure 6.5 demonstrates that the distribution of the Monte Carlo simulations, while skewed slightly toward higher temperatures, as for equilibration of a Petri dish (Section 4.5.4), was close to normal.

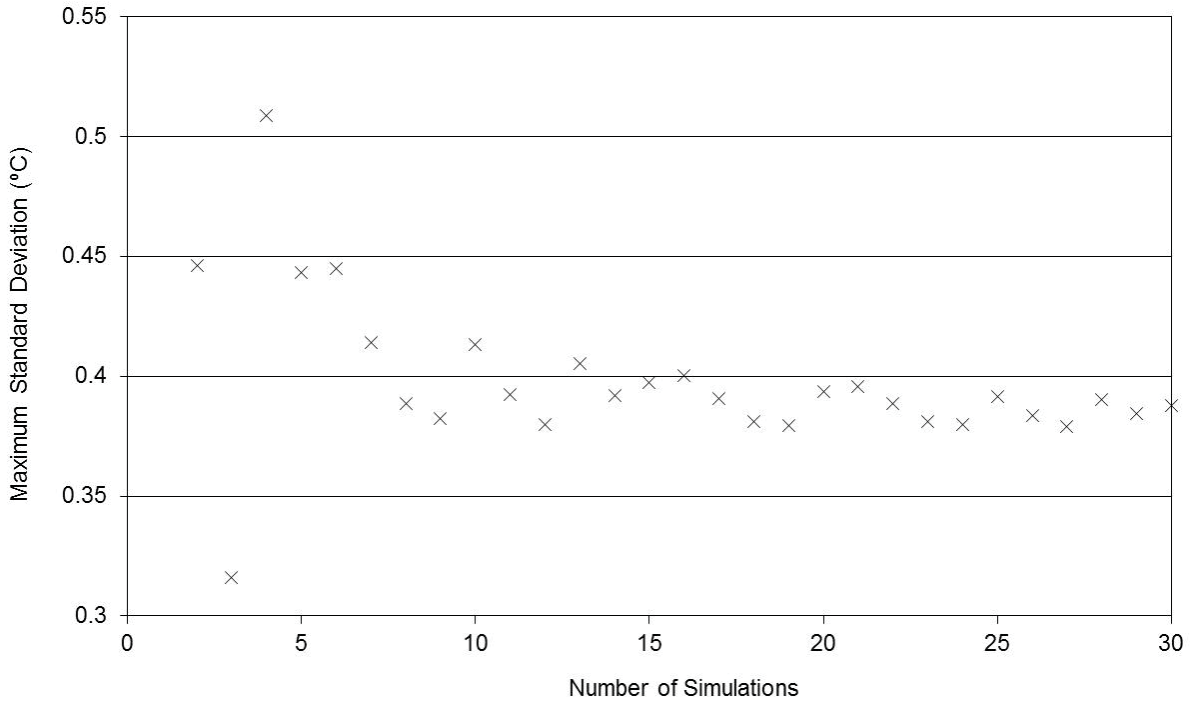

Figure 6.4: The maximum standard deviation for the first 'n' simulations (over the simulation's time steps) vs. the number of simulations run (n) for equilibration of a 4-well dish.

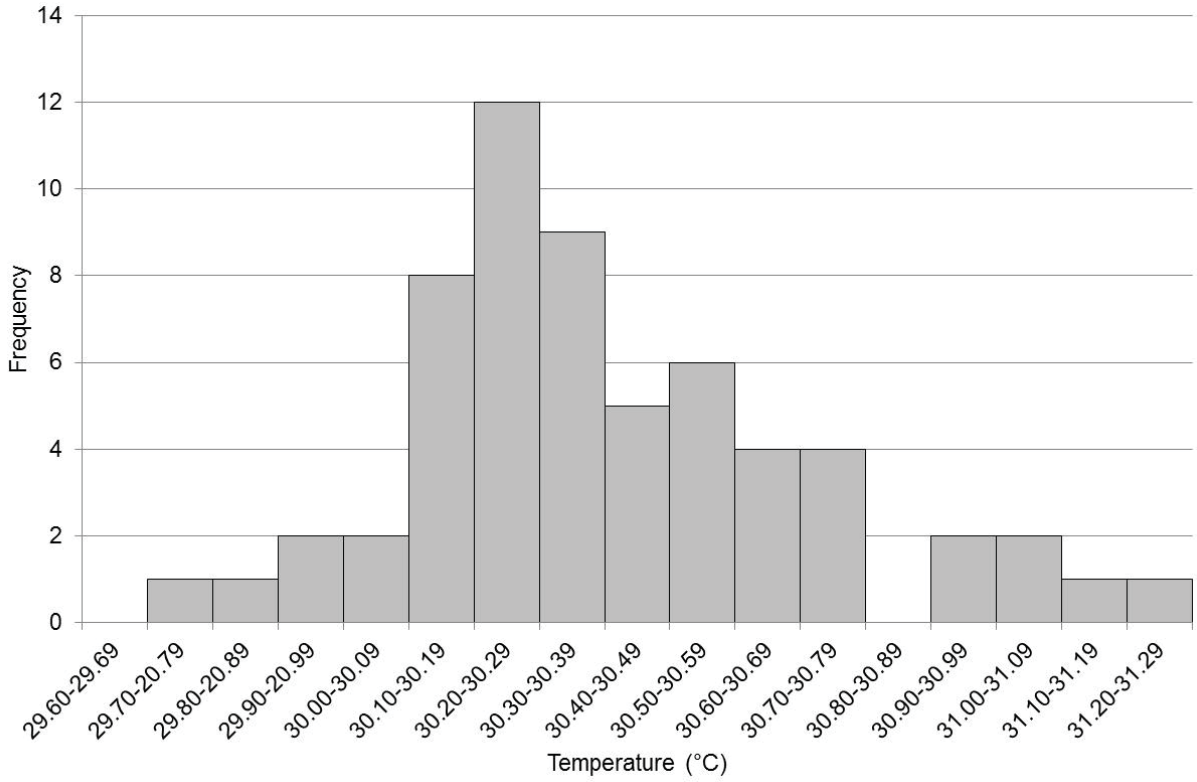

Figure 6.5: A histogram displaying the temperature frequency of 60 Monte Carlo Simulations at t=5 minutes for equilibration of a 4-well dish.

Figure 6.6 displays the comparison between the mean simulation (± 2 standard deviations) and the experimental data. For the most part the experimental data lies within two standard deviations of the mean simulation output, thus validating the model.

The exception to this is a discrepancy due to a temperature increase within the first 10 seconds of the experiment (this same temperature increase occurs in experimental replicates). During this time the dish was placed into the incubator. Moving the 4-well dish through the warm air into the incubator likely increased the rate of heat transfer (characterized by an increased convective heat transfer coefficient) to the dish. The effective convective heat transfer coefficient at the exposed boundary of a 4-well dish is possibly higher than that around a Petri dish under the same conditions due to its

geometry. The geometry impacts on fluid flow (air flow) around the boundary in question. Figure 6.7 displays the boundary between the air and the underside of both the 4-well dish and the Petri dish. The nature of the 4-well dish geometry (angular with the outer walls of the dish acting as baffles) perhaps promotes more turbulent flow around the wells of the dish while the dish is moved through the air; increasing the effective convective heat transfer coefficient.

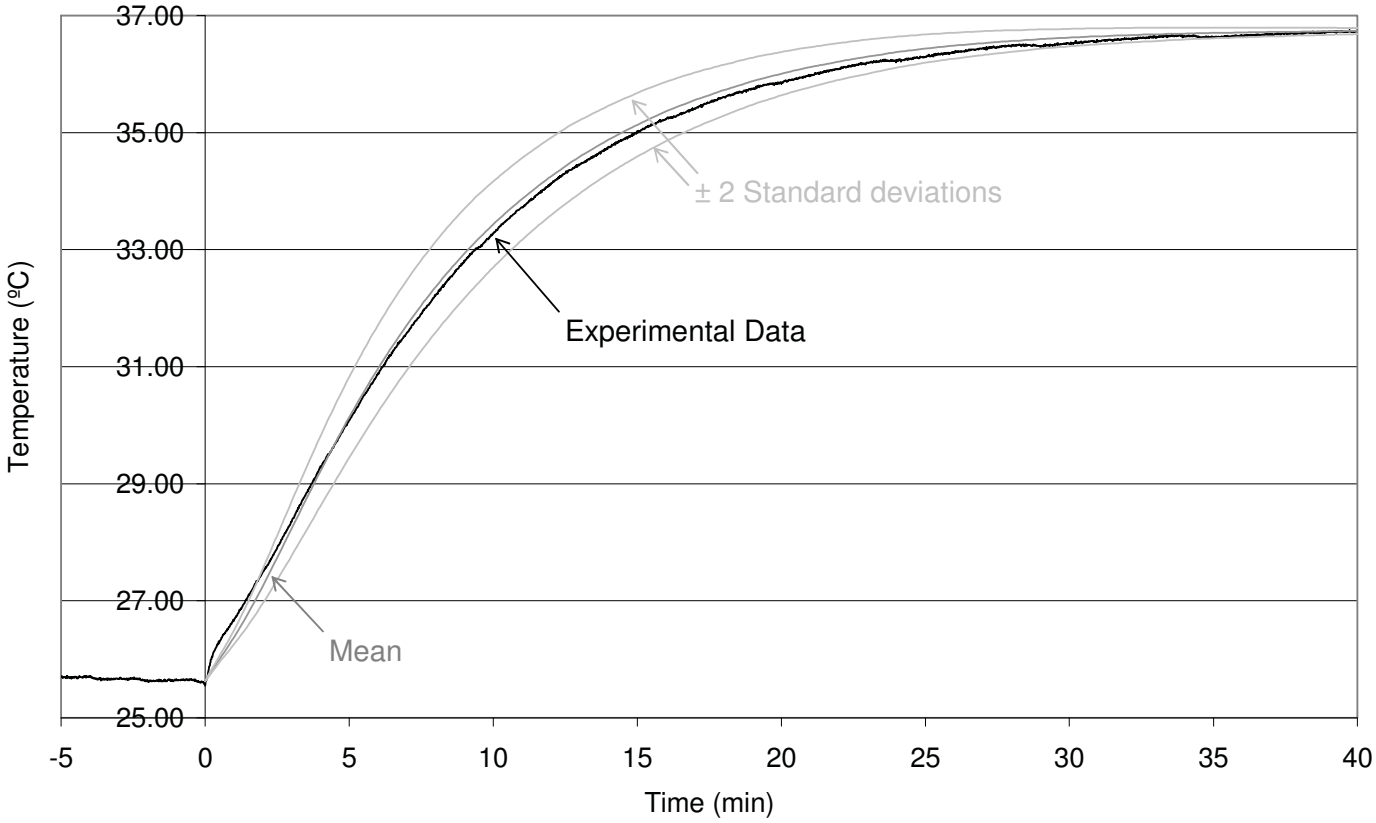

Figure 6.6: Measured temperature rise at the centre floor of a well of a 4-well dish compared with the model simulation output (mean ± 2 standard deviation of 30 Monte Carlo simulation outputs) after placement into an incubator at t=0. Initial temperature of the 4-well dish = 25.6 °C. Incubator air temperature = 36.8 °C. h=12$W.m^{-2}K^{-1}$.

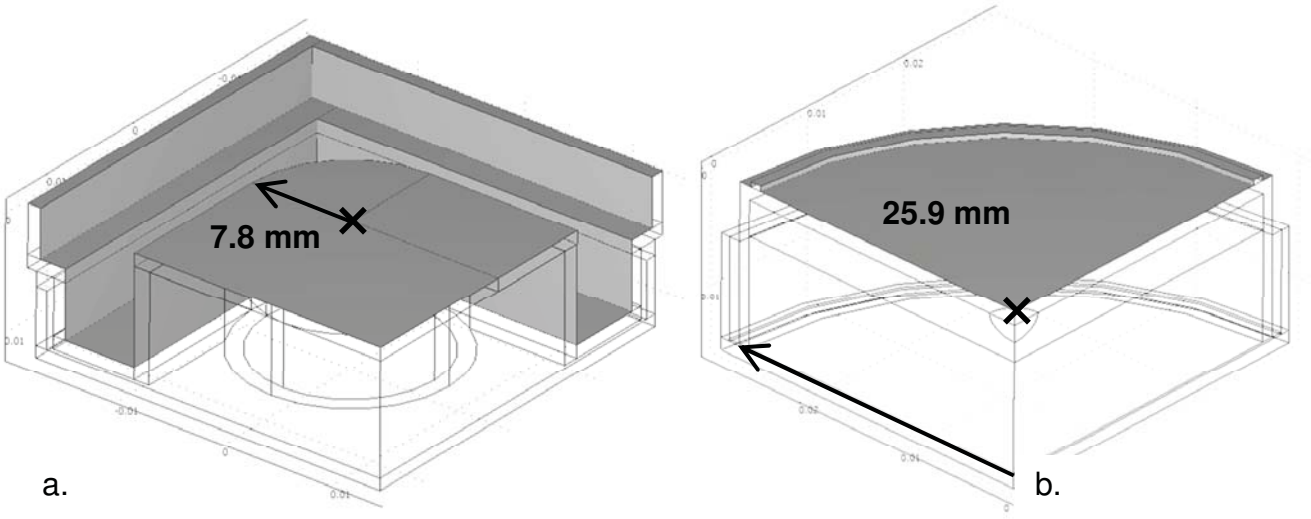

Figure 6.7: Comparing the geometry of the underside boundary of a 4-well dish (a) with a Petri dish (b).

A simulation was run in which the convective heat transfer coefficient (h) was set to 30 $W.m^{-2}K^{-1}$ for the first 10 seconds and then reduced back to 12 $W.m^{-2}K^{-1}$. The first two minutes of this simulation (mean ± 2 standard deviations) is compared with the experimental data in Figure 6.8. This shows an improved fit between the model prediction and the experimental data, demonstrating that this initial discrepancy could be due to the proposed experimental anomaly rather than any weakness in the model. Figure 6.9 shows the full simulation, throughout which the experimental data lies within two standard deviations of the mean simulation output.

The temperature at the centre floor of a well of a 4-well dish fully equilibrates in an incubator from room temperature to within 0.3 °C of the incubator temperature in 27 minutes. This is very similar to the pre-equilibration time of a Petri dish (28 minutes, as described in Section 4.5.4) therefore it will be assumed that thermal equilibration of a 4-well dish (containing ≈0.8 ml of liquid in each well) and of a Petri dish (containing ≈7 ml of oil) may be addressed together when defining equilibration time for dishes.

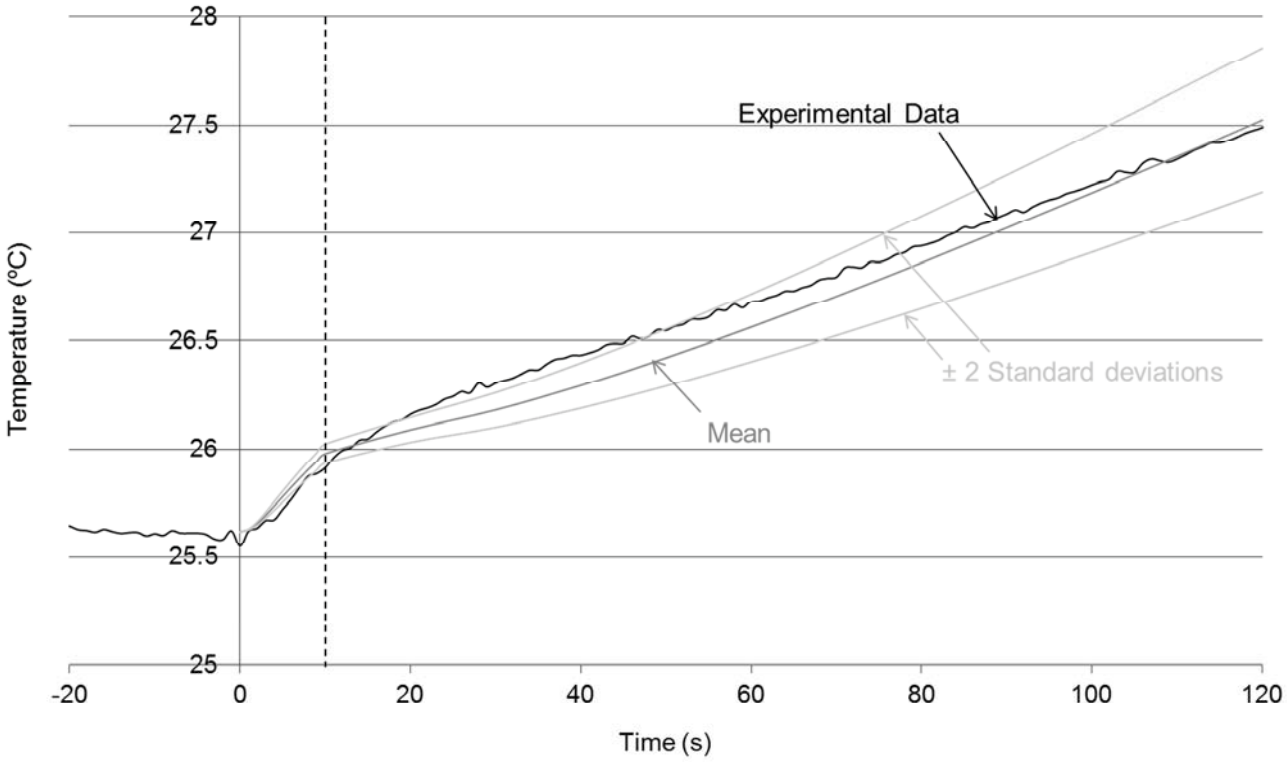

Figure 6.8: Two minutes of measured temperature rise at the centre floor of a well of a 4-well dish compared with the model simulation output (mean ± 2 standard deviation of 30 Monte Carlo simulation outputs) after placement into an incubator at t=0. Initial temperature of the 4-well dish = 25.6 °C. Incubator air temperature = 36.8 °C. For the first 10 s h=30 $W.m^{-2}K^{-1}$ then changed to h=12$W.m^{-2}K^{-1}$. Full equilibration is displayed in Figure 6.9.

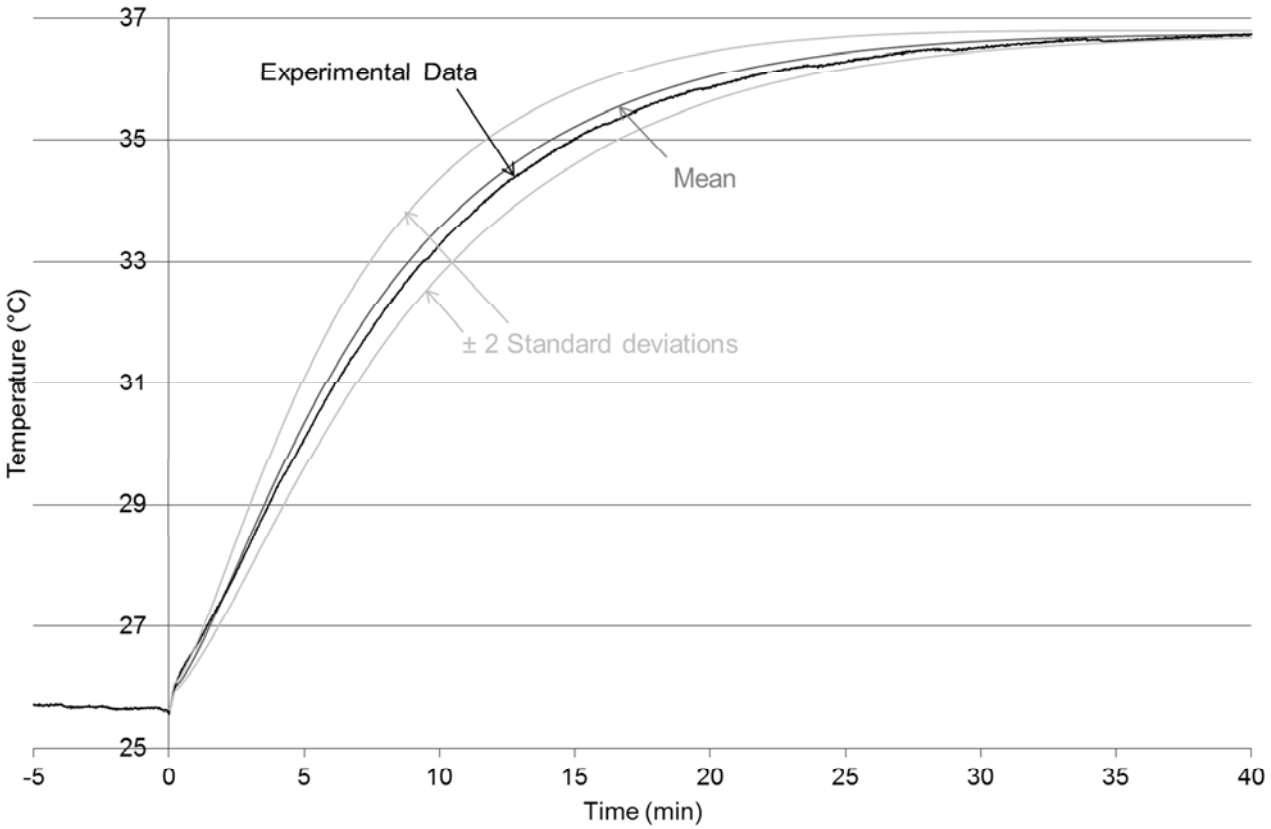

Figure 6.9: Measured temperature rise at the centre floor of a well of a 4-well dish compared with the model simulation output (mean ± 2 standard deviation of 30 Monte Carlo simulation outputs) after placement into an incubator at t=0. Initial temperature of the 4-well dish = 25.6 °C. Incubator air temperature = 36.8 °C. For the first 10 s h=30 $W.m^{-2}K^{-1}$ then changed to h=12$W.m^{-2}K^{-1}$. The first two minutes are displayed in Figure 6.8.

6.4 Model Application

The model of a 4-well dish, validated in Section 6.3, may be applied in the same fashion as the Petri dish model to investigating the thermal environment around embryos contained in this dish throughout the embryo culture process.

The 4-well dish is used at Fertility Associates for a number of tasks including rinsing embryos prior to a culture media change, stripping oocytes prior to ICSI, group embryo culture and holding embryos for an embryo replacement. In fertility clinics worldwide, 4-well dishes are utilised for other purposes. For example, they are

sometimes used in place of the Petri dish as the main culture dish, either with group culture of embryos in the wells, or for individual drop culture (3-4 drops per well).

Whenever a dish is utilised in the culture process, a similar sequence of steps is required. The following steps, which will be likely to take place when using a 4-well dish, are identical to those required when using a Petri dish:

- Equilibration of a dish in a humidified incubator
- Transfer of a 4-well dish (from the incubator onto a heated surface)
- Placement on a heated stage for embryo manipulation
- Lid removal from the dish for embryo manipulation
- Lid replacement
- Transfer back into the humid incubator
- Re-equilibration in the incubator.

Comparing the thermal environments these two dishes provide for embryos through different steps in the culture process may indicate benefits or pitfalls of one dish type over the other for use in certain tasks.

Figure 5.9, in Chapter 5, demonstrated the importance of the Petri dish's foot height (the thickness of the air layer beneath the dish) to the temperatures on the dish floor. A change of 0.3 mm to the foot height changed the steady state temperature of the centre floor of a Petri dish with its lid off by 0.64 °C. Currently NUNC 4-well dishes have a foot height of ≈ 0.73 mm. However, during 2010 NUNC released their new dish range (including Petri and 4-well dishes) without a foot so the impact of this will be considered throughout the remainder of this chapter.

6.4.1 Transfer of a 4-well dish

Transfer of a Petri dish was investigated in Section 5.3 of Chapter 5. The investigation was split into two parts, heat loss to the air and heat loss to the carrier. For the 4-well dish, the investigation solely focuses on heat loss to the air, as this will highlight differences between the dish types. The presence or absence of a dish foot is not significant to this section as the base of the dish will be exposed to the bulk air. Transfer of a 4-well dish was not incorporated as an individual step in the process flow diagram but is represented by the transition between two steps such as between steps 2.7 and 3.0 (Figure 3.10), in which a 4-well dish with its lid on is transferred from a heated stage into an incubator.

Heat transfer between the air and a 4-well dish has already been addressed in this chapter. In validating the 4-well dish model (Section 6.3.2) it was concluded that the initial rise in temperature of the centre floor of the 4-well dish (seen in several replicates of experimental data) was due to moving the dish into the incubator through warm air and this movement increased the rate of heat transfer to the dish. It appeared that the heat transfer coefficient was increased over the first 10 seconds while moving the 4-well dish into the incubator. That this phenomenon was not seen in the Petri dish suggests that the upper limit of feasible convective heat transfer coefficient for the 4-well dish could be higher than that for the Petri dish. However, this value (60 $W.m^{-2}K^{-1}$) is likely an overestimate for the Petri dish, as it was approximated experimentally by briskly walking a dish across the laboratory at a pace which would not take place in practice. It is also double the value of 30 $W.m^{-2}K^{-1}$ which explained the initial heat gain by the 4-well dish upon movement though the air into the incubator. Therefore,

this value of 60 $W.m^{-2}K^{-1}$ will be applied as the upper feasible limit to provide a comparison with the Petri dish data.

Figure 6.10 illustrates three factors which have an impact on heat loss from the 4-well dish to the laboratory air during transfer, the convective heat transfer coefficient (h), the laboratory air temperature (θ_a) and the time of transfer. This figure is similar to Figure 5.3 for the Petri dish. A model simulation was run, applying values of h and θ_a which simulated firstly the highest feasible rate (θ_a=18 °C, h=60 W.m^{-2}K^{-1}) and secondly the lowest feasible rate (θ_a=27 °C, h=10 W.m^{-2}K^{-1}) of heat transfer between the dish and the surrounding air. As for the Petri dish, a cut off temperature of 36 °C (the lower end of the desired temperature range, Section 3.6) has been assumed.

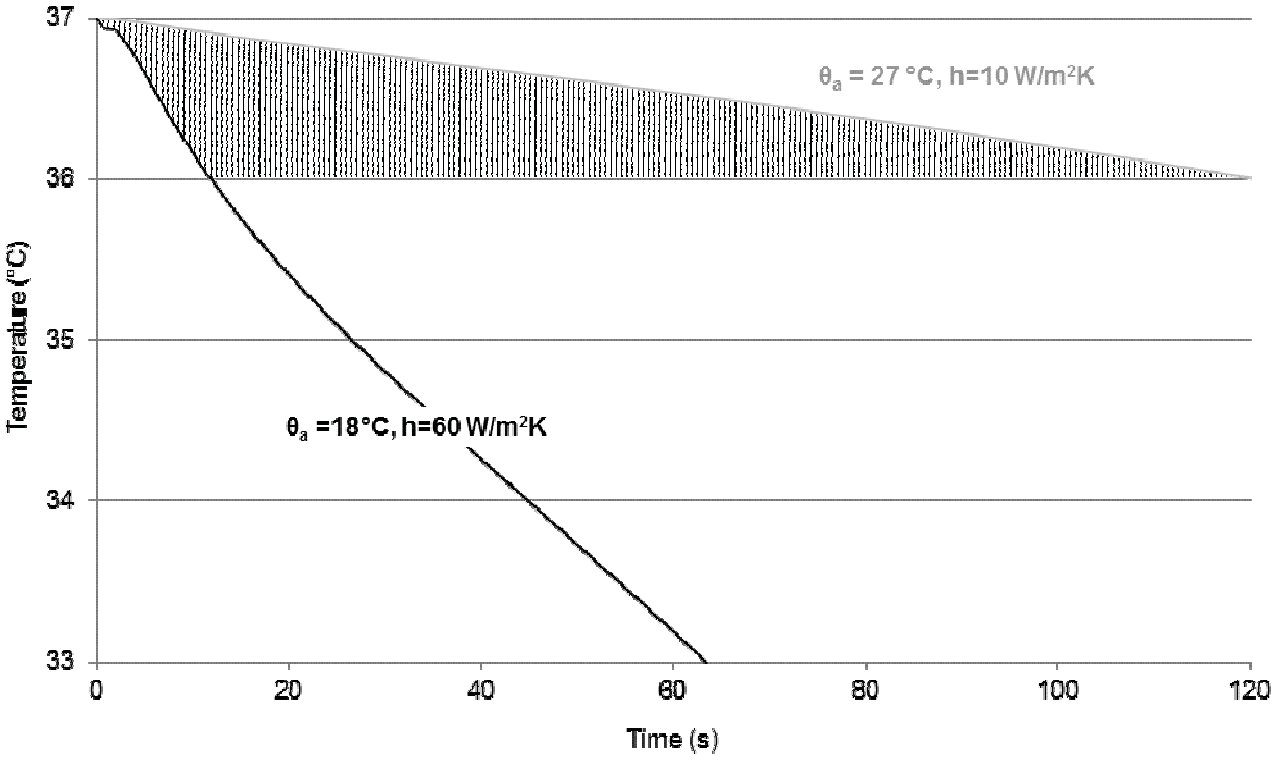

Figure 6.10: The impact of the laboratory environment on heat loss from a 4-well dish during dish transfer through air. Values of h and θ_a were chosen to give a high rate (θ_a=18°C, h=60 W.m^{-2}K^{-1}) and a low rate (θ_a=27 °C, h=10 W.m^{-2}K^{-1}) of heat transfer between the dish and the surrounding air. The shaded area represents the range of temperatures, above 36 °C, to which the centre floor of a well may feasibly drop at every time interval.

Figure 6.10 shows that the centre floor of a well is very unlikely to drop below 36 °C in less than 12 seconds, and is very likely to have dropped below 36 °C after 121 seconds of transfer through the laboratory air. Table 6.2 compares these times with those predicted for the Petri dish (Figure 5.3). It appears that when assuming identical boundary conditions the 4-well dish takes longer to drop below 36 °C. This is because the bulk of heat transfer is perpendicular to the floor of the dish or well. A well of the 4-well dish contains a total liquid depth of 4 mm and therefore a greater resistance to heat loss compared to the 3.09 mm liquid depth in a Petri dish. As stated in Section 5.3.1, in a small laboratory 11-12 seconds is a plausible time in which to move a dish from an incubator to a stage.

	Petri Dish	4-well Dish
Highest Rate (h=60, θ_a =18 °C)	11 s	12 s
Lowest Rate (h=10, θ_a =27 °C)	86 s	121 s

Table 6.2: Comparison between heat loss from a Petri dish and a 4-well dish in laboratory environments which provide either a high or a low rate of heat loss. The times reported are those required for the temperature at the centre floor of the dish or well, for the Petri dish and 4-well dish respectively, to drop from 37 to 36 °C. Values obtained from model predictions displayed in Figures 5.3 and 6.10.

6.4.2 The 4-well dish on a surface of constant and uniform temperature

As identified in Section 5.4.1, modelling a dish system on a stage of constant and uniform temperature enabled investigation of factors which impact on an embryo's thermal environment outside of the incubator. In Section 5.4, modelling was applied to investigate factors within the Petri dish system which affect the temperature embryos are exposed to. The purpose of this section was to do the same for the 4-well

dish and to compare the interaction of the 4-well dish and Petri dish with a heated stage (of constant and uniform temperature). This information was required as 4-well dishes and Petri dishes are used on the same heated surfaces in laboratories world-wide. In the process flow diagram (Figure 3.10) 25 steps involve a 4-well dish (with and without a lid) on a heated microscope stage (the first of these is step 2.6b). The effect of having no foot on 4-well dishes will be considered.

4-well dish vs. Petri dish

Figure 6.11 compares the modelled temperature changes at the centre floor of the well or dish (as appropriate) of three dishes with their lids on, a 4-well dish with a foot, a 4-well dish with no foot and a Petri dish, after placement onto a surface of constant and uniform temperature (36.7 °C). This surface temperature (36.7 °C) was the set temperature to best maintain temperatures within a 4-well dish with a foot and lid on between the assumed limits of 36 to 37.1 °C (Section 3.6).

In all three dish types the temperature at the centre floor transiently increases and then decreases after placement onto a heated surface. This response is because the oil layer has a low thermal diffusivity ($\alpha=\lambda/(\rho.cp) = 8.8\times10^{-8}$ m^2s^{-1}) compared to the other layers in the system ($\alpha=2.22\times10^{-5}$ for air, 1.11×10^{-7} for polystyrene and 1.49×10^{-7} m^2s^{-1} for water/media). This means that heat from below can reach the media droplet relatively fast but is dissipated into the oil layer more slowly. Once steady state is reached the media droplet temperature reduces based on the thermal resistances discussed above.

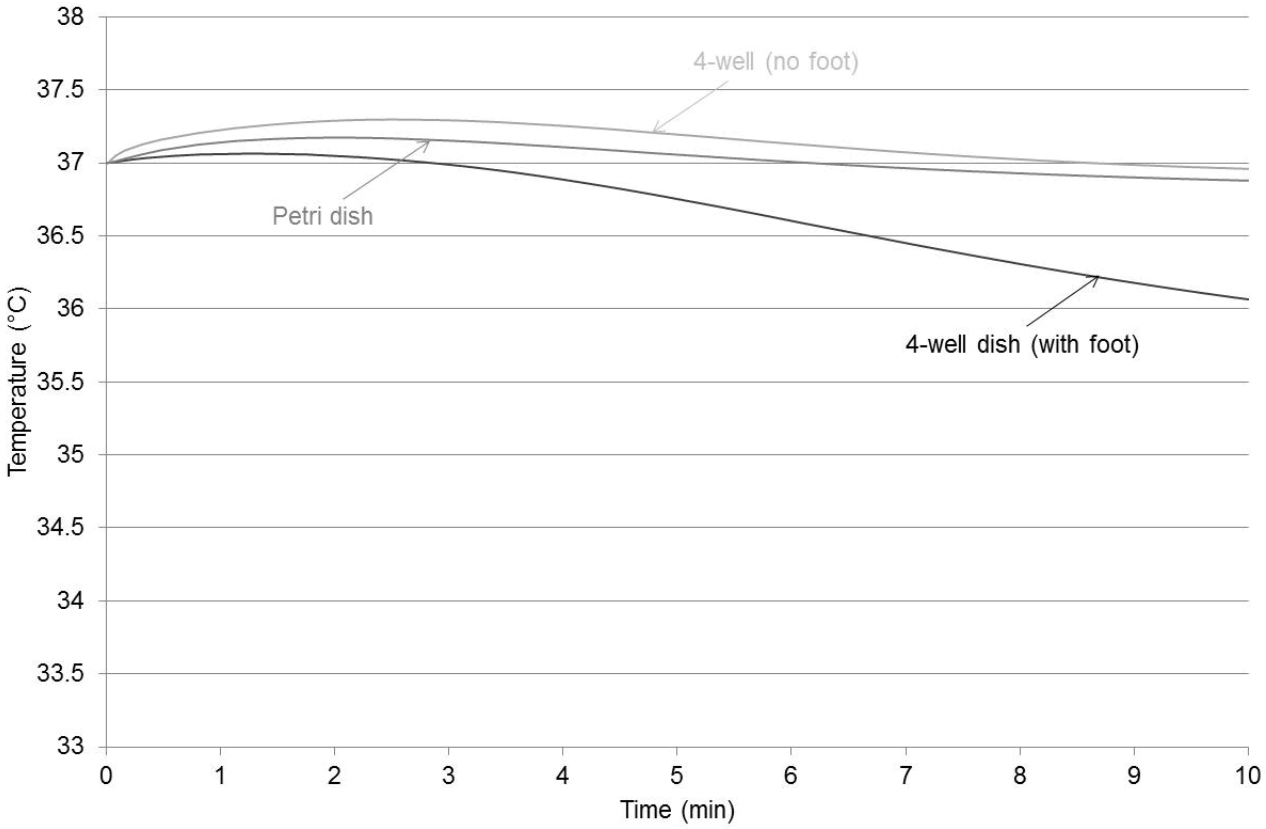

Figure 6.11: Modelled temperature profile from three dishes all with lids on, a Petri dish (centre floor), a 4-well dish with a foot height of 0.73 mm (centre floor of well) and 4-well a dish with no foot height (centre floor of well), after placement onto a heated stage (constant and uniform temperature of 37.6 °C). The Petri dish contained a single central drop overlaid by a depth of 3.09 mm of oil, the 4-well dishes contained a depth of 2.5 mm of media overlaid by 1.5 mm of oil in each well. Ambient air temperature =25°C, h=12 $W.m^{-2}K^{-1}$.

Figure 6.12 makes the same comparison for dishes with their lids off.

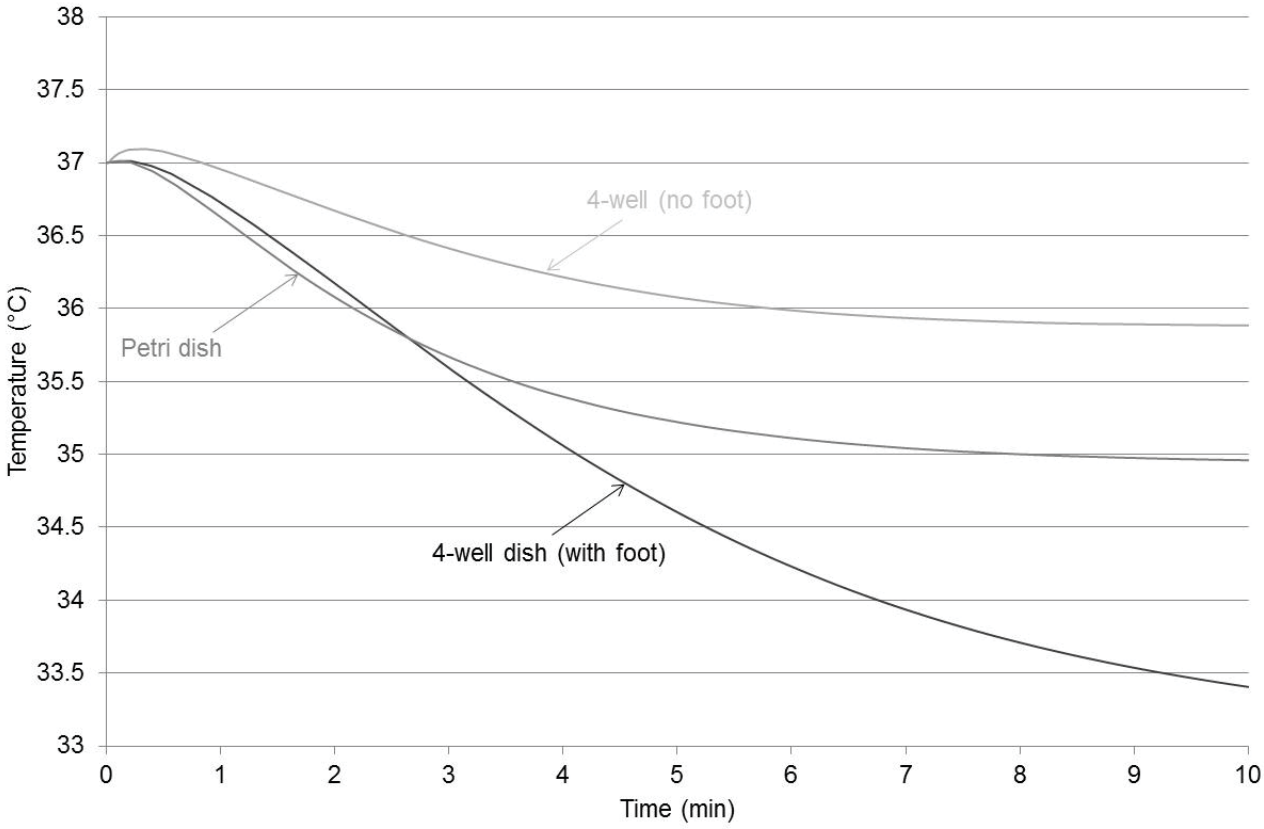

Figure 6.12: Modelled temperature drop from three dishes all with lids off, a Petri dish (centre floor), a 4-well dish with a foot height of 0.73 mm (centre floor of well) and 4-well a dish with no foot height (centre floor of well), after placement onto a heated stage (constant and uniform temperature of 37.6 °C). The Petri dish contained a single central drop overlaid by a depth of 3.09 mm of oil, the 4-well dishes contained a depth of 2.5 mm of media overlaid by 1.5 mm of oil in each well. Ambient air temperature =25°C, h=12 $W.m^{-2}K^{-1}$.

The importance of the foot height beneath the dish to heat transfer in a dish was described for the Petri dish in Section 5.4.3. The air layer created beneath the dish by the foot is the layer with the greatest resistance to heat transfer between the floor of the dish and the stage surface. This will be true for the 4-well dish which has the same air and polystyrene layers (while different thicknesses) between the heated surface and the well floor. It therefore has a significant impact on the steady state temperature at the floor of the dish or well. As expected, in both Figures 6.11 and 6.12 the steady state temperatures decline with increasing foot height in the order: 4-well dish with a

foot height of 0 mm, Petri dish with a foot height of 0.43 mm, 4-well dish with a foot height of 0.73 mm.

In both Figures 6.11 and 6.12, the stage surface temperature was set to best maintain temperatures within a 4-well dish, with a foot and its lid on, between the assumed limits of 37.1 and 36 °C (Section 3.6). This stage set point does not maintain the temperatures of the other dish configurations between these limits demonstrating the difficulties of using more than one dish type on a given stage set-up.

Liquid depth

In addition, Figure 6.13 displays the modelled heat loss from the centre floor of a well of a 4-well dish, initially at 37 °C, with lid on or off, after placement onto a stage of constant and uniform temperature (36.7 °C) for varying liquid depths in the well. The depth of liquid in a well in practise is approximately 4.1 mm (equates to 0.8 ml of liquid in the well). Varying liquid depth by 4 mm only changes the steady state temperature by ≈0.3 °C. A small change in liquid volume will therefore have little impact on heat loss from the dish system while it is sat on a heated surface.

With the lid on or off the dish, the lower the liquid depth in the well, the higher the steady state temperature at the centre floor of the well. This is counter intuitive as one would expect that the more liquid in the well the warmer the dish floor will stay.

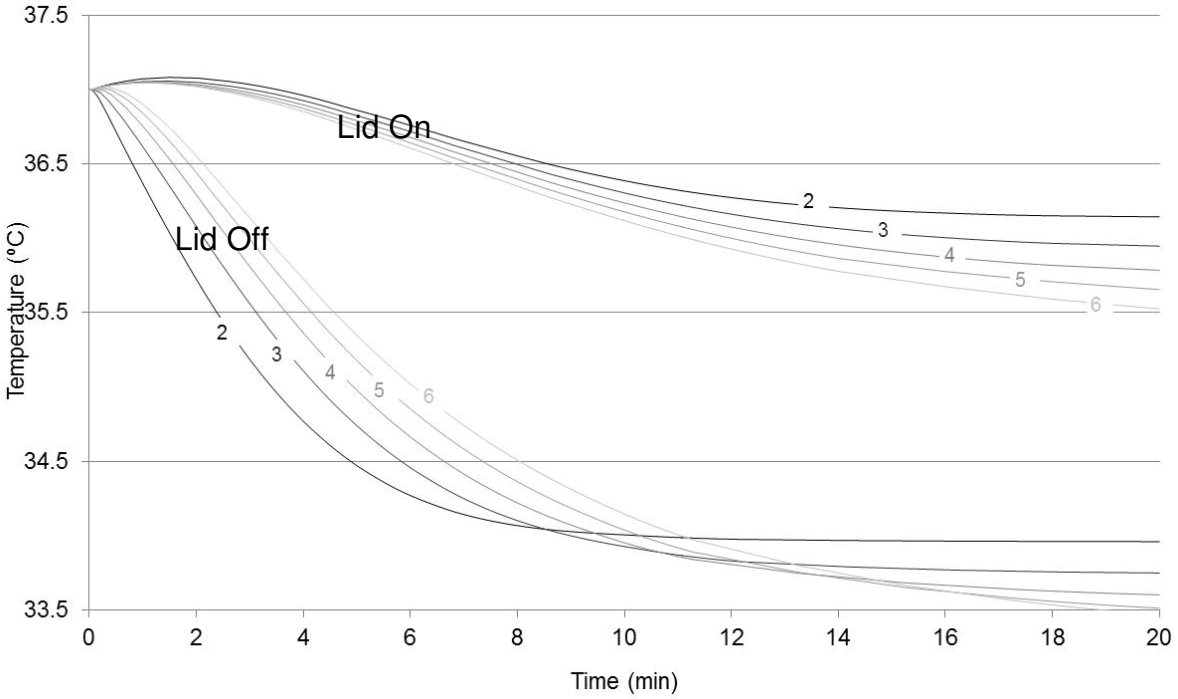

Figure 6.13: Modelled fall in temperatures at the centre floor of the well of 4-well dishes, both with lid on and off, which vary in total liquid depth between 2 and 6 mm (the oil depth remains constant at 1.5 mm) after placement on to a stage (constant and uniform temperature of 36.7 °C). Ambient air temperature=27 °C, h=12 $W.m^{-2}K^{-1}$.

Table 6.3 displays the resistances to heat transfer of each layer along the central axis of a well of the 4-well dish system. With the lid on the dish air is trapped above the liquid in each well. This air layer, as shown in Table 6.3, has the greatest resistance to heat transfer and is also dependent on the liquid depth. The lower the liquid depth the greater the thickness of the air layer trapped in the dish and the greater the resistance to heat transfer above the floor of the dish.

Figure 6.13 shows that by increasing the depth of liquid in the well the thermal mass of the system increases and thus the centre floor of the well takes longer to reach steady state. Increasing the depth also significantly increases the surface area for heat loss through the well walls and the steady state temperature falls.

	Thickness (m)	Thermal conductivity ($W.m^{-1}K^{-1}$)	Resistance ($m^2.K.W^{-1}$)
polystyrene (lid)	0.001	0.156	0.0064
air(trapped by lid)	0.00672	0.024	0.28
oil	0.0015	0.124	0.0121
media	0.0015	0.620	0.0032
polystyrene (well floor)	0.0011	0.156	0.007
air (trapped under dish)	0.00073	0.024	0.03

Table 6.3: The thickness, the thermal conductivity and the resistance to heat transfer of the layers along the central axis of a well of a 4-well dish system with its lid on (assuming a total liquid depth of 3 mm).

Position of embryo across well

Figure 6.14 displays a two dimensional temperature profile across the floor of wells in two 4-well dishes (no lids), one with a foot height of 0.73 and the other with no foot, five minutes after placement onto a stage of constant and uniform temperature. The temperature of the boundary condition was set appropriately for each foot height, 39.5 °C and 37.6 °C for the dish with a foot and the dish with no foot respectively. For each, the structure of the dish quarter surrounding the well is shown; the centre of the dish is where the lines of symmetry intersect. For both dishes point 'a' is the coolest position as it is next to the internal side of the well wall which is exposed the laboratory air (since there is no lid on the dishes). Point 'b' is the warmest as it is positioned next to the outer side of the well wall which is insulated by air trapped in beneath the dish by the outer walls of the dish.

After five minutes on the stage the temperature difference between points 'a' and 'b' is 1.27 °C for a 4-well dish with a foot height of 0.73 mm and 0.68 °C for a 4-well dish with no foot. The presence of an air gap beneath the dish, which has a resistance

to heat transfer approximately four times that of the polystyrene well floor (as shown in Table 6.3), enables a temperature gradient to build up horizontally beneath the dish. Therefore greater gradients exist across the floor of wells above an air gap compared to the situation when the polystyrene well floor is in direct contact with the heated surface.

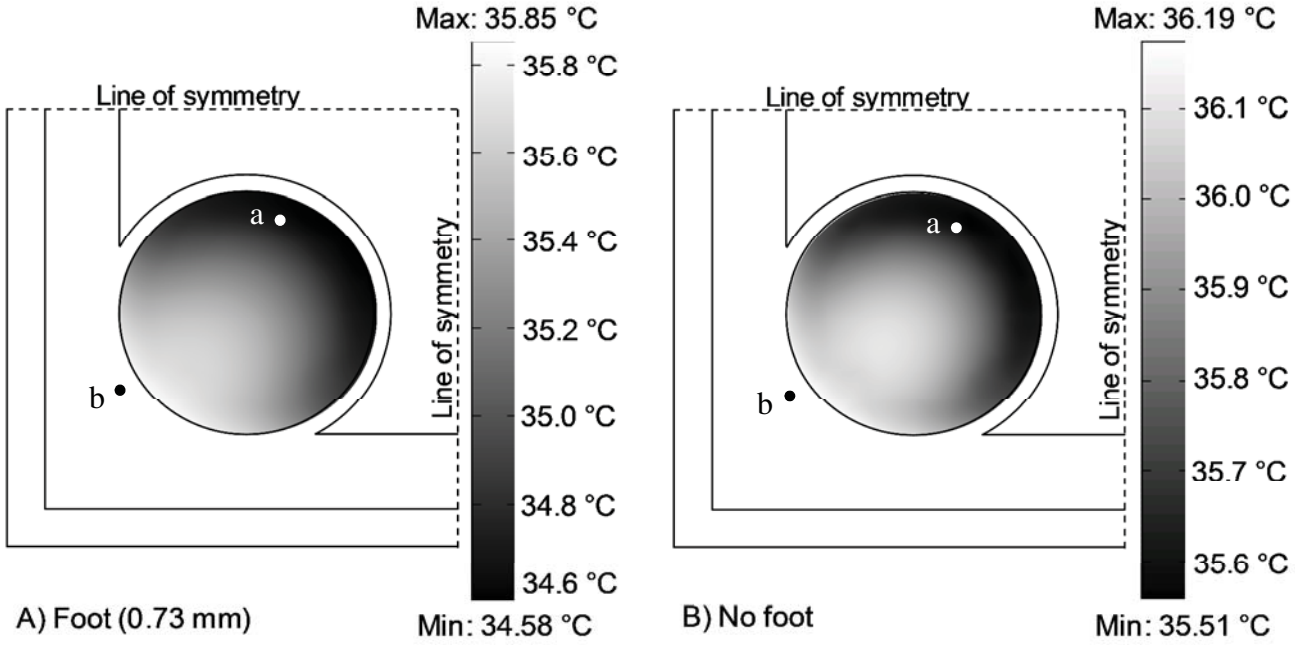

Figure 6.14: A) Modelled temperature profile across the floor of a well of a 4-well dish with a foot height of 0.73 mm at t=5 min after placement onto a stage (constant and uniform temperature of 39.5 °C) B) Modelled temperature profile across the floor of a well of a 4-well dish with no foot at t=5 min after placement onto a stage (constant and uniform temperature of 37.6 °C). For both A and B the well contained a depth of 2.5 mm of culture medium overlaid with 1.5 mm of oil, the initial temperature of the dish systems = 37 °C, ambient air = 25 °C, h=12 $W.m^{-2}K^{-1}$. Point 'b' marks the position in the well closest to the 4-well dish corner. Point 'a' marks the position in the well closest to the centre of the 4-well dish.

Figure 6.15 shows how the temperature profile across the well floor develops over time for the 4-well dish with a foot height of 0.73 mm after placement onto a surface of constant and uniform temperature (39.5 °C). The well diameter is taken from point 'a' (0 mm) to point 'b' (15.6 mm) as defined in Figure 6.14. The temperature gradient

across the diameter of the well floor at any time is steepest next to the walls of the wells.

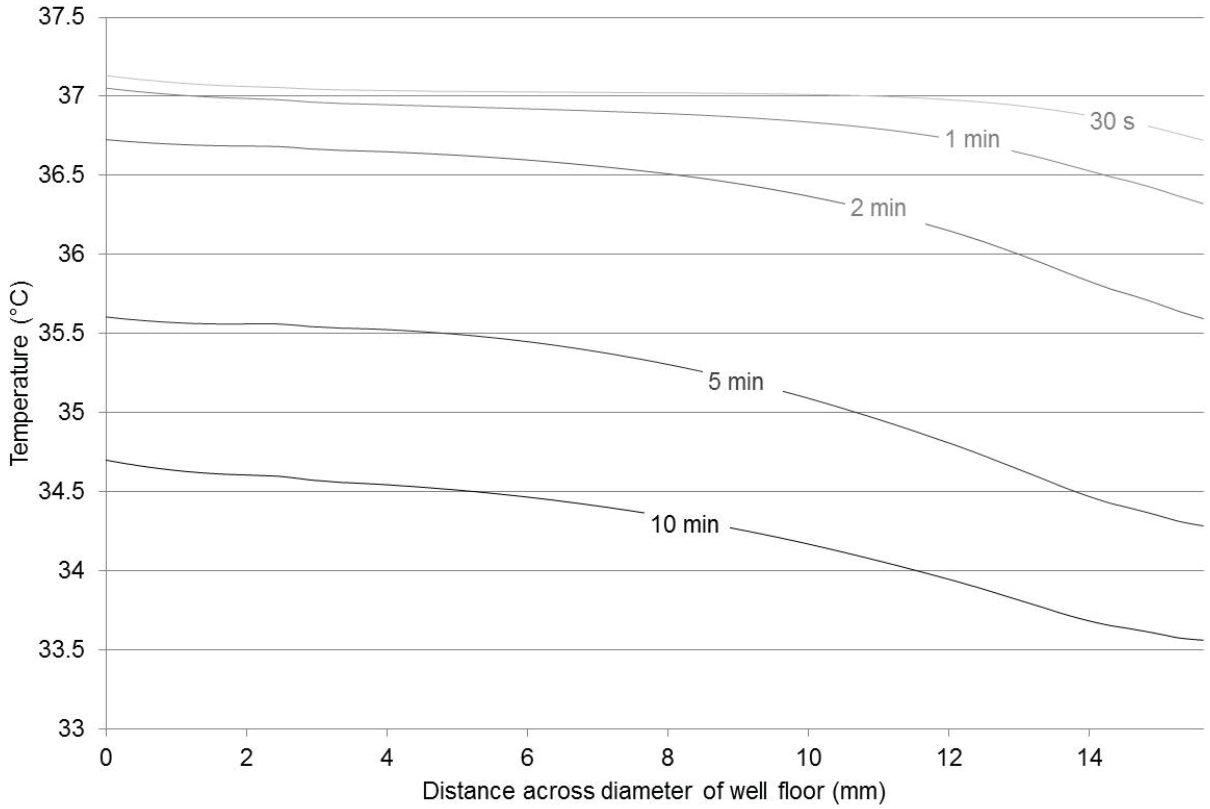

Figure 6.15: Modelled temperature profile across the diameter of the floor of a well of a 4-well dish (lid off, foot height = 0.73 mm, 2.6 mm media overlaid with 1.5 mm paraffin oil) at times 30 s, 1 min, 2 min, 5 min and 10 min after placement on a stage (constant and uniform temperature of 39.5 °C). The diameter runs across the well from the point on the circumference closest to the dish corner (point b, Figure 6.14) to the point closest to the dish centre (point a, Figure 6.14). The dish system is initially at 37 °C, ambient air 25 °C, h=12 $W.m^{-2}K^{-1}$.

Temperatures across a well of the 4-well dish vary across the whole diameter of the well as the environment beyond the wall of the well is not uniform. This is unlike the Petri dish in which the temperatures are uniform at any time for a specified distance from the centre. Figures 6.14 and 6.15 show that the warmest point across the floor of a 4-well dish (with its lid off) is point 'b', the position closest to the corner of the dish. This suggests that when setting a heated microscope stage for the use of a 4-well dish

without a lid it should be the temperature at point 'b' which is measured to ensure the temperatures do not exceed 37.1 °C (or a chosen upper limit). Restricting placement of embryos to within a set distance from the well walls could be a useful option to reduce the maximum temperature difference between any two embryos across the dish floor.

6.5 Summary

The model of heat transfer within the Petri dish (developed and validated in Chapter 4) was adapted for the 4-well dish system and validated in this chapter. The model was then applied to investigation of the thermal environments embryos are exposed to in 4-well dishes throughout the culture process. The main findings were:

- In a dry incubator the dish equilibrates to within 0.3 °C of the final steady state value in 27 minutes (similar time frame to Petri dish equilibration in a dry incubator).
- Modelling estimates that the centre floor of a well is very unlikely to drop below 36 °C in less than 12 seconds, and is very likely to have dropped below 36 °C after 121 seconds of transfer through the laboratory air.
- The importance of the foot height to heat transfer in a dish was highlighted through modelled comparison of two 4-well dishes (foot height of 0 and 0.73) and a Petri dish (foot height of 0.43) for which, after placement onto a stage of constant and uniform temperature, the steady state temperatures declined with increasing foot height.

- Comparing the 4-well dish with the Petri dish did not indicate benefits or pitfalls of one dish type over the other. Instead it demonstrated the difficulties of using more than one dish type on a given stage set-up.
- With the lid on or off the 4-well dish on a heated surface (of constant and uniform temperature), varying liquid depth by 4 mm (total liquid depth with 0.8 ml of liquid in a well is ≈ 4.1 mm) only changes the steady state temperature by ≈0.3 °C.
- For a 4-well dish system, with no lid and a foot height of 0.73 mm, on a stage of constant and uniform temperature, the temperatures of embryos placed across the well may differ by up to 1.27 °C after 5 minutes.
- For a 4-well dish system, with no lid and no foot (i.e. foot height = 0), on a stage of constant and uniform temperature, the temperatures of embryos placed across the well may differ by up to 0.68 °C after 5 minutes.

Investigation of heat transfer in the Petri dish and the 4-well dish systems covers a significant number of the steps in the embryo culture process as described in the process flow diagram (Figure 3.10). The major gap in investigation of an embryo's thermal environment throughout this process is heat transfer in pipettes which are used to transfer embryos between dishes.

7 Pipettes

In the previous chapters, models of two major dish types used in the embryo culture process (the Petri dish and the 4-well dish) were developed, validated and applied to investigate the range of temperatures embryos are exposed to in these systems. Pipettes are the tools for moving embryos between dishes. The purpose of this chapter is to develop and validate a model for heat transfer in both glass pipettes and plastic pipette tips. Understanding the temperatures embryos are exposed to in pipettes will provide a more complete picture of the temperature fluctuations that embryos are exposed to throughout the culture process. This may highlight opportunities to improve pipette use and limit environmental stress on the embryos.

7.1 Heat transfer during pipetting

7.1.1 The system

Pipettes are used to move embryos within or between dishes. At Fertility Associates two pipette types are used for embryo handling. These are finely drawn glass pipettes (commonly referred to as pulled pipettes) (VOLAC® Disposable Pasteur Pipettes, Poulten & Graf Ltd, Barking, England) and plastic (polypropylene) micro-pipette tips (T-400, Axygen Scientific, Axygen Inc., Union City, Ca).

The glass pipettes are drawn by the embryologist immediately prior to use. This involves heating the pipette in a Bunsen flame and, once it is sufficiently hot, pulling the two ends of the pipette apart thinning the pipette's glass wall and lumen. The excess glass at the tip is cleanly snapped off. Pulling pipettes is a skill in its own right

and the ease with which embryologists take to pulling glass pipettes may influence their choice of this pipette type.

Individual embryologists have their own way of pipetting which is dependent on the technique they learnt during training and how this has evolved during their careers. Influences include exposure to different techniques in different laboratories and the embryologist's own view or understanding of what is best for the embryos.

Fine control of the volume of liquid pulled into the glass pipette is obtained through slight changes in pressure on a rubber bulb (VOLAC® Teat for Pasteur Pipettes made of PVC, Poulten & Graf Ltd, Barking, England) which is attached to the end of a pipette. Pulled glass pipettes are the preferred pipette for the majority of embryologists at Fertility Associates Auckland. In contrast all embryologists at Fertility Associates Wellington use plastic pipette tips. When using the plastic pipette tips embryologists set the pipette to an arbitrary volume and control the liquid drawn into the tip by fine changes in pressure on the pipette, never fully lifting or expelling the set liquid volume.

Typically, transferring an embryo or oocyte between dishes is as follows. The pipette tip is placed into the media droplet under oil (total liquid depth of 2-4 mm in a Petri dish). The embryo(s) are lifted into the pipette within a column of culture medium. Embryologists ensure there is a depth of culture medium lifted into the pipette above the embryo(s) of approximately 5 to 20 mm in a glass pipette and approximately 3 to 10 mm in a plastic pipette tip. This is to ensure that there is sufficient liquid in the pipette above the embryo(s) to flush the embryo(s) out of the pipette on expulsion in

order to ensure that the embryo(s) do not get attached to air or oil bubbles. Embryologists also ensure there is a depth of culture medium lifted into the pipette after the embryo(s) (between 2 and 5 mm) to ensure the embryo(s) are not expelled with an air bubble. The volume of liquid lifted into the pipette in total depends on the number of embryos picked up at once (this may be anywhere between 1 and 20 embryos) and the depth of media the embryologist chooses to lift them in.

Once the embryo(s) have been drawn into the pipette it is lifted out of the dish and the embryos are placed into the new well or drop of culture medium in a new dish. The time for transfer of an embryo in a pipette to another dish is usually from 1 to 10 seconds (but may take up to 30 seconds), during which the pipette is completely surrounded by the laboratory air.

7.1.2 Conceptual model development

The aim of this section is to develop a conceptual model describing the heat transfer processes which take place within pipettes during their use. To do this, the geometries of the different pipettes will be described and assumptions regarding the mode of heat transfer, initial conditions and boundary conditions will be made.

7.1.2.1 Model geometry

Plastic pipette tips

A larger pipette tip (T-200, Axygen Scientific, Axygen Inc., Union City, Ca), pictured in Figure 3.7 D, was used for model validation since the internal diameter is sufficiently large for a thermocouple to be rigged inside it, enabling experimental data

collection. The validated model can then be applied to a smaller tip (T-400) since this pipette only differs in geometry. The T-400 tip is used in embryo handling. Both tips consist of three sections, two conical and one cylindrical section (into which the pipette holder fits).

The conical portion of each pipette consists of two sections, the dimensions of which are displayed in Figure 7.1. These sections differ in the slope of the wall relative to the pipette centre (line of asymmetry). For each pipette tip these dimensions are defined and are not simplified for use in models. As the majority of heat transfer is radially outwards from the line of symmetry, the ratio of liquid to plastic, radial from any position, is likely to influence heat transfer.

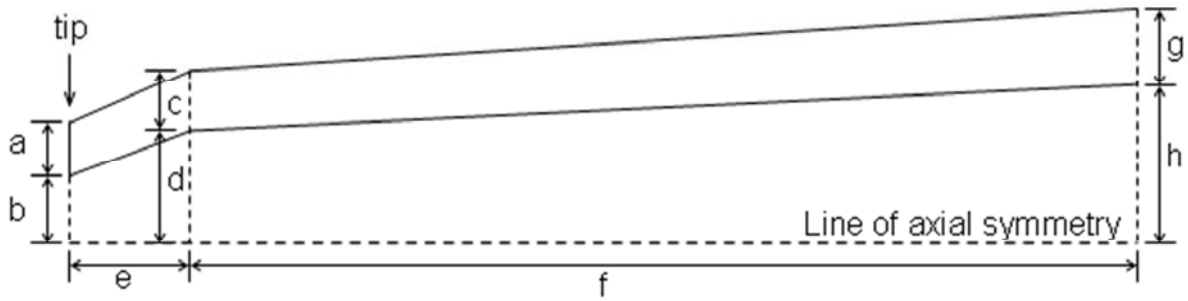

T-200		T-400	
Dimension	*Value*	*Dimension*	*Value*
A	0.15 mm	a	0.15 mm
B	0.3 mm	b	0.465 mm
C	0.5 mm	c	0.45 mm
D	0.38 mm	d	0.625 mm
E	2.5 mm	e	1.0 mm
F	32.0 mm	f	24.0 mm
G	0.5 mm	g	0.57 mm
H	1.95 mm	h	0.89 mm

Figure 7.1: Dimensions of Plastic Pipette tips. For each pipette type measurements were taken from a single pipette.

The cylindrical portion of the pipette tips is not depicted in Figure 7.1. A 10 mm cylindrical section was included in the model. While these are not depicted in Figure 7.1 they are continuous with the top of the pipette and thus have an internal diameter of ‘h’ and a wall thickness of ‘g’ (dimensions displayed in Figure 7.1).

Though the simplest form of model would be two dimensional, due to the conical nature of the geometry it proved easier to describe the geometries in three dimensions. As the time period of interest is restricted (embryos are very unlikely to remain in a pipette for longer than 30 seconds) and the geometry is very simple relative to the 4-well dish, this was not likely to significantly impact on simulation time.

Images of the three dimensional model geometries are displayed in Figure 7.2. Pipette dimensions were measured from a single pipette for each pipette type. Characterising the variation in pipette dimensions is not a focus of this thesis (as for dishes, discussed in Section 4.1.3.1).

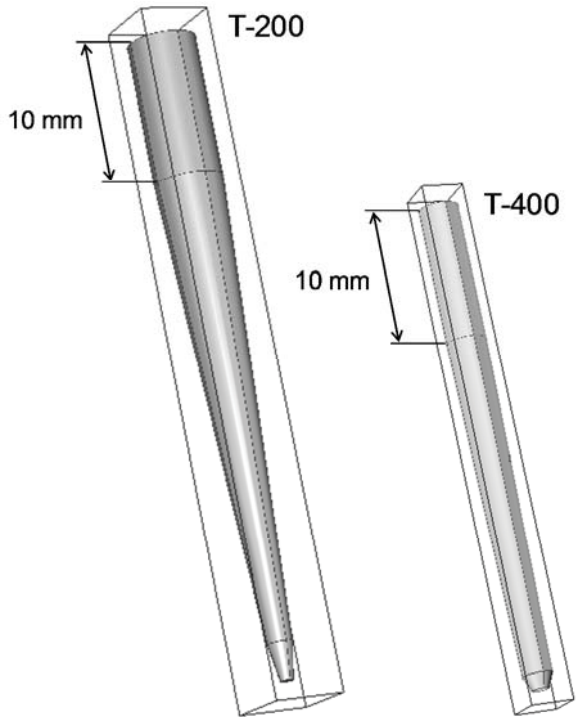

Figure 7.2: Plastic pipette tip model geometries (T-200 and T-400, Axygen Scientific, Axygen Inc., Union City, Ca).

Glass Pasteur Pipettes

The internal diameter of an un-pulled Pasteur pipette is sufficiently large so that a thermocouple can be rigged inside it enabling experimental data collection. Therefore this pipette type was used to validate the model of heat transfer in a glass pipette. Once validated against the un-pulled pipette, the model can be applied to the pulled glass Pasteur pipette which is used throughout the culture process.

Dimensions of the pulled and un-pulled Pasteur pipettes are displayed in Figure 7.3. These cylindrical pipettes may be modelled in two dimensions. The dimensions were measured under microscope from a single un-pulled and a single pulled pipette. The length was not measured since the ratio of length to diameter is very large and therefore heat transfer further up the pipette will not significantly impact heat loss from the lumen near the tip.

The pipette becomes conical away from its tip (≈30 mm), as visible in Figure 3.7, however the section of a glass pipette which contains liquid during embryo transfer will rarely exceed 30 mm in practise. Therefore the Pasteur pipette, both pulled and un-pulled, may be assumed to be cylindrical.

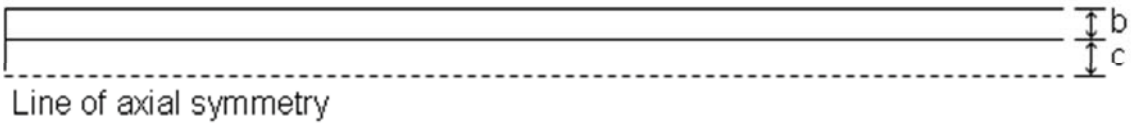

Un-pulled Pasteur Pipette		Pulled Pipette	
Dimension	*Value*		*Value*
b (wall thickness)	0.1 mm	b (wall thickness)	0.031 mm
c (internal radius)	0.35 mm	c (internal radius)	0.062 mm

Figure 7.3: Dimensions of glass pipettes. The length of the pipette is not included.

7.1.2.2 Model Assumptions

All pipettes are stored at room temperature and it may be assumed that they are at room temperature when they are picked up for use. The pipette is dipped beneath the liquid surface prior to lifting any liquid (for approximately 1 to 30 seconds). During this time the portion of the pipette beneath the liquid level will gain heat from the liquid (≈37 °C) by convection. This heat will be transferred within the pipette by conduction. Heat will be lost to the surrounding air from the portion of the pipette above the liquid level. Heat transfer during this initial period is extremely variable due to the wide time frame (1-30 s) and the variation in pipette movement which affects the degree of contact and the rate of heat transfer between the bulk liquid and the pipette.

The draw phase is the short period during which liquid is drawn up into the pipette. The length of the draw phase is difficult to measure but is estimated, by embryologists, to be a maximum of 200 ms. During this time, liquid at the bottom of the pipette is continually drawn from a source of fluid at a known and constant temperature (≈37 °C).

If the pipette is cooler than the fluid then as fluid moves up the pipette it will lose heat radially into the pipette wall. Therefore by the end of the draw phase there may be significant temperature gradients both axially and radially through both the fluid and pipette wall.

The extent to which these changes occur depends on the relative rates of heat transfer in the fluid and pipette wall at the time of the draw phase. Heat transfer rates can be

approximated as first order changes and effective time constants can be estimated. Heat transfer from a cylinder can be characterised by a time constant given by:

$$\tau = \frac{\pi^2}{4}\frac{\rho c_p r^2}{\lambda}$$ Equation 7.1

This can be applied to the loss of heat from the fluid present in the pipette to the pipette walls.

For heat transfer though the pipette wall its geometry can be approximated as a slab as, due to the small thickness of the wall (x), the internal surface area is almost the same as the outside. This is given by:

$$\tau = \frac{\rho c_p x^2}{(2.4048)^2 \lambda}$$ Equation 7.2

These time constants can be found from the exponential forms in the analytical solutions for heat conduction in a slab and a cylinder (e.g. Carslaw & Jaeger; 1947)

The rate of heat loss by convection is slow and can be negated during the draw phase. Using the properties of glass, polypropylene and media, described in Tables 4.6 and 7.2, these time constants can be estimated. To enable comparison of pipette types the plastic pipette tips were approximated to cylinders by assuming the dimensions at the thickest part of the pipette were applied (dimensions ‘g’ and ‘h’ for the wall thickness and lumen radius respectively, as described in Figure 7.1). The resulting estimates are shown in Table 7.1.

Pipette type	Time constant for loss from fluid to pipette wall (s)	Transfer through wall (s)
un-pulled glass	0.03	0.09
pulled glass	0.003	0.003
T-200 plastic tip	4.1	2.75
T-400 plastic tip	5.3	0.6

Table 7.1: Estimates of the time constant for heat transfer through the pipette wall (Equation 7.1) and through fluid in the pipette lumen (Equation 7.2) for the un-pulled and pulled glass pipette and the T-200 and T-400 plastic pipette tips.

From this analysis two conclusions can be made. In the glass pipette heat transfer is very fast, due mainly to the small distances for transport. These calculations clearly show that the fluid and wall will be approximately in equilibrium and that heat transfer from the fluid to the wall will be significant during the 0.2 s draw phase. For the plastic pipettes the opposite outcome can be seen. The time constants are much greater than the 0.2 s it takes to draw liquid into the pipette. This allows the assumption to be made to ignore the draw phase for plastic pipettes and therefore to take the initial conditions to be the fluid at the temperature of the media that is drawn into the pipette and the pipette at its initial temperature prior to the draw phase.

Mathematical modelling of the draw phase requires application of computational fluid dynamics tools which were unavailable in the base COMSOL package used in this work. As such the initial conditions were chosen assuming completion of the draw phase.

If the pipettes themselves are pre-warmed the selection of the initial conditions is straight forward as the walls of the pipette and the drawn fluid are all at the initial fluid temperature (≈37 °C). Heat losses from the walls of the pipette by convection are negligible in the time frame of the draw phase. This applies to both the glass and plastic pipette types.

When the pipette is not pre-warmed fluid drawn up first will experience the most temperature change as it will lose heat to the cold wall all the way up the pipette. This transfer will heat the pipette wall as it goes past and therefore less cooling will occur at positions closer to the tip. In this scenario, the fluid at the top of the liquid column will experience the most extreme heat loss, while at positions closer to the tip where the embryo is most likely to be (as described in Section 7.1.1) the pipette is to some degree pre-warmed.

For pipettes that are not pre-warmed, gradients in both the axial and radial direction are present after the draw phase. For the glass pipette, heat transfer rates are much faster and so significant heat transfer into the pipette wall is expected during the draw phase.

To set initial conditions for the model (at completion of the draw phase) two cases can be considered. The real conditions will fit between these cases:

1. During normal IVF practices, as discussed in Section 7.1.1., the embryo is in the bottom portion of the column of fluid within the pipette. The worst case condition the embryo would be exposed to is where no pre-warming of the pipette wall has occurred from the fluid passed over it. As such the initial

temperature of the fluid will be at the source temperature (≈37 °C) and the wall would be at its initial temperature (θ_a). In this case there will be an initial rapid cooling in this modelling as heat is lost from the fluid to the cold pipette wall. This situation will more closely reflect temperature change in the initially cool plastic pipette tips than in the glass pipettes since radial heat transfer in the plastic tips is slow relative to the length of the draw phase (see Table 7.1).

2. The other extreme is to assume a local thermal equilibrium between the fluid and the surrounding wall, as it is drawn up into the pipette. This will represent the most change that can occur to the fluid at the top of the pipette but will be a less extreme situation at the bottom due to the pre-warming effect of the fluid above (Figure 7.4).

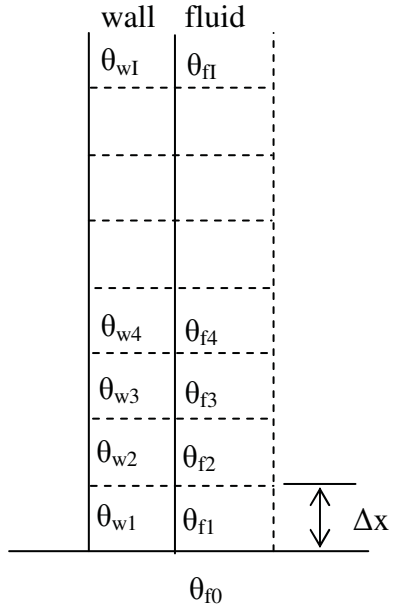

$$\theta_{wi}^{n+1} = \frac{\rho_w c_w A_w \theta_{wi}^n + \rho_f c_f A_f \theta_{f_{i-1}}^n}{\rho_w c_w A_w \theta_{wi}^n + \rho_f c_f A_f}$$

$$\theta_{fi}^{n+1} = \theta_{wi}^{n+1}$$

For i=1 to I, repeat for n=0 to N

$$A_w = \pi (r_f + x_w)^2 - \pi r_f^2$$

$$A_f = \pi r_f^2$$

$\theta_{wi} = \theta_a$ for i=1 to I, at n=0

Figure 7.4: Numerical solution for the draw phase assuming local thermal equilibrium between fluid and pipette wall. N= the total number of solutions, I = total number of segments. The subscripts 'w' and 'f' denote fluid and wall respectively.

This simple model was numerically solved using Excel to predict the temperature in a glass pipette as a function of the height as shown in Figure 7.5.

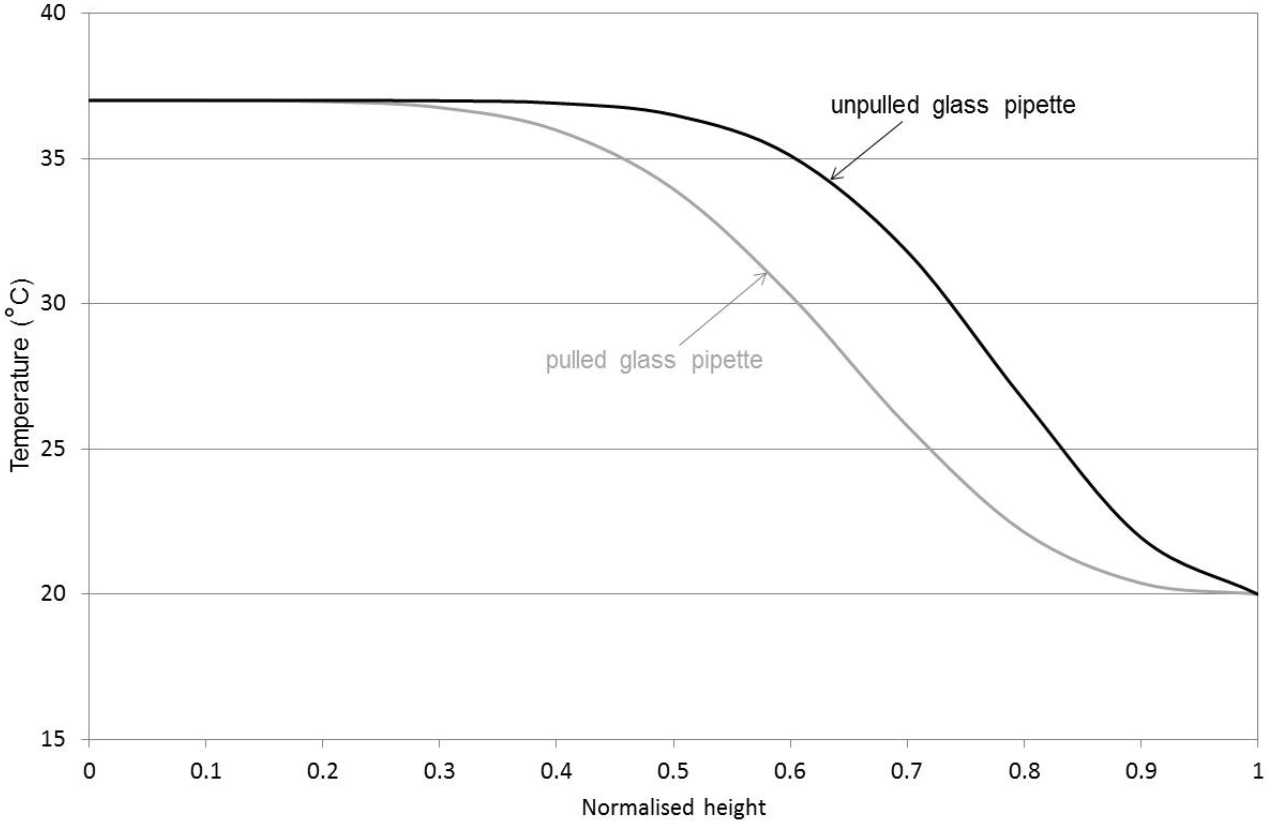

Figure 7.5: Predicted axial temperature profile in pipette after the draw phase. The height is normalised (i.e. height/final fluid height).

This analysis shows that the liquid first drawn into the pipette will cool the most, losing heat to the pipette walls. The liquid drawn up into the pipette later, after the pipette walls have been pre-warmed, loses less heat. Because of their rapid radial heat transfer rates, see Table 7.2, this analysis is most applicable to the glass pipettes.

This analysis shows that lifting embryos near the bottom of the liquid column within glass pipettes, as is done to ensure they are easily expelled (described in Section 7.1.1.), inadvertently protects them from the greater temperature changes they would be exposed to at positions further up the liquid column. This benefit should be made

known and the practice of lifting embryos in the lower half of the liquid column encouraged.

Based on this analysis two cases and initial conditions (best and worst) with respect to the embryo position can be defined.

1. The pipette is initially at the ambient temperature
   - fluid temperature = bulk fluid temperature (≈37 °C)
   - wall temperature = ambient temperature at t=0 (≈20°C)

   This will be most applicable to the use of plastic pipettes.
2. The pipette is pre-warmed
   - fluid temperature = bulk fluid temperature (≈37 °C)
   - wall temperature = bulk fluid temperature (≈37°C)

   This will be applicable to pre-warmed pipettes of either type and for the lower portion of the initially cold glass pipette.

Real practice in a plastic pipette tip will not approximate one of these cases but will fall between these limits. Real practise in the glass pipette will approximate the second, pre-warmed, case.

7.2 Model Formulation

As for the dish models it has been assumed that the sole mode of heat transfer is thermal diffusion (Equation 7.3).

$$\rho c \frac{\partial \theta}{\partial t} = \lambda \nabla^2 \theta \qquad \text{Equation 7.3}$$

There are three boundary conditions applicable to pipette models. The boundaries are labelled in Figure 7.6 and are described below**:**

Axial symmetry: For 2D pipette models there is a line of axial symmetry down the centre of the pipette. This boundary condition is not required for the 3D models of the plastic pipette tips.

$$\frac{\partial \theta}{\partial r} = 0 \qquad \text{Equation 7.4}$$

for the line of axial symmetry, $t \geq 0$.

The exposed boundary:

$$\mathrm{n}.(\lambda \nabla \theta) = h(\theta_A - \theta_S) \qquad \text{Equation 7.5}$$

for the exposed boundary of the model, $t \geq 0$.

The top boundary: The bulk of heat transfer in the pipette system is radial and it may be assumed that diffusion up the pipette wall from the liquid becomes insignificant after a short distance. Therefore a top boundary condition where no heat is transferred (thermal insulation) was appropriate.

$$\frac{\partial \theta}{\partial y} = 0 \qquad \text{Equation 7.6}$$

for the top boundary of the pipette, $t \geq 0$

As discussed above for a pre-warmed pipette of any type, and in the lower half of an initially cold glass pipette after the draw phase, the initial temperature gradient through the pipette system may be considered negligible and initial conditions will be;

$$\theta_i\,(\Omega_{\text{air (inside pipette)}},\ \Omega_{\text{pipette}},\ \Omega_{\text{media}}) = \theta_{\text{bulk liquid}} \qquad \text{at } t=0$$

'Ω' denotes the subdomain

For a cold plastic pipette tip, the pipette walls are initially assumed to be at room temperature;

$$\theta_i\,(\Omega_{media}) = \theta_{bulk\ liquid} \qquad \text{at } t=0$$

$$\theta_i\,(\Omega_{air\ (inside\ pipette)}, \Omega_{pipette}) = \theta_{ambient\ air} \qquad \text{at } t=0$$

'Ω' denotes the subdomain

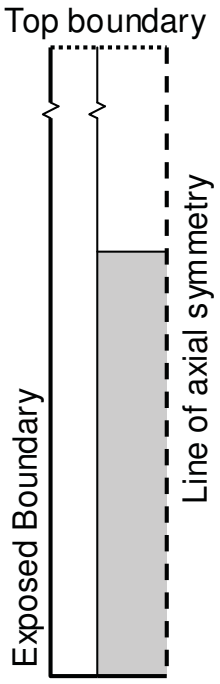

Figure 7.6: The boundaries of the pipette model. The schematic image is based on the cylindrical 2D pipette type. With the exception of the line of symmetry the same boundaries apply to the 3D plastic pipette tip models.

7.3 Parameter Estimation

In Chapter 4, Table 4.6, the values of the thermophysical properties (thermal conductivity, heat capacity and density) of air and water (culture media) and the temperature dependency of these properties were defined. Therefore only the unique pipette materials need be defined here. Table 7.2 displays values for the thermophysical properties of the various pipette materials.

The precision and accuracy required of the thermophysical properties for the models of heat transfer through the dishes was far greater than that required in the pipette model. The dish systems are large and the internal resistance to heat transfer (dependent on the thermophysical properties) was significantly important to the temperatures of interest. Every point within a pipette is close to an external boundary and therefore will be far more sensitive to the condition at this boundary than to slight changes in a subdomain property. Therefore, temperature dependency was not defined for the thermophysical properties of the pipette materials. Any uncertainty in these properties will be far outweighed by that in the convective heat transfer coefficient (h) which characterises the external resistance to heat transfer.

Pipette	Pipette Material	Parameter	Units	Value	Reference
Pasteur Pipettes	Glass	ρ_g	$kg.m^{-3}$	2203	Materials/C
		λ_g	$W.m^{-1}K^{-1}$	1.38	Materials/C
		c_g	$J.kg^{-1}K^{-1}$	703	Materials/C
		α_g	m^2s^{-1}	8.91×10^{-7}	Equation 5.
Pipette tips	Polypropylene	ρ_{pp}	$kg.m^{-3}$	900	Martienssen
		λ_{pp}	$W.m^{-1}K^{-1}$	0.22 (30°C)	Martienssen
		c_{pp}	$J.kg^{-1}K^{-1}$	1613 (30°C)	Martienssen
		α_{pp}	m^2s^{-1}	1.52×10^{-7}	Equation 5.

Table 7.2: Model Parameter Inputs. ρ=density, λ=thermal conductivity, c= heat capacity, α= thermal diffusivity. Subscripts: g=glas

7.4 Model solution

The model was solved by the finite element method in the software package COMSOL Multiphysics 3.3a (COMSOL, Stockholm, Sweden). The process required to solve the models is described in Section 4.2.1. As for the 2D Petri dish model, the 2D models of the glass pipettes were solved using the default linear system solver, the direct UMFPACK solver. As for the 4-well dish model (Section 6.2) the 3D models of the plastic pipette tips were solved using the linear solver system default for the 3D models.

Solver accuracy checks were carried out, as detailed for heat transfer in a Petri dish in Section 4.2.2.2. As a result, for all models, all subsequent simulations were run with a relative tolerance of 0.01. The mesh density varied with the model. For the 3D models a mesh of ≈17,000 elements for the larger plastic pipette tip (T200) and ≈7000 elements for the smaller plastic pipette tip (T400) were used. For the 2D models a mesh of 5,000-8,000 elements was used.

7.5 Model validation

The models of heat transfer in a plastic pipette tip and in a glass Pasteur pipette were validated against experimental data to assess assumptions and approximations made throughout model formulation and to ensure that they appropriately describe heat loss from these systems during embryo transfer.

As discussed above (Section 7.1.2.2), due to difficulties in modelling the draw phase two cases were identified in which the initial conditions could be defined at the end of the draw phase.

The first, which is applicable to the plastic pipette tips, assumes the pipette tip is initially at the ambient temperature at the end of the draw phase. This model was validated against experimental data collected in which any pre-warming is minimised by minimising contact between the plastic pipette tip and the bulk liquid before liquid is drawn into the pipette. Models of the plastic pipette tip were validated at two positions along the liquid column within the pipette. This both allowed for further validation of the model in the more complex geometry and enabled evaluation of the effect of liquid depth above the embryo on pre-warming of the pipette walls in the plastic pipette tips since transfer of heat from the liquid to the pipette walls is slower in plastic tips than in the glass pipettes.

The second, applicable to all pipette types, assumes that the pipettes are pre-warmed to the temperature of the bulk fluid at the end of the draw phase. This model was validated against experimental data collected in which pre-warming of the pipettes was ensured by repeatedly flushing the pipette with the bulk liquid before a final draw. It was also validated against experimental data collected in which any pre-warming of the glass pipette was minimised by minimising contact with the bulk liquid before liquid was drawn into the pipette. The latter tests the assumption that the pipette walls adjacent to the lower portion of a liquid column in a glass pipette are pre-warmed though contact with liquid further up the column as it was drawn up.

7.5.1 Experimental equipment and set-up

K-type thermocouples were used with an Agilent data logger. The benefits of this temperature measurement combination are described in Section 4.5.1 of Chapter 4. Of particular importance to the pipette system is the small size of the thermocouples available.

Figure 7.7 displays the positions of thermocouple junctions (labelled *a-c*) in the plastic pipette tip and glass pipette (un-pulled) during model validation experiments. For both, the uptake of liquid was controlled by manual use of a 1 ml syringe.

For the plastic pipette tip (T-200) the thermocouple (both wires encased in insulation with a solder junction) was threaded through the seal at the attachment of the pipette tip to the syringe. The length of wire within the pipette tip and the shape of this wire could be controlled to position the junction.

For the thinner glass pipette (un-pulled) the insulation was removed from the two thermocouple wires and the wires were separated (the solder broken). The end of each wire was threaded into opposite ends of the pipette, one through the seal with the syringe and the other into the tip. Each end was looped back onto itself, one through the other, pulled tight and the wire twisted to hold. The amount of each wire within the pipette controlled the position of the junction (where the two loops are pulled tight against each other).

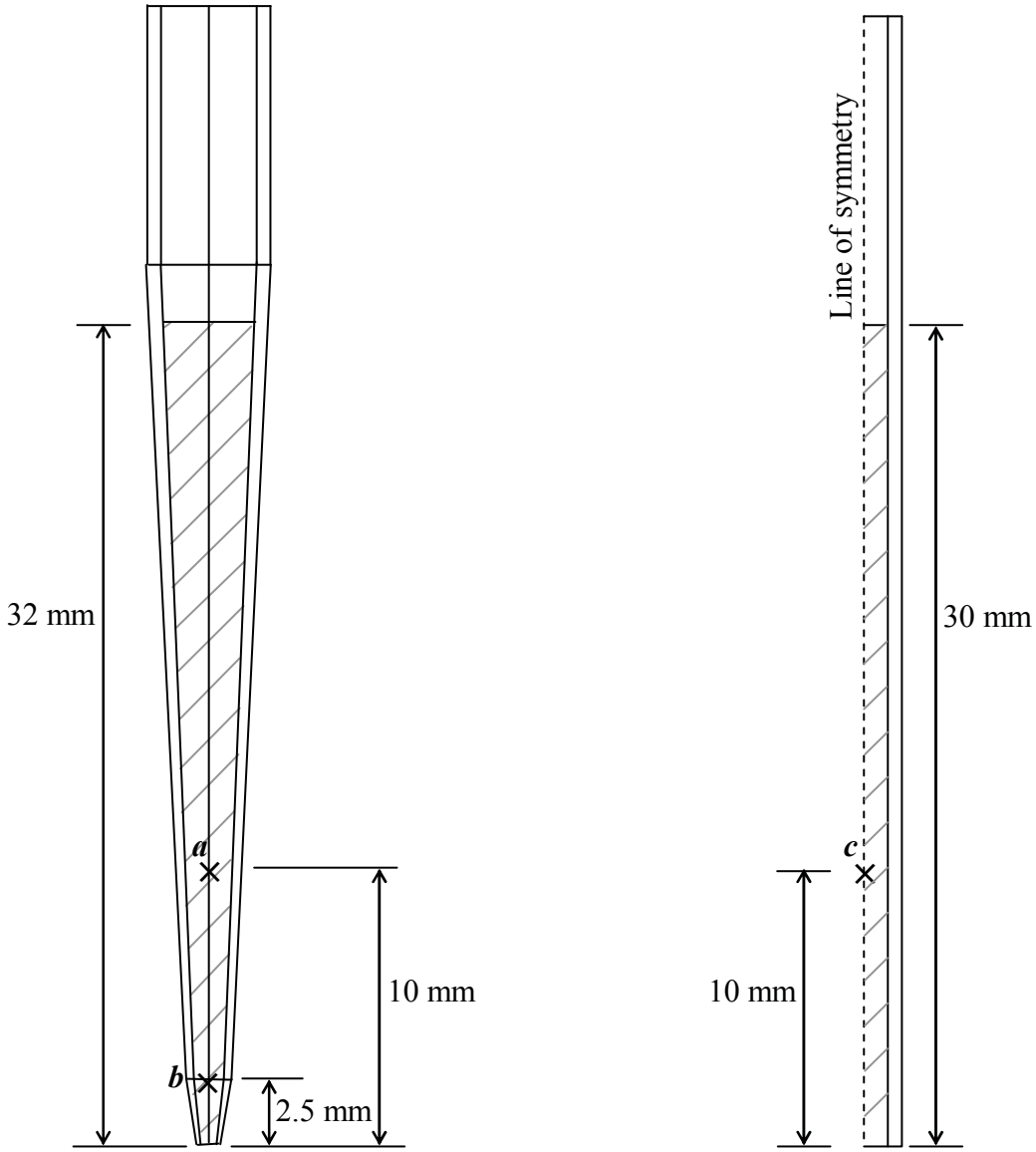

Figure 7.7: Thermocouple placement in the plastic pipette tip and glass pipette (un-pulled) during model validation experiments. × marks the thermocouple positions labelled *a-c*. / / / liquid in the pipettes.

7.5.2 Experimental Methodology

The room temperature and water bath temperature were measured continuously. Replicates were carried out for both experimental situations, in both pipette types at the positions specified in Figure 7.7. The model was compared to the average of these

replicates ± one standard deviation to indicate the degree of variation in the experimental data set.

The pre-warmed pipette

To pre-warm a pipette, water from a water bath at ≈37 □C was repeatedly lifted into and expelled from it in order to heat the pipette material to ≈37 □C. Once the thermocouple reading no longer dropped immediately from 37 □C upon expulsion of the water, liquid was lifted to a set depth (30 mm in the glass pipette and 32 mm in the plastic pipette tip) and the pipette was held in the ambient air for 30 seconds. Only the tip of the pipette was dipped into the water bath, to prevent coating of the pipette wall with water which may evaporate.

Figure 7.8 displays two thermocouple readings within a plastic pipette tip as it is pre-warmed. Lifting and expelling liquid in quick succession approximately six times pre-warmed the pipette walls. The selection of t=0 is shown for each data set. This is required for comparison with the modelling for which it is assumed that t=0 once all the fluid has been drawn into the pipette. For the pre-warmed pipette this was taken to be the highest temperature reading prior to progressive heat loss from the pipette. Accurate selection of t=0 is limited to ± 1 s since the data was sampled at 1 s intervals.

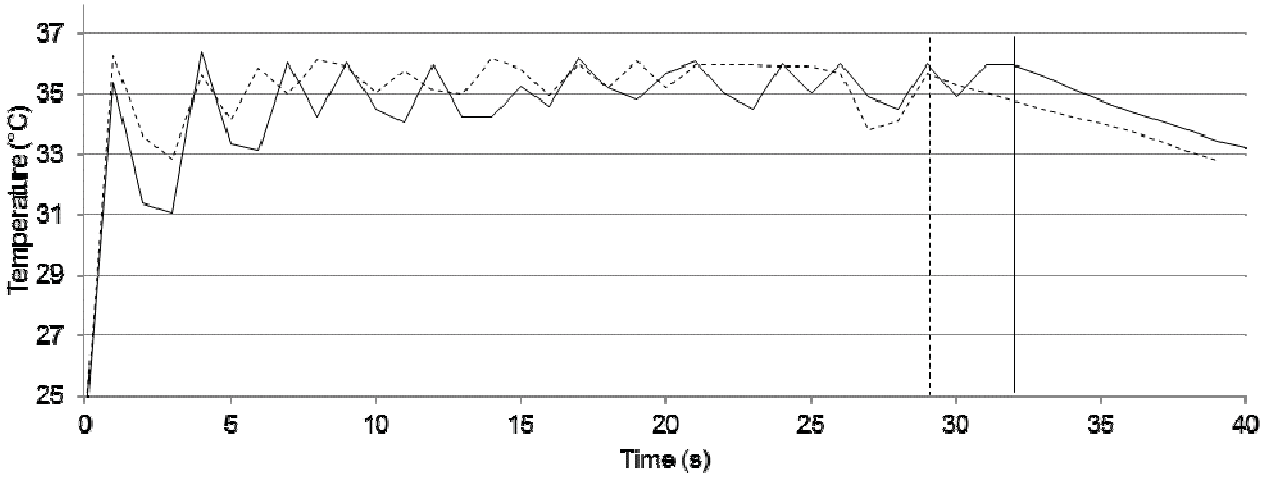

Figure 7.8: Temperature measured within a plastic pipette tip as it is pre-warmed by repeatedly lifting and expelling water (represented by a dotted and a solid line). Vertical lines mark the chosen time for 't=0' for each data set (dotted and solid respectively).

The initially cool pipette

To minimise heat transfer between the pipette and the bulk liquid prior to the draw phase only the pipette tip (as little as possible) was dipped into the water. The pipette was held in the ambient laboratory air for 30 seconds. The selection of t=0 was required for comparison with the modelling for which it is assumed that t=0 at completion of the draw phase. This was taken to be the highest temperature reading collected during a measurement. Accurate selection of t=0 is limited to ± 1 s since the experimental data was sampled at 1 s intervals.

7.5.3 Model Validation: Pre-warmed pipettes

The model of heat transfer in a pipette was first validated against experimental data collected in pipettes initially pre-warmed.

7.5.3.1 Convective heat transfer coefficient (h)

The only parameter input not provided by the experimental work or the literature was the convective heat transfer coefficient (h). This value was determined by comparing predictions with different convective heat transfer coefficients to the experimental data collected for pre-warmed pipettes until the best fit was obtained. Increments of 5 $W.m^{-2}K^{-1}$ were used in determining this fit. As a result, the uncertainty in the convective heat transfer coefficient was taken to be ± 5 $W.m^{-2}K^{-1}$ and assumed to determine the uncertainty in model predictions since uncertainty in this value will far outweigh uncertainty in the thermophysical properties of glass and polypropylene. The value of the heat transfer coefficient determined by this comparison for both the plastic pipette tips and the glass pipettes was applied in all subsequent simulations for model validation and application.

Figure 7.9 compares the experimental data for the pre-warmed plastic pipette tip (T-200) at a point 10 mm from the tip (position a, Figure 7.7) with a range of model simulations differing in the value of h. The best fit with the experimental data was at h = 50 $W.m^{-2}K^{-1}$. Uncertainty in this value of ± 5 $W.m^{-2}K^{-1}$ results in a prediction band of ± 0.27 °C at 10 s and ± 0.53 °C at 30 s.

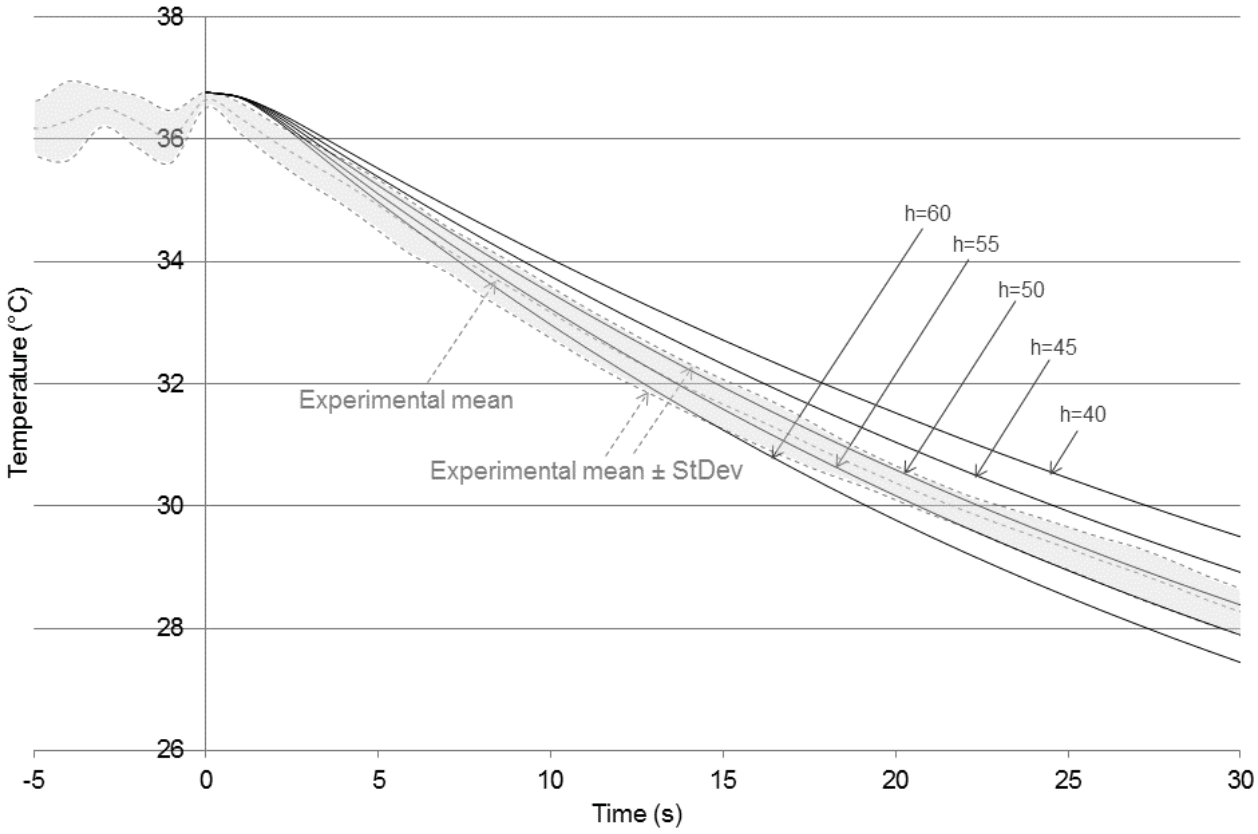

Figure 7.9: Displays the experimental mean ± standard deviation (shaded) for heat loss from a pre-warmed (36.77 °C) plastic pipette tip (T-200) containing a 32 mm column of liquid at a point 10 mm from the tip. At t=0 the pipette was lifted into the ambient air (21.1°C). Overlaid are five model simulations which vary in the value of the convective heat transfer coefficient (*h*) as displayed.

Figure 7.10 compares the experimental data for the pre-warmed un-pulled glass pipette with a range of model simulation differing in the value of *h*. The best fit with the experimental data was at h = 25 $W.m^{-2}K^{-1}$. Uncertainty in this value of ± 5 $W.m^{-2}K^{-1}$ results in a prediction band of ± 0.74 °C at 10 s and ± 1 °C at 30 s.

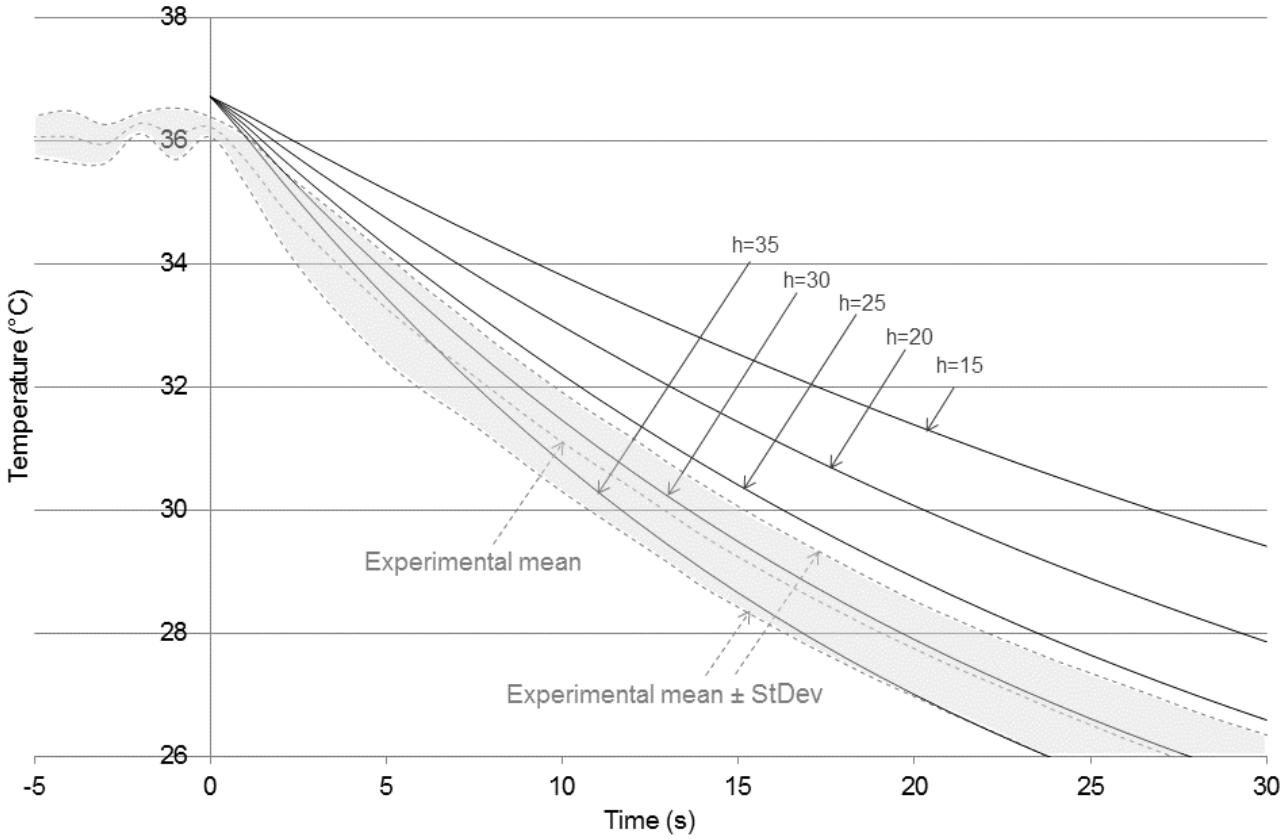

Figure 7.10: Displays the experimental mean ± standard deviation (shaded) for heat loss from a pre-warmed (36.71 °C) un-pulled glass Pasteur pipette containing a 30 mm column of liquid at a point 10 mm from the tip. At t=0 the pipette was lifted into the ambient air (21.2°C). Overlaid are five model simulations which vary in the value of the convective heat transfer coefficient (h) as displayed.

The values of 50 and 25 $W.m^{-2}K^{-1}$ are required to fit the experimental data for the pre-warmed plastic pipette tip and glass pipette respectively. Both these values are specific to these pipettes in the laboratory environment in which the experimental work was carried out. Both values are much higher than the convective heat transfer coefficient applied at the boundary of dish systems (12 $W.m^{-2}K^{-1}$, defined in Section 4.5.3) in the same laboratory environment. Chapman (1967) presented correlations for heat transfer coefficients for gas flow over cylindrical tubes. The correlation demonstrated that for a given range of Reynolds numbers, the smaller the diameter of the cylindrical tube the higher is the convective heat transfer coefficient. While the heat transfer coefficient for the thinner glass pipette is lower than that required to

justify the heat loss in the plastic pipette tip, these pipettes differ in geometry and material, both factors which have an impact on the convective heat transfer coefficient.

7.5.3.2 Plastic pipette tip (T-200)

Figures 7.11 and 7.12 compare the experimental data (mean ± standard deviation) with the model simulation for heat loss from a pre-warmed plastic pipette tip 10 mm from the tip (position 'a', Figure 7.7) and 2.5 mm from the tip (position 'b', Figure 7.7) respectively. The model simulation remains within, or close to, one standard deviation of the mean experimental temperature. This validates the model at both positions within the plastic pipette tip.

The initial temperature of the pipette system was defined as the water bath temperature. Experimental data measured at both 10 mm and 2.5 mm from the tip (Figures 7.11 and 7.12 respectively) ranges below the water bath temperature at t=0 because the highest temperature immediately prior to heat loss from the pipette may have occurred within ±1 s of the chosen t=0 for any experimental run and therefore may not have been sampled (due to collection of experimental data at 1 s intervals as described in Section 7.5.2). As a result, discrepancies between the model predictions and the experimental data may be explained by uncertainty in the placement in time of the experimental data.

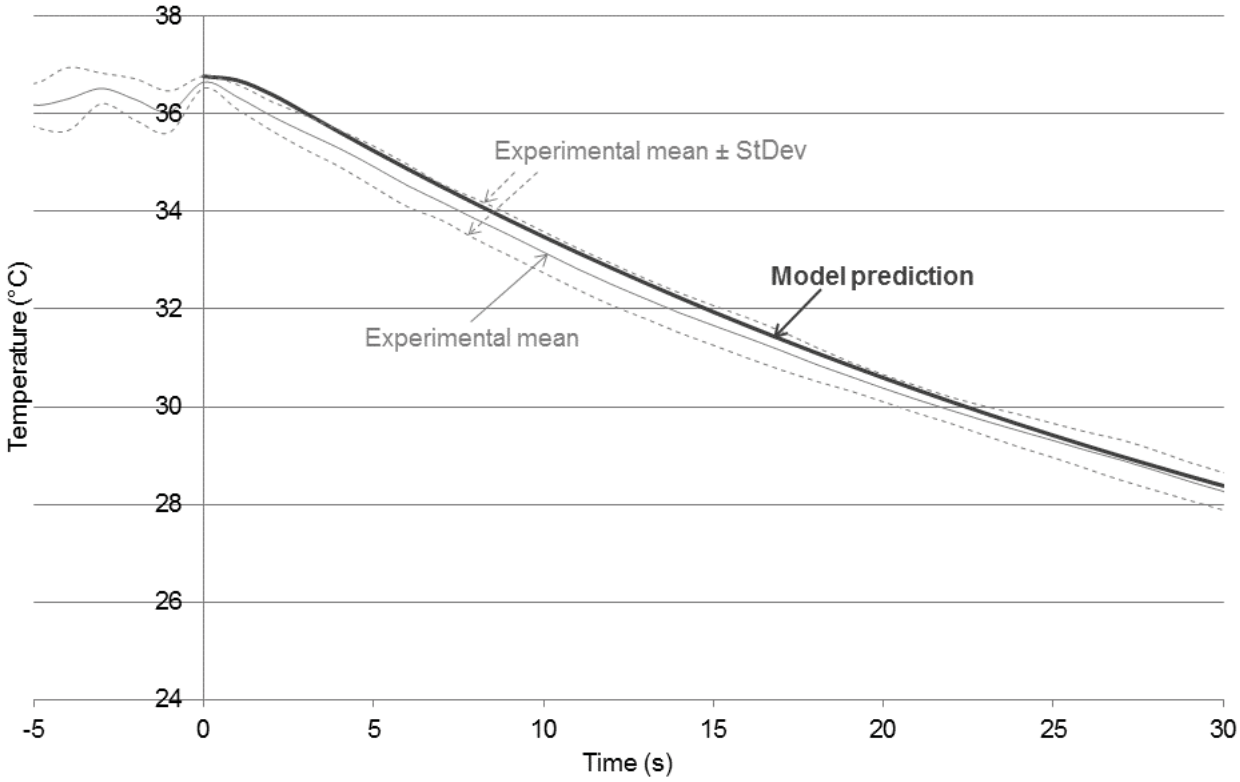

Figure 7.11: Model output vs. experimental data (mean ± standard deviations, n=8) for heat loss from a pre-warmed (36.77 °C) plastic pipette tip containing a liquid depth of 30 mm, at a point 10 mm from the pipette tip (position a, Figure 7.7). At t=0 the pipette was lifted into the ambient air (21.1°C).

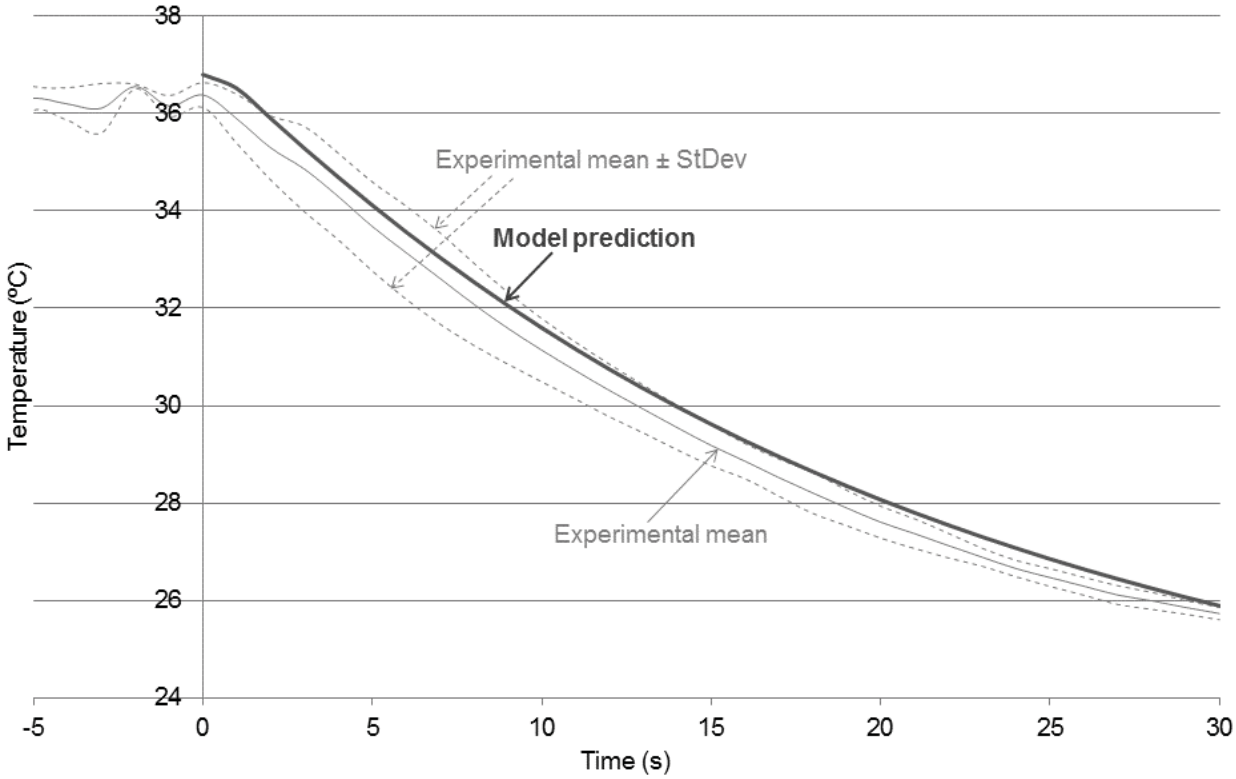

Figure 7.12: Model output vs. experimental data (mean ± standard deviations, n=3) for heat loss from a pre-warmed (36.8 °C) plastic pipette tip containing a liquid depth of 30 mm, at a point 2.5 mm from the pipette tip (position b, Figure 7.7). At t=0 the pipette was lifted into the ambient air (21.75 °C).

The discrepancies between the model predictions and experimental data sets may also be attributed to uncertainty in the model inputs. For example, uncertainty in the convective heat transfer coefficient alone (± 5 $W.m^{-2}.K^{-1}$), as defined in Section 7.5.3.1, gives a prediction band of approximately ± 0.27 °C at 10 s and ± 0.53 °C at 30 s at a point 10 mm from the pipette tip. Such a prediction band (prediction ± uncertainty) would overlap with the experimental data in Figure 7.12 at every time point.

7.5.3.3 Un-pulled glass Pasteur pipette

Figure 7.13 displays a comparison of the experimental data (mean ± standard deviation) with the model simulation for heat loss from a pre-warmed un-pulled glass pipette at a position 10 mm from the tip (position 'c', Figure 7.7). As with the plastic pipette tip the experimental data ranges below the water bath temperature at t=0 (due to the collection of experimental data at 1 s intervals). The model simulation runs close to one standard deviation above the mean experimental temperature validating the model.

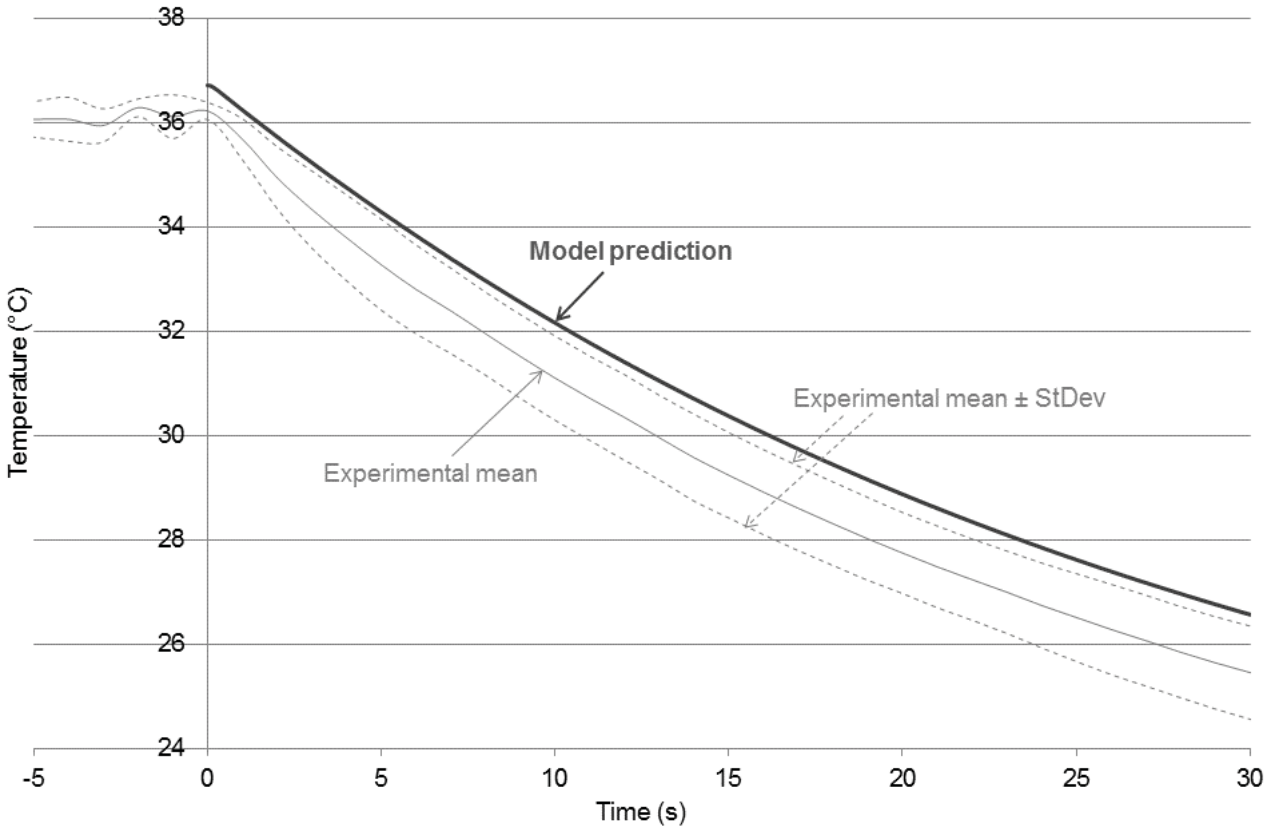

Figure 7.13: Model output vs. experimental data (mean ± standard deviations, n=10) for heat loss from a pre-warmed (36.71 °C) un-pulled glass pipette containing a liquid depth of 30 mm, at a point 10 mm from the pipette tip (position c, Figure 7.7). At t=0 the pipette was lifted into the ambient air (21.2°C).

As for the plastic pipette tip the small discrepancy between the model prediction and the experimental data set may be attributed to uncertainty in the placement in time of

the experimental data (±1 s) and uncertainty in the model inputs. Uncertainty in the convective heat transfer coefficient alone, as defined in Section 7.5.3.1, results in a prediction band of approximately ± 0.74 °C at 10 s and ± 1 °C at 30 s which would overlap with the experimental data.

The effect of uncertainly in the placement in time of the experimental data is depicted in Figure 7.14 which displays the mean, the mean + 1 standard deviation shifted forward by 1 s and the mean – 1 standard deviation shifted backwards by 1 s. The model prediction runs closely with the mean + 1 standard deviation of the experimental data when shifted forward by 1 s.

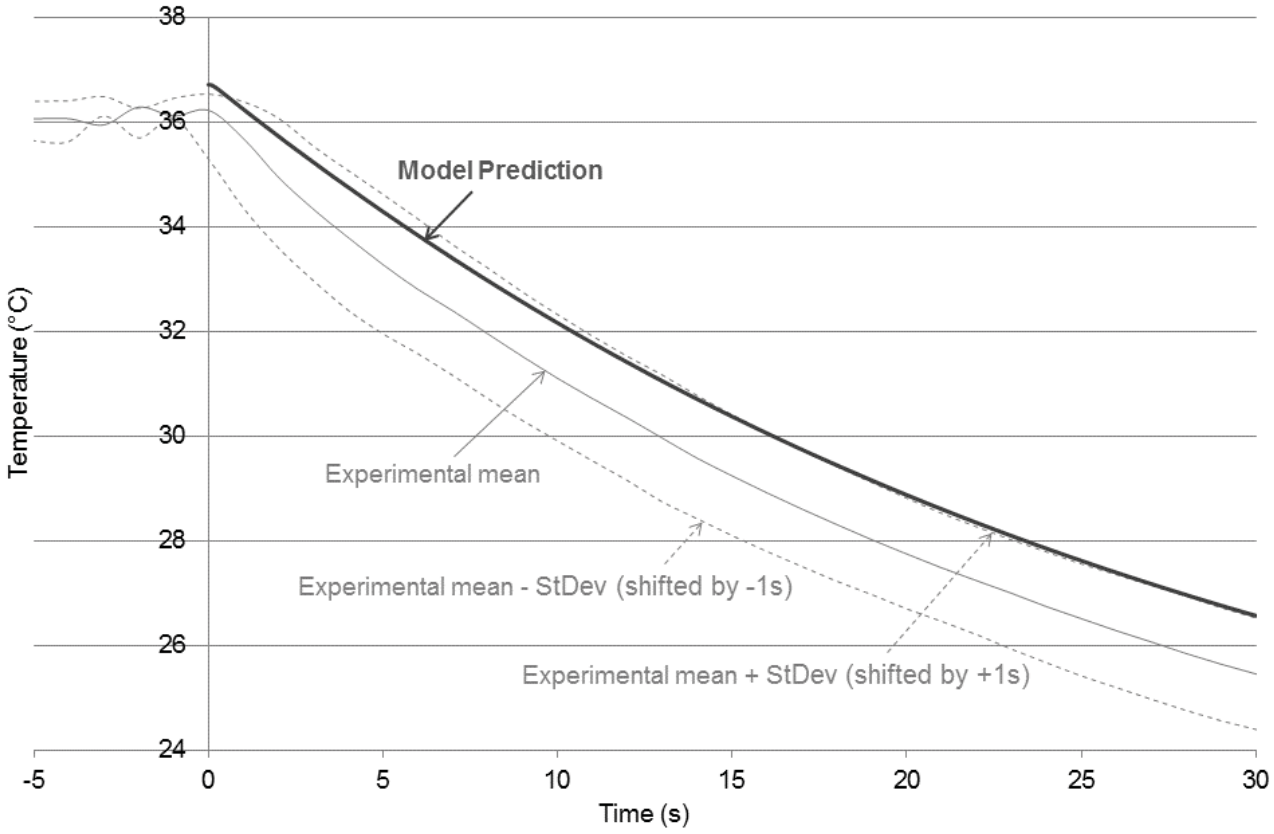

Figure 7.14: Model output vs. experimental data for heat loss from a pre-warmed (36.71 °C) un-pulled glass pipette containing a liquid depth of 30 mm, at a point 10 mm from the pipette tip (position c, Figure 7.7). The experimental data is presented as the mean, the mean + 1 standard deviation shifted forward by 1 s and the mean – 1 standard deviation shifted backwards by 1 s. At t=0 the pipette was lifted into the ambient air (21.2°C).

7.5.4 Model Validation: Pipettes initially at room temperature

Validation of heat transfer in a pre-warmed pipette has demonstrated that the model accurately predicts heat loss from plastic pipette tips and glass Pasteur pipettes during transfer when given the appropriate initial conditions. Comparison of model predictions with experimental data collected in initially cool pipettes (where initial contact with the bulk liquid and thus pre-warming was minimised) enables assessment of the validity of the following assumptions;

i. That heat transfer during the draw phase in a plastic pipette tip is not significant (as assumed in Section 7.1.2.2)
ii. That heat transfer during the draw phase alone pre-warms glass Pasteur pipettes (as predicted in Section 7.1.2.2)

7.5.4.1 Plastic pipette tip (T-200)

Figures 7.15 and 7.16 compare the experimental data (mean ± standard deviation) with the model simulation for heat loss from an initially cool plastic pipette tip at 10 mm from the tip (position ‘a’, Figure 7.7) and 2.5 mm from the tip (position ‘b’, Figure 7.7) respectively.

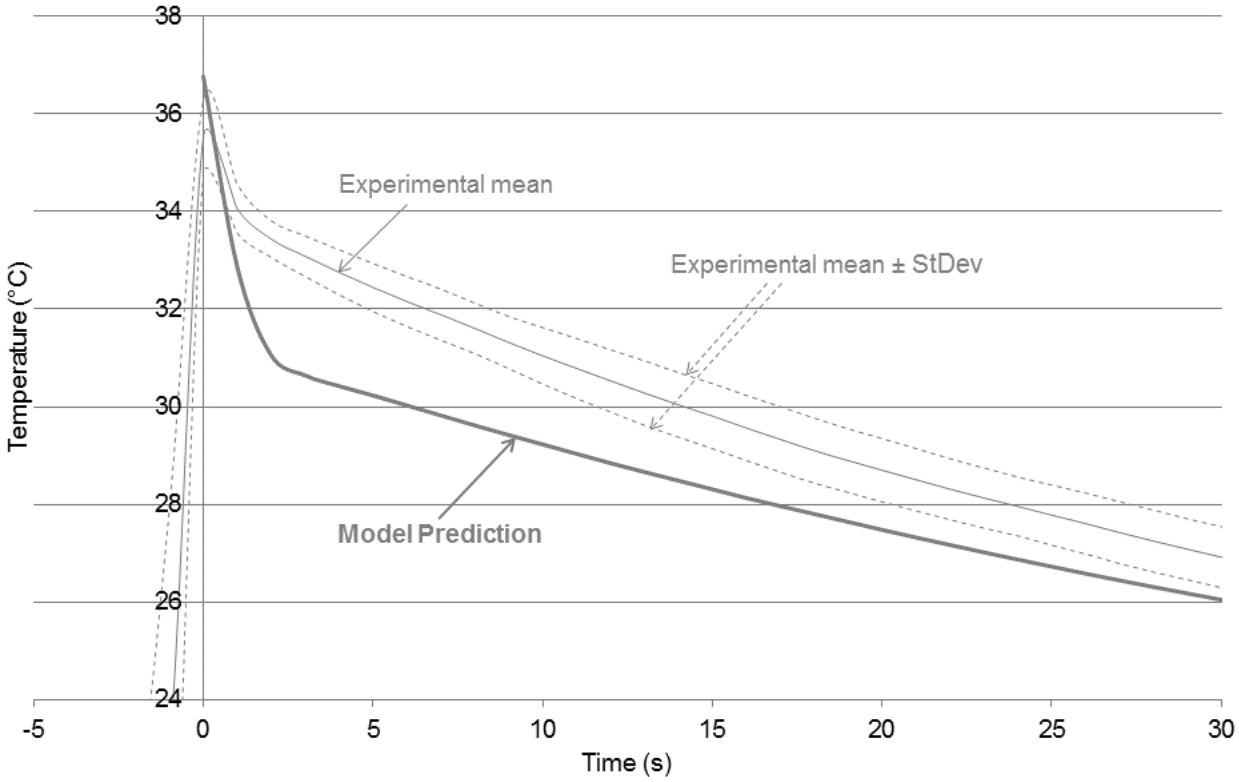

Figure 7.15: Model output (initial pipette temperature = 21.1 °C, h=50 W.m^{-2}.K^{-1}) vs. experimental data (mean ± standard deviations, n=12) for heat loss from a plastic pipette tip containing a liquid depth of 32 mm, at a point 10 mm from the pipette tip (position a, Figure 7.7). At t=0 the pipette was lifted into the ambient air (21.1°C). Water bath temperature = 36.77 °C.

As for the pre-warmed pipette, the experimental data ranges below the water bath temperature (initial temperature of the modelled dish system) at t=0. This is because for each experimental data set, the temperature at t=0 was taken to be the highest recorded temperature (as described in Section 7.5.2). Since the highest temperature immediately prior to heat loss from the pipette may have occurred within ±1 s of this recorded value, the average initial value will be underestimated.

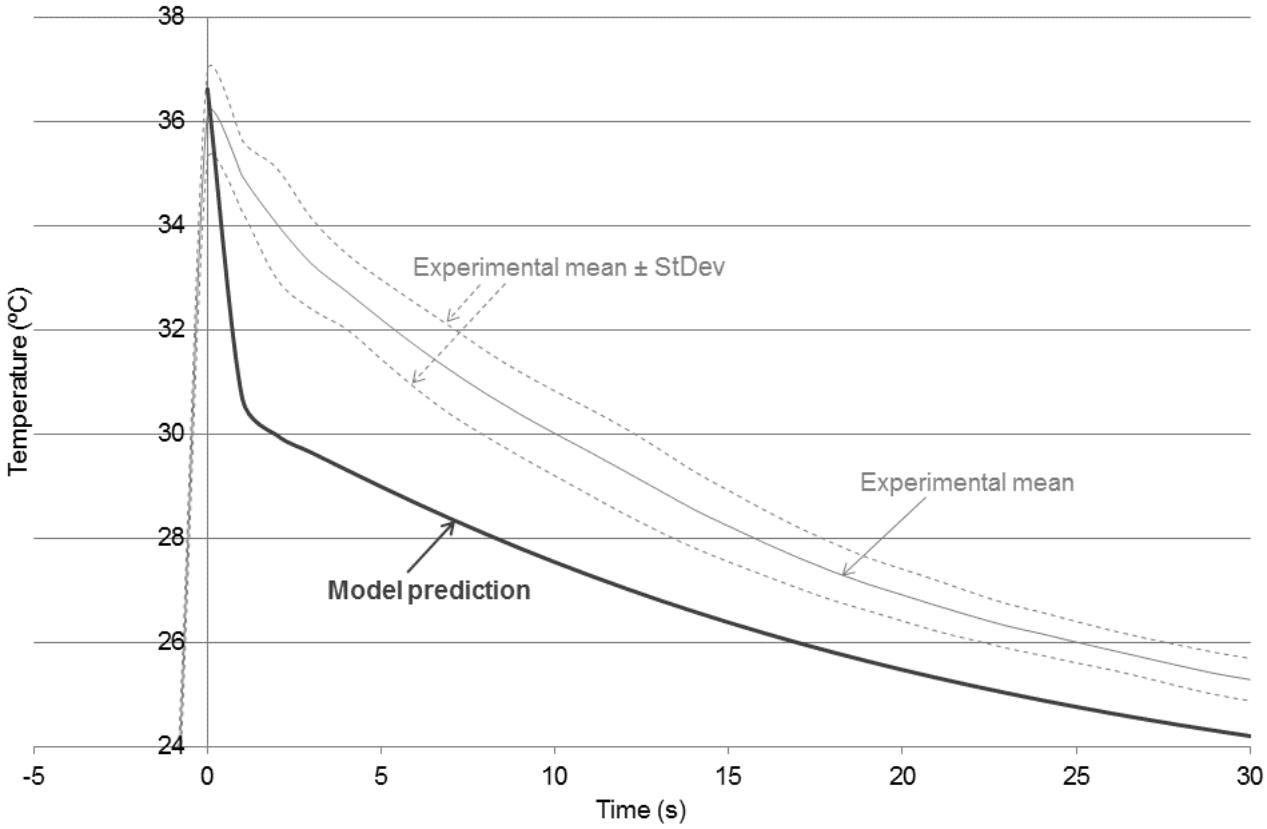

Figure 7.16: Model output (initial pipette temperature = 21.75 °C, h=50 W.m^{-2}.K^{-1}) vs. experimental data (mean ± standard deviations, n=7) for heat loss from a plastic pipette tip containing a liquid depth of 32 mm, at a point 2.5 mm from the pipette tip (position b, Figure 7.7). At t=0 the pipette was lifted into the ambient air (21.75°C). Water bath temperature = 36.8 °C.

At a point 10 mm from the tip (Figure 7.15) a sharp fall in the mean measured temperature of 2.8 °C is evident in the first two seconds. This is due to immediate heat loss from the fluid to the pipette walls demonstrating that, as expected, the wall of the plastic tip is not completely pre-warmed during the draw phase. However, the model over-predicts the magnitude of this fall demonstrating that a degree of pre-warming of the pipette occurs during the draw phase.

Similarly, at 2.5 mm from the tip (Figure 7.16) there is initially an increased rate of measured heat loss in the first 2 seconds. This is not as marked as at 10 mm (Figure 7.15) most likely because the closer the position to the tip, the greater the degree of

pre-warming by liquid drawn up into the pipette. Again the model over-predicts the magnitude of this fall demonstrating the pre-warming occurs during the draw phase.

These comparisons demonstrate that pre-warming of the walls of the plastic pipette tip does occur during the draw phase. However, the rate of heat loss measured experimentally in an initially cool plastic pipette tip is significantly greater than if they are pre-warmed (as predicted in Section 7.1.2.2). For example the measured experimental temperature 10 mm from the tip of an initially cool pipette falls below 34 °C in ≈2 s (Figure 7.15) compared with ≈7.5 s if the pipette is pre-warmed (Figure 7.11). It is important to note that pre-warming a plastic pipette tip significantly reduces the rate of cooling an embryo would be exposed to. Pre-warming of a pipette, as described in Section 7.5.2, is a simple practical step which may be used in practise to reduce the temperature changes embryos are exposed in an open culture process.

In practise, if the pipette is not actively pre-warmed, heat loss will not be approximated by either the pre-warmed or initially cool models but will fall between these limits. To apply the model to the smaller T-400 tip for prediction purposes both extremes in initial conditions will be applied. These must then be interpreted with the knowledge that assuming the pipette is initially pre-warmed is the practically achievable best case and assuming the pipette is initially at room temperature overestimates the initial rate of heat loss.

7.5.4.2 Un-pulled glass Pasteur pipette

Figure 7.17 compares experimental data (mean ± standard deviation) collected in an initially cool glass pipette at a position 10 mm from the tip (position ‘c’, Figure 7.7)

with a model simulation which assumes the pipette is pre-warmed. As with the actively pre-warmed glass pipette (Figure 7.13), the model simulation runs close to one standard deviation above the mean experimental temperature. This validates the assumption that the wall of the glass pipette adjacent to the lower portion of the liquid column, in this case $^1/_3$ up from the tip, is pre-warmed during the draw phase.

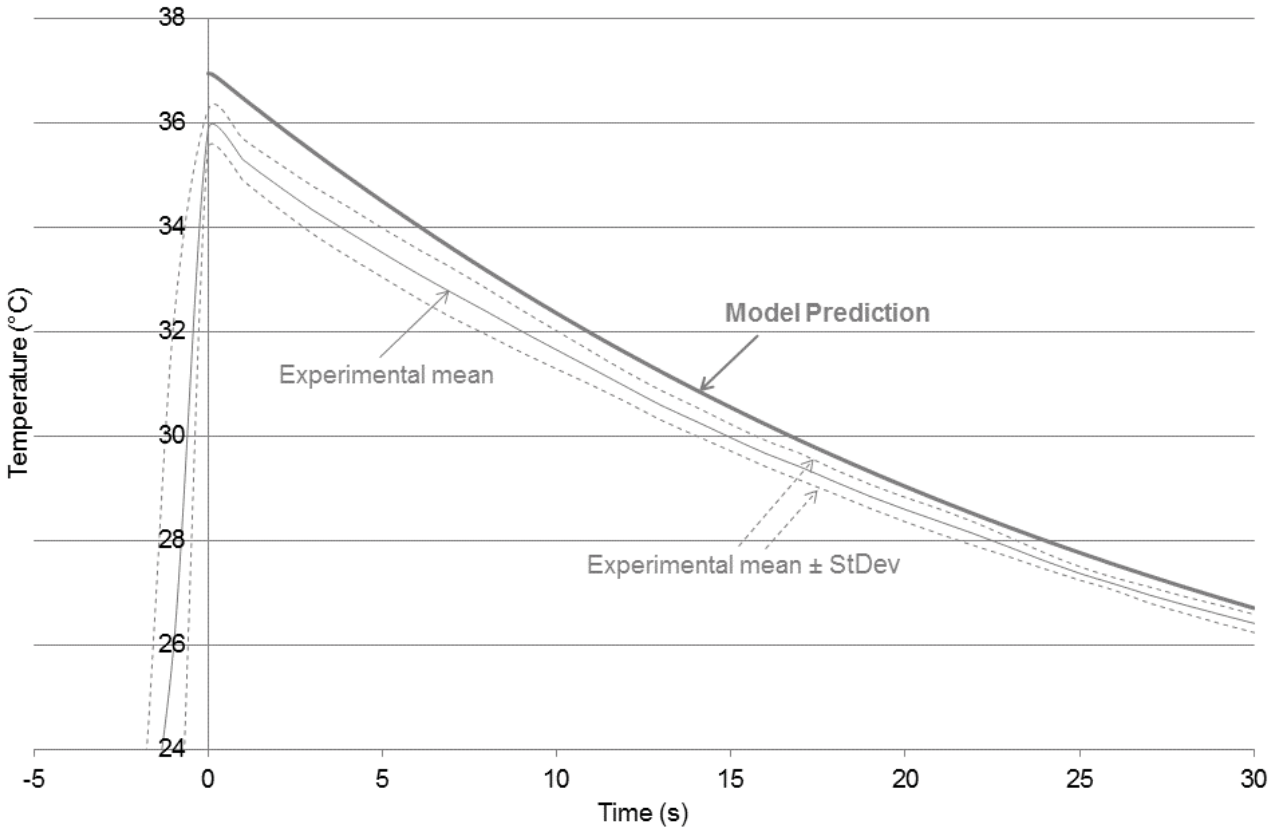

Figure 7.17: Model output (initial pipette temperature = 36.94 °C, h=25 W.m^{-2}.K^{-1}) vs. experimental data (mean ± standard deviations, n=10) for heat loss from an un-pulled glass pipette containing a liquid depth of 30 mm, at a point 10 mm from the pipette tip (position c, Figure 7.7). At t=0 the pipette was lifted into the ambient air (21.3 °C). Water bath temperature = 36.94 °C.

As was presented for the pre-warmed experimental data (Figure 7.14), the effect of uncertainly in the placement in time of the experimental data is depicted in Figure 7.18 which displays the mean, the mean + 1 standard deviation shifted forward by 1 s, and the mean – 1 standard deviation shifted backwards by 1 s. The model prediction

runs closely with the mean + 1 standard deviation of the experimental data when shifted forward by 1 s.

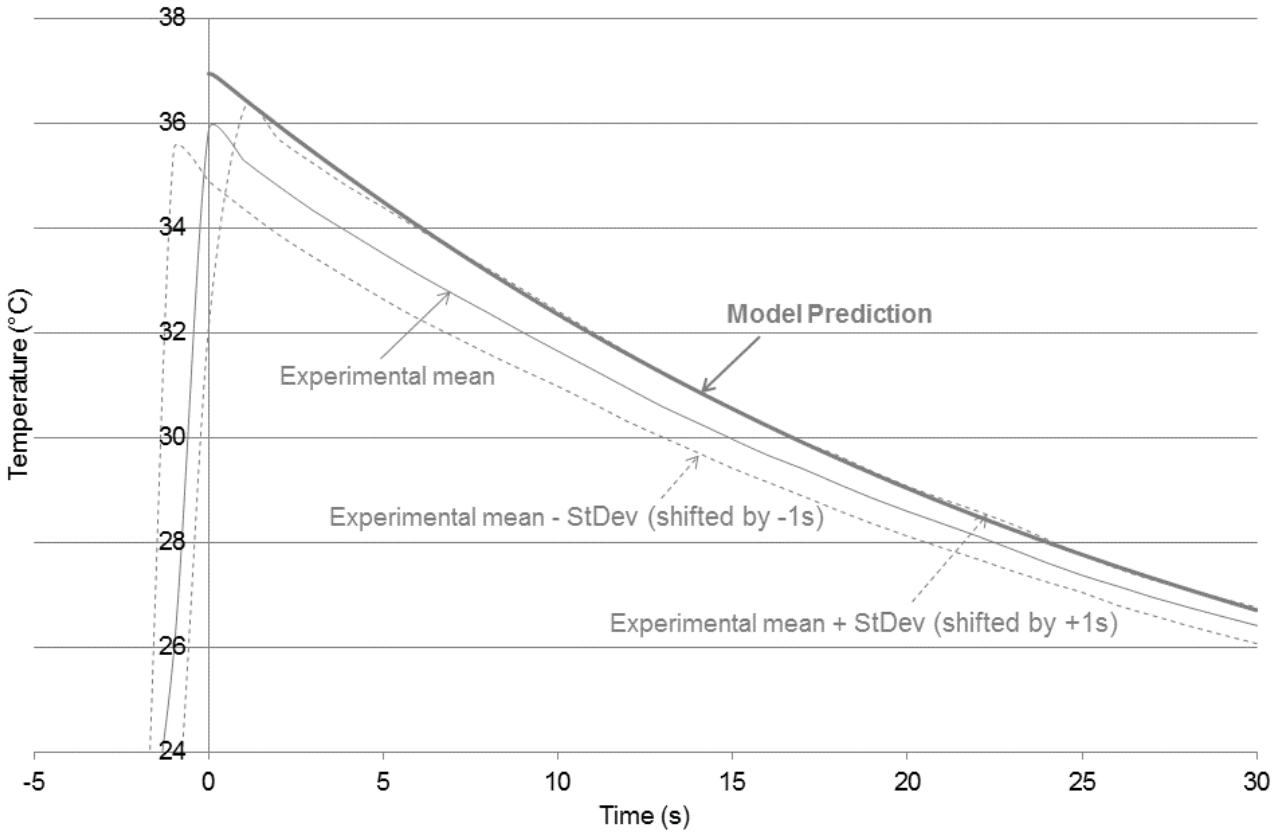

Figure 7.18: Model output (initial pipette temperature = 36.94 °C, h=25 W.m^{-2}.K^{-1}) vs. experimental data (mean, +1 standard deviation shifted by +1 s , -1 standard deviation shifted by -1s; n=10) for heat loss from an un-pulled glass pipette containing a liquid depth of 30 mm, at a point 10 mm from the pipette tip (position c, Figure 7.7). At t=0 the pipette was lifted into the ambient air (21.3 °C). Water bath temperature = 36.94 °C.

To apply the model of heat transfer in a glass Pasteur pipette to the smaller pulled pipette for prediction purposes, one may assume that the pipette will be pre-warmed to the bulk liquid temperature as long as either the pipette is actively pre-warmed or the embryo is in the lower portion of the liquid column (as is expected in current practice, see Section 7.1.1).

7.6 Model Application

The purpose of this section is to apply the models of heat transfer in pipettes, validated in Section 7.5, to the pipettes use in the culture process, outlined in Chapter 3, in order to characterise the temperatures embryos are subjected to. Within the embryo culture process pipettes are used for embryo manipulation (movement and transfer). The step within the embryo culture process which has the most impact on an embryo's thermal environment, with the greatest magnitude and rate of temperature change, is likely the transfer of an embryo through the laboratory air in a pipette system. During the embryo culture process embryos are transferred between two culture dishes a minimum of approximately ten times. This step will be the focus of this section.

As mentioned in Section 7.5.3.1, Chapman (1967) showed that for gas flow over cylindrical tubes, given the same environmental conditions, the convective heat transfer coefficient will increase with a decrease in the diameter. Therefore, applying the validated models to the smaller pipette systems used throughout the culture process without altering the convective heat transfer coefficients possibly underestimates heat loss from these systems. This possibility will be discussed below for the plastic pipette tips and the glass pipettes separately.

7.6.1 Pipette Tip: T-400

As described in Section 7.1.1, when using a plastic pipette tip to move embryos approximately 3-10 mm of culture media is lifted into the pipette before the embryo, and 2-5 mm is lifted after the embryo. To enable prediction of the best case

temperature profile the maximum likely depth (15 mm), and therefore thermal mass of the liquid column, was applied assuming the embryo would be positioned 5 mm from the tip. The culture media temperature was set to 37 °C and the ambient air temperature to 25 °C (as stated in Chapter 3, this is typically 23-27 °C in the Fertility Associates laboratory).

Figure 7.19 displays the two model predictions. The best case model (slowest rate of heat loss) assumes the pipette is initially pre-warmed to the bulk liquid temperature, this was shown to be practically achievable in Section 7.5.2. The worst case model (greatest rate of heat loss) assumes the pipette is initially at ambient air temperature, this is an overestimate of the initial rate of heat loss as the pipette wall is pre-warmed , to some extent, during the draw phase (see Section 7.5.4.1).

As discussed in Section 3.6, 34 °C is a somewhat arbitrarily assigned value commonly considered to be a temperature below which embryos should not be exposed (since there have been no dose-response experiments with respect to embryo temperature). Minimising temperature fluctuations within the culture process will contribute to minimising stress on the embryos. In practise, as shown in Figure 7.19, the temperature of an embryo within this system will fall below 34 °C at some point in time between 0.9 s and 9.5 s after the embryo has been lifted into the pipette. While 0.9 seconds will be an underestimate of the minimum time it takes for the temperature to fall below 34 °C, the real time frame will still be large. It is important to note that by ensuring the pipette tip is pre-warmed embryologists may transfer an embryo between two dishes without its temperature falling below 34 °C, since 9.5 s is certainly sufficient of time to carry out this task. As demonstrated in Section 7.5.2,

pre-warming a pipette may be achieved by lifting and expelling liquid in the pipette in quick succession approximately 6 times which takes < 30 seconds.

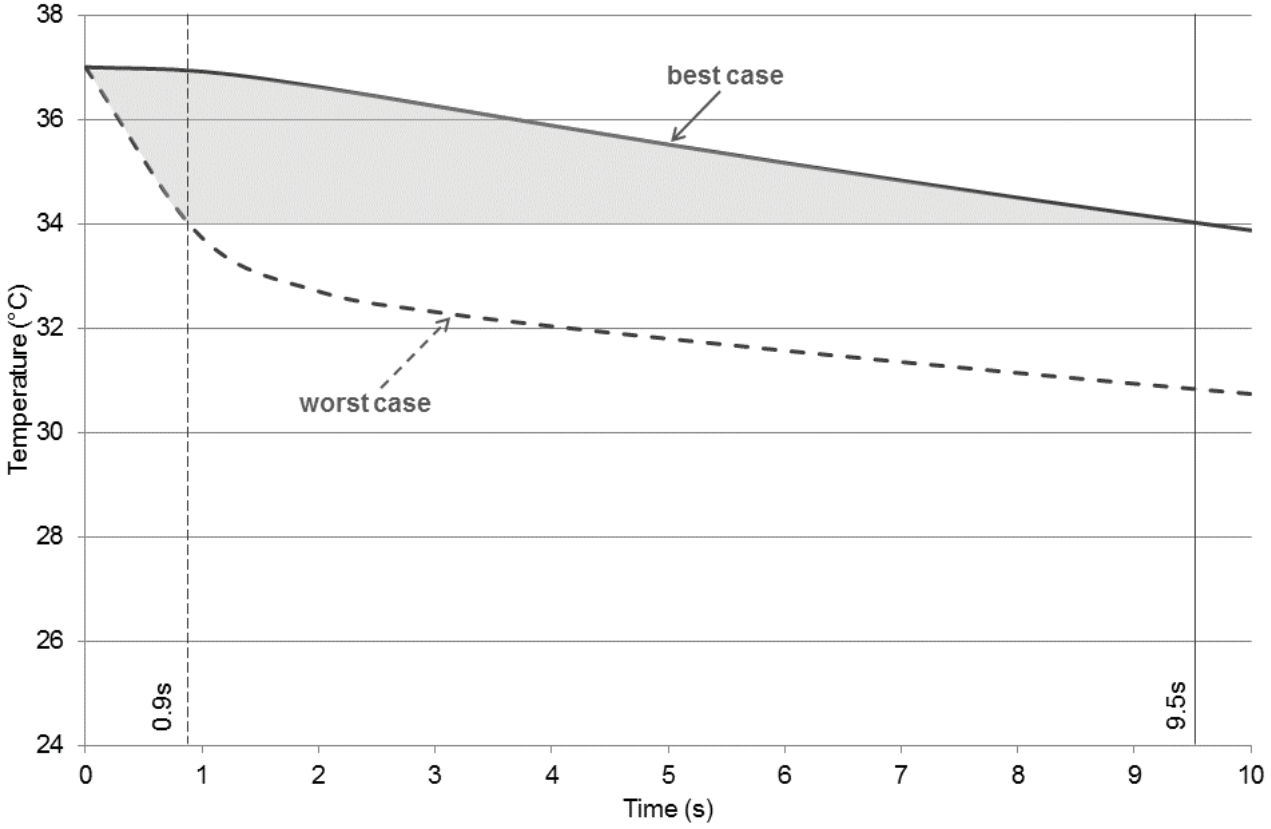

Figure 7.19: Displays the best case temperature profile (the pipette is initially pre-warmed (37 °C)) and worst case temperature profile (the pipette is at ambient air temperature (25°C) prior to the draw phase) for heat loss from a point 5mm from the tip of a T-400 plastic pipette tip which contains culture media to a depth of 15 mm. The temperature of an embryo may be maintained above 34°C (shaded) for between 0.9 and 9.5 seconds.

The T-400 and T-200 plastic pipette tips are depicted in Figure 7.2. The larger T-200 tip is more conical, narrower closer to the tip and much wider at the top, while the smaller T-400 tip is more cylindrical. The diameter 5 mm from the tip of the T-400 pipette tip is ≈2.3 mm. This value is in between the diameters at distances 2.5 mm (1.76 mm) and 10 mm from the tip (2.5 mm) of the larger T-200, points at which the model was validated, so it will be assumed that the same convective heat transfer

coefficient (of 50 $W.m^{-2}K^{-1}$) may be applied. The effect of the difference in the geometry of these two pipette types cannot be quantified.

7.6.2 Pulled glass Pasteur pipettes

As described in Section 7.1.1, in a glass pipette approximately 5-20 mm of culture media is lifted into the pipette before the embryo is picked up and 2-5 mm of extra liquid is lifted up after the embryo. As for the plastic tip, to enable prediction of the best case temperature profile the maximum likely depth of the liquid column, 25 mm, will be applied assuming the embryo would be positioned 5 mm from the tip. Figure 7.20 displays the model prediction for heat loss in a glass pipette. As determined in Section 7.5.4.2, if the embryo is in the lower portion of the liquid column the walls of the glass pipette adjacent to the embryo will be pre-warmed during the draw phase alone. Therefore a single model of heat loss from a pulled glass pipette will provide a prediction of any use of the pipette for embryo transfer in the culture process.

Figure 7.20 shows that the temperature of an embryo within a pulled glass pipette will fall below 34 °C approximately 1.4 seconds after the pipette has been lifted into the air. This is a very short time and is not sufficient time to transfer an embryo between dishes. After 30 s the temperature of an embryo within a pulled glass pipette would be 25 °C (ambient air temperature).

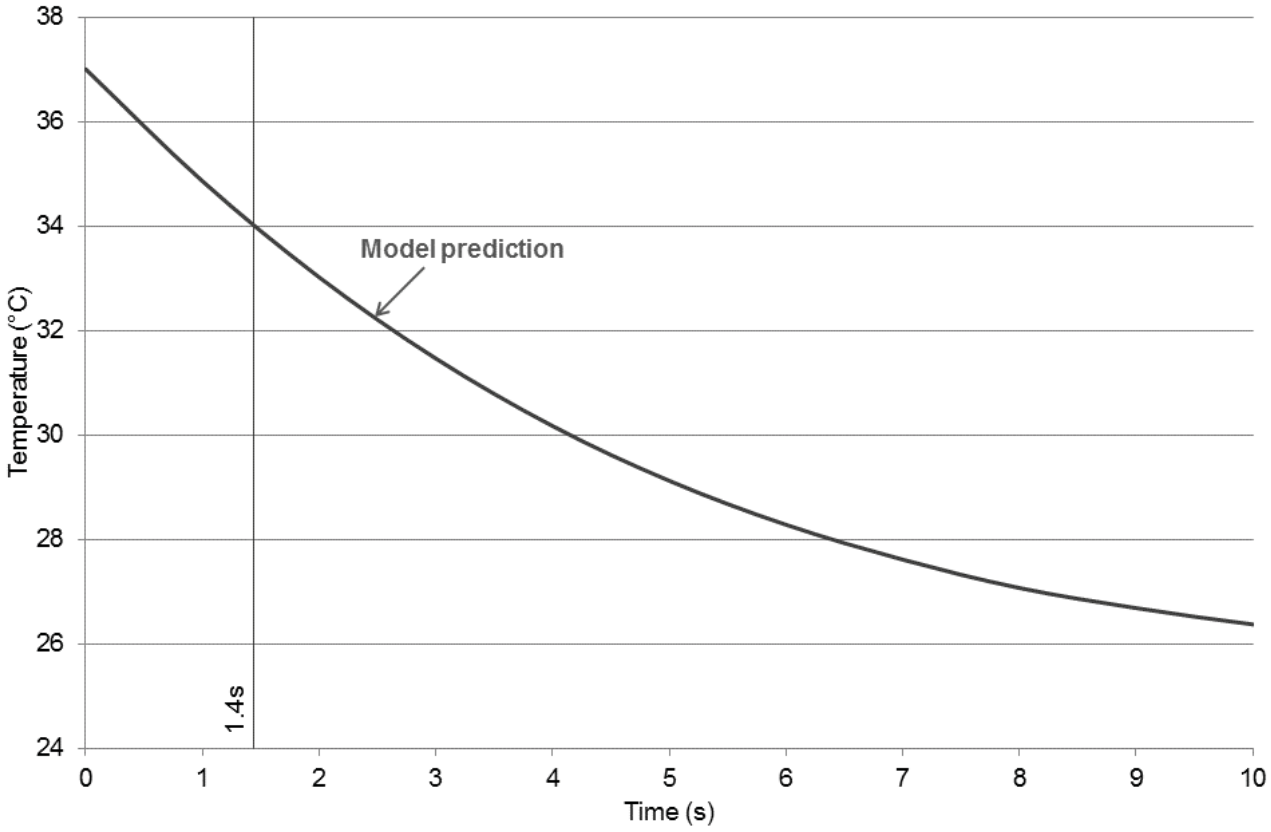

Figure 7.20: Displays the best case temperature profile (the pipette is initially pre-warmed (37 °C)) for heat loss from a point 5mm from the tip of a pulled glass pipette which contains culture media to a depth of 25 mm. The temperature of an embryo may be maintained above 34°C for a maximum of 1.4 seconds.

This model indicates that embryos transferred between dishes within a pulled glass pipette will be exposed to temperatures below 34°C. That pulled glass pipettes are used so frequently in practise highlights the fact that embryos are resilient to such changes in temperature. However, the use of the plastic pipette tips (T-400), which may be pre-warmed to provide a thermal environment above 34 °C for a sufficient time for embryo transfer, would reduce thermal stress on the embryos and perhaps improve embryo viability.

Scaling down the model of heat loss in the glass Pasteur pipette without being able to re-assess the convective heat transfer coefficient is a potential shortfall of this

modelling process. Given that the laboratory environment remains the same, the convective heat transfer coefficient would be expected to increase (>25 $W.m^{-2}K^{-1}$) with the smaller diameter. Therefore the model prediction, displayed in Figure 7.20 and discussed above, possibly underestimates the rate of heat loss from the glass pipette and therefore the temperature profile for an embryo within this pipette would be worse than predicted. This adds strength to the argument for the use of plastic pipette tips.

7.7 Summary

Models of heat transfer within plastic pipette tip and glass Pasteur pipette systems were developed and validated within this chapter. These models were applied to investigate the range of thermal environments an embryo within a pipette system may be exposed to. The main findings were:

- The draw phase may be incorporated into the model by approximating heat gain by the pipette wall during the draw phase and setting initial pipette temperature appropriately.
- Ensuring embryos are placed in the lower half of the liquid column should be encouraged so that liquid, which is drawn into the pipette before the embryo, pre-warms the pipette wall.
- The temperature of an embryo within a plastic pipette tip (T-400) will fall below 34 °C between 0.9 and 9.5 seconds after the pipette has been lifted into the air. (Assuming culture media temperature = 37 °C, ambient air temperature = 25°C, and the convective heat transfer coefficient = 50 $W.m^{-2}K^{-1}$)

- Pre-warming plastic pipette tips prior to use is a simple practical means to reduce temperature fluctuations embryos are exposed to within the culture process.
- The temperature of an embryo within a pulled glass pipette will fall below 34 °C within 1.4 seconds (best case) after the pipette has been lifted into the air (Assuming culture media temperature = 37 °C, ambient air temperature = 25°C, and the convective heat transfer coefficient = 20 $W.m^{-2}K^{-1}$)
- Transfer of embryos between dishes within a plastic pipette tip, not a glass pipette, will minimise both the magnitude and rate of temperature changes an embryo is exposed to.

Characterisation of the thermal environment in the Petri dish, 4-well dish and in the pipette systems has covered the majority of the steps in the embryo culture process (Figure 3.10). A similar approach may be taken to investigate mass transport of oxygen and carbon dioxide (therefore pH) throughout this process.

8 Mass Transfer of Oxygen in Dishes

Human embryo culture is carried out in 5 vol. % oxygen to replicate the oxygen environments in the oviduct and uterus of mammalian species (Burton *et al*., 2002). A higher oxygen content (e.g. atmospheric oxygen is ~21 vol. % O_2) results in higher concentrations of reactive oxygen species (ROS) which cause embryo damage and reduced embryo quality (Jana *et al*., 2010). A low oxygen (5%) environment is maintained in incubators, but changes are likely when embryos are removed into the atmospheric environment for manipulation and handling. Characterisation of the oxygen environment throughout *in vitro* embryo culture through the development of mathematical models allows the identification of the changes in oxygen environment embryos experience and the factors which impact on this environment. This may identify changes in practice which minimise changes in the oxygen environment in order to reduce the exposure of embryos to ROS, thus potentially improving IVF success rates.

The validated model of heat transfer in a Petri dish (Chapters 4 and 5) provides a good starting point for developing a model for oxygen transfer in the same system. The geometry of the system is identical. In addition, the diffusion equation for mass transfer is analogous to that for heat transfer so a similar set of equations may be defined.

It is convention in this field to define the oxygen concentration in volume percent (vol %). This means that the oxygen concentration in the solution is in equilibrium with a gas of this concentration. Typically the concentration of gases dissolved in liquid is

linear (follows Henry's law) up to a point, but may reach a saturation concentration when equilibrated with gases at very high concentrations (e.g. Langmuir behaviour). At atmospheric pressure water follows Henry's law up to an oxygen concentration in gas of 100 vol. %. This convention is useful as a common unit value can be used to describe any fluid (e.g. blood, plasma, culture media) even though they have different Henry's law coefficients.

8.1 Drop culture in a Petri Dish

Drop culture in a Petri dish was described in Section 4.1. The purpose of this section is to develop a model for mass transfer of oxygen in this system, using the previously developed model of heat transfer as a basis. The similarities between the heat and the mass transfer models and the changes needed to convert them will be identified.

8.1.1 Conceptual Model Development

The aim of this section is to outline the development of a conceptual model describing the mass transfer processes, with respect to oxygen, which take place within and at the boundaries of the drop culture in a Petri dish system.

8.1.1.1 Model geometry

Figure 8.1 displays the model geometry required for modelling mass transfer of oxygen in the drop culture in a Petri dish system. Most aspects are identical to that described in Section 4.1.3.1.

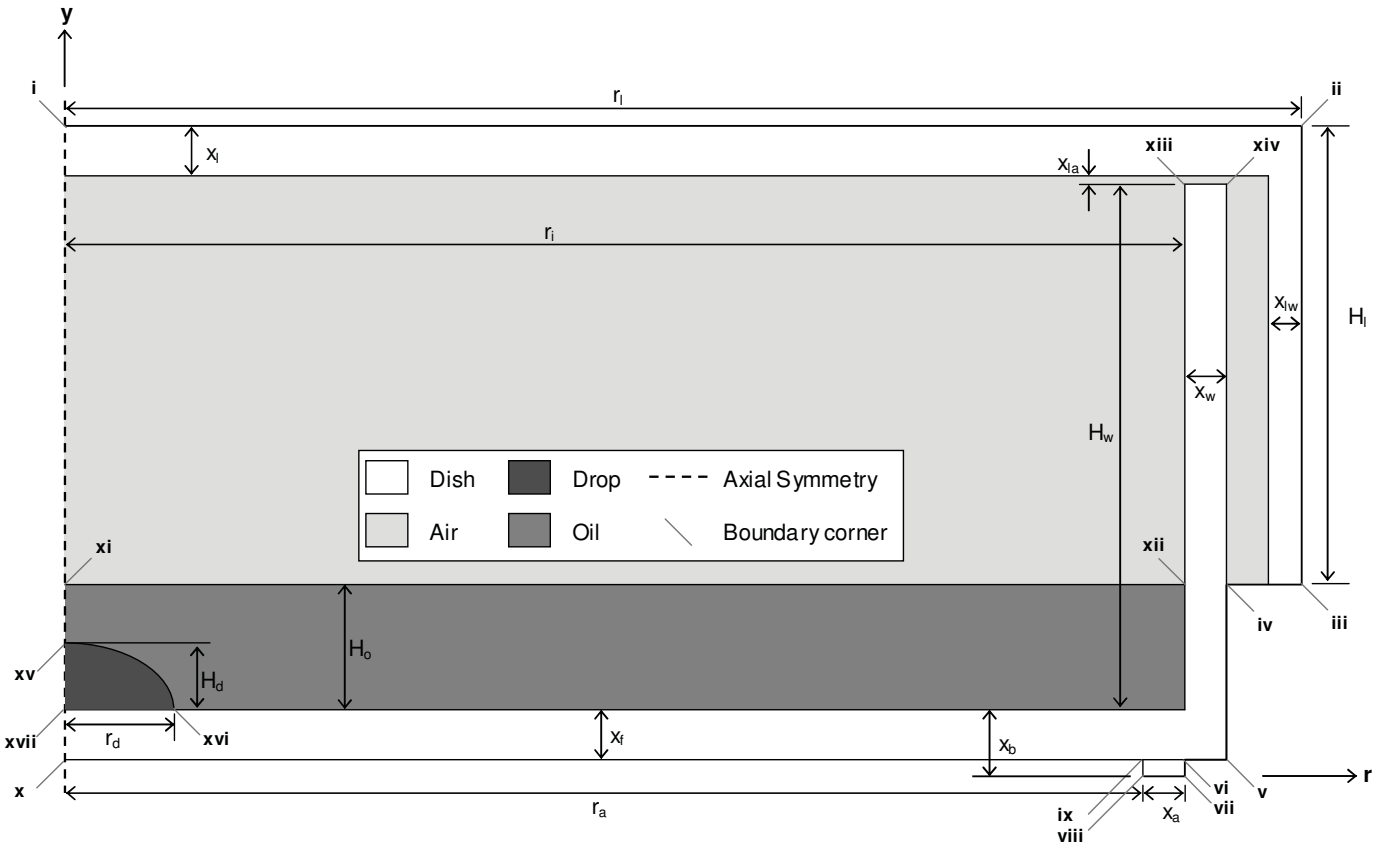

Figure 8.1: The 2D model geometry of drop culture in a Petri dish. Roman numerals (i-xiv) label corners of the dish system boundaries. Dimensions are defined in Table 8.1.

The key difference is that the trapped air beneath the dish will not be incorporated into the model as part of the system. It will be assumed that the oxygen content within the air beneath the dish will be equal to that in the bulk air surrounding the dish; whether in an incubator or in the laboratory environment. This is a valid assumption as placing the dish on a tray or a stage will not form an air tight pocket beneath the dish. In addition, mass transfer of oxygen through the polystyrene is slow relative to through air, oil and aqueous solution.

Dimension	Length (mm)	Dimension	Length (mm)
r_i	25.9	x_l	1.03
r_a	24.85	x_{la}	0.17
r_l	28.62	x_{lw}	0.89
r_d	2.45	H_d	1.43
x_f*	1.09	H_w	12.71
x_b*	1.51	H_{lw}	9.65
x_a	0.93	H_o*	3.09
x_w	0.94		

Table 8.1: The dimensions for the 2D model geometry of drop culture in a Petri dish (Figure 8.1). Values marked (*) are example values only and represent dimensions which were characterised for each individual dish during model validation due to their significant impact on simulation results.

8.1.1.2 Mass Transfer Assumptions

Several assumptions were made to define the means by which oxygen is transferred both within and around the dish system.

Diffusion

It was assumed that the diffusion coefficient of oxygen was constant and independent of oxygen concentration. This is a valid assumption for dilute aqueous solutions.

Bulk flow

Rayleigh numbers were calculated for the oil and air layer in the Petri dish system in Section 4.1.3.2. The values, 809 and 443, for the air and the paraffin oil layers respectively, were below the critical value (1000) and therefore it was assumed that natural convection would not occur in the system. It was also assumed that bulk flow

from within the system would be minimal due to careful handling of dishes given their delicate contents. Both forced and natural convection were not incorporated into the heat transfer model which was successfully validated through Chapters 4-7. Therefore, it was assumed that bulk movement of fluid does not occur within the dish system and that mass transfer of oxygen is only due to diffusion.

It was assumed that the bulk air in the incubator around the dish was well mixed as the incubators are designed to provide appropriate oxygen and carbon dioxide environments to dishes placed at any position. Therefore it was assumed that the oxygen environment was uniform around the dish boundary.

8.1.2 Model Formulation

As discussed in the previous section the sole mode of oxygen mass transfer may be assumed to be diffusion. Diffusion of oxygen is described by Equation 8.1.

$$\frac{\partial C_{O_2}}{\partial t} = D\nabla^2 C_{O_2} \qquad \text{Equation 8.1}$$

However, the use of oxygen partial pressure instead of concentration makes the oxygen gradient through the dish easier to describe as it simplifies comparison of levels in different subdomains. The concentration at every point in the model and at the model's boundaries will be dependent on the solubility of O_2 in the particular material (polystyrene, air, media and paraffin oil) whereas the partial pressure gradient would be continuous. Partial pressure, at normal atmospheric pressure, may be easily converted to volume percentage oxygen, Equation 8.2.

$$\%O_2 = \frac{P_{O_2}}{760} \times 100$$

Equation 8.2

Solubility is the liquid phase concentration of a species that is in equilibrium with a gas containing a vapour pressure of that same species. The relationship between concentration and pressure for dilute systems may be defined by a constant of proportionality, known as Henry's Law coefficient. It has various manifestations depending on the units chosen to express the concentrations (mole fraction, molar concentration, mass concentration, pressure, mass/mass (e.g. humidity)). In this work Henry's law coefficient is given the units m^3mmHg.mol^{-1}. The relationship between concentration and partial pressure of oxygen can thus be described as:

$$C = S \times P$$

Equation 8.3

where S = solubility = $\frac{1}{K_h}$, where K_h = Henry's law coefficient (m^3mmHg.mol^{-1})

Therefore the diffusion of oxygen may be described by Equation 8.4;

$$S\frac{\partial P_{O_2}}{\partial t} = SD\nabla^2 P_{O_2}$$

Equation 8.4

where P_{O_2} is the partial pressure of oxygen, S is the solubility of oxygen and D is the diffusion coefficient of oxygen

This is analogous to the equation for thermal diffusion (Equation 4.6). This relationship is displayed in Table 8.2.

Heat transfer $\rho c \frac{\partial \theta}{\partial t} = \lambda \nabla^2 \theta$	Mass transfer $S \frac{\partial P_{O_2}}{\partial t} = SD \nabla^2 P_{O_2}$
Temperature θ (°C)	Partial pressure P (mmHg)
The product of the density and the specific heat capacity ρc ($J.m^{-3}K^{-1}$)	Solubility S ($mol.m^{-3}.mmHg^{-1}$)
Thermal conductivity λ ($J.s^{-1}m^{-1}K^{-1}$)	The product of the diffusion coefficient and the solubility (permeability) DS ($mol.s^{-1}m^{-1}.mmHg^{-1}$)

Table 8.2: The mass and heat transfer analogy

When considering mass transfer of oxygen there are only two arrangements of boundary conditions for the Petri dish within the culture process. These are described below. Each condition is applied to a boundary as indicated by roman numerals in reference to Figure 8.1.

1. The line of axial symmetry down the centre of the dish, about which the 2D model rotates.

$$\frac{\partial P_{O_2}}{\partial r} = 0 \qquad \text{Equation 8.5}$$

for i-x, $t \geq 0$

2. The exposed boundary of the model.

$$P_{O_2} = P_{aO_2} \qquad \text{Equation 8.6}$$

for i-ii-iii-iv-v-vi-vii-viii-ix-x, $t \geq 0$*, when the lid is on the dish*

for xi-xii-xiii-xiv-iv-v-vi-vii-viii-ix-x, $t \geq 0$*, when the lid is off the dish*

where P_{aO_2} = atmospheric oxygen

Initial conditions

If it is assumed that the initial oxygen gradient through the dish is negligible the initial conditions are:

$P_{iO_2}(\Omega_a, \Omega_p, \Omega_m, \Omega_o) = P_{eO_2}$ at t=0

'Ω' denotes the subdomain (with the subscripts: *a*=air, *p*=polystyrene, *m*=media, *o*=Paraffin oil), P_{iO_2} = the initial partial pressure of oxygen and P_{eO_2} = experimentally recorded oxygen content.

If it cannot be assumed that the oxygen gradient through the dish is negligible then the initial partial pressure values are defined as the output values from the model of the preceding situation.

$P_{iO_2(x)}(y,r) = P_{fO_2(x-1)}(y,r)$ at t=0

$P_{iO_2(x)}$ = Initial partial pressure of oxygen in step process step number *x*, $P_{fO_2(x-1)}$ = Final partial pressure of oxygen in the process step number *x-1*.

8.2 Parameter estimation

The final model must be able to produce reliable predictions upon which decisions about future work may be based. For this to be possible the values of the model's subdomain parameters, the transport properties of oxygen in the subdomain material, must be suitably accurate.

Lango *et al*. (1996) and Weathersby & Homer (1980) provide reviews of experimentally determined diffusion coefficients and solubilities for O_2 and CO_2 (diffusion of CO_2 covered in Chapter 9) in water, biological fluids and in oil (various

vegetable oils). The values collected in these reviews, supplemented by those recorded in more recent papers, provide a comprehensive range of values within which the solubility or diffusion coefficient may vary. A number of available values in Lango *et al*. (1996) were excluded due to the authors suggesting inaccuracies in their determination, or the authors noting that the value has been disputed within the literature.

8.2.1 Solubility

Solubility, as specified above, is the liquid phase concentration of a species that is in equilibrium with a gas containing a vapour pressure of that same species. All gases, with the exception of helium, show a decreasing solubility in aqueous solvents with increasing temperature. Values of solubility have been collected over the range of temperatures experienced throughout the IVF process, when possible, to provide an accurate assessment of the range within which each parameter will sit at a given temperature.

8.2.1.1 Media (Water)

Figure 8.2 displays the relationship between oxygen solubility in water and temperature (this data is displayed, with references, in Table 8.3). A line of best fit was applied to approximate the solubility's temperature dependency. There were few values available and not enough at any one temperature to determine the variability. Discounting obvious outlying values, a conservative estimate of error was taken to be the value of the greatest percentage residual (±12.5%). It was assumed, for Monte Carlo simulations, that the standard deviation is 6% (half the presented error).

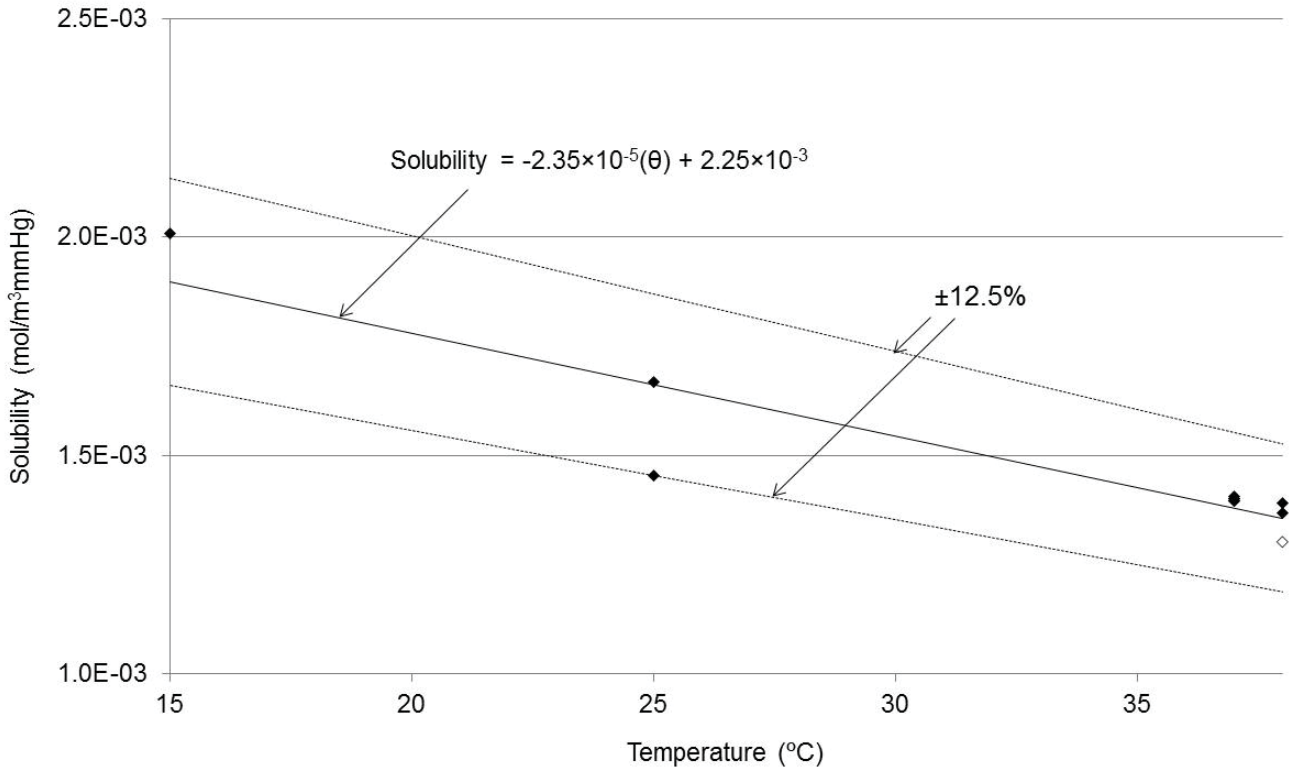

Figure 8.2: Values of the solubility of O2 in water (♦) over at a range of temperatures collected from the literature. A linear fit as an approximation of the solubility's temperature dependency is displayed with an error margin of ±12.5% (references for each value are displayed in Table 8.3). Oxygen solubility in a physiological saline solution = ◊ at 38 °C.

The impact of the salinity of water is an important consideration. In general, added salt decreases gas solubility in aqueous liquids, but most gases will dissolve in physiological saline to at least 90% of their solubility in pure water. In Figure 8.2 the solubility of O_2 at 38 °C in a physiological saline solution (Lango *et al.*, 1996) is displayed. While this is lower than the solubility of oxygen in water at 38 °C the effect of salinity is minor compared to the temperature sensitivity of O_2 solubility. Therefore the solubility of oxygen in culture media will be defined as that in water.

Temp (°C)	Solubility (mol. m^{-3}.$mmHg^{-1}$)	Reference
15	2.008×10^{-3}	Lango *et al*., 1996
25	1.455×10^{-3}	Arain *et al*., 2005
25	1.667×10^{-3}	Robertson, 2006
37	1.406×10^{-3}	Weathersby & Homer, 1980
37	1.396×10^{-3}	Weathersby & Homer, 1980
37	1.401×10^{-3}	Weathersby & Homer, 1980
37	1.401×10^{-3}	Weathersby & Homer, 1980
37	1.396×10^{-3}	Lango *et al*., 1996
38	1.391×10^{-3}	Lango *et al*., 1996
38	1.368×10^{-3}	Lango *et al*., 1996
38	1.302×10^{-3}	Lango *et al*., 1996

Table 8.3: The solubility of O2 in water at a range of temperatures collected from the literature. Values have been converted to units consistent with this work.

8.2.1.2 Paraffin oil

Figure 8.3 displays the values of oxygen solubility collected from the literature in a number of oil types and the temperatures at which these values were determined (this data is displayed in Table 8.4 with references). Only a single value of the solubility of oxygen in paraffin oil was identified in the literature (Arain *et al*., 2005). This lies between the solubility in transformer oil and that in olive oil.

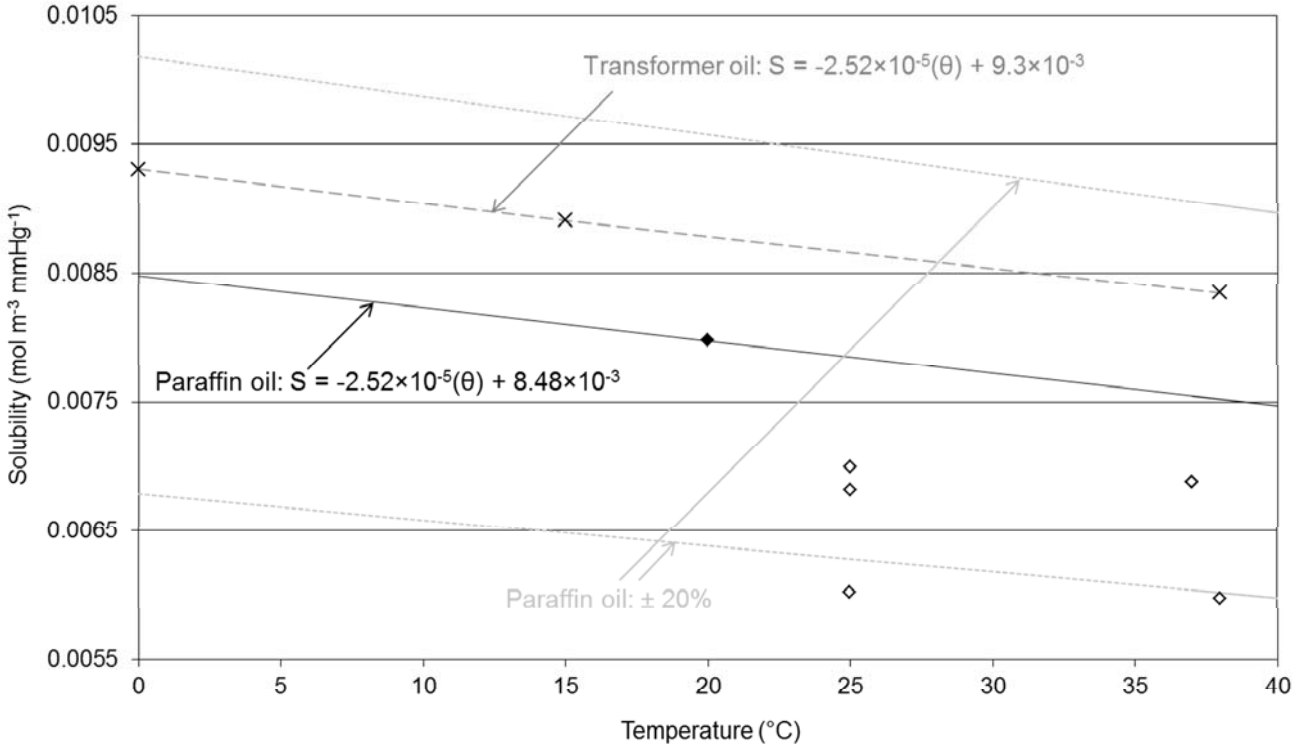

Figure 8.3: The solubility of oxygen in several oil types over a range of temperatures. × = transformer oil, ♦ = paraffin oil, ◊ = olive oil. The data is displayed in Table 8.3 with references. A linear fit as an approximation of the temperature dependency of the solubility of transformer oil is displayed (dashed line). The slope of the temperature dependency for transformer oil is applied to approximate the temperature dependency of the solubility of paraffin oil, this is displayed with error margin of ±20% (references for each value are displayed in Table 8.4)

Transformer oil (Shell Diala AX) is, like paraffin, a refined mineral oil and it is likely that the values of oxygen solubility in transformer oil better represent that in paraffin oil than solubilities in plant derived oils such as olive oil. In addition transformer oil has a density of 885 kg/m^3, closer to that of paraffin oil (~843 kg/m^3) than vegetable oil (olive, corn, cotton seed) which range from around 910-940 kg/m^3 (Perry *et al.*, 1997).

Temp (°C)	Type of oil	Solubility (mol. $m^{-3}.mmHg^{-1}$)	Reference
20	paraffin oil	7.979×10^{-3}	Arain *et al*., 2005
25	Olive	6.992×10^{-3}	Lango *et al*., 1996
25.1	Olive	6.819×10^{-3}	Lango *et al*., 1996
25.3	Olive	6.023×10^{-3}	Lango *et al*., 1996
37	Olive	6.876×10^{-3}	Lango *et al*., 1996
37	Olive	6.876×10^{-3}	Weathersby & Homer, 1980
38	Olive	5.978×10^{-3}	Lango *et al*., 1996
0	Transformer oil	9.305×10^{-3}	Shahsiah *et al*., 2007
15	Transformer oil	8.9092×10^{-3}	Shahsiah *et al*., 2007
38	Transformer oil	8.3434×10^{-3}	Shahsiah *et al*., 2007

Table 8.4: The solubility of oxygen in several oil types (paraffin, olive and transformer) at a range of temperatures (0-38 °C) collected from the literature. Values have been converted to units consistent with this work.

The temperature dependency of the solubility of oxygen in transformer oil was taken as an estimate of that in paraffin oil. The slope from a linear best fit of the values for transformer oil was applied to intercept the single value for paraffin oil at 20 °C to produce an equation approximating the temperature dependency of paraffin oil ($S = -2.52\times10^{-5}(\theta) + 8.48\times10^{-3}$). A conservative estimate of error of 20% was applied which encapsulates the values of transformer oil and the bulk of the values of olive oil solubility.

8.2.1.3 Polystyrene

Table 8.5 displays the values gathered from the literature for oxygen solubility in polystyrene.

Temperature	Value (mol. m^{-3}.$mmHg^{-1}$)	Reference
25 °C	7.848×10^{-3}	Arain *et al*., 2005
35 °C	7.290×10^{-3}	Rios-Dominguez *et al*., 2006
35 °C	7.285×10^{-3}	Puleo *et al*., 1989

Table 8.5: Solubility of Oxygen in Polystyrene: Values have been converted to units consistent with this work.

A linear fit was applied to the three values displayed in Table 8.5 ($S = -5.605\times10^{-5}(T) + 9.249\times10^{-3}$). Once again, as there was little available data, 20% was applied as a conservative estimate of error.

8.2.1.4 Air

In the air phase, a way of converting molar concentration driving force for diffusion to partial pressure is required. The amount of oxygen per unit volume of air per unit of pressure is the gaseous equivalent to solubility of gas in liquids and solids discussed above. It may be calculated from the ideal gas law.

$$PV = nR_g(\theta + 273.15), \text{ therefore } \frac{n}{VP} = \frac{1}{R_g(\theta + 273.15)}$$

$$\frac{1}{R_g(\theta + 273.15)} = \frac{1}{0.082057(\theta + 273.15)} \quad \frac{mol}{l.atm}$$

The desired units of are $\frac{mol}{m^3 mmHg}$,

$$\frac{1}{0.082057(273.15 + \theta)} \frac{mol}{l.atm} \times \frac{1}{760} \frac{atm}{mmHg} \times 1000 \frac{l}{m^3},$$

Therefore the conversion of gaseous concentration to partial pressure is

$$= \frac{16.035}{(\theta + 273.15)} \frac{mol}{m^3 mmHg}$$

8.2.2 Diffusion coefficients

The diffusion coefficient is a measure of the rate of gas transfer and, like solubility, has a temperature dependency. Values of the diffusion coefficients of oxygen have been collected over the range of temperatures experienced throughout the IVF process.

8.2.2.1 Media (Water)

Figure 8.4 displays values of the diffusion coefficient of oxygen in water collected from the literature (this data is displayed in Table 8.6 with references) and the temperatures at which these values were determined. Since there was sufficient data, an exponential curve was fitted to the data ($D = 1.26 \times 10^{-9} e^{2.265 \times 10^{-2} (\theta)}$). The standard deviation of the values at 25 °C (n=13) was 2.49×10^{-10}. Twice this standard deviation was taken as a conservative estimate of error (approximately ± 18%) and presented as the limits in Figure 8.4 (dotted line) between which all the values lie.

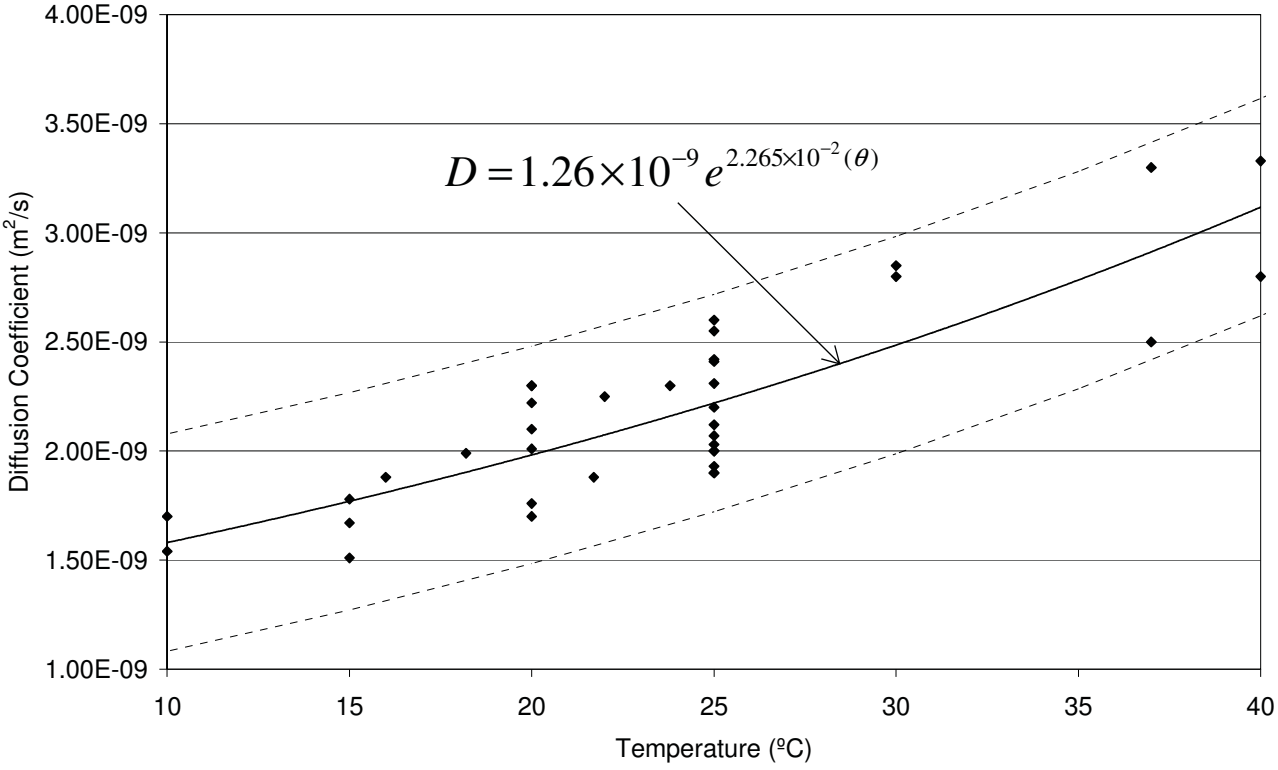

Figure 8.4: Diffusion coefficient of Oxygen in Water: The plot displays the diffusion coefficients of water gathered from the literature over a range of temperatures (The data is displayed in Table 8.6 with references). The exponential curve fitted to the data is displayed with an error margin of ±18% (2×standard deviation of the values at 25°C).

Temp (°C)	Diffusivity ($m^2.s^{-1}$)	Reference
10	1.7×10^{-9}	Lango *et al*., 1996
10	1.54×10^{-9}	Lango *et al*., 1996
15	1.67×10^{-9}	Lango *et al*., 1996
15	1.51×10^{-9}	Lango *et al*., 1996
15	1.78×10^{-9}	Lango *et al*., 1996
16	1.88×10^{-9}	Lango *et al*., 1996
18.2	1.99×10^{-9}	Lango *et al*., 1996
20	2.01×10^{-9}	Lango *et al*., 1996
20	1.76×10^{-9}	Lango *et al*., 1996
20	2.22×10^{-9}	Lango *et al*., 1996
20	1.7×10^{-9}	Lango *et al*., 1996
20	2.3×10^{-9}	Lango *et al*., 1996
20	2.3×10^{-9}	Lango *et al*., 1996
21.7	1.88×10^{-9}	Lango *et al*., 1996
22	2.25×10^{-9}	Lango *et al*., 1996
23.8	2.3×10^{-9}	Lango *et al*., 1996
25	2.6×10^{-9}	Lango *et al*., 1996
25	1.93×10^{-9}	Lango *et al*., 1996
25	1.9×10^{-9}	Lango *et al*., 1996
25	2.12×10^{-9}	Lango *et al*., 1996
25	2.42×10^{-9}	Lango *et al*., 1996
25	2.03×10^{-9}	Lango *et al*., 1996
25	2.55×10^{-9}	Lango *et al*., 1996

Temp (°C)	Diffusivity (m
25	2.41×10^{-9}
25	1.90×10^{-9}
25	2×10^{-9}
25	2.2×10^{-9}
25	2.07×10^{-9}
25	2×10^{-9}
29.6	3.5×10^{-9}
30	2.8×10^{-9}
30	2.85×10^{-9}
37	2.5×10^{-9}
37	3.3×10^{-9}
40	2.8×10^{-9}
40	3.33×10^{-9}
20	2.1×10^{-9}
25	2.31×10^{-9}

Table 8.6: The diffusion coefficient c
collected from the literature. Values ha
this work.

8.2.2.2 Paraffin Oil

The diffusion coefficient of oxygen in paraffin oil was determined by Kekedy & Teuca (1994) and Stokes (2009). These values are displayed in Figure 8.5 alongside the diffusion coefficients in olive oil (this data is displayed in Table 8.7 with references). The Kekedy & Teuca (1994) value is approximately 1.5 times that of Stokes *et al.* (2009). A similar range of values is available for the diffusion coefficient of oxygen in olive oil. These wide ranges are likely to be partially due to differences in the composition of oils within either type (olive or paraffin). The diffusion coefficient of oxygen in paraffin oil is important to this model since the rate at which the oxygen level changes at the position of an embryo is most dependent on both this value and the diffusion coefficient in water, which is relatively well defined.

Stokes et al. (2009) determined the diffusion coefficient of oxygen in paraffin oil by fitting a diffusion model to experimental data which had been collected by Houghton et al. (1996) to evaluate oxygen consumption of pre-implantation mouse embryos. The paraffin oil used by Houghton et al. was appropriate for embryo culture (produced by BDH, Poole, Dorset, UK). The value determined by Stokes et al. (2009) will therefore be used in this modelling in preference to the value measured by Kekedy & Teuca (1994) on the basis of the likely similarity to the paraffin oil used for model validation experiments (OVOIL, Vitrolife Sweden AB, Kungsbacka, Sweden) A conservative estimate of error of 20% was applied.

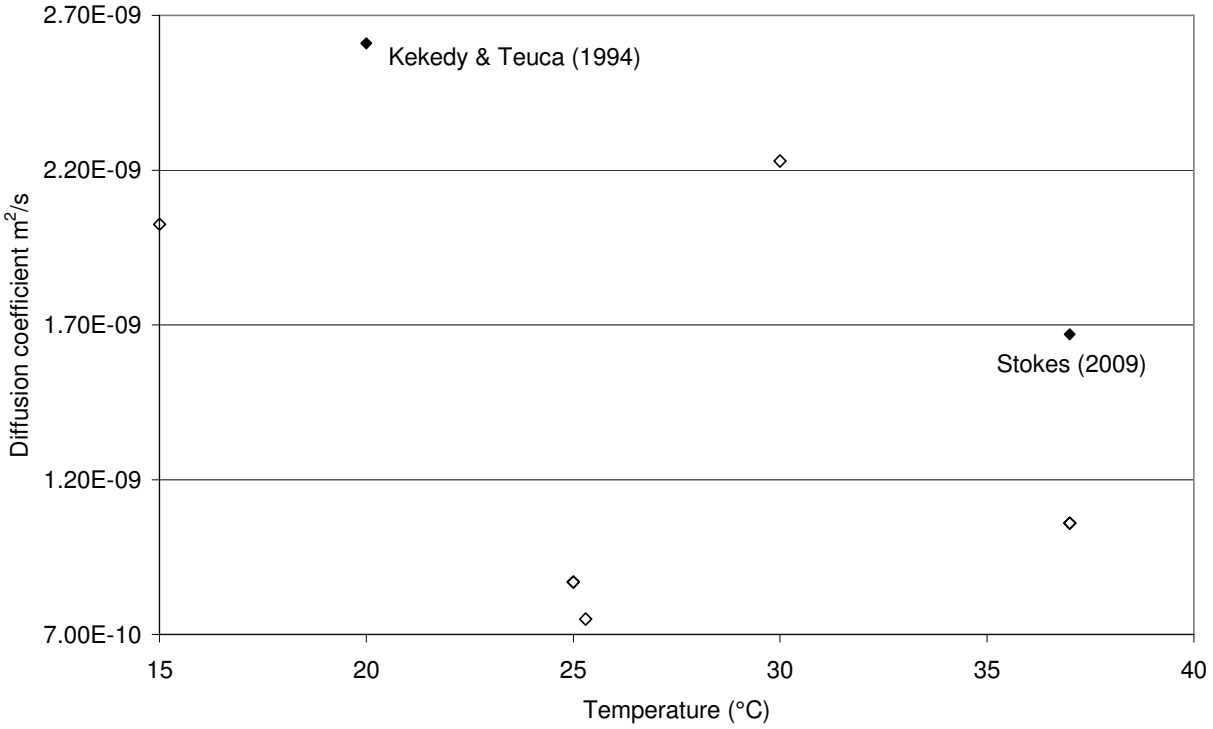

Figure 8.5: The diffusion coefficient of oxygen in several oil types over a range of temperatures. The oil type of each point is specified as follows; ♦ = paraffin oil, ◊ = olive oil. (The data is displayed in Table 8.7 with references)

Temperature (°C)	Oil type	Value ($m^2.s^{-1}$)	Reference
15	Olive	2.025×10^{-9}	Coutelieris, 2006
25	Olive	0.87×10^{-9}	Crowe *et al.*, 1986
25	Olive	0.87×10^{-9}	Crowe *et al.*, 1986
25.3	Olive	0.75×10^{-9}	Lango *et al.*, 1996
30	Olive	2.23×10^{-9}	Coutelieris, 2006
37	Olive	1.06×10^{-9}	Crowe *et al.*, 1986
37	Olive	1.06×10^{-9}	Crowe *et al.*, 1986
20	Paraffin	2.61×10^{-9}	Kekedy & Teuca, 1994
37	Paraffin	1.67×10^{-9}	Stokes *et al.*, 2009

Table 8.7: The diffusion coefficients of O2 in several types of oil at a range of temperatures collected from the literature. Values have been converted to units consistent with this work.

8.2.2.3 Polystyrene

Table 8.8 displays the gathered literature values of the diffusion coefficient of oxygen in polystyrene.

Temperature	Diffusivity ($m^2.s^{-1}$)	Reference
25 °C	1.1×10^{-11}	Arain *et al*., 2005
35 °C	1.65×10^{-11}	Puleo *et al*., 1989

Table 8.8: Diffusion coefficient of oxygen in polystyrene. Values have been converted to units consistent with this work.

As there was such limited data available, it was assumed that the relationship between the two available values (displayed in Table 8.8) was linear. This provided an approximation of the temperature dependency ($D = 5.5\times10^{-13}(\theta) - 2.75\times10^{-12}$) and 20% was applied as a conservative estimate of error.

8.2.2.4 Air

Table 8.9 displays the gathered literature values of the diffusion coefficient of oxygen in air.

Temperature	Diffusivity ($m^2.s^{-1}$)	Reference
0 °C	1.775×10^{-5}	Cussler, 1976
25 °C	2.03×10^{-5}	Robertson, 2006

Table 8.9: Diffusion Coefficient of oxygen in air. Values have been converted to units consistent with this work.

Again due to the limited data available it was assumed that the relationship between the two available values (displayed in Table 8.9) was linear. This provided an

approximation of the temperature dependency ($D = 1.02\times10^{-7}(\theta) + 1.775\times10^{-5}$) and 20% was applied as a conservative estimate of error.

8.2.3 Parameter Summary

Table 8.10 summarises the mass transfer properties of each subdomain in the dish system and their percentage error estimates. In order to implement a Monte Carlo simulation a value for the standard deviation of every thermophysical property is required. The reasoning for this was described in Section 4.3. The standard deviation was taken to be half the estimated errors which are displayed in Table 8.10.

Material	Diffusion Coefficient of O_2 ($m^2.s^{-1}$)	Solubility of O_2 ($mol.m^{-3}mmHg^{-1}$)
Water	$1.26\times10^{-9}e^{2.27\times10^{-2}(\theta)}$ (±18%)	$-1.999\times10^{-5}(\theta) + 2.124\times10^{-3}$ (±12.5%)
Paraffin Oil	1.67×10^{-9} (±20%)	$-2.52\times10^{-5}(\theta) + 8.48\times10^{-3}$ (±20%)
Polystyrene	$5.5\times10^{-13}(\theta) - 2.75\times10^{-12}$ (±20%)	$-5.605\times10^{-5}(\theta) + 9.249\times10^{-3}$ (±20%)
Air	$1.02\times10^{-7}(\theta) + 1.775\times10^{-5}$ (±20%)	$\frac{16.035}{(273.15+\theta)}$ (±20%)

Table 8.10: Diffusion coefficients and solubility's of oxygen, including temperature dependency, in the model subdomains. The estimated percentage error is displayed.

The values of the solubility of oxygen in water, paraffin oil and polystyrene are of the same magnitude, however the diffusion coefficients of oxygen in water and paraffin oil are respectively 166 and 95 times greater than that in polystyrene. This indicates that the majority of oxygen diffusion to and from the floor of the Petri dish will be through the media drop and the oil layer within the dish rather than through the dish floor itself. The value of the diffusion coefficient of oxygen in air is >7000 times that

in water, suggesting that diffusion of oxygen from the ambient environment to and from the air trapped by the lid of the dish will be relatively rapid facilitating oxygen transfer through the liquid layers.

8.3 The model solution

The model was solved by the finite element method in the software package COMSOL Multiphysics 3.3a (COMSOL, Stockholm, Sweden). Solving the 2D model solution for O_2 mass transfer in a Petri dish was the same as solving the 2D model of heat transfer in a Petri dish, for more detail see Section 4.2.1.

Solver accuracy checks were carried out, as detailed for heat transfer in a Petri dish in Section 4.2.2.2. As a result all subsequent simulations were run, as for the heat transfer mode, with a relative tolerance of 0.01 and a mesh density of ≈7000 elements.

8.4 Model Validation

The model of oxygen mass transfer in the Petri dish was validated against data collected during equilibration of a dish system through a change in oxygen partial pressure, at 37 °C, in a Sanyo incubator. Pre-equilibration of a Petri dish is represented by steps 5.5a and 9.2.8a as defined in the process flow diagram (Figure 3.10).

For model validation the media drop was not included in the dish set-up. The oxygen probe is significantly larger than a thermocouple used for temperature measurement in this system, and it was not possible to position it within a media drop. It was assumed

that the media drop may be incorporated into the model for model application without being validated against experimental data, since the mass transfer properties of oxygen in water are well characterised compared with those of the other subdomains in this system.

8.4.1 Experimental Design

8.4.1.1 Equipment

Oxygen measurement

The NeoFox (NeoFox® Phase Measurement System, Ocean Optics, Dunedin, FL, USA) was used with a FOXY-R oxygen probe (Ocean Optics, Dunedin, FL, USA). This system employs a fluorescence based method to measure the partial pressure of oxygen based on the florescence lifetime. The NeoFox system may log data from two probes simultaneously. The FOXY-R probe is a needle probe, 75 mm in length and 1.587 mm in external diameter. It has a response time of 30-50 seconds in liquids (sufficiently quick given the measurement period of hours) and is accurate to within 5% of the reading.

The oxygen probes were calibrated prior to use via a two point calibration at atmospheric oxygen (20.9% O_2), and at 0% oxygen (achieved by flushing the probe with nitrogen).

Incubator

The Sanyo incubator (MCO-5M: 1.7 cu. ft. CO_2 Cell Culture Incubator, SANYO Biomedical, Wood Dale IL, USA) monitors the oxygen partial pressure within with "a high-precision zirconia electrolyte oxygen sensor" and the microprocessor injects

nitrogen or oxygen gas as required. A port in the back of the incubator provided entry for the fibre optic cables of the oxygen probes used for model validation.

The lag time for the incubator to reach a new partial pressure of oxygen was significant, especially when increasing the oxygen partial pressure (~1 hour). Therefore, a second oxygen probe was employed to record the partial pressure of oxygen in the incubator to be used for the boundary condition of the model.

8.4.1.2 Experimental methodology

Calibration of the oxygen probes, as described in Section 8.4.1.1, was the first step in any experimental work. Figure 8.6 displays the set up of the oxygen probe in the dish. A hole, of approximately the probe diameter (~1.6 mm), was melted into the base of the dish wall and the probe inserted so that it lay flat along the dish floor. The probe was held in place with a thin piece of aluminium tape and the small hole was sealed with silicone. While silicone is permeable to oxygen, the use of silicone as a seal was thought not to impact on measurement since the majority of oxygen mass transport to and from the dish floor will be vertical (as predicted in Section 8.2.3). Once the silicone had set, the paraffin oil was added to the dish. The mass of the dish was recorded before and after oil was added in order to enable accurate determination of the oil depth (from the relationship described in Equation 4.1).

The dish set up was placed into the incubator and the probe was connected to a fibre optic cable. Another probe, to measure the incubator partial pressure for the boundary condition, was taped to the tray in the incubator, next to the dish, and connected to a second fibre optic cable.

Data was recorded from the outset as the dish system was equilibrated in the incubator. Once steady state had been reached, the oxygen content in the incubator was stepped up or down as appropriate and data collection continued until the new steady state had been reached.

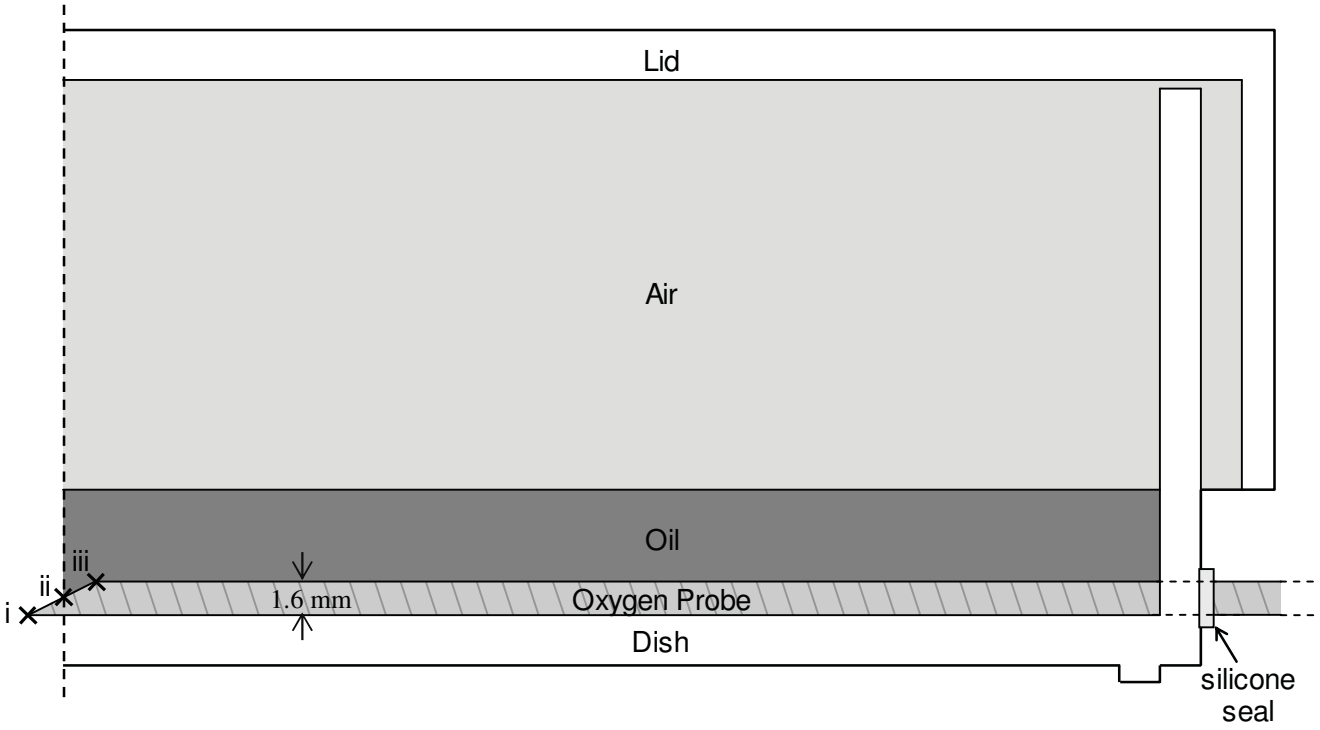

Figure 8.6: Diagram of the oxygen probe placement for model validation experiments including the oxygen probe and silicone seals. Point 'i' = active surface of the probe meets the dish floor. Point 'ii' = the centre of the active probe surface (0.8 mm above the dish floor). Point 'iii' = top of the active surface of the probe (1.6 mm above the dish floor). The dashed line marks the line of axial symmetry of the dish.

8.4.2 Model Validation

The experimental data was compared to the Monte Carlo simulation output (n=30, mean ± two standard deviations) in which the mass transfer properties of the subdomain materials are randomly selected from their individual approximated normal distributions. The decision to use 30 Monte Carlo simulations was made by running increasing numbers of simulations until the standard deviation remained

constant (the same methodology as described for heat transfer in a Petri dish and 4-well dish models, outlined in Section 4.5.4). In addition, due to the larger probe size, the experimental data was compared to the mean model output at three depths of oil; on the dish floor, at ½ the probe (0.8 mm) diameter, and at the probe diameter (1.6 mm). The probe measures over an area that lies between these three positions as depicted by points i, ii, and iii in Figure 8.6.

8.4.2.1 Equilibration from 15% to 5% O2

Figure 8.7 displays the data collected while equilibrating a dish, initially fully equilibrated in a 15% oxygen environment, to 5% oxygen at 37 °C in a Sanyo incubator. The oxygen partial pressure outside the dish provided a data set for the exposed boundary condition of the dish. The mass of paraffin oil was measured (5.826 g) and its depth calculated (3.25 mm)

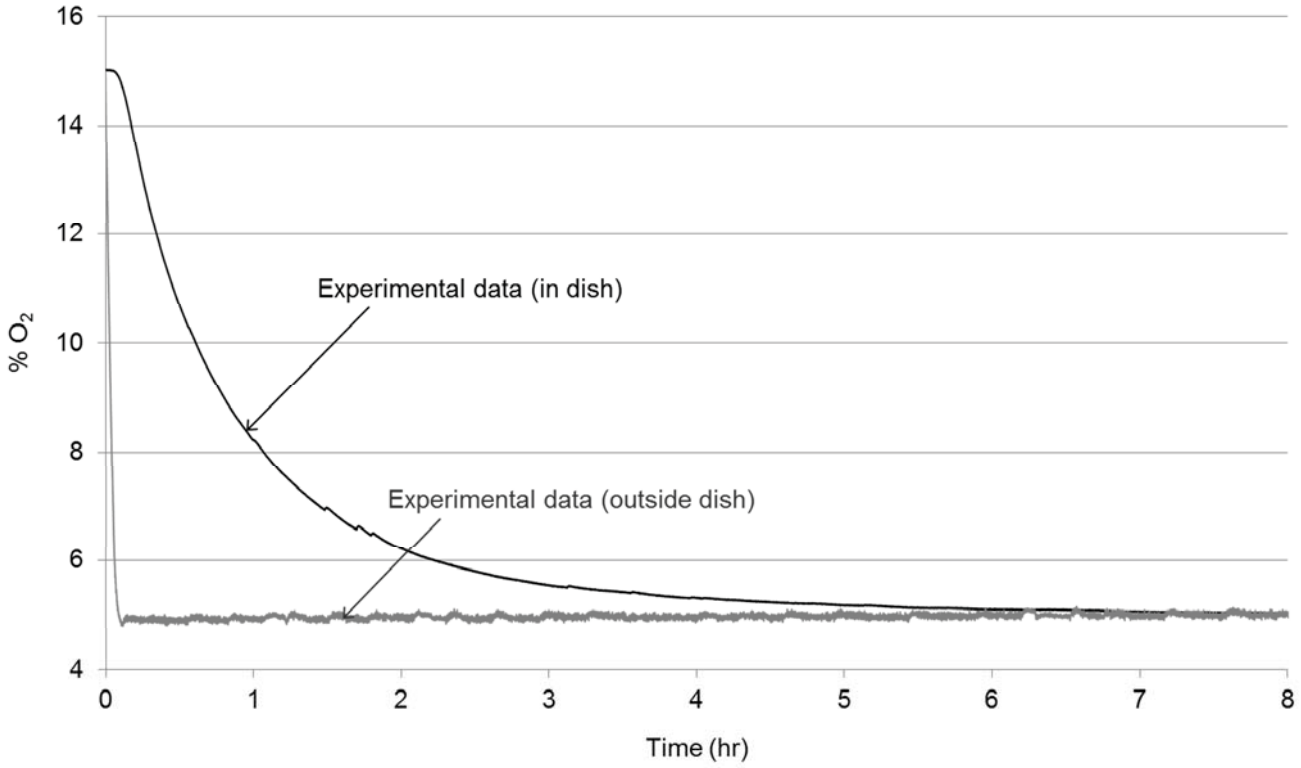

Figure 8.7: The experimentally measured fall in oxygen content in a dish, initially fully equilibrated to 15% oxygen, after dropping the incubator oxygen content to 5% at t=0 and the measured oxygen content within the incubator over an 8 hour time period. Temperature = 37 °C. Oil depth = 3.25 mm.

Figure 8.8 displays the comparison between the mean simulation (± 2 standard deviations) and the experimental data. The experimental data remained within two standard deviations of the mean simulation output. This provides confidence in the model.

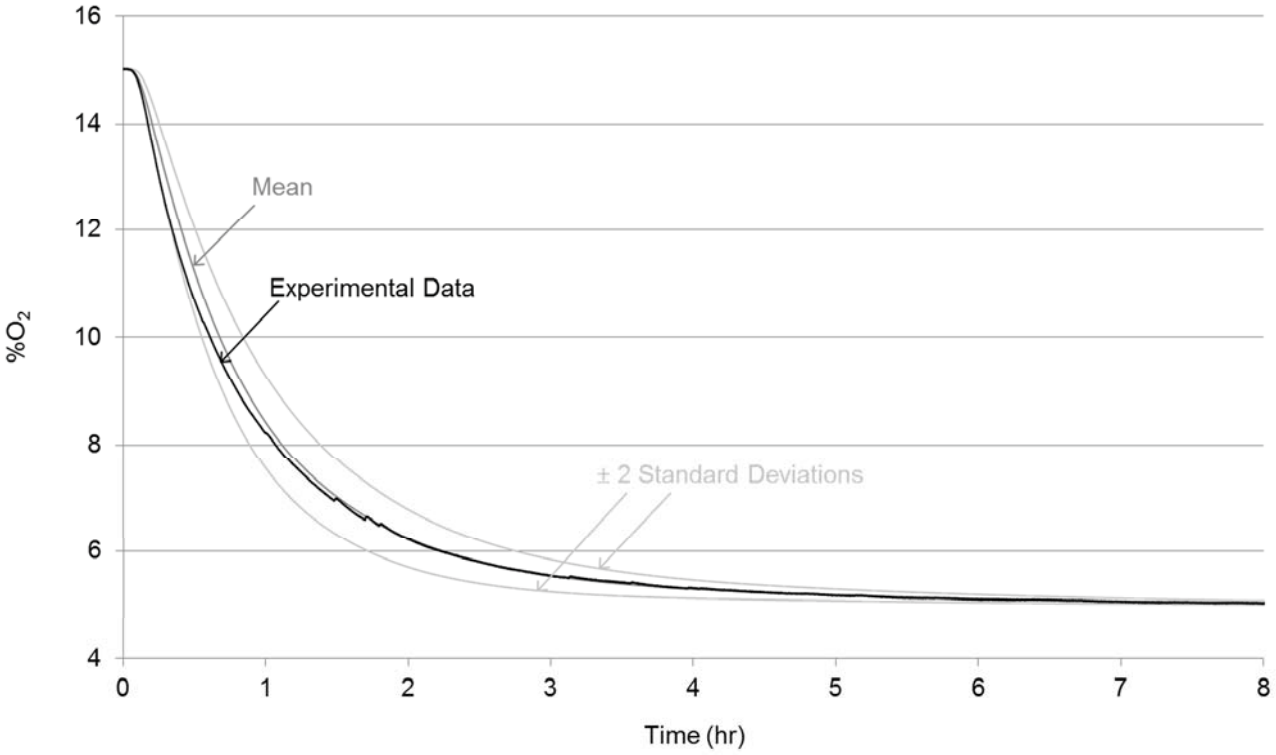

Figure 8.8: The experimentally measured fall in oxygen content in a Petri dish, initially fully equilibrated in 15 % O2, after a change in the incubator to 5% oxygen at t=0, compared with the modelled fall in oxygen (mean ± 2 standard deviations of 30 Monte Carlo simulations) at a point 0.8 mm above the centre floor of the dish. Oil depth = 3.25 mm.

Figure 8.9 compares the modelled fall in oxygen content at three positions along the axis of symmetry; at the centre floor of the dish, at 0.8 mm (the probe radius) above the centre floor of the dish and at 1.6 mm (the probe diameter) above the centre floor of the dish (as depicted by points i, ii, and iii in Figure 8.6). The mean experimental predictions at each point are displayed. The experimental data remains within the prediction band, close to the central prediction (the probe radius).

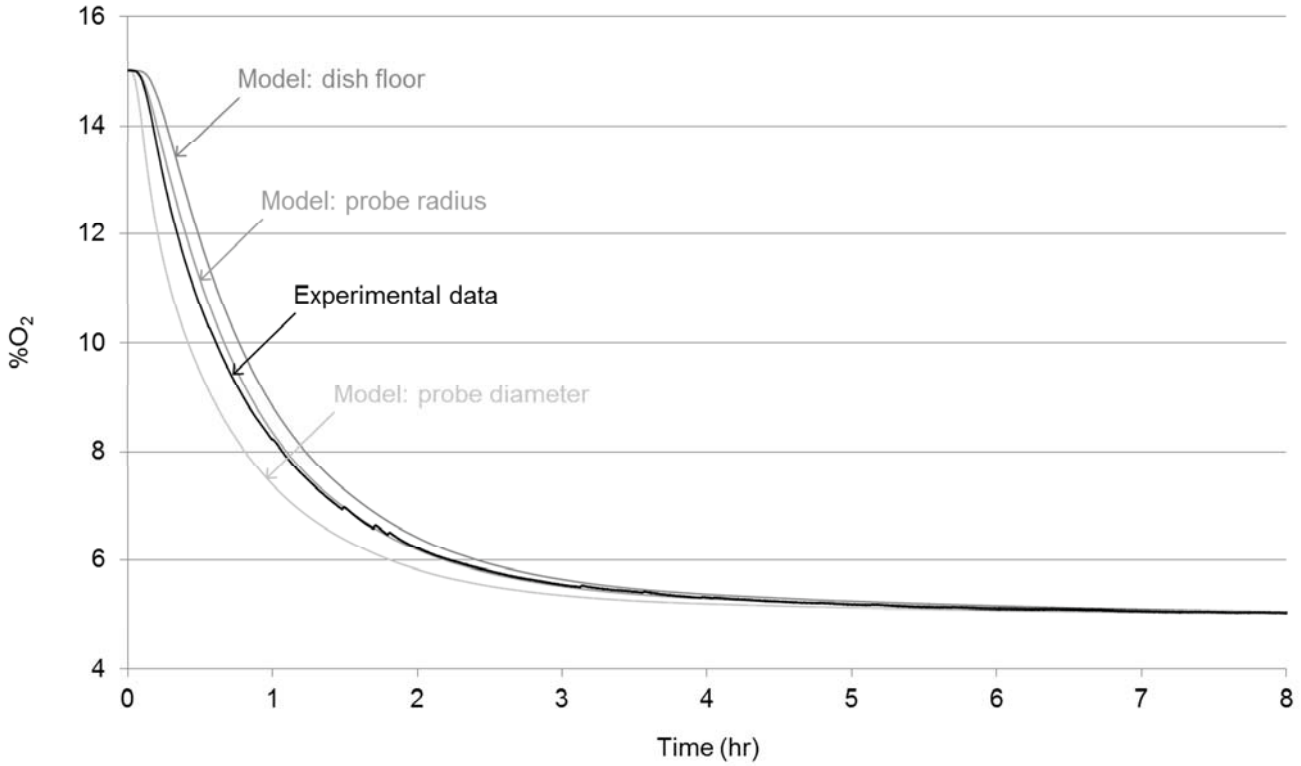

Figure 8.9: The experimentally measured fall in oxygen content in a Petri dish, initially fully equilibrated in 15 % O2, after a change in the incubator to 5% oxygen at t=0, compared with the modelled fall in oxygen content at three positions along the axis of symmetry: at the centre floor of the dish, at 0.8 mm (the probe radius) above the centre floor of the dish and at 1.6 mm (the probe diameter) above the centre floor of the dish. Oil depth = 3.25 mm. Temperature = 37 °C.

8.4.2.2 Varying the oxygen partial pressure

Figure 8.10 displays the data collected while subjecting a dish (the same system as validated above in Section 8.4.2.1 with an oil depth of 3.25 mm), initially fully equilibrated to 5% oxygen, to a series of three changes of incubator setting for O_2 partial pressure at 37 °C in a Sanyo incubator. At t=0 the incubator setting was stepped from 5% O_2 to 15% O_2. Once the partial pressure in the incubator reached 15% O_2 (t≈1.3 hr) the setting was stepped down to 11% O_2 for 30 minutes and then set back to 15% O_2 (t≈1.8 hr). The oxygen partial pressure outside the dish provided a

data set for the exposed boundary condition of the dish. The initial partial pressure of all model subdomains was set to 5% O_2 (38 mmHg).

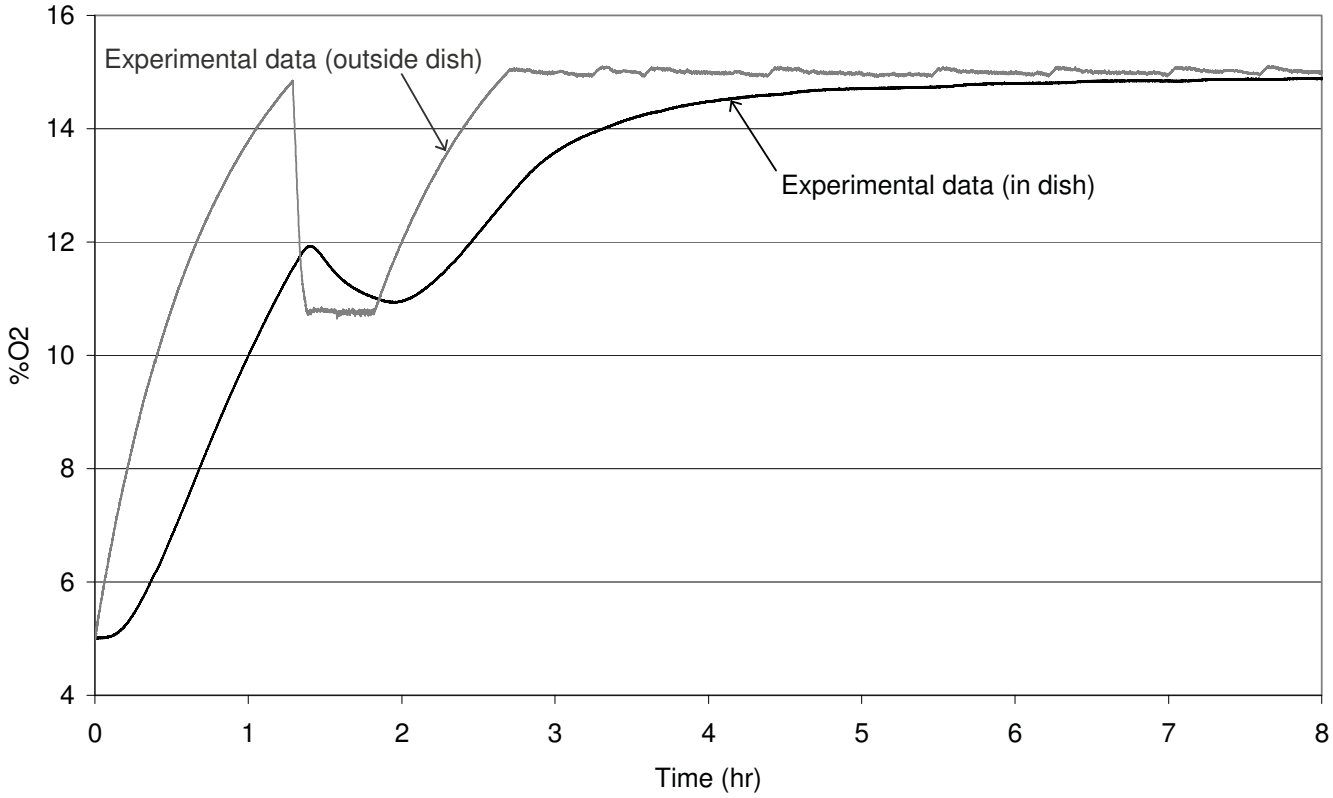

Figure 8.10: The experimentally measured change in oxygen content within the incubator and within a Petri dish, initially fully equilibrated to 5% oxygen, through a series of changes in the incubators partial pressure of oxygen: set to 15% at t=0, to 11% at t=1.3 hr and to 15% at t=1.8 hr. Oil depth = 3.25 mm. Temperature = 37 °C.

Figure 8.11 compares the modelled change in oxygen content (mean ± 2 standard deviations of 30 Monte Carlo simulations) at a point 0.8 mm above the centre floor of the Petri dish (½ the probe diameter) with the experimental data. The experimental data remains close to the modelled prediction band but not within it at all times. The model under predicts the rate of oxygen transfer while accurately predicting the steady state oxygen content (11% and 15% oxygen).

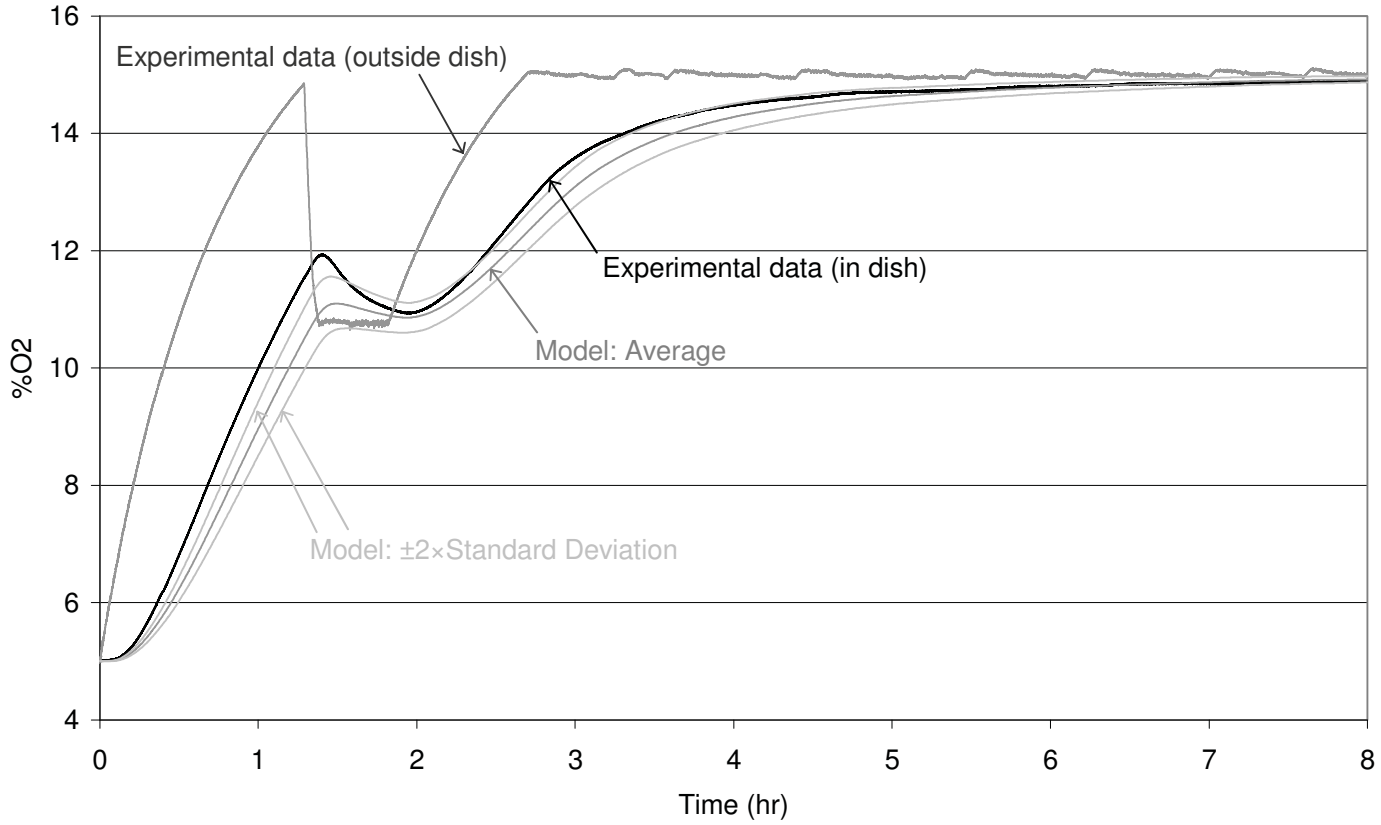

Figure 8.11: The experimentally measured change in oxygen content within the incubator and within a Petri dish, initially fully equilibrated to 5% oxygen, through a series of changes in the incubator's oxygen content: set to 15% at t=0, to 11% at t=1.3 hr and to 15% at t=1.8 hr. This data is compared with the modelled change in oxygen content (mean ± 2 Standard Deviations of 30 Monte Carlo simulations) at a point 0.8 mm above the centre floor of the Petri dish. Oil depth = 3.25 mm.

Figure 8.12 compares the experimental data with the modelled change in oxygen content at three positions along the axis of symmetry; at the centre floor of the dish, at 0.8 mm (the probe radius) above the centre floor of the dish and at 1.6 mm (the probe diameter) above the centre floor of the dish (as depicted by points i, ii, and iii in Figure 8.6). The experimental data closely follows the prediction output at the probe's diameter (i.e. a probe diameter above the dish floor). If the uncertainty in the experimental measurement was taken into account, ±5 % of the measured value, then validation is further justified. The prediction bands in Figure 8.12 would overlap the measured value at all times.

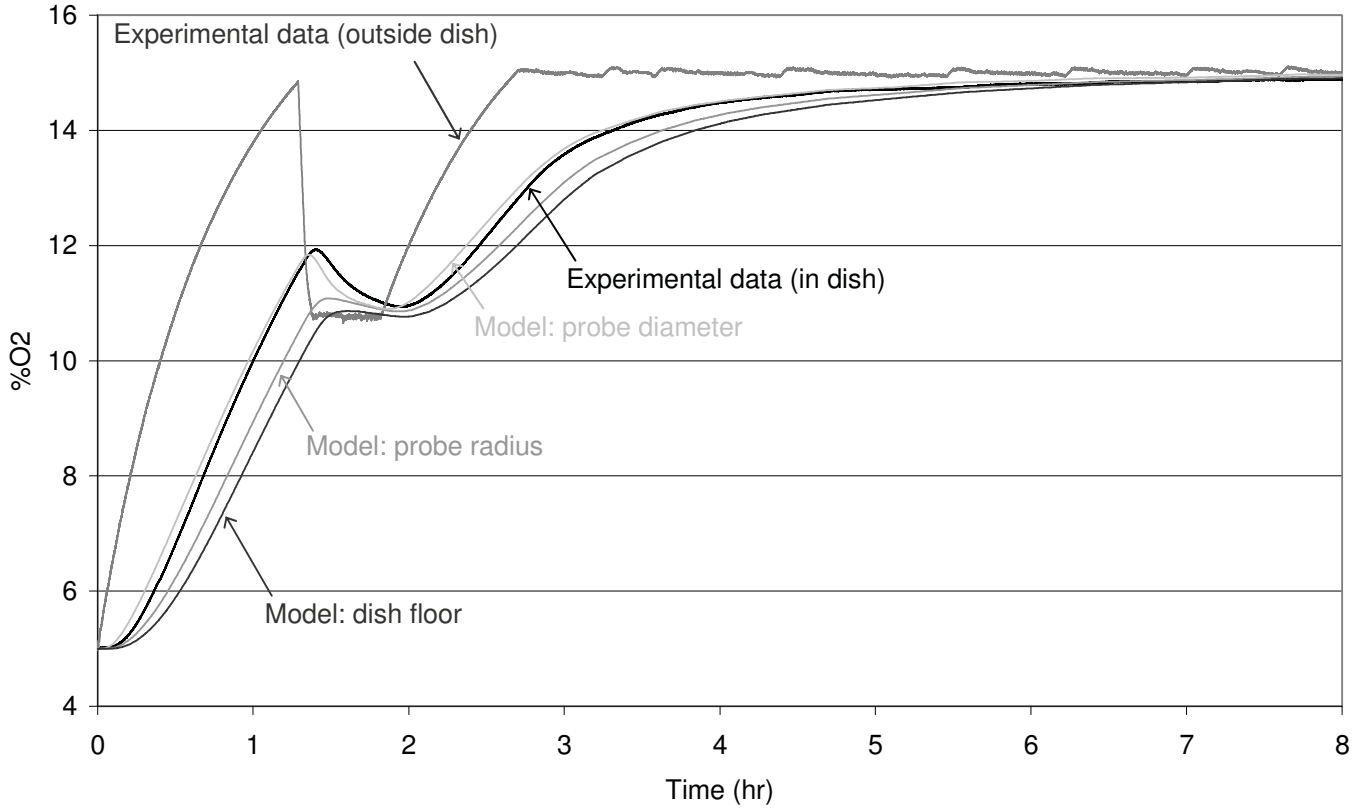

Figure 8.12: The experimentally measured change in oxygen content within the incubator and within a Petri dish, initially fully equilibrated to 5% oxygen, through a series of changes in the incubator's oxygen content: set to 15% at t=0, to 11% at t=1.3 hr and to 15% at t=1.8 hr. This data is compared with the modelled change in oxygen content at three positions along the axis of symmetry: at the centre floor of the dish, at 0.8 mm (the probe radius) above the centre floor of the dish and at 1.6 mm (the probe diameter) above the centre floor of the dish. Oil depth = 3.25 mm

8.5 Model Application

Throughout the embryo culture process the dish system is exposed to two oxygen environments; atmospheric oxygen in the laboratory air and 5% oxygen in the incubator (this may vary with IVF laboratory). A third, more temporary environment is the re-equilibrating incubator as nitrogen is flushed into the incubator in order to drop the oxygen content back down to the set point (5%). In the process flow diagram (Figure 3.10) the embryo, in a Petri dish, is transferred a maximum of 13 times between the incubator and laboratory environments. The purpose of this section is to

apply the model of mass transfer of oxygen in a Petri dish, as validated in the previous section, to investigate situations which may occur in the embryo culture process.

8.5.1 The Model for Application

For model validation the dish system was simplified by excluding the media drop to enable experimental data collection (as described in Section 8.4). Since the mass transfer properties of oxygen in water are well characterised compared with those of the other subdomains in this system it was assumed appropriate to incorporate the media drop back into the model for application to the embryo culture process.

Figure 8.13 compares the modelled fall in oxygen content at the centre floor of two dish systems, one with and one without a central media drop, during equilibration from atmospheric to 5% oxygen. Both dish systems have a total oil depth of 3.09 mm. This shows that there is little difference between the two systems due to the small volume of the media drop and the relatively similar oxygen mass transfer properties of oil and water, further supporting incorporation of the media drop into the model for application to the embryo culture process.

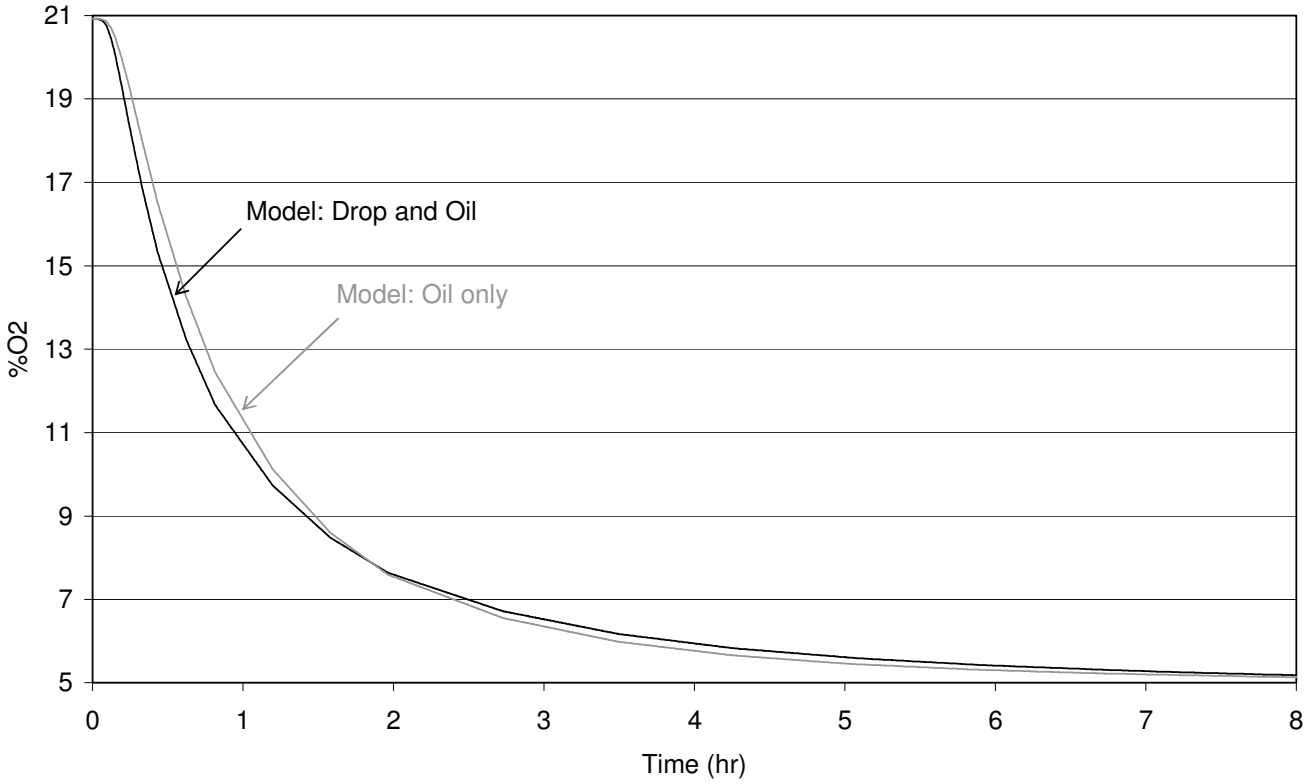

Figure 8.13: The modelled fall in oxygen content at the centre floor of two Petri dish systems, initially fully equilibrated at atmospheric oxygen (20.9 %), after placement into a 5% oxygen environment at t=0. One Petri dish system has an oil layer with no media drop and the other incorporates a media drop. In both cases the oil depth = 3.09 mm and the lid is on the dish.

8.5.2 The impact of a lid on oxygen mass transfer

It is a common assumption in embryo laboratories that the lid is a significant barrier to mass transfer of O_2 and CO_2. As a result, it is frequently considered preferable to leave the lid on when a dish is removed from an incubator in order to slow oxygen and carbon dioxide change (thus pH change) and to cock the lids on a dish when first placed into an incubator in order to speed change of oxygen and carbon dioxide back to culture levels.

Figure 8.14 compares the modelled change in oxygen content over 30 minutes at the centre floor of two Petri dish systems (with and without a lid), initially fully equilibrated to 5% O_2, after placement into an atmospheric environment (20.9% O_2).

This comparison over-estimates the effect of the presence of a lid since the model assumes no bulk movement of the air beneath the lid (even between the external wall of the dish and the lip of the lid). This is likely not the case, especially during transfer of the dish from an incubator onto a microscope stage.

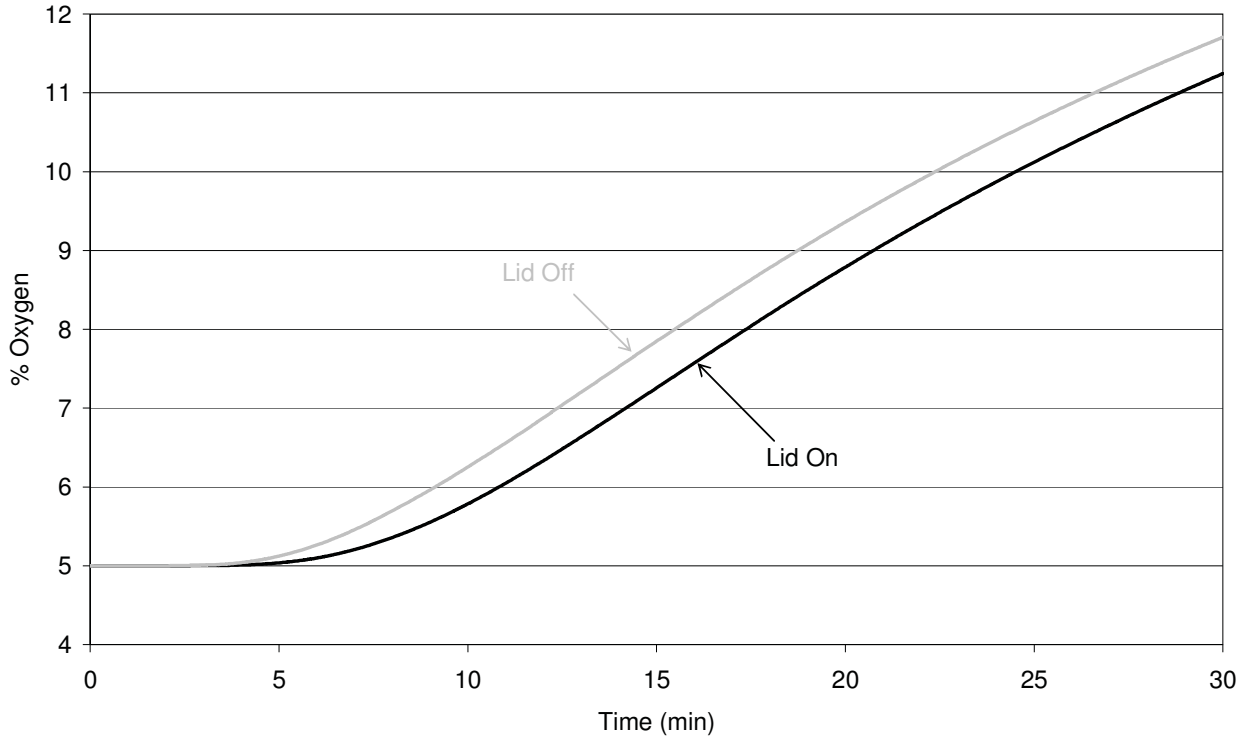

Figure 8.14: The modelled rise in oxygen content at the centre floor of two Petri dish systems, one with a lid and the other without a lid, initially fully equilibrated to (5% O2), after placement into a 20.9% oxygen environment at t=0. Oil depth = 3.09 mm.

Figure 8.14 displays a minimal difference in oxygen content between a dish with its lid on (black) and a dish without a lid (light grey). After 30 minutes out of an incubator (an extended period which is not likely to occur during the culture process)

the oxygen content at the centre floor of the dish differs by <0.5% and it takes a dish with a lid ≈2 minutes and 14 seconds longer to reach 11% O_2 than a dish with its lid off. This difference in oxygen profiles, which is an overestimate, represents little or no difference to the environment an embryo is exposed to, and hence embryo viability. The presence of a lid will likely have a similar minimal effect on mass transfer of CO_2, and therefore pH change. This is because it is the diffusive mass transfer properties of these gasses in air which promote fast equilibration of the air trapped by the lid of the dish with the surrounding bulk air essentially cancelling out the presence of the lid.

8.5.3 Oxygen changes throughout the embryo culture process

8.5.3.1 Oxygen equilibration

Throughout the culture process the air surrounding a Petri dish system will be at atmospheric oxygen (20.9%) or at 5 % (the incubator set point). Identifying the changes in oxygen environment at the position of an embryo when the dish is exposed to either of these extremes is potentially beneficial.

Figure 8.15 displays equilibration of the dish system, in both directions, between 20.9% (~atmospheric) and 5% oxygen. To reach 67% and 95% of the final value, in both directions, takes 1 hour and 4.1 hours respectively.

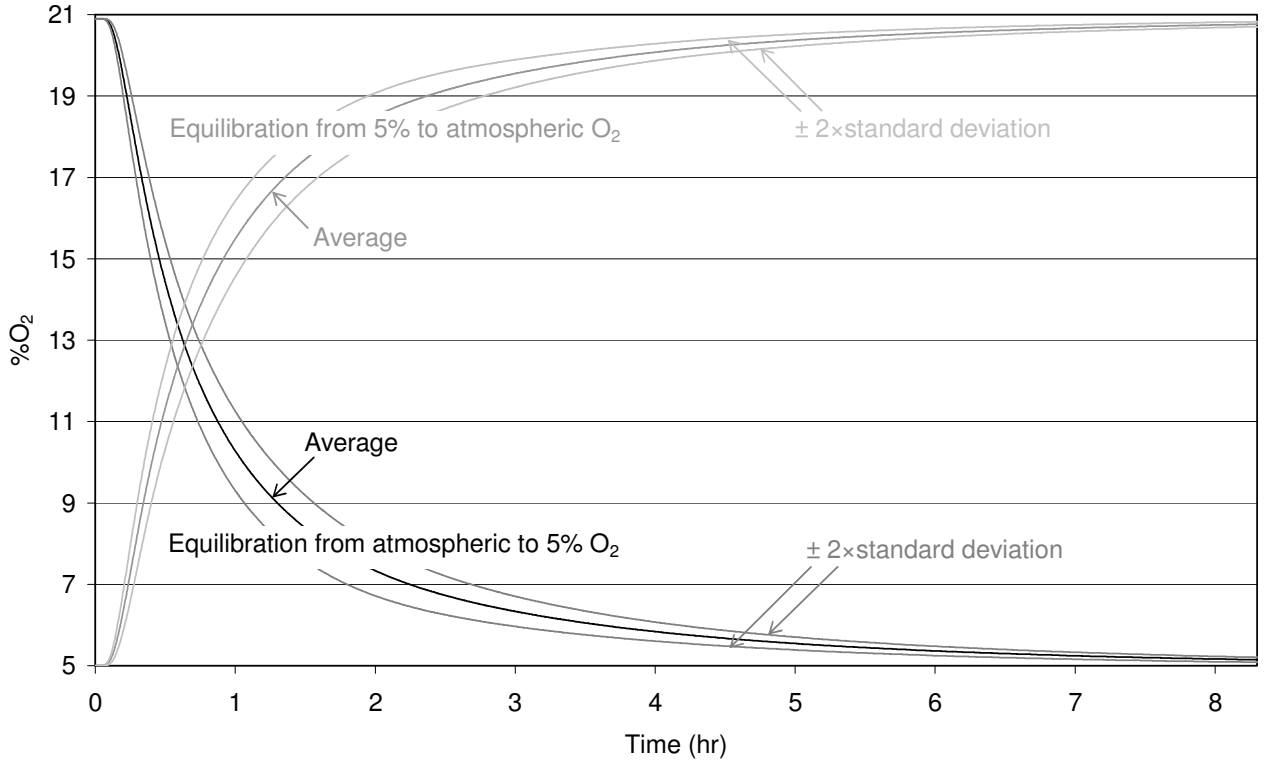

Figure 8.15: Modelled equilibration of oxygen content at the centre floor of a Petri dish (mean ± 2 standard deviations of 30 Monte Carlo simulations) in both directions between atmospheric oxygen (20.9 %) and a 5% oxygen environment. The petri dish system: lid on, depth of 3.09 mm of oil and a central media drop.

Effect of opening incubator doors

Figure 8.16 displays the percentage oxygen in a 1.7 cu ft (48.1 L) incubator recorded experimentally through a series of door openings to simulate a busy laboratory. Each opening of the door lasted 10 seconds. The measured oxygen content in the incubator, displayed in Figure 8.16, was applied as the exposed boundary condition of the Petri dish model in order to identify the impact that door openings may have on the oxygen content at the centre of the dish floor.

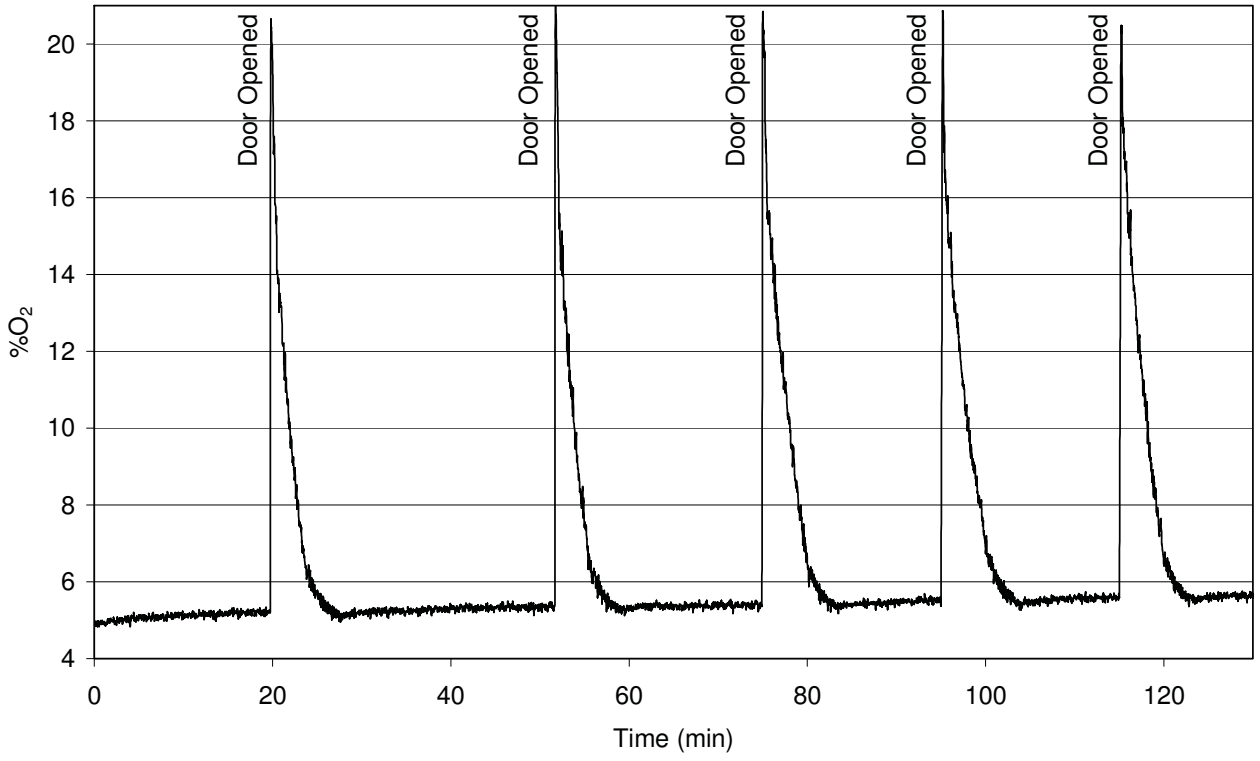

Figure 8.16: Experimentally measured change in incubator oxygen content as the door is opened (for a period of 10 seconds) five times over 130 minutes.

Figure 8.17 displays the modelled change in oxygen content (mean ± 2 standard deviations of 30 Monte Carlo simulations) at the centre floor of a Petri dish. The Petri dish was initially fully equilibrated at 5% O_2 and the experimentally measured changes in oxygen content within an incubator due to openings of the incubator door (displayed in Figure 8.16) were applied at the exposed boundary. As shown in Figure 8.16, the baseline oxygen concentration in the incubator steadily increased from 5 to 5.7%, this change is much smaller than the stepwise increase in oxygen concentration modelled at the floor of the dish (5 to 6.7%). This work demonstrates that if the time between two openings is less than the dish's or the incubator's recovery time then the oxygen content within the dish will rise. The magnitude of the rise in oxygen content within the dish after a single door opening is dependent on the incubator size, design

(a single door or multiple hatches for removing dishes from different parts of the incubator) and the gas flow rate when the incubator is flushed to return the low oxygen environment.

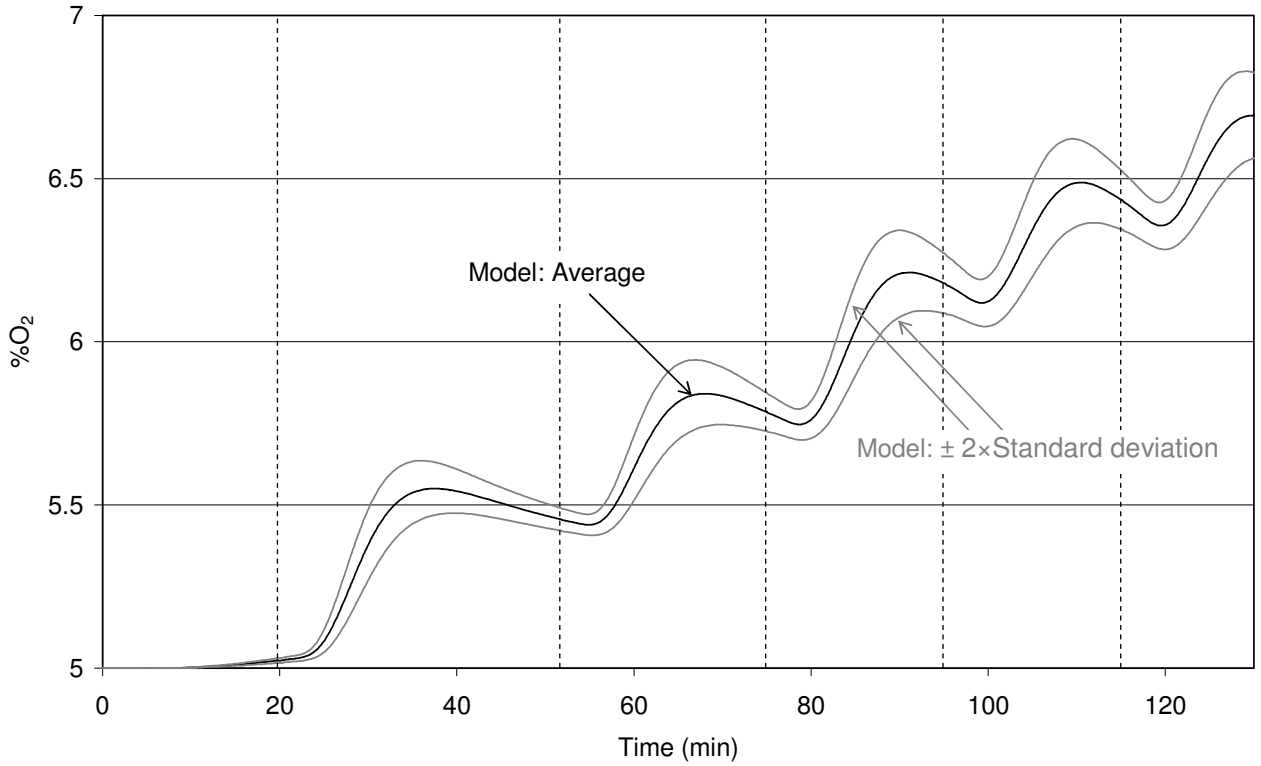

Figure 8.17: Modelled changes in the oxygen content at the centre floor of a Petri dish as the incubator door is opened multiple times (at times marked with a dashed line) causing the fluctuations in incubator partial pressure displayed in Figure 8.16. Petri dish has lid on, an oil depth of 3.09 mm and a central media drop.

8.6 Summary

A model of mass transfer of oxygen in the Petri dish system was developed and validated within this chapter. This model was applied to investigate the changes in oxygen content in an embryos environment throughout the culture process and factors which impact on these changes. The main findings were;

- A Petri dish system equilibrating from atmospheric oxygen (20.9% O_2) to 5 % oxygen, takes 4 hours to reaches 95 % of its total change.
- The presence of a lid on the dish system makes minimal difference to the oxygen environment an embryo in the dish is exposed to. Therefore, setting heated microscope stages for dishes without lids would optimise embryo temperature during embryo manipulation (as discussed in Section 5.4.3) without adversely affecting their oxygen environment.
- Modelling demonstrated how fluctuation in incubator oxygen content, due to a series of openings of an incubator door, can lead to a progressive rise in oxygen content at the centre floor of a Petri dish system.

This validated model of the mass transfer of oxygen in a Petri dish provides a good starting point for developing a model of pH change which, due to the bicarbonate buffer in the culture media, is dependent on the mass transfer of carbon dioxide in the system.

9 pH changes in a Petri dish

In the previous chapter a model of mass transfer of oxygen in the Petri dish system was developed and validated. Using this model as a starting point, this chapter aims to develop and validate a model of carbon dioxide mass transfer in the Petri dish system and subsequently use it to estimate the pH in the media drop. This model will then be applied to characterising the pH changes an embryo may be exposed to throughout the culture process and identify factors which may impact on these changes. As for oxygen it is convention in this field to define the carbon dioxide levels as volume present of a gas in equilibrium with the sample. Throughout this chapter all percentage carbon dioxide values refer to volume percentages.

The pH (defined by Equation 9.1) of the embryo culture media is buffered by the bicarbonate buffer system (the chemical equilibrium displayed in Equation 9.2). It is therefore dependent on the surrounding concentration of carbon dioxide (CO_2). Culture dishes are pre-equilibrated and embryos are cultured in incubators with a 6% CO_2 atmosphere to maintain the pH close to 7.3.

$$pH = -\log_{10}[H^+] \qquad \text{Equation 9.1}$$

$$CO_2 + H_2O \rightleftharpoons H_2CO_3 \rightleftharpoons HCO_3^- + H^+ \qquad \text{Equation 9.2}$$

A change in the concentration of CO_2 in the media impacts the pH through the equilibrium represented in Equation 9.2. The aim of this chapter is to predict the pH changes that an embryo experiences in a Petri dish at stages throughout the embryo culture process. Two processes must be considered. Firstly the diffusion of CO_2

through the dish system and secondly the impact of CO_2 on the pH as described by the equilibrium reaction in Equation 9.2.

9.1 Drop culture in a Petri dish

Drop culture in a Petri dish has been described in Chapter 4 Section 4.1. Mass transfer of oxygen in this system was modelled in Chapter 8 and, though the parameter inputs will differ, the same model will apply to predicting the diffusion of carbon dioxide (CO_2), but will also need to account for reaction of CO_2 via the described buffer reaction. As the interest in modelling CO_2 is due to its impact on the pH of the culture media the challenge in this section will be predicting this relationship within the culture media.

9.1.1 Conceptual model development

As discussed in the Petri dish heat transfer model development (Section 4.1.3.2) it was assumed that natural and forced convection are negligible within the dish system. Therefore the sole mode of mass transfer within the dish system is diffusion.

In the Petri dish system CO_2 will diffuse through the paraffin oil above the media drop. When CO_2 diffuses into the drop, the equilibrium is shifted to the right (of Equation 9.2) increasing the concentration of HCO_3^- and H^+ thereby decreasing the pH. When CO_2 diffuses out of the drop the opposite occurs, and the pH increases. In order to effectively model pH in the drop, the impact of a change in CO_2 concentration must be predicted to a suitable degree of accuracy.

The pH is an important environmental factor to an embryo. As described in Section 3.6, a pH of 7.4 is commonly considered the upper limit of pH tolerated in embryology laboratories.

9.1.1.1 Model geometry

The Petri dish drop culture geometry displayed in Figure 8.1 and the dimensions defined in Table 8.1 of Chapter 8 for the model of O_2 diffusion in a Petri dish are applicable to the model of CO_2 diffusion in a Petri dish. The only difference is that the lid, and the air trapped by the lid, will not be incorporated into the model geometry since modelling of oxygen transport in the Petri dish system (Section 8.5.2) suggested that the presence of the lid on the dish has minimal impact on mass transfer in the system.

9.1.1.2 Mass Transfer Assumptions

The assumptions made when defining the mode of oxygen mass transfer in the Petri dish apply equally to CO_2 transport in a Petri dish. Hence the assumptions made here are the same as those made for oxygen transfer (see Section 8.1.1.2).

9.1.2 Model Formulation

The driving force for CO_2 diffusion is dependent on the CO_2 concentration gradient. The concentration of aqueous carbon dioxide at any point in a media drop is dependent on the proportion which is converted to other species in the buffering reactions.

The following set of equations, derived from the equilibrium reaction (Equation 9.2), may be solved simultaneously to obtain the concentration of each species throughout a media drop:

$$\frac{\partial[CO_2]}{\partial t} = D\nabla^2[CO_2] + R_{CO_2}$$

$$\frac{\partial[H_2CO_3]}{\partial t} = D\nabla^2[H_2CO_3] + R_{H_2CO_3}$$

$$\frac{\partial[HCO_3^-]}{\partial t} = D\nabla^2[HCO_3^-] + R_{HCO_3^-}$$

$$\frac{\partial[H^+]}{\partial t} = D\nabla^2[H^+] + R_{H^+}$$

Where the reaction term in each equation is derived from the equilibrium as;

$$R_{CO_2} = -k_{+1}[CO_2][H_2O] + k_{-1}[H_2CO_3]$$

$$R_{H_2CO_3} = k_{+1}[CO_2][H_2O] + k_{-2}[HCO_3^-][H^+] - k_{-1}[H_2CO_3] - k_{+2}[H_2CO_3]$$

$$R_{HCO_3^-} = k_{2+}[H_2CO_3] - k_{-2}[HCO_3^-][H^+]$$

$$R_{H^+} = k_{2+}[H_2CO_3] - k_{-2}[HCO_3^-][H^+]$$

However, this full model requires diffusion coefficients for all species and the rate constants for every relationship. Many of these values are unavailable in the literature. Poor characterisation of such input parameters would lead to inaccuracies in the modelling and therefore the detail of such a model could add to prediction error rather than improving accuracy. By assuming that $R_{CO_2} \approx 0$ this full model may be simplified.

From the maximum pH change during equilibration of the culture media from atmospheric to 6% CO_2, the maximum change in H^+ concentration may be determined. This will correspond to the maximum concentration of CO_2 converted to bicarbonate and hydrogen in the buffer reaction since the stoichiometry is 1:1 (Equation 9.2).

With a partial pressure of 6% CO_2, as in an incubator, the concentration of CO_2 in the media is ≈1.482 mol.m^{-3} and the pH is ≈7.33. With an atmospheric partial pressure of 0.03% CO_2 the concentration of CO_2 in the media is ≈0.00741 mol.m^{-3} and the pH is ≈9.63 (assuming the solubility of CO_2 in media at 37 °C is 0.0325 mol.m^{-3}mmHg^{-1}, Table 9.5). The maximum change in the concentration of CO_2 in the media due to diffusion of CO_2 into the media is therefore ≈1.475 mol.m^{-3}. The maximum change in pH equates to a change in H^+ of 4.65×10^{-5} mol.m^{-3}. Since the change in H^+ concentration is equal to the change in CO_2 due to the buffer reaction, the proportion of CO_2 change due to the buffer reaction relative to that of diffusion is only 0.003% ($\frac{4.65\times10^{-5}}{1.475}\times100$). Therefore the reaction term (R_{CO_2}) may be assumed negligible and it may be assumed that the changes in CO_2 concentration within the dish are solely due to diffusion as described by Equation 9.3. As for the model of oxygen transport partial pressure units were used, the reasoning being described in Section 8.1.2.

$$\frac{\partial P_{CO_2}}{\partial t} = D\nabla^2 P_{CO_2} \qquad \text{Equation 9.3}$$

By assuming diffusion of CO_2 through the media is much slower than the reaction (Equation 9.3) it may be assumed that all species reach equilibrium instantaneously. At equilibrium the Henderson-Hasselbalch Equation (Equation 9.4) defines the relationship between CO_2 concentration and pH. Thus the pH can be calculated directly from the concentration of CO_2.

$$pH = \mathrm{pK_a} + \log\left(\frac{[HCO_3^-]}{[CO_2]}\right) \qquad \text{Equation 9.4}$$

where the CO_2 concentration is as predicted by solution of Equation 9.3

The concentration of bicarbonate in the culture media is high: ≈25mol/m^3. Since the stoichiometry is 1:1 for H^+ and HCO_3^- (Equation 9.2), the maximum change in [H^+], calculated above, is equal to the maximum change in $[HCO_3^-]$. $[HCO_3^-]$ will only change by ≈0.0002% ($\frac{4.65\times10^{-5}}{25}\times100$) and therefore may be assumed constant.

9.1.2.1 Boundary Conditions

When considering mass transfer of CO_2, since the lid is negated, there is one possible boundary condition arrangement for the Petri dish within the culture process. Each condition is applied to a boundary as described by roman numerals in reference to Figure 8.1.

1. The line of axial symmetry down the centre of the dish, about which the 2D model rotates.

$$\frac{\partial P_{CO_2}}{\partial t} = 0 \qquad \text{Equation 9.5}$$

$$for\ xi\text{-}x,\ t \geq 0$$

2. The exposed boundary of the model.

$$P_{CO_2} = P_{aCO_2} \qquad \text{Equation 9.6}$$

$$\textit{for xi-xii-xiii-xiv-v-vi-vii-viii-ix-x, } t \geq 0$$

9.1.2.2 Initial Conditions

In a given situation, it can be assumed that the initial carbon dioxide gradient through the dish is negligible, the initial conditions are:

$$P_{iCO_2}\ (\Omega_p, \Omega_o) = P_{aCO_2} \qquad \text{at } t=0$$

$$P_{iCO_2}(\Omega_m) = f(\textit{initial pH}) \qquad \text{at } t=0$$

'Ω' denotes the subdomain (with the subscripts: *p*=polystyrene, *m*=media, *o*=Paraffin oil), P_{iCO_2} = the initial partial pressure of carbon dioxide and P_{aCO_2} = atmospheric CO_2 concentration.

If it cannot be assumed that the carbon dioxide gradient through the layers of the dish is negligible then the initial temperature values were defined as the output values from the model of the preceding situation:

$$P_{iCO_2(x)}(y,r) = P_{fCO_2(x-1)}(y,r) \qquad \text{at } t=0$$

$P_{iCO_2(x)}$ = Initial partial pressure of CO_2 in process step number x, $P_{fCO_2(x-1)}$ = Final partial pressure of CO_2 in process step number x-1.

9.2 Parameter Estimation

The final model must be able to produce reliable predictions upon which decisions about future work may be based. For this to be possible the values of the model's subdomain parameters, the transport properties of carbon dioxide in the subdomain

material, are required. In addition, suitable estimates of the constants required for pH determination must be made.

The temperature dependence of each parameter must be taken into account. Embryo culture takes place at ~37 °C so for application of the model, the model parameters are required to be well defined at 37 °C. However for practical reasons the experiments for model validation took place at 20 °C (see Section 9.4.1) and therefore, in order to compare the model with the experimental data, suitable estimates of the parameter inputs were also required at 20 °C.

9.2.1 Media (Water)

Figure 9.1 displays the values of carbon dioxide solubility in water as gathered from the literature and the temperatures at which these values were determined (this data is displayed, with references, in Table 9.1). As for the solubility of O_2 in water, a line of best fit was applied to approximate the temperature dependency of the solubility. Only a single value from these sources was determined outside the 37-38 °C range (25 °C) greatly increasing the possibility of error in this fit. Since there was more data available for the value of O_2 solubility in water and assuming measurement of the two solubilities would be carried out by similar techniques, the percentage error estimate for oxygen solubility was used as an error estimate for CO_2 solubility (±12.5%). This is presented as the limits in Figure 9.1 (dotted line).

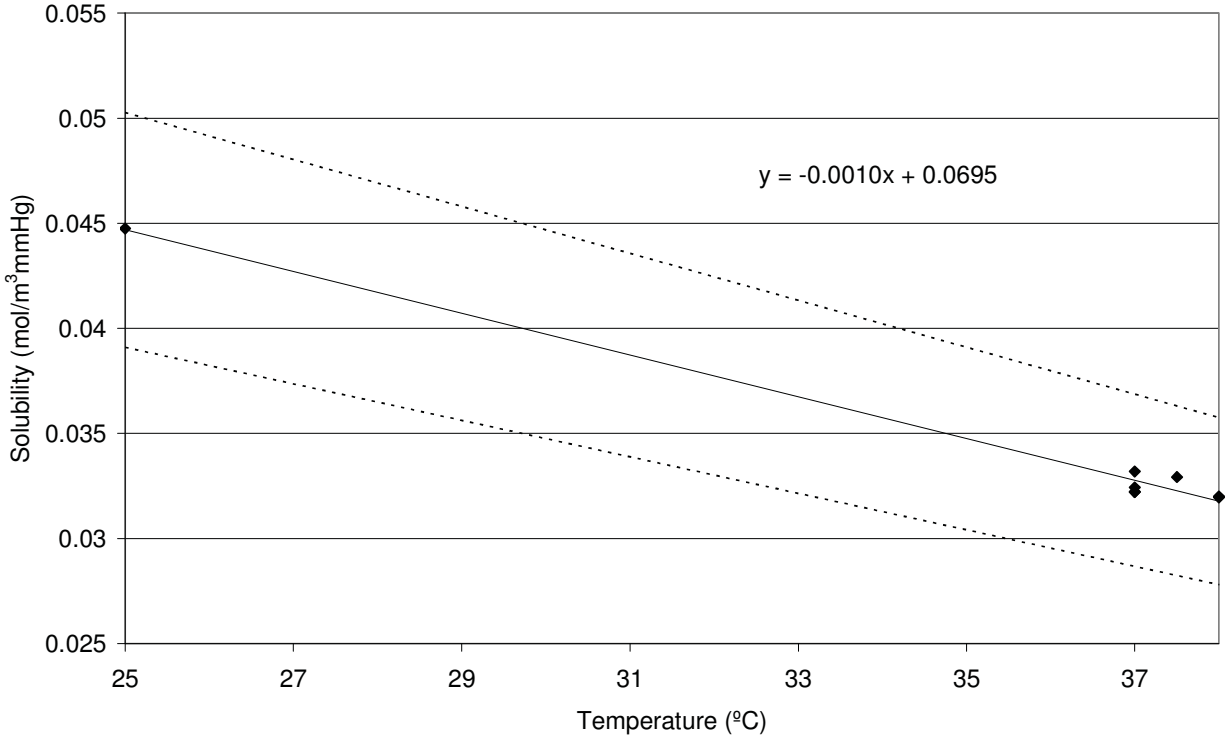

Figure 9.1: Values of the solubility of CO_2 in water (♦) over at a range of temperatures as collected from the literature. A linear fit approximating the solubility's temperature dependency is displayed with error margin of ±12.5% (references for each value are displayed in Table 9.1)

Temp (°C)	Solubility (mol. m^{-3}.$mmHg^{-1}$)	Reference
37	3.319×10^{-2}	Weathersby & Homer, 1980
37	3.221×10^{-2}	Weathersby & Homer, 1980
37	3.242×10^{-2}	Weathersby & Homer, 1980
37	3.221×10^{-2}	Lango et al., 1996
37.5	3.293×10^{-2}	Lango et al., 1996
38	3.200×10^{-2}	Lango et al., 1996
38	3.195×10^{-2}	Lango et al., 1996
25	4.475×10^{-2}	Robertson, 2006

Table 9.1: The solubility of CO_2 in water at a range of temperatures as collected from the literature. Values have been converted to units consistent with this work.

Figure 9.2 displays values of the diffusion coefficient for CO_2 in water and the temperatures at which these values were determined (this data is displayed, with references, in Table 9.2). Since diffusion coefficients are known to have an exponential relationship with temperature and there are sufficient values available, an exponential curve was fitted to the data. The standard deviation of the values at 25 °C (n=13) was 1.43×10^{-10}. Twice this standard deviation was taken as a conservative estimate of error (approximately ± 12%) and is presented as the limits (dotted line) in Figure 9.2.

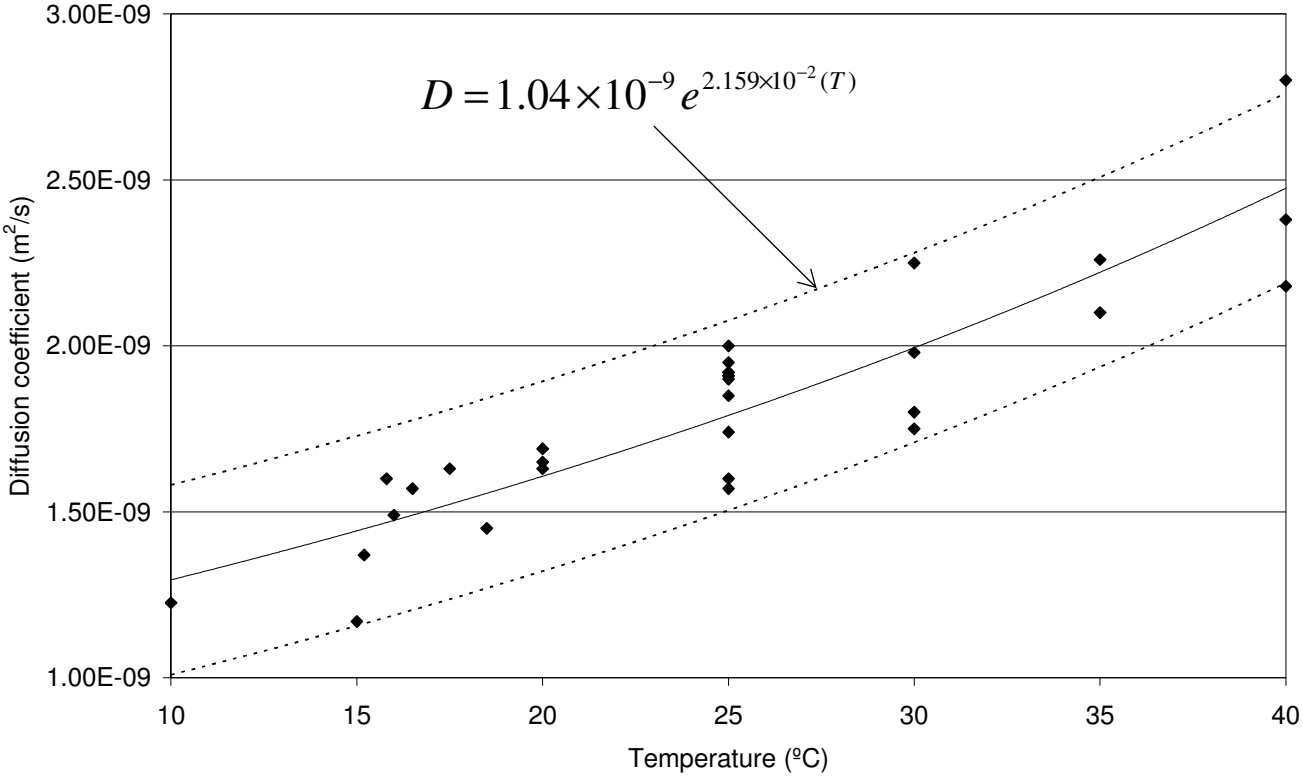

Figure 9.2: Diffusion coefficient of CO_2 in Water: The plot displays the diffusion coefficients of water as gathered from the literature over a range of temperatures (The data is displayed in Table 9.2 with references). The exponential curve fitted to the data is displayed with an error margin of ±12% (2×standard deviation of the values at 25 °C).

Temp (°C)	Diffusion Coefficient ($m^2.s^{-1}$)	Reference
10	1.226×10^{-9}	Lango et al., 1996
10	1.17×10^{-9}	Lango et al., 1996
15	1.37×10^{-9}	Lango et al., 1996
15.2	1.6×10^{-9}	Lango et al., 1996
15.8	1.49×10^{-9}	Lango et al., 1996
16	1.57×10^{-9}	Lango et al., 1996
16.5	1.63×10^{-9}	Lango et al., 1996
17.5	1.45×10^{-9}	Lango et al., 1996
18.5	1.65×10^{-9}	Lango et al., 1996
20	1.63×10^{-9}	Lango et al., 1996
20	1.69×10^{-9}	Lango et al., 1996
20	1.6×10^{-9}	Lango et al., 1996
25	1.74×10^{-9}	Lango et al., 1996
25	1.57×10^{-9}	Lango et al., 1996
25	1.91×10^{-9}	Lango et al., 1996
25	1.9×10^{-9}	Lango et al., 1996
25	1.92×10^{-9}	Lango et al., 1996
25	1.85×10^{-9}	Lango et al., 1996
25	2×10^{-9}	Lango et al., 1996
25	1.91×10^{-9}	Lango et al., 1996
25	1.95×10^{-9}	Lango et al., 1996
25	1.92×10^{-9}	Lango et al., 1996
25	1.98×10^{-9}	Lango et al., 1996
30	1.75×10^{-9}	Lango et al., 1996
30	1.8×10^{-9}	Lango et al., 1996
30	2.25×10^{-9}	Lango et al., 1996
30	2.1×10^{-9}	Lango et al., 1996
35	2.26×10^{-9}	Lango et al., 1996
35	2.18×10^{-9}	Lango et al., 1996
40	2.38×10^{-9}	Lango et al., 1996
40	2.8×10^{-9}	Lango et al., 1996
25	1.98×10^{-9}	Robertson, 2006

Table 9.2: The diffusion coefficient of CO_2 in water at a range of temperatures as collected from the literature. Values have been converted to units consistent with this work.

9.2.2 Paraffin Oil

Figure 9.3 displays the values of carbon dioxide solubility in a number of oil types and the temperatures at which these values were determined (this data is displayed, with references, in Table 9.3). The black diamonds are solubility values of CO_2 in plant derived oils (olive, linseed and cottonseed) while the pale grey crosses are the solubility values of CO_2 in transformer oil.

As discussed in Section 8.2.1.2 transformer oil (Shell Diala AX) is, like paraffin, a refined mineral oil and it is likely that the values of carbon dioxide solubility in transformer oil better represent that in paraffin than solubilites in the plant derived oils. Therefore, the values of carbon dioxide solubility in transformer oil were assumed to be the best available estimate of the values in paraffin oil. A line of best fit was applied to the values and a conservative estimate of error of 20% was applied.

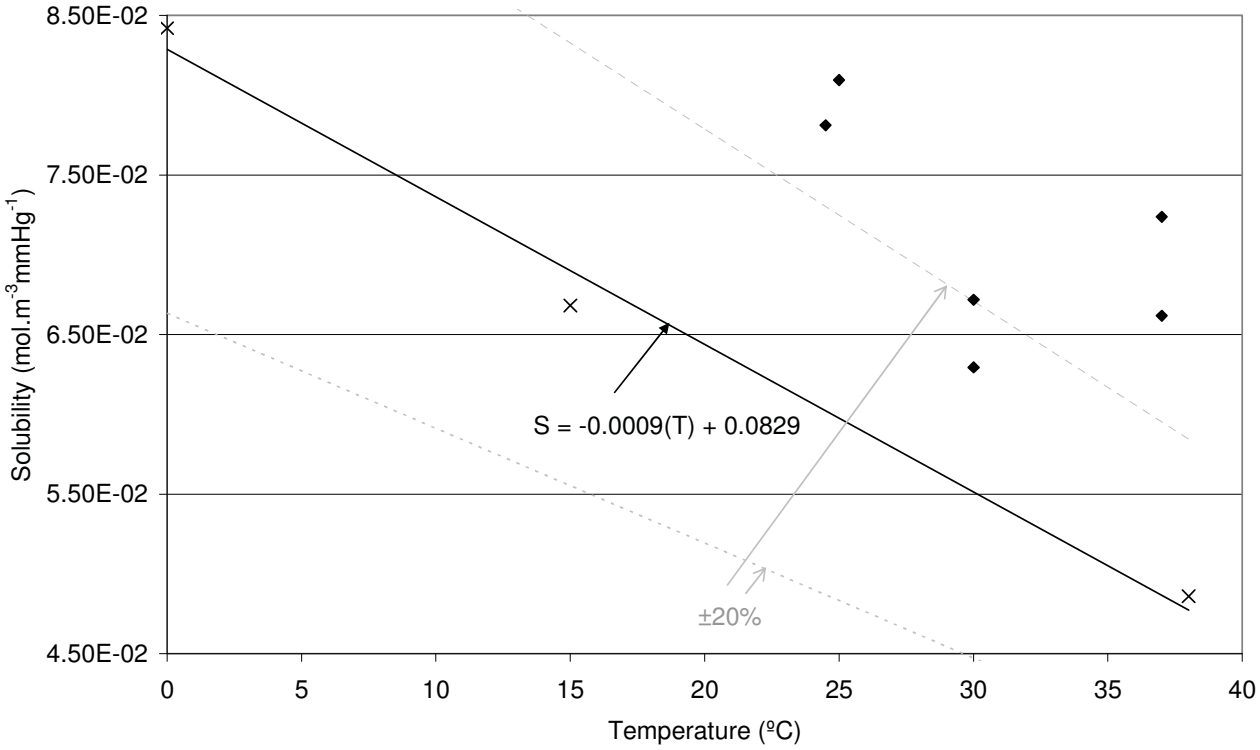

Figure 9.3: The solubility of CO_2 in several oil types over a range of temperatures as collected from the literature. The oil type of each point is specified as follows; ♦ = plant oil, × = transformer oil. References for each value are displayed in Table 9.3.

Temp (°C)	Type of oil	Solubility (mol. $m^{-3}.mmHg^{-1}$)	Reference
20	olive	7.238×10^{-2}	Weathersby & Homer, 1980
25	olive	6.618×10^{-2}	Weathersby & Homer, 1980
25.1	olive	8.095×10^{-2}	Lango et al., 1996
25.3	olive	6.294×10^{-2}	Lango et al., 1996
37	linseed	6.718×10^{-2}	Lango et al., 1996
38	cottonseed	7.811×10^{-2}	Lango et al., 1996
0	transformer oil	6.682×10^{-2}	Shahsiah et al., 2007
15	transformer oil	4.859×10^{-2}	Shahsiah et al., 2007
37	transformer oil	8.420×10^{-2}	Shahsiah et al., 2007

Table 9.3: The solubility of CO_2 in several oil types (olive, linseed, cottonseed and transformer) at a range of temperatures (0-38 °C) as collected from the literature. Values have been converted to units consistent with this work.

In gaseous mass transfer the diffusion coefficient is dependent on the molecular size of the gas molecule; it follows that the ratio of the diffusion coefficient of oxygen to that of carbon dioxide will be relatively constant in different materials/liquids and with temperature. Figure 9.4 displays the ratio of D_{O_2} to D_{CO_2} in water calculated at a number of temperatures using data from Tables 8.6 and 9.2. This demonstrates that D_{O_2}/D_{CO_2} is approximately constant with temperature. The average ratio (D_{O_2}/D_{CO_2}) was 1.29.

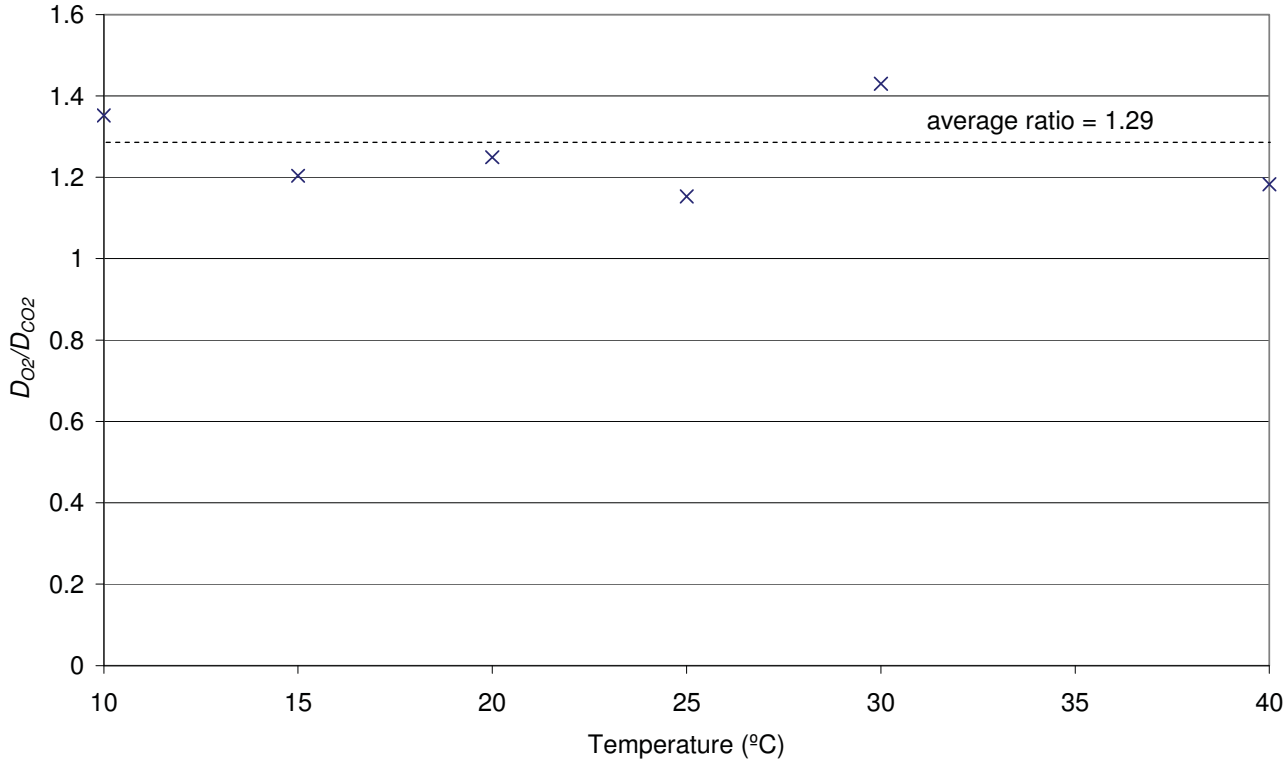

Figure 9.4: The ratio of the oxygen diffusion coefficient in water to the carbon dioxide diffusion coefficient in water as a function of temperature. The average ratio (1.29) is marked with a dotted line.

The diffusion coefficient of CO_2 in paraffin oil was predicted from the coefficient of O_2 in paraffin oil. The value of the diffusion coefficient of O_2 in paraffin oil, defined in Chapter 8, was 1.67×10^{-9} m^2s^{-1} at 37 °C (Stokes, 2009). This value was divided by the average ratio of D_{O_2}/D_{CO_2}, 1.29, to give a prediction of the diffusion coefficient of CO_2 in paraffin oil: 1.295×10^{-9} m^2s^{-1} at 37 °C.

The temperature dependence of D_{O_2} in paraffin oil was not defined in Chapter 8. In order to estimate the D_{CO_2} at 20 °C the value of D_{O_2} at 20 °C was predicted. It was assumed that the percentage change in D_{O_2} between 20°C and 37 °C was the same for oxygen mass transport in both water and paraffin oil. Therefore, since the change in D_{O_2} between 20 and 37 °C in water is 32% of the value at 37 °C, then D_{O_2} in paraffin

oil would be 1.136×10^{-9} m^2s^{-1} at 20 °C. Dividing this by the average ratio of D_{O_2} / D_{CO_2} (1.29) gave a prediction of D_{CO_2} in paraffin oil, 8.8×10^{-10} m^2s^{-1} at 20 °C.

9.2.3 Polystyrene

Table 9.4 displays literature values of the diffusion coefficient and the solubility of carbon dioxide in polystyrene. These were the only available values. While they were determined at 35 °C, out of necessity they were applied to the model when simulating either at 20 °C or 37 °C. As the temperature dependency was not available and there was little available data, 20% was applied as a conservative estimate of error.

Property	Temperature	Value	Reference
Solubility	35 °C	5.724×10^{-2} $mol.m^{-3}mmHg^{-1}$	Puleo et al., 1989
Diffusion coefficient	35 °C	8.8×10^{-12} m^2s^{-1}	Puleo et al., 1989

Table 9.4: The solubility and diffusion coefficient of carbon dioxide in polystyrene

9.2.4 Summary of the mass transfer properties of CO_2

Tables 9.5 and 9.6 summarise the mass transfer properties of CO_2 in the subdomains of the dish system at 37 °C and 20 °C respectively. The mass transfer properties of polystyrene are not changed since only single values of these properties (35 °C) were found in the literature. In order to implement a Monte Carlo simulation a value for the standard deviation of every thermophysical property is required. The reasoning for this was described in Section 4.3. The standard deviation was taken to be half the estimated errors which are displayed in Tables 9.5 and 9.6.

Material	Diffusion Coefficient of CO_2 (m^2s^{-1})	Solubility of CO_2 ($mol.m^{-3}mmHg^{-1}$)
Water	2.3197×10^{-9} (±12%)	0.0325 (±12.5%)
Paraffin Oil	1.798×10^{-9} (±20%)	0.0496 (±20%)
Polystyrene	8.8×10^{-12} (±20%)	0.0572 (±20%)

Table 9.5: The diffusion coefficients and solubilities of CO_2 in the model subdomains at 37 °C. The estimated percentage error is displayed, in brackets, next to each value.

Material	Diffusion Coefficient of CO_2 (m^2s^{-1})	Solubility of CO_2 ($mol.m^{-3}mmHg^{-1}$)
Water	1.602×10^{-9} (±12%)	0.0495 (±12.5%)
Paraffin Oil	8.8×10^{-10} (±20%)	0.0649 (±20%)
Polystyrene	8.8×10^{-12} (±20%)	0.0572 (±20%)

Table 9.6: Summary of diffusion coefficients and solubilities of CO_2 in the model subdomains at 20 °C. The estimated percentage error is displayed, in brackets, next to each value.

9.2.5 Constants for pH determination

The most common concentration of bicarbonate in culture media used for human embryo culture is 25 mM (Fleming & Cooke, 2009), or close to this value. Though the exact value will vary with manufacturer and batch this value was applied throughout this work.

The equilibrium constant K, or the negative log of this value (the pK_a) has been well characterised for the bicarbonate buffer system at 37 °C since the buffering of blood is dependent on the same mechanism. Though the rates of the reaction in the body are far greater due to the presence of an enzyme which catalyses the reaction (carbonic anhydrase), the equilibrium is identical. The pK_a of this reaction (Equation 9.2) is 6.1. Applying this pK_a value to the Henderson-Hasselbalch equation (Equation 9.4) the pH of media under a 6% CO_2 atmosphere containing 25 mol/m^3 of bicarbonate is

≈7.33; this is within the range specified by Vitrolife for the G5 series bicarbonate buffered media. The G5 series Vitrolife culture media specifies that the pH of the culture media under a 6% CO_2 atmosphere is 7.27±0.07.

The equilibrium constant, and thus the pKa, of bicarbonate buffer is temperature dependent. This is displayed in Figure 9.5 (Hansen & Gesser, 1980; cited from Severinghaus, 1965). The pKa of the bicarbonate buffer system at 20 °C was estimated to be ≈6.2 from this relationship.

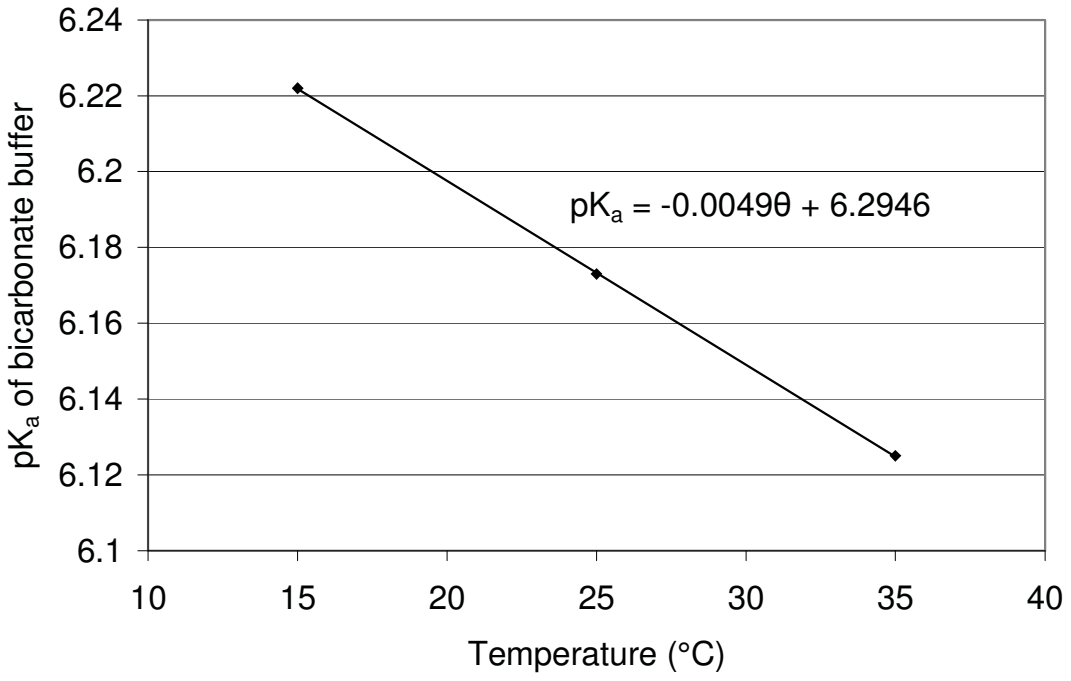

Figure 9.5: The temperature dependence of the bicarbonate buffer pK_a between 15 °C and 35 °C (Hansen & Gesser, 1980)

9.3 The Model Solution

The model was solved by the finite element method in the software package COMSOL Multiphysics 3.3a (COMSOL, Stockholm, Sweden). This 2D model of

CO_2 mass transfer in a Petri dish was similar to solving the 2D models of O_2 mass transfer and heat transfer in a Petri dish. For more detail see Section 4.2.1.

Solver accuracy checks were carried out, as detailed for heat transfer in a Petri dish in Section 4.2.2.2. As a result all subsequent simulations were run, as for the heat transfer mode, with a relative tolerance of 0.01 and a mesh density of ≈7000 elements.

9.4 Model Validation

The primary difference in experimental validation of this model of CO_2 diffusion as opposed to heat transfer or oxygen diffusion is that the CO_2 concentration was not directly measured. Instead, the pH was measured and the model of CO_2 diffusion was validated together with the assumed relationship between CO_2 concentration and pH.

This approach presents difficulties. Discrepancies between the model and the experimental data may be attributed to a model parameter, an error in conversion of CO_2 concentration to pH, an experimental measurement error or a combination of all three and it is not simple to discern which. However, diffusion of oxygen through the same system was successfully validated in Chapter 8 and therefore, though transport parameters of CO_2 are not so well defined in the literature, a similar model should accurately describe CO_2 mass transfer. Since pH was the factor of interest, not the CO_2, measuring pH as an endpoint was justified.

As for the oxygen probe, since the pH probe is relatively large (2 mm in diameter) it was not possible to position the probe within a standard media drop. However, culture media could not be excluded from the dish system for validation as the purpose of this

model was to assess how the pH varies with the concentration of CO_2 in the culture media. Therefore the pH probe was submerged in a layer of culture media and paraffin oil was layered over the top.

9.4.1 Experimental Design

9.4.1.1 pH probes

The pH probe used for the experimental validation was a PHR-146 Micro Combination pH Electrode (Lazar Research Laboratories, Inc., Los Angeles, USA). This is a solid state micro pH electrode designed for the measurement of small samples. The probe is 2 mm in diameter. The probe was connected to a Jenco Model 60 portable Digital pH meter (Jenco Electronics Ltd, San Diego, USA), for pH display.

Calibration was carried out against pH 7 and pH 4 buffers immediately prior to an experimental run in accordance with the manufacturer's instructions.

The use of this pH probe proved problematic but it was the only probe available that was sufficiently small to measure in a Petri dish system. The precision of initial pH readings was ±0.2 pH units, a broad range considering the total pH range in question was 2-3 pH units. In addition the probe reading drifted throughout experimental runs and the final probe reading was frequently ±0.5 pH units from the known steady-state value. The containment of the probe within the dish system did not allow for recalibration of the probe at frequent intervals throughout the experimental run.

To determine the initial pH of the media (to the nearest 0.1 pH unit) an IQ 125 miniLab pH meter (Hach Company, Colorado) was used. The inbuilt electrode was calibrated with pH 7 and pH 10 buffers immediately prior to use. A drop of medium was removed from the dish with a glass pipette and placed onto the probe tip. Once the reading had stabilised its value was recorded to the nearest 0.1 pH unit.

9.4.1.2 Experimental methodology

Calibration of the pH probe, as described above in Section 9.4.1.1., was the first step in each experimental run. Figure 9.6 displays the set up of the needle probe in the dish. A hole, of approximately the probe diameter, was melted at the base of the dish wall and the probe (just calibrated) was inserted so that it lay flat along the dish floor. The probe was held in place with a thin piece of aluminium tape and the hole was sealed with silicone. Once the silicone had set, the culture medium was added to the dish to cover the probe. A layer of paraffin oil was added over the culture medium. The mass of the dish was recorded before and after addition of the culture medium and the oil layers to accurately determine the depths of each layer.

Once the dish was set-up it was placed, along with the pH meter (cordless), into a sealed culture chamber. This culture chamber (Incubator chamber, Billups-Rothenburg Inc., Del Mar, CA, USA.) had gas inlets and outlets. The purpose of the chamber was to reduce the volume of gas required for an experiment (to reduce the expense) and to ensure the gas environment around the dish reached 6% CO_2 quickly. The gas flow was turned on (~1 $L.min^{-1}$ of 6% CO_2 in nitrogen) and the data was logged until steady state had been reached. The large gas flow meant any diffusion of

CO_2 through the walls of the culture chamber (moulded polycarbonate) may be negated.

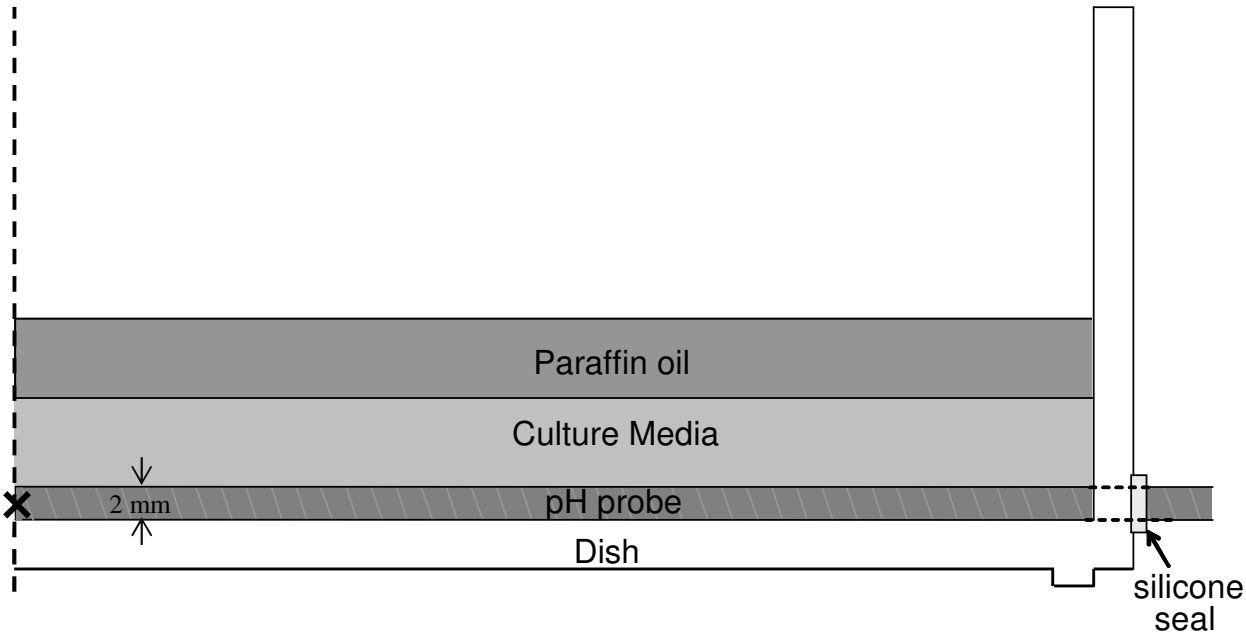

Figure 9.6: Diagram of pH probe placement for model validation experiments including the pH probe and silicone seals. The pH is measured at the centre of the dish, 1mm from the floor (labelled ×).

The culture chamber did not have temperature control. Experimental work was carried out at a room temperature of 20 °C. For model validation the mass transfer properties and pKa at 20 °C were used.

9.4.2 Model Validation

The experimental data was compared to the Monte Carlo simulation output (n=30), mean ± two standard deviations, in which the mass transfer properties of the subdomain materials are randomly selected from individual approximated normal distributions. The decision to use 30 Monte Carlo simulations was made via the same methodology described for heat transfer in a Petri dish (Section 4.5.4.). The

simulation output was taken 1 mm (half the probe diameter) from the floor of the dish at the dish centre.

The depths of the culture media and the paraffin oil were calculated to be 3.50 mm and 2.38 mm respectively, after correction for the volume of the pH probe, from the mass of each liquid added into the dish. The initial pH of the media was recorded by the IQ 125 miniLab pH meter as pH 8.5

From the Henderson-Hasselbalch equation (Equation 9.4), using the values of CO_2 solubility in water and the pKa of bicarbonate buffer at 20 °C, the final pH may be determined as follows:

$$pH = \mathrm{pK_a} + \log\left(\frac{HCO_3^-}{CO_2}\right)$$

$$\therefore pH = 6.2 + \log\left(\frac{25}{(P_{CO_2} S_{CO_2})}\right) = pH = 6.2 + \log\left(\frac{25}{\left(\left(\frac{760}{100}\right) \times 6 \times 0.0495\right)}\right) = 7.244$$

This is further verified by the IQ 125 miniLab pH meter which measured the final pH of the culture media, after equilibration with 6 % CO_2, as pH7.2 (to the nearest 0.1 pH unit).

The pH data recorded in the dish by the micro pH electrode was converted to an H^+ concentration. An offset correction was used to adjust the measured change in H^+ concentration to fit the more accurate initial and final pH values. A linear relationship

was assumed between the actual change in H^+ (determined from the initial and final pH measurements and the Henderson-Hasselbalch equation) and the measured change in H^+ by the pH electrode in the dish. The data was adjusted to the actual H^+ change and converted back into pH units.

Figure 9.7 displays the comparison between the experimentally measured fall in pH and the calculated fall in pH (from the modelled rise in CO_2 content using the best values of each parameter determined at 20 °C as defined in Table 9.6) at three points on the line of axial symmetry: the dish floor, at half the probe radius (1 mm) and at the interface of the media and oil layers.

There is little difference between the model predictions at the dish floor and 1 mm above this point. The experimental data closely follows these predictions. The model prediction at the floor of the dish for the most part slightly under predicts the actual pH change. The degree by which this under-predicts the actual change in pH is likely to be dependent on the rates of the equilibrium reactions and the diffusion of hydrogen ions through the media. The model prediction at the media-oil interface was significantly higher than the experimental pH change as expected, since the probe is measuring a mean value across its diameter (2 mm) and the media-oil interface is 1.5 mm above the probe diameter.

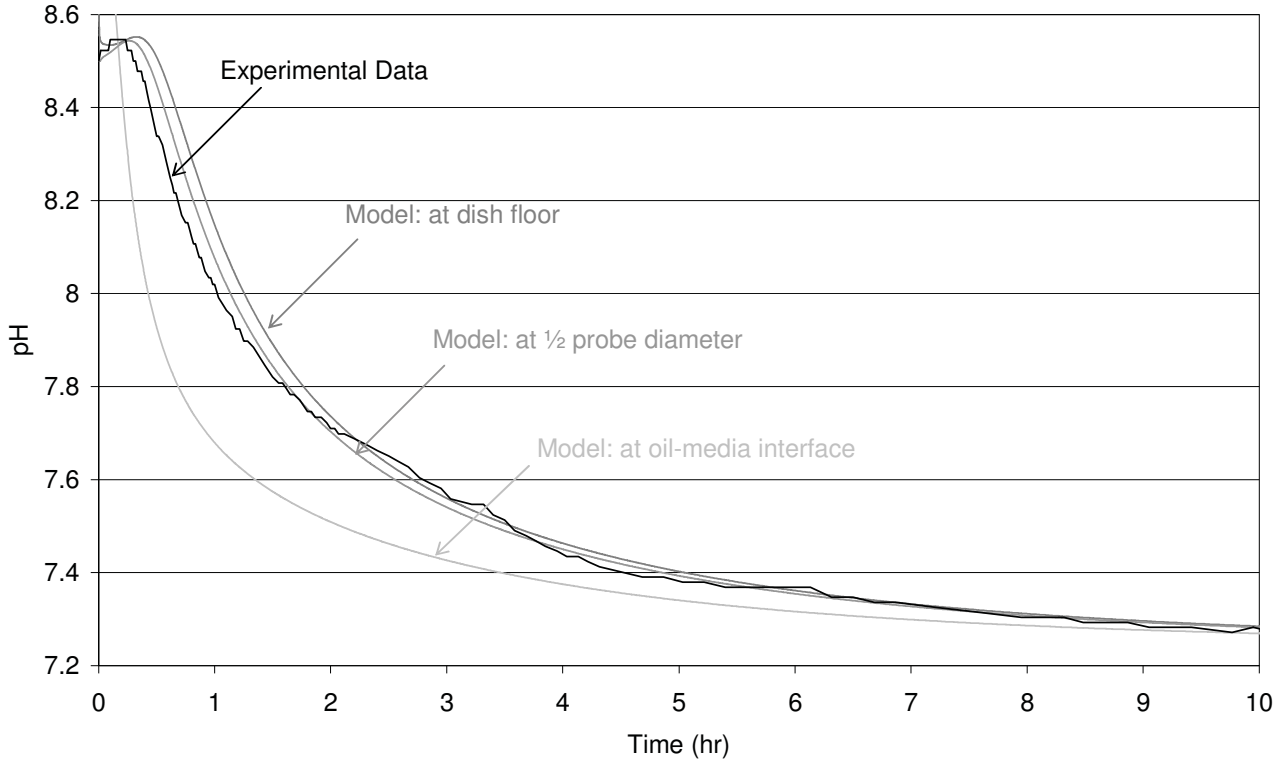

Figure 9.7: The experimentally measured fall in pH in a Petri dish, initially at a steady state pH of 8.5, after placement into a 6% carbon dioxide atmosphere compared with the fall in pH (calculated from the modelled rise in CO_2 content) at three positions along the axis of symmetry: on the dish floor, at ½ the probe diameter (1 mm) above the dish floor and at the oil-media interface (3.5 mm above the dish floor). Depth of culture medium = 3.5 mm, depth of paraffin oil = 2.38 mm. No lid on the dish.

Figure 9.8 displays the comparison between the experimentally measured fall in pH and the calculated fall in pH (from the modelled rise in CO_2 content (mean ± 2 standard deviations of 30 Monte Carlo simulations) at a point 1 mm (half the probe diameter) above the dish floor. The experimental data remains within two standard deviations of the mean simulation output validating the model.

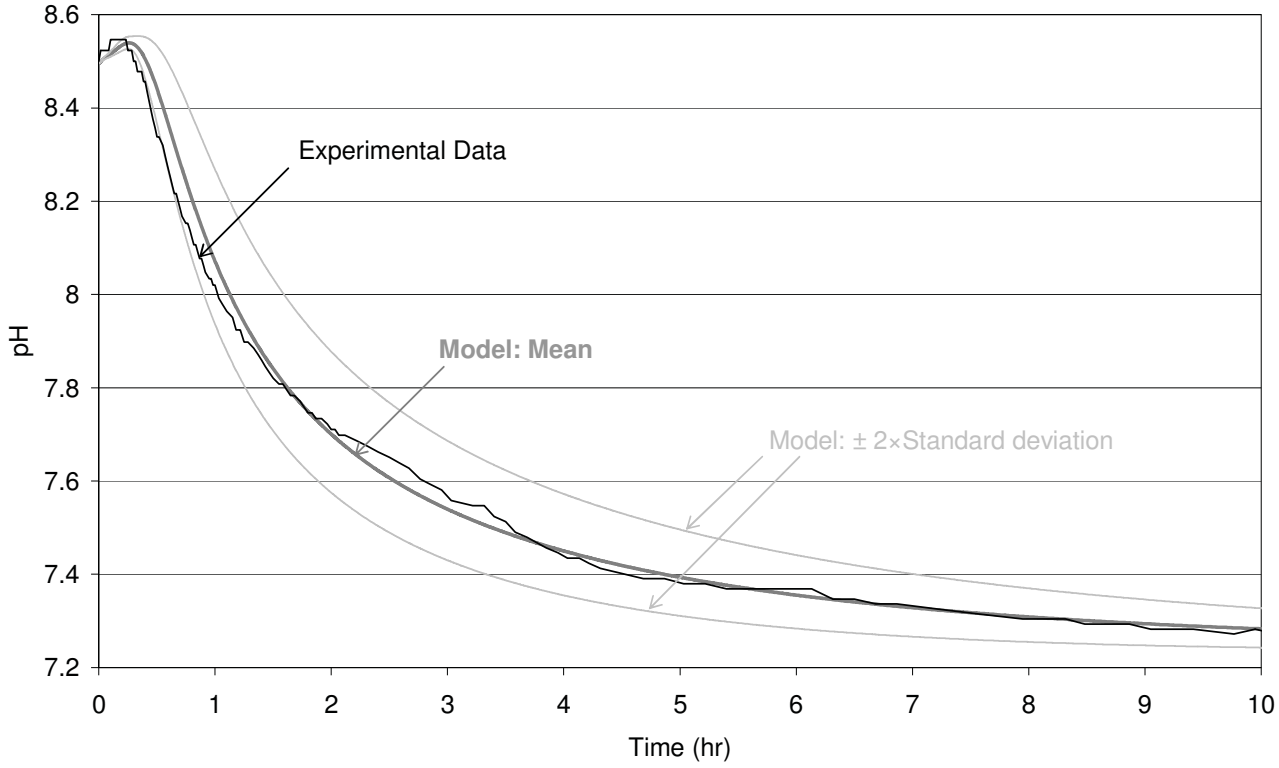

Figure 9.8: The experimentally measured fall in pH in a Petri dish, initially at a steady state pH of 8.5, after placement into a 6% carbon dioxide (at t=0) compared with the fall in pH (calculated from the modelled rise in CO_2 content, mean ± 2 standard deviations of 30 Monte Carlo simulations) at a point 1 mm above the centre floor of the dish. Depth of culture medium = 3.5 mm, depth of paraffin oil = 2.38 mm. No lid on the dish.

Figure 9.9 compares the experimentally measured fall in pH with the calculated fall in pH (from the modelled rise in CO_2). The pH was calculated from the mean partial pressure of carbon dioxide in the media layer (found by integrating across the media subdomain). The experimental data follows this model prediction closely, the model prediction slightly over-predicting the rate of pH change. This method of pH determination will be used throughout model application to determine the mean carbon dioxide content in the 15 µl media drop.

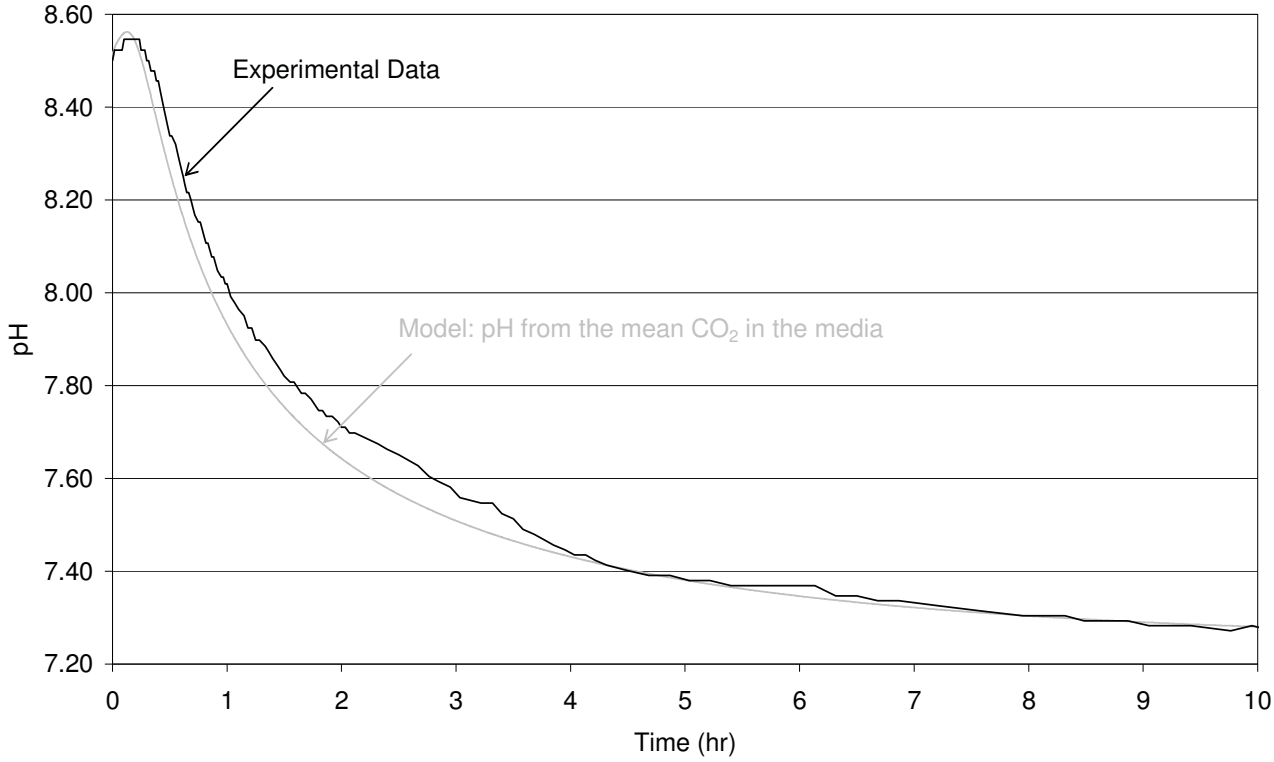

Figure 9.9: The experimentally measured fall in pH in a Petri dish, initially at a steady state pH of 8.5, after placement into a 6% carbon dioxide (at t=0) compared with the fall in pH calculated from the rise in the mean CO_2 partial pressure in the media layer (the integrated partial pressure across the media subdomain).

9.5 Model Application

The purpose of this section was to apply the model of carbon dioxide transfer in a Petri dish and the relationship between CO_2 and pH, as validated in Section 9.4, to investigate steps in the embryo culture process.

The model was validated against pH data measured in a Petri dish set-up which differed to the normal culture set-up. This was because the probe was too large to measure the pH within a culture drop. For model application the drop culture geometry (Figure 8.1) used in clinical practice was investigated. Throughout the embryo culture process the dish system will be exposed to two carbon dioxide

environments; atmospheric CO_2 in the laboratory air (0.03% CO_2) and 6% CO_2 in the incubator (this value may vary with IVF laboratory).

The model was validated against experimental data collected at 20 °C (applying best estimates of the mass transfer properties at 20 °C, displayed in Table 9.6) to ensure the pH meter remained well within its range of safe operating temperatures. Best estimates of the mass transfer properties at 37 °C (displayed in Table 9.5) were used for application of the model to the culture process.

9.5.1 pH equilibration

Figure 9.10 displays the model output for equilibration of CO_2 in the media drop between 0.03% (atmospheric) and 6% CO_2. The mean CO_2 in the drop, the CO_2 at the top of the drop (point of fastest change) and the CO_2 on the dish floor (point of slowest change) are displayed. In both directions the equilibration time is equal. Figure 9.11 displays the pH change in each direction as determined from the data for CO_2 equilibration displayed in Figure 9.10. Equilibration between atmospheric and 6% CO_2 is fast. It takes ≈20 minutes to reach 67% and <1.5 hours to reach 95% of the total pH change. Equilibration from 6% to atmospheric CO_2 is significantly slower. To reach only 67% of the pH change takes 4 to 4.5 hours.

pH change due to equilibration from 0.03 to 6% CO_2 is fast compared to pH change due to equilibration from 6 to 0.03% CO_2. This is due to the bicarbonate buffer buffering against an increase in pH. This result is favourable for embryo culture. The fast pre-equilibration of pH in a dish with a change in CO_2 from atmospheric to 6% quickly produces the environment required for embryos. The relatively slow change

in pH when a dish, fully equilibrated in 6% CO_2, is exposed to the atmospheric CO_2 concentration is good since pH change is not desired when removing embryos from an incubator for observation and manipulation.

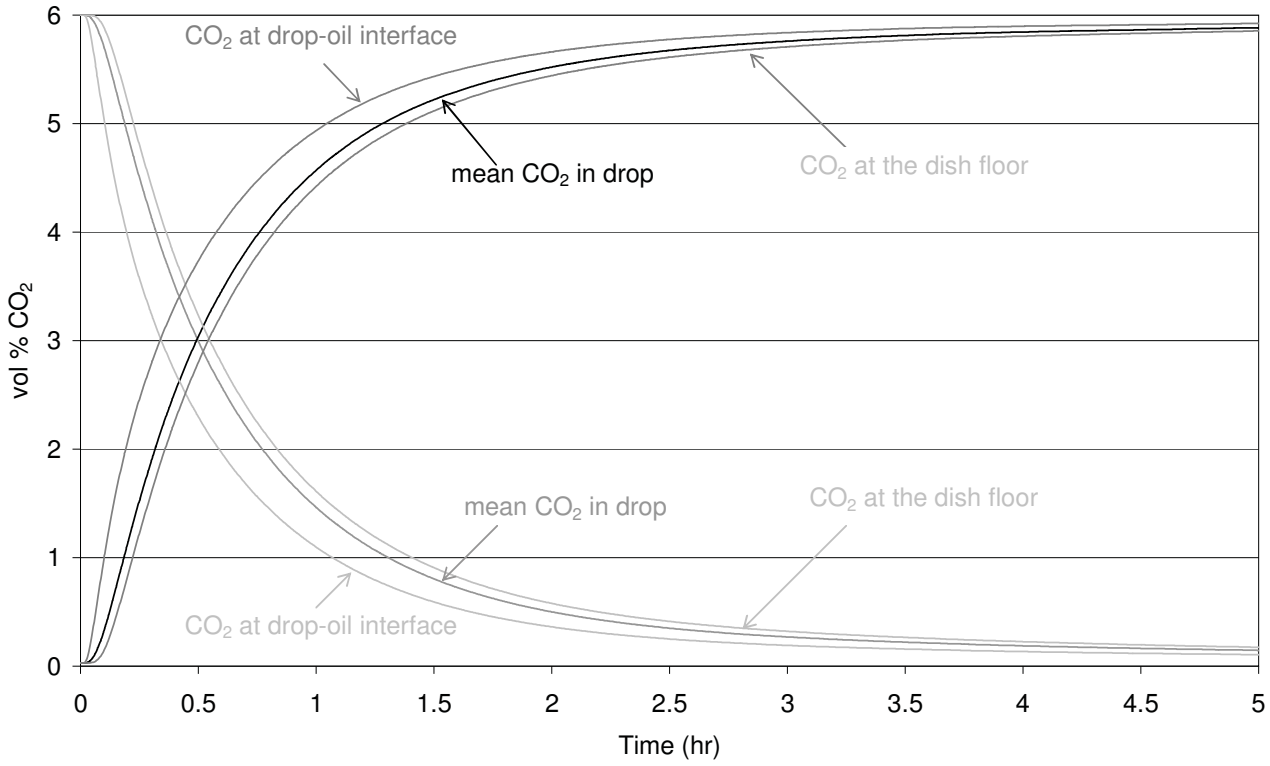

Figure 9.10: Modelled equilibration of carbon dioxide content at the centre floor of a Petri dish in both directions between atmospheric CO_2 (0.03 %) and a 6% CO_2 environment: changes in the mean CO_2 in the drop, the CO_2 at the top of the drop and the CO_2 at the centre floor of the dish floor. The Petri dish system: no lid, depth of 3.09 mm of oil and a central media drop.

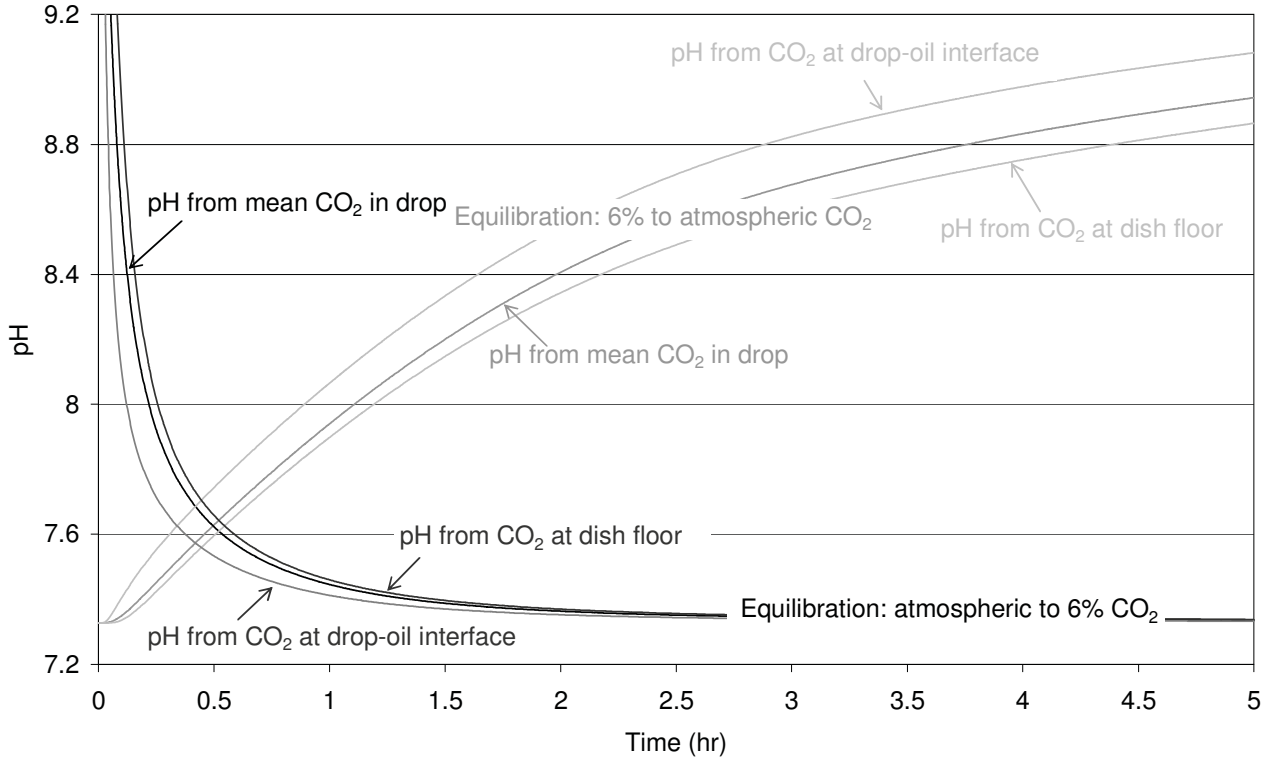

Figure 9.11: pH change calculated from the modelled equilibration of carbon dioxide content at the centre floor of a Petri dish in both directions between atmospheric CO_2 (0.03 %) and a 6% CO_2 environment: changes in the mean CO_2 in the drop, the CO_2 at the top of the drop and the CO_2 at the centre floor of the dish floor. The Petri dish system: no lid, depth of 3.09 mm of oil and a central media drop.

9.5.2 The impact of temperature on pH change

One option to reduce media breakdown during pre-equilibration is to equilibrate the dish systems in the desired gas environment overnight at 4 °C (fridge temperature). As the majority of parameter inputs to the model were not suitably defined at 4 °C the pH change due to equilibration from atmospheric to 6% CO_2 was compared between 20 °C (as used for model validation) and 37 °C.

Figure 9.12 compares the pH change during equilibration from atmospheric to 6% CO_2 at 20 °C with that at 37 °C. The diffusion of CO_2 and the buffering system are

both temperature dependent. At lower temperatures the diffusion coefficient of CO_2 is reduced while the solubility of CO_2 increases. The pK_a of the buffer also increases slightly. The impact of the temperature dependency of mass transfer properties is that at lower temperatures, equilibration of pH is slower and the steady state pH at a given CO_2 concentration (i.e. 6% CO_2) is slightly lower. This 17 °C change slows equilibration by an hour; to reach 95% of full equilibration takes ~1.5 hours at 37 °C and ~2.5 hours at 20 °C.

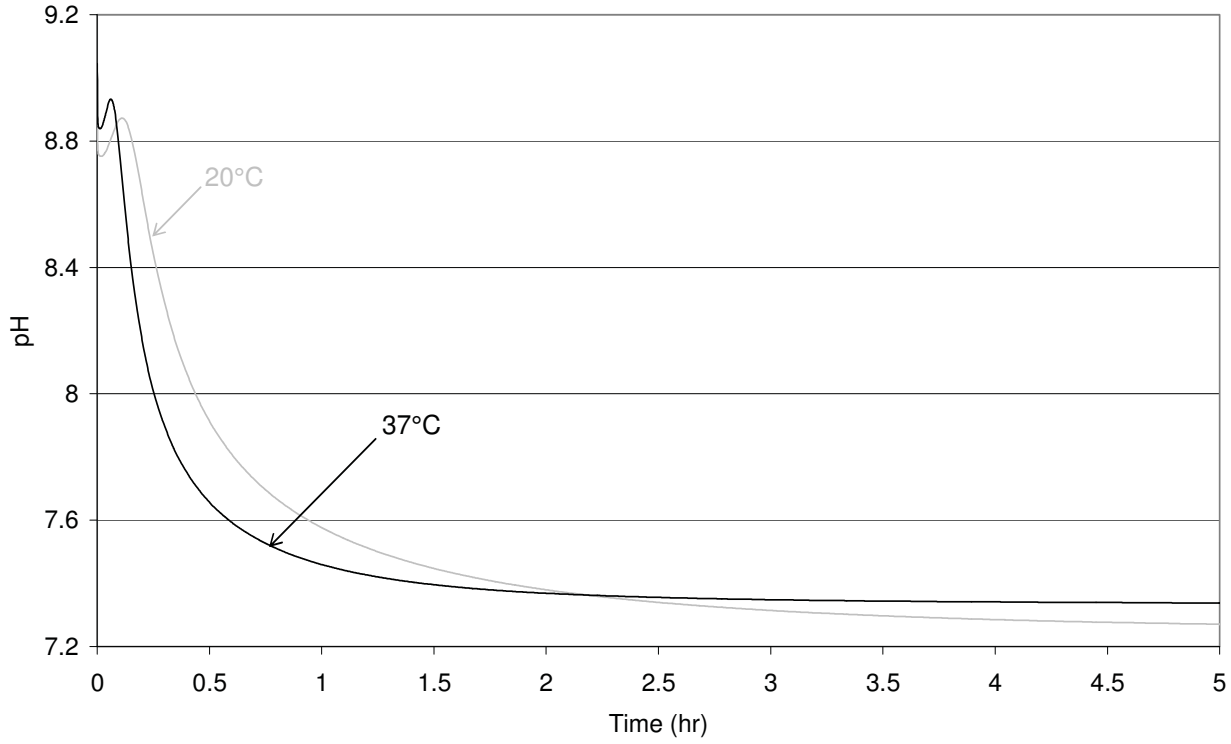

Figure 9.12: Compares the pH change (calculated from the modelled mean CO_2 content in the media drop) during equilibration of a Petri dish from atmospheric CO_2 (0.03 %) to 6% CO_2 at 20°C and 37 °C. The Petri dish system: no lid, depth of 3.09 mm of oil and a central media drop.

Since the temperature change from 37 °C to 20 °C (17 °C) increases the time it takes to reach 95% of pH equilibration from 1.5 to 2.5 hours it is likely that a further temperature decrease of 16 °C (to 4 °C) will have a similar impact on this time (perhaps taking approximately 3 ½ hours). Therefore ~12 hours (overnight) of CO_2

pre-equilibration at 4 °C is very likely to be sufficient for the required pH change. Pre-equilibration of temperature in the dishes may then be carried out in an incubator at 37 °C for approximately 1 hour prior to use.

9.5.3 pH change during embryo manipulation

Figure 9.13 displays the pH rise (calculated from the mean CO_2 concentration in the drop) when a dish is removed from the incubator for 5 minutes (for observation or manipulation) and compares the rise in pH when the 15 µl media drop is overlaid with 5, 5.5, 6, 6.5 or 7 ml of paraffin oil (equating to total oil depths of 2.35, 2.59, 2.82, 3.06 and 3.29 mm respectively). The majority of manipulations throughout embryo culture, with the exception of some ICSIs, will take less than five minutes, therefore this section will look at the pH changes which will occur when a dish is removed from the 6% CO_2 environment into the ambient laboratory air (0.03% CO_2). Some dishes will remain out of the incubator for a longer period due to the large variation in the time taken for steps in the culture process (As describes in Section 3.4).

Figure 9.13 shows that the less paraffin oil over the media drop, the greater the change in pH since there is a shorter distance for CO_2 diffusion out of the drop. Since a pH of 7.4 is considered the maximum upper limit for the pH of an embryo (Section 3.6), the current use of 7 ml over a 15 µl media drop appears appropriate (since the pH does not exceed pH 7.4 after 5 minutes out of an incubator). The minimum volume of oil over 15 µl media drops which will prevent the pH not exceeding 7.4 after 5 minutes out of the incubator is 6 ml (to the nearest 0.5 ml).

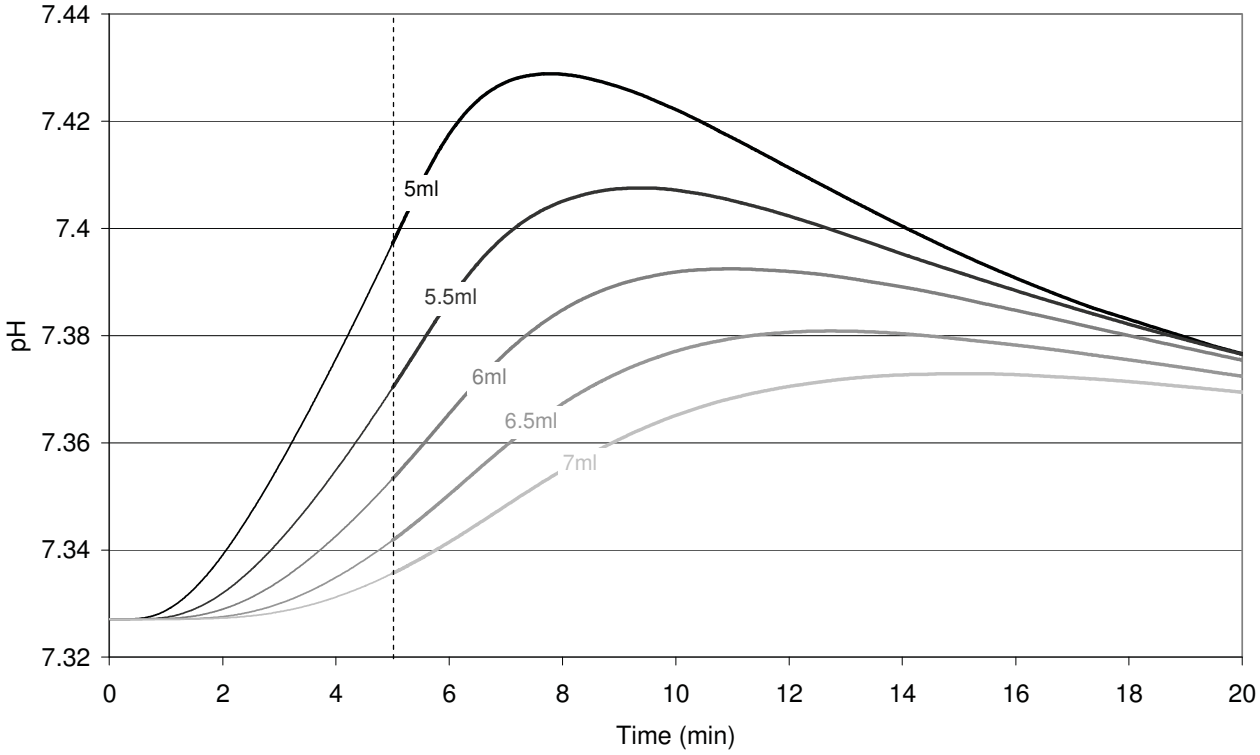

Figure 9.13: The rise in pH (calculated from the modelled mean CO_2 content in the media drop) after transfer of the Petri dish, initially fully equilibrated in a 6% CO_2 environment, from a 6% CO_2 environment into atmospheric CO_2 (0.03 %) at t=0 and return of the Petri dish into a 6% CO2 environment at t=5 minutes (dotted line). This change in pH is compared for dish set ups with varying volume of paraffin oil (5, 5.5, 6, 6.5 and 7 ml of paraffin oil) overlaying the media drop. Dish system: central media drop, no lid.

9.6 Summary

A model of pH change in a media drop was developed based on the mass transfer of CO_2 through the Petri dish system. The model was validated against measured pH data validating the modelling of two simultaneous processes; the diffusion of carbon dioxide through the dish system and the assumed relationship between the pH and the CO_2 concentration in the drop. This model was then applied to investigate the pH changes in an embryo's environment throughout the culture process and factors which impact on these changes. The main findings were:

- pH equilibration, due to carbon dioxide equilibration (from atmospheric (0.03%) to 6% CO_2), of a media drop in the Petri dish system reaches 95% of the pH change in approximately 1.5 hours (at 37 °C)
- pH equilibration, due to carbon dioxide equilibration (from 6% to atmospheric (0.03%) CO_2), of a media drop in the Petri dish system reaches 95% of the pH change in approximately 2.5 hours (at 37 °C)
- Modelling showed that 6 ml of oil in the Petri dish is the minimum volume which will prevent the pH in a media drop exceeding 7.4 after 5 minutes out of the incubator (to the nearest 0.5 ml and assuming a media drop height of 1.43 mm). Normal practice is to overlay a media drop with 7 ml of oil, so this result suggests that significant pH changes will not occur when embryo manipulation and observation takes 5 minutes or less.

10 Discussion and future work

This thesis has studied key aspects of the physical environment that human embryos are exposed to throughout open *in vitro* culture: temperature, oxygen and pH (dependent on carbon dioxide concentration).

There are a limited number of published studies in this area and these have been descriptive and without a theoretical framework (Cooke *et al*., 2002; Lane *et al*., 2008; Wang *et al*., 2001; Higdon *et al*., 2008). Descriptive studies have been hindered by difficulties in measuring temperature, O_2 and pH *in situ* during embryo incubation and handling. These difficulties are due to two main factors - the small size of the embryo, and its immediate environment such as a dish or pipette and limitations in the available measurement technology. Mathematical modelling helps to free the investigator from these limitations.

This study set out to methodically develop mathematical models of heat transfer and of mass transfer for oxygen and carbon dioxide that could be applied to all steps of the culture process. Though embryo culture is a long process consisting of numerous steps, as displayed in Figure 3.10, every use of a dish consists of the same few simple steps (equilibration of the dish in an incubator, transfer of the dish onto a heated surface, removal of the lid from the dish, return of the lid to the dish and return of the dish to the incubator) and pipettes transfer embryos between dishes. Therefore investigation of these few steps covered the majority of the culture process.

Before discussing the outcome and applications of the study it is useful to make an important observation. There is very limited knowledge of:

a) the *in vivo* environment of an embryo with respect to temperature and oxygen concentration
b) the impact on an embryo *in vitro* of changes in temperature and oxygen concentration away from what is considered appropriate.

Due to the technological limitations of measurement *in vivo* there is limited knowledge of the embryo's *in vivo* environment, perhaps the 'ideal' which should be replicated *in vitro*. Nevertheless, there is evidence that changes in temperature and in oxygen concentration exist *in vivo*, with endothermic cooling of the follicles in mammals around ovulation (Hunter *et al*., 2006; Leese *et al*., 2008) and decreased oxygen concentrations in the uterus at the time of implantation (Harvey *et al*., 2007). Such variation in the physical environment has been ignored in embryological practice thus far.

With the introduction of *in vitro* maturation (IVM) into common practice, temperature control is likely to be even more important since there is evidence that mammalian oocytes *in vivo* are cooled around ovulation (Hunter *et al*., 2006; Leese *et al*., 2008) below the standard temperature applied to *in vitro* culture (37 °C) and developing oocytes are more sensitive to cooling than embryos due to de-polymerization of the meiotic spindle (Rama Raju *et al*., 2007; Almeida & Bolton, 1995; Azambuja *et al*., 1998; Pollard *et al*., 1996). Therefore a narrower temperature tolerance for oocytes is likely.

While there has been a great deal of research into the metabolic requirements of human and animal embryos and resulting improvements in embryo culture media, there has been no systematic study of the physical environment throughout embryo culture.

There have been no dose-response experiments on the effect of *in vitro* temperature on embryo development in mammals and, due to ethical considerations, these may never be done in humans. Therefore it has not been possible to objectively define limits for safe practice. Limits have had to be estimated. Embryologist arbitrarily aim to keep embryos within a range of 36 - 37.1 □C and, where this is not possible, between 33 and 37.5 □C, although 34 °C is sometimes interchanged with 33 °C as the desired lower limit.

The results of this study show that the open culture system has the potential to temperature stress oocytes and embryos, the impact of these stresses are not known until the effect of such temperature changes, both in rate and magnitude, have been experimentally determined for embryos and oocytes. Until this is done, as a precaution, it would be prudent to aim to minimise stressors.

10.1 Evaluation of the modelling

10.1.1 Heat transfer in Dishes

The model of heat transfer in the Petri dish and 4-well dish systems were validated against experimental data. The model successfully predicted the experimental data which consistently lay within two standard deviations of the model's mean.

Though the models were well validated, the application of these models had limitations. Prediction of the boundary conditions proved difficult since the placement of a dish onto a heated microscope stage formed a complex thermal environment. In most situations the boundary between the stage and the dish should not be assumed to be of a constant and uniform temperature. Models of specific heated stages may be incorporated into the dish model. However, there are a large variety of heated microscope stages and surfaces so modelling one specific stage would be of limited use. For model application in both dishes, the boundary was assumed to be of a constant and uniform temperature and this enabled investigation of factors in the dish systems which may affect embryo temperature while on a heated surface in the ambient laboratory environment.

A simplification in modelling the 4-well dish was that, due to the greater complexity of the geometry compared to the Petri dish, only a quarter of the dish was modelled in three dimensions with symmetry applied to the two internal boundaries of the dish segment. The full three dimensional dish could be modelled but it was not possible to run a simulation due to limitations in available computing memory. This forced the assumption that the contents of each well are identical and did not enable investigation of any alternatives. This was not considered to be detrimental as a) on many occasions all wells of a 4-well dish will contain a similar volume of culture media and oil and b) the impact one well has on a neighbouring well is likely to be minimal. The influence of a neighbouring well is minimised during the steps of most interest, since during embryo manipulation, when the potential for temperature change is greatest, the lid is off the dish and all that connects the wells is the thin air gap beneath the dish and the thin polystyrene dish floor.

10.1.2 Heat transfer in a pipette

The use of pipettes (as described in Section 7.1.1) is highly variable and the initial temperature of a pipette system used to transfer an embryo will vary greatly in practice.

Heat will be transferred between the liquid in the pipette lumen and the pipette wall as liquid is drawn up into the pipette, the draw phase. Mathematical modelling of the draw phase requires application of computational fluid dynamics tools which were unavailable in the base COMSOL package used in this work. As such the initial conditions were chosen assuming completion of the draw phase.

Calculated time constants showed that heat transfer in the glass pipette from the fluid to the wall will be fast. Therefore, it may be assumed that a local thermal equilibrium between the fluid and the surrounding wall is reached during the 0.2 s draw phase. Since, in normal practice, embryos are lifted into pipettes near the bottom of the liquid column to ensure they are easily expelled, it may be assumed that the pipette wall adjacent to an embryo's position has been pre-warmed by the liquid drawn into the pipette above the embryo. Therefore, for the glass pipette the temperature of the system at the end of the draw phase, the model's initial conditions, may be assumed to be uniformly the temperature of the bulk liquid.

Calculated time constants showed that heat transfer from the fluid to the wall will be slower in the plastic pipette tips. Therefore thermal equilibrium will not be reached between liquid in the pipette lumen and the pipette wall during the draw phase. Two model predictions provide the best and worst case temperature profiles for an embryo

in a plastic pipette tip. Best case assumes the pipette is pre-warmed, worst case assumes no heat is transferred between the liquid in the pipette lumen and the pipette wall during the draw phase.

The models of heat transfer in a glass Pasteur pipette and in a plastic pipette tip were successfully validated for the situation in which the pipette was initially pre-warmed to the temperature of the liquid to be drawn into it. Modelling heat loss from a pre-warmed pipette in the laboratory environment predicted the temperature profile of an embryo within a glass pipette during transfer and provided the best case temperature profiles an embryo may experience in the plastic pipette tip during transfer.

For the worst case model of heat transfer in a plastic pipette tip it was assumed that no heat is transferred between the liquid in the pipette lumen and the pipette wall during the draw phase and thus the pipette wall is initially at room temperature and the liquid within the pipette is initially at bulk liquid temperature. This overestimates initial heat loss from the pipette tips since some heat is transferred during the draw phase. Application of this model was interpreted with this knowledge in mind. In practice, if the pipette is not actively pre-warmed, heat loss will not be approximated by either the pre-warmed or initially cool models but will fall between these limits.

Modelling a static system reduced the potential application of a model since lifting liquid into and out of a pipette, which can occur repeatedly during washing or denuding an embryo, cannot be simulated.

All the observations made through application of the pipette model are new, since the difficulty of measuring temperature in pipettes means such information has never been reported.

10.1.3 Oxygen mass transfer in a Petri dish

A model of oxygen (O_2) mass transfer through the dish system was developed. Model validation was carried out with some simplification. The oxygen probe was large and it was not possible to position it within a 15 µl drop. Therefore the drop was not included in the experimental validation. The result of this was that the transport properties of oxygen in culture media were not experimentally validated. This was not considered problematic since the transport properties of oxygen in water are well characterised (Lango *et al*., 1996; Weathersby, 1980).

The current model was not set up to predict the O_2 content immediately adjacent to an embryo in a droplet where local consumption may deplete O_2 (Stokes *et al*., 2009). However, the model could be extended to include the embryo as an oxygen sink.

10.1.4 Mass transfer of carbon dioxide in a Petri dish and prediction of pH change

A model of pH change in a media drop was developed based on mass transfer of CO_2 through the Petri dish system. This validated two processes simultaneously, the diffusion of carbon dioxide through the dish system and the assumed relationship between the pH and the CO_2 concentration in the drop. A direct relationship between

pH and the concentration of CO_2, as described by the Henderson-Hasselbalch Equation, was assumed at any point in the media drop. This assumption was possible as the concentrations of both bicarbonate and carbon dioxide in the media are significantly greater than the concentration of H^+ and thus the rate of change of each may be assumed independent.

The model validation was carried out with simplifications.

The measurement of pH was used to validate both the diffusion of CO_2 through the dish system and the relationship between the CO_2 concentration and pH in the media. This meant that any discrepancies between the model and the experimental data could not be directly attributed to either part of the model. Several factors made this validation process easier. For example the successful validation of oxygen diffusion in a Petri dish system had already validated the assumption that diffusion is the mode of gas transport in this system.

The pH probe was large and it was not possible to position within a 15 μl drop. As the relationship between CO_2 and the pH in the culture media was of interest, the probe was submerged within a layer of culture media overlaid with paraffin oil. This layer of media was incorporated into the model for comparison with the experimental data.

The measurement of pH proved difficult over the time frame of interest (~10 hours). The probe used to log the change in pH with time had initial readings with an accuracy of ±0.2 pH units and in addition the probe readings drifted throughout experimental runs. Therefore a second probe, which read the pH to the nearest 0.1 pH

unit, was used to record the actual initial pH of the media. The final pH was determined from the Henderson-Hasselbalch equation. The experimental curve was fitted between these two values (a linear relationship was assumed between readings from the two different pH probes).

In spite of these simplifications there was sufficient agreement between the model output and the experimental data to indicate that the parameters describing the diffusion of CO_2 and the simplifications made to the full model of the relationship between CO_2 and H^+ in the culture media were appropriate for a culture system comprising of relatively small droplets under oil.

10.2 Recommendations for embryo culture

From the modelling and experimental work carried out, several recommendations were made on how clinical practices could be changed to optimise the environment the embryo is exposed to throughout the IVF culture process.

Pipette use

Recommendations: Embryos are exposed to the greatest temperature changes, both in rate and magnitude, during transfer in a pipette. To minimise these changes plastic pipette tips should be used in preference to glass Pasteur pipettes. Pipettes should be pre-warmed, immediately prior to use by repetitively drawing up and expelling 37 °C culture medium in quick succession, six times would ensure pre-warming. (Section 7.6)

Dish set-up

Recommendations: Embryo placement in a Petri dish:

Restrict the placement of media drops, and therefore embryos, to within 15 mm of the dish centre (Section 5.4.3)

or

Restrict drop placement to a ring at a set distance from the dish centre, e.g. 20 mm (Section 5.4.3). *Note: with the stage set appropriately temperatures closer to the centre of the dish will reach >37 °C.*

Oil depth:

Maximising oil depth within practical limits will help buffer against changes in O_2 and CO_2 during embryo manipulation (Section 9.5.3). As long as heated stages are set appropriately the volume of oil in a dish has minimal impact on embryo temperature.

Setting heated stage temperature:

Recommendations:

- Heated stages should be set to maintain the temperatures within dish systems with their lids off (Sections 5.4.3 and 8.5.2)
- The temperature should be measured *in situ* at the position an embryo would be within the dish system and under the exact conditions (e.g. lid on/off, height of oil etc.) after removal from the 37 ^{0}C incubator.

- The temperature should be measured with a minimally invasive (Section 4.5.1.1) and calibrated probe.
- Since placement of a dish onto a heated stage forms a dynamic thermal environment (Sections 5.4.4) the temperature should be recorded over time for the period a dish is likely to be on the stage.
- For a dish system in which embryos may be at different temperatures, the 'warmest' position (e.g. the centre floor of a Petri dish) should be measured to avoid overheating.
- Where multiple dish types or set-ups are to be used on the same stage the dynamics of all should be measured.
- The setting of stages should be carried out whenever there is a change to the system. For example moving the stage within the laboratory or a change to dish type or set-up.
- The setting of stages should be checked periodically to ensure nothing has changed inadvertently (for example changes in dish geometry as described in Section 4.1.3.1).

Heated stage use

Recommendations:

- Only dishes for which the stages have been set appropriately should be used.
- Glass heated stages provide a heated surface while an embryo is directly under the microscope, likely better maintaining embryo temperature compared to metal stages which have a hole in the centre to enable light to

pass through for the microscopy.

- If stages have been set for dishes without lids, then the lids should be removed immediately as dishes are placed onto the heated stage.
- Wafts from liquid nitrogen tanks, near heated stages, should be avoided especially while they are in use, as the cold air can cool a stage's feedback sensor triggering a spike in stage temperature. (observed with glass heated stages: Thermoplate, Tokai Hit, Japan)
- The use of glass heated stages to hold multiple dishes should be avoided as this can affect the temperature the stage is controlled to. (Section 5.4.4 and observed with glass heated stages: Thermoplate, Tokai Hit, Japan)

Pre-equilibration of the Petri dish

Recommendations: The times required for equilibration of temperature, O_2 and pH in a Petri dish in a typical incubator environment (to 37 °C, 5% O_2 and 6% CO_2) from the laboratory environment (25 °C, 21% O_2 and 0.03% CO_2) are 1 hr, 4 hr and 2 hr respectively in order to provide a safe environment for embryos and oocytes. (Sections 5.2, 8.5.3.1 and 9.5.1)

Limiting the equilibration time may be beneficial to embryos (Section 2.6.4). Four hours required for oxygen equilibration is shorter than the overnight incubation currently used, however

practically this may be problematic if dishes are required in the early morning. An alternative is to equilibrate dishes overnight to 5% O_2 and 6% CO_2 at 4 °C (Section 9.5.2) and equilibrate the dishes for an hour in the morning at 37 °C.

Though not investigated in this work, it is important to note that temperature differences exist within traditional incubators between different shelves and positions on the shelves. Temperature differences have been observed between dish positions within other incubator systems (e.g. Minc, Planar X) and within enclosed culture systems in which both the bench surface and the surrounding air are heated. Temperature gradients within incubator systems and the interaction between these environments and different dish systems should be investigated through measurement.

10.3 Recommendations for future work

Knowledge of the temperatures, pH and oxygen concentrations which an embryo may experience are only partly useful as the optimal environment for an embryo has not been fully defined. Technological advances which may allow improved *in vivo* investigation or investigations into the impact of changing the *in vitro* environment on embryos from an animal model would be beneficial to the field. Such research would help set specifications for a culture system.

The development of good models of specific heated stages, incorporating the stages' control system would, when coupled with a dish model, enable accurate predictions of temperatures in the dish on the stage and potential for improved stage design.

Models of O_2 and CO_2 mass transport should be developed for steps other than those which involve the Petri dish, for example, within pipettes.

The development of software which would provide an interface to enable an embryologist to use modelling as a tool would be beneficial to a laboratory and for the design of commercial products. An embryologist would then be able to define a sequence in the process themselves, select the relevant geometries (e.g. dish) and boundary conditions (e.g. room temperature), and run the sequence to see the temperature, oxygen concentration, and pH an embryo would be experiencing. This would aid research, staff awareness and training, and the introduction and development of new technologies, or simply optimization of existing systems.

This project has utilised engineering knowledge and mathematical modelling to characterise the physical environment of temperature, oxygen and pH that oocytes and embryos may be exposed to throughout an open culture system, used by the majority of IVF clinics worldwide. It has extended understanding of the temperature changes beyond what can be achieved by experiments alone. The modelling framework enabled changes in the thermal environment to be quantified and validated for pipettes, which had not been done before, and which would mostly be impractical without modelling. Description of O_2 and pH changes during a key step, the movement of a Petri dish in and out of an incubator, is also new. Key phenomena

were uncovered which were not readily apparent to embryologists, particularly the importance of a dish as an insulator on a warmed surface. The findings of this study will allow better design of open culture systems for human and animal embryology and will hopefully prompt continued interest in mathematical modelling as a valuable tool for investigating developments in embryo culture systems.

References

Abu-Isa, I. & Doyle, M. (1965). “Specific Heat of Synthetic High Polymers. XII. Atactic and Isotactic Polystyrene”. Journal of Physical Chemistry. 69(8): 2668-2675.

Almeida, P. A., Bolton, V. N., (1995) “The effect of temperature fluctuations on the cytoskeletal organisation and chromosomal constitution of the human oocyte.” Zygote. 3:357-365

Arain, S. Weiss, S. Heinzle, E. John, G. T. Krause, C. Kilmant, I. (2005). “Gas sensing in microplates with optodes: Influence of oxygen exchange between sample, air, and plate material”. Biotechnology and Bioengineering. 90(3):271-280.

Azambuja, R. M., Kraemer D. C., Westhusin, M. E. (1998) “Effect of low temperatures on *in vitro* matured bovine oocytes” Theriogenology 49:1155-1164.

Bahçeci1, M., Çiray, H. N., Karagenc, L., Ulug, U., Bener, F. (2005) “Effect of oxygen concentration during the incubation of embryos of women undergoing ICSI and embryo transfer: a prospective randomized study.” Reproductive BioMedicine Online. 11(4): 438-443.

Barati, F., Agung, B., Wongsrikeao, P., Taniguchi, M., Nagai, T., Otoi, T. (2008) “Meiotic competence and DNA damage of porcine embryos exposed to an elevated temperature “. Theriogenology. 69:767–772

Barrett, C., Wang, S., Powers. R. (2001) “:Maintaining temperature in IVF culture dishes: do aluminum warming blocks reduce the rate of cooling.” Fertility and Sterility.76 (3):S228-229.

Bastemur, E., Shevlin, M., Sutcliffe, A. (2010) “Growth of children conceived by IVF and ICSI up to 12years of age.” Reproductive BioMedicine Online. 20(1):144-149

Baumann, C. G. Morris, D.G. Sreenan, J. M. Leese, H. J. (2007). ”The quiet embryo hypothesis: Molecular characteristics favouring viability”. Molecular Reproduction and Development. 74(10):1345-1353.

Bavister, B. D. (2002). “Early history of in vitro fertilization”. Reproduction. 124(2):181-196.

Bavister, B. D. (2004). “Oxygen concentration and preimplantation development.” Reproductive BioMedicine Online. 9(5):484-486.

Bavister, B. D., Poole K. A. (2005) “Duration and temperature of culture medium equilibration affect frequency of blastocyst development” Reproductive Biomedicine online: 10(1):124-129.

Boone, W. R., Shapiro, S. S. (1990) “Quality control in the *in vitro* fertilisation laboratory” Theriogenology. 33(1):23-50.

Booth, P.J. Humpherson, P.G. Watson, T. J. Leese, H. J. (2005). “Amino acid depletion and appearance during porcine preimplantation embryo development in vitro”. Reproduction. 130:665-668.

Brandrup, J., Immergut, E. H., Grulke, E. A., Abe, A., Bloch, D. R. (2005) “Polymer Handbook (4th Edition).” John Wiley & Sons.

Braude, P., Bolton, V., Moore, S. (1988) “Human gene expression first occurs between the four- and eight-cell stages of preimplantation development.” Nature. 332:459-461.

Brinsden, P. R. (1999) “Thirty years of IVF: the legacy of Patrick Steptoe and Robert Edwards.” Human Fertility. 12(3):137-143.

Burton., G. J., Hempstock, J., Jauniaux, E. (2002) “Oxygen, early embryonic metabolism and free radical-mediated embryopathies.” Reproductive BioMedicine Online. 6(1):84-96.

Cagnacci, A. Volpe, A. Paoletti, A. M. Melis, G. (1997). “Regulation of the 24 hour rhythm of body temperature in menstrual cycles with spontaneous and gonadotropin-induced ovulation”. Fertility and Sterility. 68(3):421-425.

Campagne, D. M. (2006). “Should fertilisation treatment start with reducing stress?” Human Reproduction. 21(7):1651-1658.

Carslaw, H. S. & Jaeger, J. C. (1947). “Conduction of heat in solids” Clarendon Press. Oxford.

Carwile, L. C. K. & Hoge, H. J. (1966). “Technical Report 66-27-PR Thermal Conductivity of Polystyrene: Selected Values.” U. S. Army Natick Laboratories. Natick.

Cetin, M. T., Kumtepe, Y., Kiran, H., Seydaoglu, G. (2010) “Factors affecting pregnancy in IVF: age and duration of embryo transfer” Reproductive BioMedicine Online. 20:380-386.

Chapman, A. J. (1967) “Heat Transfer, Second Edition” The Macmillan Company. New York.

Choi, Y. & Okos, M. R. (1986). Effects of temperature and composition on the thermal properties of foods. In, Food Engineering and Process Applications (Vol. 1), Jelen P (Ed.), Elsevier Applied Science, London.

Christians, E. S., Zhoub, Q., Renard JP., Benjamin. I. J. (2003) “Heat shock proteins in mammalian development” Seminars in Cell and Developmental Biology.14:283-290.

Ciray, H. N., Aksoya, T., Yaramancia, K., Karayakaa I., Bahceci, M. (2009) ” In vitro culture under physiologic oxygen concentration improves blastocyst yield and quality: a prospective randomized survey on sibling oocytes.” Fertility & Sterility. 91(4):1459-1461.

Cooke, S., Tyler, J. P.P., Driscoll, G. (2002) “Objective Assessments of Temperature Maintenance Using In Vitro Culture Techniques.” Journal of Assisted Reproduction and Genetics. 19(8):368-375.

Correa, G. A., Rumpf, R., Mundim, T. C. D., Franco, M. M., Dode, M. A. N. (2007) “Oxygen tension during in vitro culture of bovine embryos: Effect in production and expression of genes related to oxidative stress” Animal Reproductive Sciences. 104: 132-142.

Coutlieris, F. A., Kanavouras, A. (2006) “Shelf-life predictions for packaged olive oil based on simulations.” Food Chemistry. 96(1):48-55.

Coyne M. D. Kesick, C. M. Doherty, T. J. Kolka, M. A. Stephenson, L.A. (2000). “Circadian rhythm in core temperature over the menstrual cycle: method for noninvasive monitoring.” American Journal of Physiology: Regulatory, Integrative and Comparative Physiology. 279:R1316-R1320.

Cronin, J., Gleeson, J. P. (2006). “Monte Carlo Simulation”. In Sablani, S. S. (Ed.), Datta, A. K. (Ed.), Rahman, M. S. (Ed.), Mujumdar, A. S. (Ed.), “Handbook of Food and Bioprocess Modelling Techniques.” CRC Press, Boca Raton.

Crowe, M. O’conner, P. E. Masterson, B. (1986). “Oxygen Diffusion in natural oils and triglycerides”. Biochemical Society Transactions. 15:260-261.

Cussler, E. L. (1976) “Multicomponent Diffusion.” Elsevier. Amsterdam.

Dale B. Menezo, Y. Cohen, J. DiMatteo, L. Wilding, M. (1998). “Intracellular pH regulation in the human oocyte.” Human Reproduction. 13(4):964-970.

de Castro e Paula, L. A., Hansen, P. J. (2007) “Interactions between oxygen tension and glucose concentration that modulate actions of heat shock on bovine oocytes during in vitro maturation.” Theriogenology. 68:763-770.

Dincer, I. (2003). “Refrigeration systems and applications”. Wiley. Chichester.

Edwards, J. L. Ealy, A. D. & Hansen P. J. (1995) “Regulation of heat shock protein 70 synthesis by heat shock in the pre-implantation murine embryo.” Theriogenology. 44:329-337.

Edwards J. L. Williams DA. Gardner DK. (1998). “Intracellular pH of the mouse preimplantation embryo:amino acids as buffers of intracellular pH.” Human Reproduction. 13(12):3441-3448.

Elder, K. Dale, B. (2000). “In Vitro Fertilization”. Cambridge University Press. Cambridge.

Fauser, B. C. J. M. Rutherford, A. J. Strauss, J. F. Van Steirteghem, A. (Ed.) (1999). “Molecular Biology in Reproductive Medicine”. Parthenon Publishing. London.

Favetta, L. A., St John, E. J., King, W. A., Betts, D. H. (2007) “High levels of p66shc and intracellular ROS in permanently arrested early embryos” Free Radical Biology & Medicine. 42:1201-1210.

Fleming, S. & Cooke, S. (2009) “Textbook of Assisted Reproduction for Scientists in Reproductive Technology” Vivid Publishing. Fremantle.

Fox, T. G., Jr. and Flory P. J. (1949). “Second-order Transition Temperatures and related properties of polystyrene. I. Influence of molecular weight”. Journal of Applied Physics. 21. 589-591.

Frydman, N., Fanchin, R., Le Dû1, A., Bourrier, M. C., Tachdjian, G., Frydman, R. (2004). “Improvement of IVF results and optimisation of quality control by using intermittent activity.” Reproductive Biomedicine Online. 9(5):521-528.

Gaudina, M., Brogni, A. & Caldwell, D. (2011) "Irradiating Heat in Virtual Environments: Algorithm and Implementation" in Springer Berlin Heidelberg, Berlin, Heidelberg, pp. 194-203.

Geankoplis, C. J. (2003) “Transport Processes and Separation Process Principles.” Prentice Hall. New Jersey.

Gopichandran N. Leese H. J. (2006). “The effect of paracrine/autocrine interactions on the in vitro culture of bovine preimplantation embryos”. Reproduction. 131:269-270.

Guérin, P., El Mouatassim, S. & Ménézo, Y. (2001) "Oxidative stress and protection against reactive oxygen species in the pre-implantation embryo and its surroundings." Human reproduction update. 7(2):175-189.

Gutiérrez Diez, P. J., Russo, I. H., & Russo, J. (2012). “The evolution of the use of mathematics in cancer research.” Springer Science & Business Media. New York.

Hansen, H. D., Gesser, H. (1980).” Relationship between non-bicarbonate buffer value and tolerance of cellular acidosis: a comparative study of myocardial tissue.” Journal of experimental biology. 84:161-167.

Harvey, A. J. Navarrete Santos, A. Kirstein, M. Kind, K. L. Fischer, B. Thompson, J. G. (2007). “Differential expression of oxygen regulated genes in bovine blastocysts”. Molecular Reproduction and Development. 74:290-299.

Higdon, H. L., Blackhurst, D. W., Boone, W. R. (2008) “Incubator management in an assisted reproductive technology laboratory.” Fertility and Sterility. 89(3):703-710.

Houghton, F. D. Thompson, J. G. Kennedy, C. J. Leese, H. J. (1996). “Oxygen consumption and energy metabolism of the early mouse embryo”. Molecular Reproduction and Development. 44:476-485.

Hunter, R. H. F., Einer-Jensen, N., Greve, T., (2006) “Presence and Significance of Temperature Gradients Among Different Ovarian Tissues” Microscopy Research and Technique. 69:501–507.

Jana, S. K., Babu, N. K., Chattopadhyay, R., Chakravarty, B., Chaudhury, K. (2010) “Upper control limit of reactive oxygen species in follicular fluid beyond which viable embryo formation is not favourable.” Reproductive Toxicology. 29:447-451.

Jelinkova, L., Brucker, C., Reeka, N., Gagsteiger, F. (2004) “Effect of oxygen concentration on early cleavage of human embryos in vitro.” International Congress Series. 1271:147– 150

Jeppson, R. (2011) “Open Channel Flow: Numerical Methods and Computer Applications.” CRC Press. Boca Raton.

Johnson, M. T. Mahmood, S. Patel, M. S. (2003) “Intermediary metabolism and energetics during murine early embryogenesis”. Journal of Biological Chemistry. 278(34):31457-31460.

Kalan, M. J., Francis, M. M., Lewis, D. E., Allen, R. B., Landay, M. F., Paulson, R. J. (2008) “Temperature Fluctuation in Culture Media in the IVF Lab: Is the Isolette a Better Environment Than the Bench Top?” Fertility and Sterility. 89(4):S21.

Karja, N. W. K., Wongsrikeao, R., Murakami, M., Agung, B., Fahrudina, M., Nagai, T., Otoi, T. (2004) “Effects of oxygen tension on the development and quality of porcine in vitro fertilized embryos.” Theriogenology. 62:1585–1595.

Kaye, G. W. C., & Higgins, W. F. (1928). “The thermal conductivities of certain liquids”. Proceedings of the Royal Society of London. Series A, Containing Papers of a Mathematical and Physical Character. 117(777):459-470.

Keefe, D., Liu, L., Wang, Wei., Silva, C. (2003) “Imaging meiotic spindles by polarization light microscopy: principles and applications to IVF” Reproductive Biomedicine Online. 7(1):24-29.

Kekedy, L. Teuca, I. (1994). “Investigation of oxygen permeability of thin protective organic liquid layers using a clark-type oxygen sensor.” Magyar Kemiai Folyoirat. 100(6):248-250.

Kilani, S. S., Cooke, S., Kan, A. K., Chapman, M. G. (2006). “Do age and extended culture affect the architecture of the zona pellucida of human oocytes and embryos?” Zygote. 14(1):39–44.

Kim, S. B., Kwon, H., Kim, E. K., Kim, J. M., Choi, D. H., Cha K. Y. (2005) “The Comparison of Embryo Developments and Pregnancy Rates in Human in Vitro Culture Conditions at Different Oxygen Gas Phase.” Fertility & Sterility. 84(1):S16.

Kitagawaa, Y., Suzukib, K., Yoneda, A., Watanabe, T. (2004) “Effects of oxygen concentration and antioxidants on the in vitro developmental ability, production of reactive oxygen species (ROS), and DNA fragmentation in porcine embryos.” Theriogenology. 62:1186–1197.

Koster, J. N. (1997) “Experimental study of stability in a layer of a model alloy with a liquid miscibility gap.” Heat and Mass Transfer. 33(3): 193-199

Kovačič, B., Vlaisavljević, V. (2008). “Influence of atmospheric versus reduced oxygen concentration on development of human blastocysts in vitro: a prospective study on sibling oocytes”. Reproductive BioMedicine Online. 17(2):229-236.

Lane, M. & Gardner, D.K. (1994) "Increase in postimplantation development of cultured mouse embryos by amino acids and induction of fetal retardation and exencephaly by ammonium ions" Journal of reproduction and fertility. 102(2):305-312

Lane, M., Mitchell, M., Cashman, K. S., Feil, D., Wakefield, S., Zander-Fox, D. L., (2008) “To QC or not to QC: the key to a consistent laboratory?” Reproduction, Fertility and Development. 20(1):23-32.

Lango, T. Morland, T. Brubakk, A. O. (1996). “Diffusion coefficients and solubility coefficients for gases in biological fluids and tissues: a review.” Undersea and Hyperbaric Medine. 23(4):247-272.

Laughton, M. A. (Ed.), Warne, D. F (Ed.). (2003) “Electrical engineer's reference book.” Newnes. Oxford.

Lazzari, G., Wrenzycki, C., Herrmann, D., Duchi, R., Kruip, T., Niemann, H., Galli, C. (2002) “Cellular and Molecular Deviations in Bovine In Vitro-Produced Embryos Are Related to the Large Offspring Syndrome.” Biology of Reprodiuction. 67:767-775.

Lee E, Fukui Y. (1996). “Synergistic effect of alanine and glycine on bovine embryos cultured in a chemically defined medium and amino acid uptake by in vitro produced bovine morula and blastocysts.” Biology of reproduction. 55:1383-1389.

Lee, M. A., Grazi, R., Seifer, D. B. (2008) “Incorporation of the Cool K-Minc-1000 triple gas incubator and media system into the clinical IVF lab.” Fertility and Sterility. 90:S413-S414.

Leese, H. J. (2002) “Quiet please, do not disturb: a hypothesis of embryo metabolism and viability.” Bioessays. 24(9):845-849.

Leese, H. J., Baumann, C. G., Brison, D. R., McEvoy, T. G., Sturmey, R. G. (2008) “Metabolism of the viable mammalian embryo: quietness revisited” Molecular Human Reproduction. 14(12):667-672.
Lindenau, A. & Fischer, B. (1994) “Effect of oxygen concentration on the incubators gas phase on the development of cultured pre-implantation rabbit embryos.” Theriogenology. 41:889-898.

Magli, M. C., Van den Abbeel, E., Lundin K., Royere, D., Van der Elst, J., Gianaroli, L. (2008) “Revised guidelines for good practice in IVF laboratories.” Human Reproduction. 23(6): 1253-1262.

Mark, J. E., (2009) “Polymer Data Handbook.” Oxford University Press. Oxford.

Martienssen, W., & Warlimont, H. (2005). “Springer handbook of condensed matter and materials data.” Springer-Verlag. Heidelberg.

McCabe, W. L., Smith, J. C., Harriot, P. (2005) “Unit Operations of Chemical Engineering.” McGraw-Hill Science/Engineering/Math. Boston

Meintjes, M., Chantilis, S. J., Douglas, J. D., Rodriguez, A. J., Guerami, A. R., Bookout, D. M., Barnett, B. D., Madden, J. D. (2000) “A controlled randomized trial evaluating the effect of lowered incubator oxygen tension on live births in a predominantly blastocyst transfer program” Human Reproduction. 24(2):300-307.

Mikheyev. M. (1968) “Fundamentals of Heat Transfer.” Peace Publishers. Moscow.

Mishra, V., Misra, A. K., Sharma, R. (2007) “Effect of ambient temperature on in vitro fertilization of Bubaline oocyte.” Animal Reproduction Science. 100:379-384.

Neuer, A., Spandorfer, S. D., Giraldo, P., Dieterle, S., Rosenwaks, Z., Witkin, S. S. (2000) “The role of heat shock proteins in reproduction.” Human Reproduction Update. 6(2):149-159.

Pepperell, Hudson, & Wood. (Ed). (1987). “The infertile couple”. Churchill Livingstone. Edinburgh.

Perry, R.H., Green, D.W. & Maloney, J.O. (1997) “Perry's chemical engineers' handbook” McGraw-Hill. New York

Petersen, C., Oliveira, J., Mauri, A., Massaro, F., Baruffi, R., Pontes, A., Franco, J. (2009) “Relationship between visualization of meiotic spindle in human oocytes and ICSI outcomes: a meta-analysis.” Reproductive BioMedicine Online. 18(2):235-243.

Pollard, J. W., Martino, A., Rumph N. D., Songsasen, N., Plante, C., Leibo, S. P. (1996) “Effect of ambient temperatures during oocyte recovery on in vitro production of bovine embryos.” Theriogenology. 46:849-858

Puleo, A. C. Muruganandam, N. Paul, D. R. (1989) “Gas sorption and transport in substituted polystyrenes.” Journal of Polymer Science: Part B: Polymer Physics. 27(11):2385-2406.

Rama Raju, G. Prakash, G. Krishna, K. Madan, K. (2007). “Meiotic spindle and zona pellucida characteristics as predictors of embryonic development: a preliminary study using polscope imaging”. Reprod Biomed Online. 14(2):166-174.

Rief, S. Sinowatz, F. Stojkovic, M. Einspanier, R. Wolf, E. Prelle, K. (2002). “Effect of a novel culture system on development, metabolism and gene expression of bovine embryos produced in vitro.” Reproduction. 124:543-556.

Rios-Dominguez, H. Ruiz-Trevino, F. A. Contreras-Reyes, R. Gonzalez-Montiel, A. (2006). “Syntheses and evaluation of gas transport properties in polystyrene - POSS membranes.” Journal of Membrane Science. 271:94-100.

Redding, G. P., Bronlund, J. E., Hart, A. L. (2006) “The effects of IVF aspiration on the temperature, dissolved oxygen levels, and pH of follicular fluid” Journal of Assisted Reproduction and Genetics. 23(1):37-40.

Redding, G. P., Bronlund, J. E., Hart, A. L. (2007) “Mathematical modelling of oxygen transport-limited follicle growth.” Reproduction. 133(6):1095-1106.

Redding, G. P., Bronlund, J. E., Hart, A. L. (2008) “Theoretical investigation into the dissolved oxygen levels in follicular fluid of the developing human follicle using mathematical modelling.” Reproduction, Fertility and Development. 20(3):408-417.

Robertson, G. L. (2006) “Food packaging: principles and practice.” Taylor & Francis/CRC Press. Abingdon.

Rocha A, Randel RD, Broussard JR, Lim JM, Blair RM, Roussel JD, (1998) “High environmental temperature and humidity decrease oocyte quality in Bos taurus but not in Bos indicus cows.” Theriogenology. 49:657–65.

Sathananthan, H., Menezes, J., Gunasheela, S. (2003) "Mechanics of human blastocyst hatching in vitro." Reproductive Biomedicine Online. 7(2):228-234.

Severinghaus, J. W. (1965). *Handbook of Physiology: Respiration* 3, section 3, 1480 pp.

Shahsiah, A. Degeneff, R. C. Nelson, J. K. (2007). “A study of the temperature-based dynamic nature of characteristicf gases in oil-cellulose insulation systems”. IEEE Transactions on Dielectrics and Electrical Insulation. 14(2):471-479.

Smuts, M. P., M. Miller, Ramdas-Navale, K., Aoki, V.W. “Improved High-Quality Blastocyst Formation Rates Result From In Vitro Embryo Culture in the Cook Minc Incubator Platform.”

Soucasaux, N. (1993). “The Female Sexual Organs: Shape, Function, Symbol and Archetype”. Imago Editora. Rio de Janeiro.

Stokes, J. S., Abeydeera, L. R., Leese, H. J. (2005). “Development of porcine embryos in vivo and in vitro; evidence for embryo ‘cross talk’ in vitro”. Developmental Biology. 284:62-71.
Stokes, Y. M. Clark, A. R., Thompson, J. G. (2008). “Mathematical modelling of glucose supply toward successful in vitro maturation of mammalian oocytes.” Tissue Engineering: Part A. 14(9):1539-1547.

Stokes, Y. M. (2009) “Quantifying oxygen diffusion in paraffin oil used in oocyte and embryo culture”. Molecular Reproduction & Development. 76:1178-1187.

Sugiyama, S., McGowan, M., Kafic, M., Phillips, N., Young, M., (2003) “Effects of increased ambient temperature on the development of in vitro derived bovine zygotes.” Theriogenology. 60:1039-1047.

Sutton, M. L., Gilchrist, R. B., Thompson, J. G. (2003) “Effects of in-vivo and in-vitro environments on the metabolism of the cumulus oocyte complex and its influence on oocyte developmental capacity” Human Reproduction Update. 9(1):35-48.

Takahashi, M., Keicho, K., Takahashi, Z. H., Ogawa, H., Schultz, R. M. Okano, A., (1999) “Effect of oxidative stress on development and DNA damage in *in vitro* cultured bovine embryos by comet assay.” Theriogenology. 54:137-145.

Tavares, R. S., Martins, F. C., Oliveira, P. J., Ramalho-Santos, J., Peixoto, F. P. (2009) “Parabens in male infertility—Is there a mitochondrial connection?” Reproductive Toxicology. 27(1):1-7.

Tennent, R. M. (2001).”Science Data Book”. Oliver & Boyd, London.

Thompson, J. G., Partridge, R. J., Houghton, F. D., Cox, C. I. & Leese, H. J. (1996) "Oxygen uptake and carbohydrate metabolism by in vitro derived bovine embryos." Journal of reproduction and fertility. 106(2):299-306.

Thompson J. G. McNaughton, C. Gasparrini, B. McGowan, L. T. Tervit, H. R. (2000). “Effect of inhibitors and uncouplers of oxidative phosphorylation during compaction and blastulation of bovine embryos cultured in vitro.” Journal of reproduction and fertility. 118:47-55.

Thompson, J. G., Mitchell, M., and Kind, K. L. (2007). “Embryo culture and long-term consequences”. Reprod. Fertil. Dev. 19: 43–52.

Thompson, J. G. Partridge, R. J. Houghton, F. D. Cox, C. I. Leese, H. J. (1996). “Oxygen uptake and carbogydrate metabolism by *in vitro* derived bovine embryos.” Journal of reproduction and fertility. 106(2):299-306.

Vajta, G., Rienzi, L., Cobo, A., Yovich, J. (2010) “Embryo culture: can we perform better than nature?” Reproductive BioMedicine Online. 20:453-469.

Van Blerkom, J. (2004). “Mitochondria in human oogenesis and preimplantation embryogenesis: engines of metabolism, ionic regulation and developmental

Wang, W.-H., Meng, L., Hackett, R. J., Odenbourg, R., Keefe, D. L. (2001) “The spindle observation and its relationship with fertilization after intracytoplasmic sperm injection in living human oocytes” Fertility and Sterility. 75(2):348-353.

Wang, W.-H., Meng, L., Hackett, R. J., Keefe, D. L. (2001) “Developmental ability of human oocytes with or without birefringent spindles imaged by polescope before insemination.” Human Reproduction. 16(7):1464-1468.

Wang, W.H. Sun, Q. Y. (2006). “Meiotic spindle, spindle checkpoint and embryonic aneuploidy”. Frontiers in Bioscience. 11(1):620-636.

Wang, J. F., Li, C. X., Wang, Z. H. (2007) “Measurement and Prediction of Vapor Pressure of Binary and Ternary Systems Containing 1-Ethyl-3-methylimidazolium Ethyl Sulfate.” Journal of chemical and engineering data. 52(4):1307-1312.

Weatherby, P. K. Homer, L. D. (1980). “Solubilities of inert gases in biological fluids and tissues: a review”. Undersea Biomedical Research. 7(4):277-296.

Wilson, A. C. (1959). “Industrial thermal insulation: materials, application methods, specifications. McGraw-Hill.” New York.

Yang, W., Sokhansanj, S., Tabil Jr, . (1997). “Measurement of heat capacity for borage seeds by differential scanning calorimetry.” Journal of Food Processing and preservation. 21:395-407.

Yuan, Y. Q., Soom, A. V., Coopman, F. O. J., Mintiens, K., Boerjan, M. L., Van Zeveren, A., de Kruif, A., Peelman, L. J. (2003) “Influence of oxygen tension on apoptosis and hatching in bovine embryos cultured in vitro.” Theriogenology.

Zhang, J. Q., Li, X. L., Peng, Y., Guo X., Heng, B. C., Tong, G. Q. (2010) “Reduction in exposure of human embryos outside the incubator enhances embryo quality and blastulation rate.” Reproductive BioMedicine Online. 20:510-515.

Appendices

MATLAB and COMSOL files used to solve the models developed in this thesis can be found on the accompanying CD. The CD is arranged into four separate folders labelled Appendices A-D.

- Appendix A – Petri dish heat transfer files contains files for the models developed in chapters 4 and 5.
- Appendix B – 4-well dish heat transfer files contains files for the models developed in chapter 6.
- Appendix C – Pipette heat transfer files contains files for the models developed in chapter 7.
- Appendix D – Petri dish mass transfer files contains files for the models developed in chapters 8 and 9.

The files contained in each appendix are summarised below.

Appendix A – Petri dish heat transfer files

"Petri Dish HT" (COMSOL Model File)

"2D Petri dish geometry" (MATLAB m-file)

"HT Petri dish model validation MC" (MATLAB m-file)

"HT Petri dish lid removed MC" (MATLAB m-file)

"HTPetridishmodelvalidationMC" (MPHM File)

"HTPetridishlidremovedMC" (MPHM File)

Appendix B – 4-well dish heat transfer files

"3D 4-well geometry" (MATLAB m-file)

"4-well 3D" (COMSOL Model File)

"4-wellMC" (MATLAB m-file)

"4-wellMC" (MPHM File)

Appendix C – Pipette heat transfer files

"2D HT Glass Pasteur pipette" (COMSOL Model File)

"2D HT Pulled glass pipette" (COMSOL Model File)

"2D pipette geometry" (MATLAB m-file)

"3D HT Plastic pipette tip - T200" (COMSOL Model File)

"3D HT Plastic pipette tip - T400" (COMSOL Model File)

"plastic pipette T-200 geometry" (MATLAB m-file)

"plastic pipette T-400 geometry" (MATLAB m-file)

Appendix D – Petri dish mass transfer files

"2D MT Carbon Dioxide Petri dish" (COMSOL Model File)

"2D MT Oxygen Petri dish" (COMSOL Model File)

"CO2Validation" (MATLAB m-file)

"CO2Validation" (MPHM File)

"ExpIncubatorO2" (Text Document)

"OxygenValidationMC" (MATLAB m-file)

"OxygenValidationMC" (MPHM File)